UNIVERSITY OF RIJEKA

FACULTY OF BIOTECHNOLOGY AND DRUG DEVELOPMENT

Bobana Samardžija

Aggregation, parallel aggregation and co-aggregation of proteins in chronic mental illnesses

DOCTORAL THESIS

Rijeka, 2025

UNIVERSITY OF RIJEKA

FACULTY OF BIOTECHNOLOGY AND DRUG DEVELOPMENT

Bobana Samardžija

Aggregation, parallel aggregation and co-aggregation of proteins in chronic mental illnesses

DOCTORAL THESIS

Mentor: Assoc. Prof. Nicholas J. Bradshaw, PhD

Rijeka, 2025

SVEUČILIŠTE U RIJECI
FAKULTET BIOTEHNOLOGIJE I RAZVOJA LIJEKOVA

Bobana Samardžija

Agregacija, paralelna agregacija i koagregacija proteina u kroničnim mentalnim bolestima

DOKTORSKI RAD

Mentor: izv. prof. dr. sc. Nicholas J. Bradshaw

Rijeka, 2025

Mentor: Assoc. Prof. Nicholas J. Bradshaw

Doctoral thesis was defended on _____

at the University of Rijeka, Faculty of Biotechnology and Drug Development, in front of the Evaluation Committee:

1. Assoc. Prof. Jelena Ban (FABRI)
2. Prof. Ivana Munitić (FABRI)
3. Assoc. Prof. Dubravka Švob Štrac (IRB)

Zahvala

S poštovanjem i zahvalnošću priznajem izniman doprinos svih donora i njihovih obitelji, čija je velikodušna donacija uzoraka omogućila provođenje većine ovog istraživanja. Zahvaljujem svom mentoru na pruženoj prilici da radim na ovom projektu i na uloženom vremenu. Njegovi komentari i sugestije pridonijeli su oblikovanju ovog rada.

Ovaj rad je samo jedna polovica puzzle jer drugi dio živi kroz "my better half" Beti, koja doslovno prošla najbolje i najgore dane sa mnom. Moja iskrena zahvala ide Maji i Matei koje su pročitale ovaj rad više puta nego ja. Nadam se da ćete uvijek biti pametnije od mene. Neophodno je istaknuti neprocjenjiv doprinos Maje Juković ovim eksperimentima, koji su objavljeni 2022. godine. Njezina predanost i stručnost bili su od presudne važnosti za uspjeh ove teze i očuvanje mog mentalnog zdravlja. Posebno se zahvaljujem svim studentima i studenticama s kojima sam surađivala sve ove godine, njihov trud i predanost postavili su čvrste temelje za moje istraživanje. Oni su i najljepša stvar koja je nastala kroz moj doktorat, čvrsto vjerujem kako su oni više toga mene naučili nego ja njih. Zahvalna sam svim kolegama i kolegicama na fakultetu koji su uvijek imali vremena za kavu, bez vas ovaj posao stvarno ne bi imao smisla.

Ispunjenog srca se zahvaljujem svim svojim prijateljima (mlađima i starijima) te svojoj obitelji na nepresušnoj ljubavi i podršci.

"PhD is a lonely journey, but I never walked it alone."

Izvori financiranja:

„CANDiD: Characterisation of aggregating proteins in neuropsychiatric diseases, including Drosophila models", financirano of strane Hrvatske zaklade za znanost (IP-2018-01-9424)

„DeSPERADo: Depression, suicide and proteinopathy: elucidating the relationships between aggregation and pathological development", financirano of strane Hrvatske zaklade za znanost (IP-2022-10-2745)

DOK-2020-01-8580 (2020-2024), financirano of strane Hrvatske zaklade za znanost

„DISC1: Its Structure, Causes of Aggregation and Relevance to Disease (the DISCARD collaboration)", financirano od strane Alexander von Humboldt Foundation

Abstract

Chronic mental illnesses (CMIs), including schizophrenia (SZ), bipolar disorder (BiPD), and major depressive disorder (MDD), present a substantial burden on individuals and healthcare systems worldwide. CMIs exhibit complex etiologies involving a mixture of genetic and environmental factors. While protein aggregation is a well-established hallmark of neurodegenerative diseases, its role in CMIs remains poorly understood. Key questions remain unanswered, such as whether aggregation occurs uniformly across brain regions, whether different proteins aggregate within the same individuals, what drives this aggregation, and how it may contribute to behavioral symptoms. This thesis aims to address these knowledge gaps by investigating the causes and effects of protein aggregation in CMIs, with a focus on the potential for co-aggregation of key candidate proteins.

This research utilizes *post-mortem* human brain samples, *in vitro* cell models, and a transgenic *Drosophila* model. Analysis of human brain samples revealed distinct patterns of insolubility and aggregation for CRMP1, DISC1, NPAS3, and TRIOBP-1 across different brain regions linked to SZ, MDD, and suicide. Notably, these proteins were found to co-aggregate within the same individuals, including some healthy controls, suggesting either shared physiological mechanisms or differential pathological thresholds. The extent and location of aggregation varied between brain regions and individuals, showing that it does not follow a consistent pattern based on diagnosis.

Moreover, the link between protein aggregation, genetic mutation, and environmental susceptibility was investigated using wild-type and mutant forms of NPAS3 in cell culture experiments. While previous research showed that mutation alone can cause NPAS3 aggregation, my findings demonstrated that loss of nuclear localization and potential aggregation can also occur under physiological and stress conditions, even in the absence of mutation. This suggests that these changes may be less dependent on genetic alterations than previously assumed.

Region-specific analysis further revealed that the PAS1 domain strongly influences NPAS3 localization in cells, promoting its retention in the cytoplasm rather than the nucleus. This mislocalization may reduce NPAS3's functional activity and increase its susceptibility to

aggregation. Additionally, CRMP1 showed potential for co-aggregation with DISC1 and TRIOBP-1 in cells, echoing findings from human brain analyses. Additionally, the Drosophila model expressing human DISC1 variants shows potential for revealing behavioral and molecular alterations. However, the model requires thorough validation due to lack of expression control.

These findings establish that protein aggregation in CMIs is a heterogeneous, region-dependent process, with multiple proteins aggregating within the same individuals. It also provides new evidence that co-aggregation may be a contributing molecular mechanism in CMIs. Moreover, it highlights how both genetic and environmental stressors can influence aggregation. This study is limited by variability in brain tissue quality, protein aggregation detected in controls, and reliance on overexpression models in cell culture. Also, the *Drosophila* model showed leaky gene expression and requires further validation. Taken together, these factors highlight the need for improved models and normalization methods in future research. Nevertheless, the results from this thesis lay the groundwork for future research into protein aggregation as a potential biomarker or therapeutic target, offering novel molecular insights into the pathophysiology of CMIs.

Keywords: Protein aggregation, co-aggregation, schizophrenia, bipolar disorder, major depressive disorder, CRMP1, DISC1, NPAS3, TRIOBP-1.

Sažetak

Kronične mentalne bolesti (KMB), uključujući shizofreniju (SZ), bipolarni poremećaj (BiPD) i kliničku depresiju (KD), predstavljaju značajan teret za pojedince i zdravstvene sustave diljem svijeta. KMB imaju složenu etiologiju koja uključuje kombinaciju genetskih i okolišnih čimbenika. Iako je agregacija proteina dobro poznata značajka neurodegenerativnih bolesti, njezina uloga u KMB još uvijek nije dovoljno istražena. Ključna pitanja ostaju neodgovorena: događa li se agregacija ravnomjerno u različitim regijama mozga, agregiraju li različiti proteini unutar istih pojedinaca, što pokreće agregaciju i kako ona može pridonijeti razvoju simptoma. Ova disertacija ima za cilj popuniti te praznine u znanju istraživanjem uzroka i posljedica agregacije proteina u KMB, s posebnim naglaskom na mogućnost koagregacije ključnih kandidata proteina.

Opisano istraživanje uključuje analize *post-mortem* uzoraka ljudskog mozga, *in vitro* stanične modele i transgenični model vinske mušice (*Drosophila*). Analiza ljudskog moždanog tkiva otkrila je različite obrasce netopljivosti i agregacije proteina CRMP1, DISC1, NPAS3 i TRIOBP-1 u različitim regijama mozga povezanim sa SZ, MDD i suicidalnim ponašanjem. Analizirani proteini koagregirali unutar određenih pojedinaca sa dijagnozom i u kontrolnim uzorcima, upućujući na zajedničke fiziološke mehanizme ili različite patološke pragove. Opseg i lokalizacija agregacije varirali su među regijama mozga i pojedincima te agregacija nije bila dosljedna ni specifična za dijagnozu.

Nadalje, povezanost agregacije proteina, genetskih mutacija i osjetljivosti na okoliš istražena je pomoću divljeg i mutiranog oblika proteina NPAS3 u staničnim kulturama. Iako su prethodna istraživanja pokazala kako sama mutacija može uzrokovati agregaciju NPAS3, moji rezultati pokazuju kako gubitak nuklearne lokalizacije i potencijalna agregacija mogu nastupiti i pod fiziološkim i stresnim uvjetima, čak i bez mutacije. Stoga opisane promjene mogu biti manje ovisne o genetici nego što se prethodno mislilo. Analiza regija proteina NPAS3 dodatno je pokazala kako PAS1 domena snažno utječe na lokalizaciju NPAS3 u stanicama, potičući njegovu lokalizaciju u citoplazmi umjesto u jezgri. Opisana promjena u lokalizaciji može smanjiti funkcionalnu aktivnost NPAS3 i povećati njegovu sklonost agregaciji. Također, pokazala sam kako CRMP1 može koagregirati s DISC1 i TRIOBP-1 u

stanicama, što je u skladu s rezultatima analize uzoraka ljudskog mozga. Transgenični model vinske mušice koji eksprimira ljudski DISC1 pokazuje potencijal za otkrivanje bihevioralnih i molekularnih promjena, ali zahtijeva detaljnu validaciju zbog nedostatka kontrole ekspresije.

Opisani rezultati potvrđuju heterogenost i specifičnost agregacija proteina u KMB, pri čemu više proteina može agregirati unutar istih pojedinaca. Disertacija također nudi nove dokaze kako koagregacija može biti molekularni mehanizam koji doprinosi razvoju KMB te ističe utjecaj genetskih i okolišnih čimbenika na agregaciju. Ovo istraživanje ima ograničenja, uključujući varijabilnost kvalitete tkiva, agregaciju proteina kod kontrola te prekomjernu ekspresiju proteina u staničnim kulturama. Također, *Drosophila* model pokazuje manjak kontrole ekspresije proteina, zbog čega zahtijeva dodatnu validaciju. Sveukupno, korišteni modeli i metode zahtjevaju značajnu modifikaciju u budućim istraživanjima. Unatoč tome, rezultati ovog rada postavljaju temelje za daljnja istraživanja agregacije proteina kao potencijalnog biomarkera ili terapijskog cilja, nudeći nove molekularne uvide u patofiziologiju KMB.

Ključne riječi: agregacija proteina, koagregacija, shizofrenija, bipolarni poremećaj, klinička depresija, CRMP1, DISC1, NPAS3, TRIOBP-1.

Abbreviations

aa – amino acids

Aβ- amyloid-β

BDNF - brain-derived neurotrophic factor

BiPD – bipolar disorder disease

BA - Brodmann area

BACS - Brief Assessment of Cognition in SZ

CBT - cognitive-behavioral therapy

COMT - catechol-O-methyltransferase

CMIs – chronic mental illnesses

CNS – central nervous system

CRMP1 - Collapsin response mediator protein 1

CRP - C-reactive protein

DISC1 - Disrupted in Schizophrenia 1

DSM - Diagnostic and Statistical Manual of Mental Disorders

FC – frontal cortex

GABA - Gamma-aminobutyric acid

GWAS - Genome-wide association study

h – hour

HPA - hypothalamic-pituitary-adrenal

hrs – hours

H_2O_2 - hydrogen peroxide

IC – insular cortex

I/A – insoluble/aggregating

iPSC - induced pluripotent stem cell

LOG - lateral orbitofrontal gyrus

KDP - kronični depresivni poremećaj

MCCB - MATRICS Consensus Cognitive Battery

MDD – major depressive disorder

min – minutes

N/A - not applicable

NDs – neurodegenerative disorders

NDE1- Nuclear distribution protein nudE 1

NDEL1- Nuclear distribution protein nudE-like 1

NMDA - N-methyl-D-aspartate

NPAS3 - Neuronal PAS domain-containing protein 3

NRG1 - Neuregulin1

PC - parietal cortex

PDE4B - cAMP-specific 3',5'-cyclic phosphodiesterase 4B

PiFC - piriform cortex

ScoRS - Cognition Assessment Scale in SZ

sec – seconds

SFG - superior frontal gyrus

SNPs - single-nucleotide polymorphisms

SZ – schizophrenia

TC - temporal cortex

TRIOBP-1 – Trio and F-actin binding protein isoform 1

UAS- upstream activation sequence

wt – wild-type

Contents

1 Introduction

1.1 Chronic mental illnesses

Chronic mental illnesses (CMIs) are long-term psychiatric conditions that profoundly affect an individual's emotional, cognitive, and social functioning, often leading to significant impairment in quality of life[1,2]. Examples of CMIs include major depressive disorder (MDD), schizophrenia (SZ), and bipolar disorder (BiPD), all of which exhibit diverse symptoms and complex profiles. These conditions are widespread, with the World Health Organization (WHO) reporting that mental disorders contribute significantly to the global burden of disease, affecting approximately one in eight individuals worldwide[2,3]. Recent data suggests that more than one in ten individuals worldwide, approximately 293 million people aged 5 to 24 years, live with a diagnosable mental disorder[4].

The etiology of CMIs includes a complex interaction between genetic predispositions and environmental factors[5]. Genetic studies have shown a strong heritable component, with closer relatives having a higher risk of developing CMIs than the general population[6,7]. Initial twin studies estimated the heritability of SZ and BiPD to be between 70% and 80%[8–10]. A sizeable Danish twin study later estimated the heritability of SZ to be as high as 79%[11,12], while data from the SZ and BiPD Twin Study in Sweden reported a heritability of 73% for psychosis[13]. For MDD, early twin studies suggested heritability ranging from 48% to 75%[14]. Subsequent data from a Swedish national twin study revealed that heritability was higher in women (42%) compared to men (29%)[15]. Another Swedish twin study estimated the heritability of MDD at approximately 37%[16], consistent with findings that less severe forms of MDD in population-based studies showed heritability around 38%, with environmental factors accounting for the remainder[17,18]. Molecular genetic studies have identified numerous specific genetic polymorphisms contributing to SZ, BiPD, and other CMIs across populations[19–21]. A large genome-wide association study (GWAS) identified over 250 loci associated with SZ, many within genes critical for synaptic function and neuronal communication[22]. Certain genetic variants are associated with SZ and BiPD[23], while others are linked to SZ, BiPD, and MDD[20]; indicating that specific genetic variants may contribute to the risk of multiple mental illnesses.

A variety of environmental factors can contribute to CMIs, including adverse childhood experiences (maltreatment, trauma) and tobacco smoking[24–27], which were seen to be cross-diagnostic for multiple CMIs. In addition, previous studies suggested that other environmental factors like prenatal exposures (infections and maternal stress) and perinatal complications could increase the risk of SZ development[28–31]. The research was done on the impact of these factors by analyzing epigenetic mechanisms like DNA methylation and histone modifications[32–35]. Specifically, traumatic events like famine can lead to heritable epigenetic changes, potentially increasing the risk of psychiatric disorders in future generations[36,37]. Additionally, social factors like socioeconomic disadvantage and minority status[38], as well as substance abuse (cannabis), were associated with increased CMI risk[39,40]. For example, the strong influence of the urban environment on developing children and adolescents, can lead to an expression of a psychosis-like mental state in later life[41].

The development of CMIs is unlikely to come from a single environmental factor. Instead, it is more plausible that multiple factors interact and accumulate over time, collectively increasing the risk of these conditions.

1.1.1 Schizophrenia

Schizophrenia (SZ) is a complex neuropsychiatric illness with underlaying genetic, environmental, and neurobiological factors. This chapter explores its symptoms, etiology, underlying molecular mechanisms, current therapeutic strategies, and emerging treatments.

1.1.1.1 Symptoms of SZ

Severe symptoms of SZ are usually divided into positive, negative, and cognitive symptoms. Positive and negative symptoms are measured with the Positive and Negative Syndrome Scale (PANSS)[42].

Positive symptoms, also referred to as psychotic symptoms, are symptoms that are not normally experienced, but are present in people during a psychotic episode, including persistent hallucinations, delusions, and disorganized behavior. Delusions include fixed beliefs that something is true despite evidence of the contrary. Hallucinations, defined as sensory perceptions without an external stimulus, can be

auditory, olfactory, visual, tactile, or somatic. Disorganized behavior includes bizarre or purposeless things or unpredictable and inappropriate emotional responses. Moreover, the individual exhibits disorganized thinking, reflected in jumbled or irrelevant speech[1,2].

Negative symptoms refer to previously present behaviors that are lost since the onset of SZ, like affective flattening, social withdrawal, and avolition. Those symptoms contribute significantly to functional impairment[1,2]. People with this condition face intense and widespread stigma, leading to social exclusion and straining relationships with family and friends. This stigma fuels discrimination, further restricting their access to essential healthcare, education, housing, and employment opportunities[43]. One of the core symptoms of SZ is anhedonia, the inability to experience pleasure or enjoyment from activities that typically bring happiness or satisfaction. Due to the disruption of reward anticipation or effort valuation, patients with SZ can experience altered emotional behavior, leading to poor functional outcomes[44]. Beyond anhedonia, there is a high level of co-morbidity of MDD and anxiety in patients with SZ diagnosis[45–47]. Additionally, recent studies showed significant genetic correlations between these illnesses[48].

Cognitive symptoms, which include deficits in memory, executive function, and attention [1], frequently persist throughout the illness with a severe impact on daily living and treatment outcomes[49].

1.1.1.2 Diagnosis of SZ

Kurt Schneider developed the most influential model for classifying SZ symptoms, identifying specific "first-rank symptoms." These include "delusional perceptions," auditory hallucinations (voices), and seven types of delusions: somatic passivity, thought withdrawal, thought broadcasting, thought insertion, the belief that one's emotions are not one's own, and the belief that an external force controls impulses or actions[49,50].

Under the previous guidelines outlined in the Diagnostic and Statistical Manual of Mental Disorders, Fourth Edition (DSM-IV), a diagnosis of SZ typically required two positive symptoms, although, one Schneiderian first-rank symptom could suffice[51]. However, the updated DSM-V diagnosis of SZ mandates the presence of at least two psychotic symptoms for at least 1 month, which are not caused by

mood disorder, such as MDD or BiPD, or substance abuse. Moreover, it requires the presence of symptoms and signs of functional impairment (interpersonal or occupational disruptions) for a period of at least 6 months[1].

There are many neurophysical tests for assessing cognitive state, varying in duration and complexity, but the most commonly used are MATRICS Consensus Cognitive Battery (MCCB) and the Brief Assessment of Cognition in SZ (BACS)[52]. MCCB takes about 60 min and includes an assessment of seven cognitive domains (speed of processing, attention, working memory, visual and verbal learning, reasoning and problem-solving, and social cognition). BACS is shorter (duration is about 30 min) and assesses six cognitive domains (verbal learning and memory, working memory, motor function and speed, verbal fluency, attention and processing speed, and executive function). However, BACS lacks assessment of the social cognitive domain, which is severely affected in patients with SZ and closely related to patient recovery. In addition to cognitive testing, simplified clinical scales can be used during clinical interviews, such as the Cognition Assessment Scale in SZ or shorter ScoRS. Interestingly, these interviews are conducted with the patient, as well as with patient's frequent day-to-day contacts, such as family members, friends, colleagues, and social workers[52].

1.1.1.3 Epidemiology and life quality in SZ

In 2019, the global population of individuals with SZ diagnosis reached 23.6 million, marking a 65.85% increase since 1990. The United States recorded the highest age-standardized disability-adjusted life years rate for the condition[53].

In most cases, the first occurrence of SZ is reported at age 20-24. Schizophrenia affects around 0.3–0.7% of the general population and is diagnosed 1.4 times more frequently in males than females[27].

SZ impacts individuals' quality of life, manifesting in various psychosocial challenges and increased health risks[54]. The employment of individuals with diagnosed SZ varies between 4 and 50.4%. It is affected by factors like negative and cognitive symptoms, age of onset, and duration and course of the disease has a negative impact. Individuals with diagnosed SZ frequently experience significant social isolation and loneliness, which can exacerbate physical, emotional, and

cognitive challenges[55,56]. In contrast, a strong support system, whether through family or friends, is crucial in managing symptoms and improving adaptation to life with SZ[57–59]. There is also a high prevalence of comorbid conditions, including MDD and substance abuse disorders, among individuals with SZ, significantly elevating the risk of suicide in this population[60]. Individuals with SZ face a reduced life expectancy, living an estimated 14.5 years less than the general population, primarily due to increased rates of cardiovascular disease, diabetes, and pulmonary disorders[61].

1.1.1.4 Etiology of SZ

Heritability is known to play a significant role in SZ, with twin studies estimating a genetic contribution between 70% and 80%[8,10,12,13]. GWAS links over 250 loci to SZ, many of which are involved in synaptic function and neuronal communication[22].

One of the first discovered genetic risk factors for SZ is the *Neuregulin1* (*NRG1*) on chromosome 8p21-p12[62]. While the association is validated across populations, the precise alleles remain unidentified. Some SNPs (single-nucleotide polymorphisms) of *NRG1* have been implicated in psychosis, and others were linked to cognitive changes after antipsychotic treatment[63–66]. *NRG1* plays a crucial role in gliogenesis, myelin formation, synaptic plasticity, and neuronal survival and is expressed throughout life. The NRG1 receptor ERBB4 is similarly implicated in neurogenesis and synaptic plasticity, with mutations in the *ERBB4* also being associated with the SZ[62,67–69].

Another known genetic factor is *Disrupted-in-Schizophrenia 1* or *DISC1*, which will be discussed in more detail later in this thesis, in *Chapter 1.2.3.2*. Briefly, DISC1 has many roles, from neuronal development to synaptic plasticity through a complex network of protein interactions[62]. Initially discovered in a Scottish family with a chromosomal translocation, disruptions in *DISC1* have been linked to attention and cognition deficits[70,71]. There are also many specific SNPs in the *DISC1* associated with SZ risk[72,73]. Interestingly, DISC1 interacts with many other known SZ risk factors, such as NRG1 and PDE4B, highlighting a synergistic effect in SZ pathogenesis[62,74,75].

The *DTNBP1* gene encoding Dysbindin-1, which influences dopaminergic and glutamatergic neurotransmission, is also a risk gene associated with SZ. Mutations reducing dysbindin-1 function can

disrupt these pathways, contributing to the disorder. Dysbindin-1 also regulates neuronal development, synaptic vesicle formation, and receptor activity. Variations in *DTNBP1* affect its expression in SZ, thus making it a potential therapeutic target[62,76].

It is not surprising that the *DRD2* gene, which encodes for dopamine D2 receptors, represents risk gene for SZ, as heightened dopamine activity in the brain is linked to the disorder. This risk gene is discussed in more detail below. Genetic variations in the *DRD2* gene, such as the rs1076560 polymorphism, are associated with cognitive deficits and altered brain function[77–79].

One of the most studied risk genes for SZ is *COMT*, coding for catechol-O-methyltransferase, which regulates dopamine metabolism, especially in the prefrontal cortex. One of the most investigated polymorphisms of *COMT* connected to SZ is the Val158Met polymorphism, which is associated with higher dopamine levels and potential effects on cognition and symptom severity. However, *COMT* role in SZ risk is complex and likely involves genetic and environmental interactions[79–81].

Another known genetic risk factor for SZ is the *RELN* gene, which encodes reelin. Reelin is a glycoprotein produced by gamma-aminobutyric acid(GABA)ergic interneurons that regulates neuronal migration and differentiation during brain development[62]. Hypermethylation and reduced reelin expression in the hippocampus and other brain regions are observed in SZ patients[62,82,83].

The last example of known genetic risk factors for SZ, highlighted in this thesis, is a gene coding for brain-derived neurotrophic factor (BDNF). BDNF is a crucial factor in neuronal survival, synaptic plasticity, and cognitive function[62], with significant links to SZ pathology[84–87].

So far, various environmental risk factors for SZ are backed by strong evidence, such as: famine during pregnancy, small birth weight, low birth weight relative to gestational age and cannabis use. Additionally, childhood adversities were highly associated with SZ[27]. Beyond that, a systematic review and meta-analysis[88] demonstrated a generalized risk for psychosis associated with a combination of other factors, including maternal infection, perinatal stress, childhood infection, ethnic minority status, migration, urban living, and stressful

life events later in life. Additional research highlights that prenatal and childhood factors[24,31,41,89] and substance abuse in later life[40] significantly contribute to SZ risk.

Several molecular mechanisms have been proposed to underlie development of SZ including the disruption of neurotransmitters, neuroinflammation, structural brain changes, and altered neurodevelopment.

Neurotransmitter hypothesis of SZ has been proposed based on the effectiveness of antipsychotics on SZ symptoms. The most prominent dopamine dysregulation hypothesis has been observed in two manners: an excess of dopamine transmission in the mesolimbic pathway can lead to positive symptoms observed in SZ, while a lack of dopamine signaling in the mesocortical pathway can result in negative symptoms like anhedonia and social withdrawal[62,90,91]. This can explain why typical antipsychotics targeting only dopamine 2 receptors are often effective for the treatment of positive but less for negative symptoms.

On the other hand, the efficacy of atypical antipsychotics, which have lower affinity for dopamine 2 receptors and high affinity for serotonin 5-HT2A receptors, suggest involvement of serotonin in SZ. 5-HT receptor dysfunction is shown to affect both cognition and emotional regulation[92,93], and therefore atypical antipsychotics improve negative and cognitive symptoms in SZ. Previous studies showed that normalizing serotonergic transmission in SZ may improve cognitive performance and mitigate especially negative symptoms[94,95].

Another theory about the imbalance in neurotransmitters in SZ involves GABA deficiency. Reduced levels of glutamate decarboxylase, which synthesizes GABA, lead to weakened GABAergic transmission, disrupting the brain's excitation-inhibition balance[62]. Studies have shown lower GABA levels and reduced GABA receptor activity in brain regions linked to cognition[96–99]. Additionally, lower GABA concentrations in cerebrospinal fluid correlate with symptom severity in SZ patients[100]. However, changes in proteins connected to the GABA system and reduced GABA activity could be due to other factors like the use of antipsychotic drugs[101]. Nevertheless, evidence from clinical studies and animal models supports altered GABA balance in SZ pathology[62,102–105].

Moreover, disruptions of glutamate signaling were investigated as possible mechanisms for SZ. N-methyl-D-aspartate (NMDA) glutamate receptor hypofunction disrupts glutamatergic and dopaminergic systems, contributing to positive, negative, and cognitive symptoms[62]. Similarly, excessive glutamate accumulation can contribute to structural brain changes seen in SZ where dysfunction of NMDA receptors was observed in *post-mortem* studies and pharmacological models of SZ[106–109].

Lastly, drugs targeting cholinergic receptors have shown promise in clinical trials of SZ since acetylcholine plays a role in memory and movement, and its dysfunction has been previously linked to SZ[110,111].

Neuroinflammation, demonstrated as microglial activation and synaptic pruning, has also been implicated in SZ. Microglia are primary immune cells in the brain. When they are overactive, they can contribute to synaptic dysfunction, white matter damage, and impaired neuronal regeneration[112]. Elevated levels of pro-inflammatory cytokines have been detected in the peripheral blood and central nervous system (CNS) of SZ patients[113,114]. Additionally, reactive oxidative species and glutathione antioxidant levels, which can also contribute to neuroinflammation, were recently associated with SZ[115–118]. Immunomodulatory treatments, such as minocycline, may reduce glutamate excitotoxicity and neuronal apoptosis, offering potential therapy for cognitive symptoms[119].

Finally, one theory encompassing the majority of previously mentioned possible causes and mechanisms in SZ is the neurodevelopmental theory of SZ. This theory suggests that disruptions in early brain development, influenced by genetic and environmental factors, contribute to the onset of the disorder. Although SZ is not formally classified as a neurodevelopmental disorder in the DSM-V, its shared pathophysiological mechanisms with conditions such as autism further support this hypothesis[62,120–122]. Moreover, functional imaging studies have identified altered connectivity patterns in the brain of patients with SZ in the specific brain regions: the prefrontal cortex, temporal regions, and limbic structures[123]. These regions will be discussed in more detail later in this thesis.

1.1.1.5 Animal and cell models of SZ

Creating an animal model for SZ is challenging since SZ symptoms, like hallucinations or delusions, are uniquely human. However, some animal endophenotypes can be connected to SZ symptoms: increased locomotor activity after administering psychoactive substances and changes in social interaction can be used as indicators of positive and negative SZ symptoms, several tests can assess cognitive symptoms, such as changes in memory, reasoning, and problem-solving in animals[124,125].

Animal models for SZ can be developmental, drug-induced, genetic, or a combination of them.

Developmental animal SZ models can be created by neonatal hippocampal lesions, postnatal social isolation, prenatal administration of methylazoxymethanol, or by infecting pregnant rodents[124–126]. Rats who had neonatal hippocampal lesions show hyperactivity, cognitive deficits, and social impairments[127,128], while postnatal social isolation leads to anxiety, aggression, and sensorimotor gating deficits[129].

Administration of methylazoxymethanol in pregnant rodents can invoke reduced medial prefrontal cortex volume, increased dopamine activity, impaired memory, and heightened anxiety in offspring. Methylazoxymethanol is an anti-mitotic agent that inhibits DNA synthesis by methylating guanine residues during neurodevelopment and leads to reduced medial prefrontal cortex volume, increased dopamine activity, impaired memory, and heightened anxiety in offspring[130,131]. Viral infection of pregnant rodents triggers immune responses, and their offspring exhibit cognitive deficits and altered parvalbumin interneurons[132–134].

Drug-induced models of SZ primarily involve dopamine enhancers, like amphetamine, and NMDA receptor antagonists, like phencyclidine (PCP). While amphetamine induces hyperactivity and psychotic-like behavior[135], PCP evokes hyperlocomotion, social withdrawal, and cognitive deficits[136,137]. In addition, microinjections of GABA receptor antagonists (e.g., bicuculline) into the prefrontal cortex result in cognitive deficits and impaired emotional regulation[138,139].

Many animal models are suitable for studies on genetic background and predisposition of SZ onset. In this thesis, three of them will be explained briefly. Mouse models expressing mutant *Disc1*

display enlarged ventricles, reduced cortical thickness, altered parvalbumin interneurons, and hyperactivity[140–142]. Similarly, a mouse model expressing mutant *Nrg1* shows hyperactivity, cognitive impairments, but does not represent a complete SZ model[143]. Finally, a mouse model expressing mutant *Reln* demonstrates increased neuronal packing and decreased dendritic spine density in the frontal cortex (FC) and hippocampus[144]. It is important to note that these genetic models yielded conflicting results across different research groups, with differences mainly regarding sex and sample size[126,145].

In addition to most common rodent models, another more recently used genetic model is *Drosophila*, which will be discussed later.

Cell-based models, particularly those derived from human induced pluripotent stem cells (iPSCs), have emerged as powerful tools in SZ research[146]. iPSCs models capture patient-specific genetic backgrounds, providing an opportunity to study gene-environment interactions and the effects of risk variants. When integrated with animal models, iPSC-derived systems enhance translational relevance by allowing cross-validation of findings[147]. Furthermore, stem cell-based approaches offer a promising platform for therapeutic discovery, especially for targeting cognitive deficits and synaptic dysfunctions that are poorly addressed by current treatments[148].

1.1.1.6 Current treatment of SZ

Current treatment of SZ involves typical and atypical antipsychotics.

Typical antipsychotics, also known as first-generation antipsychotics, include medications such as chlorpromazine and haloperidol, which act as antagonists of the dopamine D2 receptor and are effective in controlling positive symptoms. As for adverse effects, these drugs induce movement-related or extrapyramidal side effects (tremors, muscle stiffness, uncontrolled movements) or can cause excess production of the hormone prolactin[149].

Atypical antipsychotics or second-generation antipsychotics such as risperidone, olanzapine, quetiapine, and clozapine target both dopamine D2 receptors and serotonin 5-HT2A receptors. They exhibit lower D2 receptor blockage and fewer movement side effects[149]. On the

other hand, they induce metabolic side effects such as obesity, hyperglycemia, dyslipidemia, and metabolic syndrome, associated with type 2 diabetes mellitus and cardiovascular disease.

More recently, third-generation antipsychotics like aripiprazole and cariprazine were developed[149]. They have high D2 receptor occupancy but act as partial agonists; hence, the antipsychotic effect is present with even fewer motor side effects[150].

For a patient to be declared as responding to therapy with antipsychotics, the reduction of positive symptoms needs to be higher than 20%. Nevertheless, about 30% of patients with SZ diagnosis do not respond to at least two different first-line antipsychotics over six weeks[151,152] and this patients have "Treatment-resistant SZ" or TRS[153]. TRS can manifest in two forms: early-onset resistance (present from illness onset, in most cases) and acquired resistance (developing over time). Patients with TRS have different neurochemical profiles: increased glutamate levels in the anterior cingulate cortex, normal presynaptic dopamine function, and improved connectivity in striatum and frontal cortical areas with reduced dopamine synthesis. In contrast, patients responding to typical and atypical antipsychotics have normal levels of glutamate in the anterior cingulate cortex, increased presynaptic dopamine function, and decreased connectivity in striatum and frontal cortical areas. Hence, patients responding to antipsychotics (so-called "non-TRS") have elevated dopamine synthesis capacity. Additionally, the differences can be observed by neuroimaging: non-TRS patients have less gray matter in frontal brain regions and increased volume of white matter. As for clinical features, TRS patients have an earlier onset of symptoms, a family history of psychosis, and more significant impairments in verbal learning, memory, processing speed, and executive functioning, compared to non-TRS and patients responding to treatment.

So far, clozapine remains the only approved treatment for TRS patients[153–155]. Clozapine is an atypical antipsychotic that has a high affinity for dopamine D2 and D4 receptors and is an agonist of serotonin 5-HT2A receptors. Also, it affects α2 adrenergic, muscarinic cholinergic, and histaminergic receptors, and its metabolite desmethyl clozapine affects muscarinic cholinergic M1 receptors[155,156]. Furthermore, clozapine decreases apoptosis in neuronal stem cells[157] and can affect neuronal plasticity in rat hippocampal neurons[158].

Adverse reactions on clozapine treatment, like agranulocytosis and tachycardia, have been thoroughly researched[159], especially in context of ethnicity[160], and clozapine use is strictly regulated worldwide[161]. However, the overall efficacy of clozapine is the highest compared to placebo and other antipsychotics[155,162]. Moreover, clozapine can be prescribed for suicide and self-injury prevention[163] and manic episodes in BiPD[164]. However, about 70% of TRS patients do not respond to clozapine, and that group of patients then has "ultra-treatment resistant SZ" (UTRS)[153].

Oral forms of antipsychotics are most commonly used, but drugs like olanzapine, risperidone, aripiprazole, and paliperidone can be used in long-acting injectable forms. Long-acting injectables are mainly used to prevent relapse, and they have shown fewer adverse reactions[165].

A study including 16 countries worldwide showed that quetiapine, risperidone, and olanzapine were the most frequently used antipsychotics in the period from 2005 to 2014[166]. In the United States of America (USA), the most dispensed antipsychotics in 2024 were quetiapine, aripiprazole, and risperidone[167]. In Croatia, a recent study by Vukićević et al., showed an increase in psychotropic drug use in period from 2012 to 2021, with clozapine, olanzapine, and quetiapine as the most prescribed antipsychotics[168]. In 2016, a study involving seven countries from Central and Eastern Europe, including Croatia, showed that the most commonly prescribed atypical antipsychotics were olanzapine, clozapine, and risperidone[169]. In addition, recently published research showed that paliperidone in a long-acting injectable form was effective in reducing psychiatric hospitalizations[170].

Recent advancements in therapeutic approaches underscore the importance of personalized medicine in SZ, with several drugs currently in clinical trials. Among them is glycine transporter type-1 inhibitors, which showed slight improvement in positive SZ symptoms[171], but failed to show better results than clozapine. Moreover, the KarXT, which acts as an agonist of muscarinic cholinergic receptors, showed enhanced improvement in positive and negative SZ symptoms[172]. TAAR1 agonists like Ulotaront inhibited dopamine signaling and significantly improved PANSS scores with fewer metabolic side effects[173].

In literature, some authors emphasize the importance of consistent and accurate terminology: current treatment available

should be referred to as "drugs for psychosis." In contrast, any novel treatment focused on multiple SZ symptoms should be called "anti-SZ" treatment[174].

Examples of non-pharmacological interventions used in SZ treatment include cognitive remediation, digital therapeutics, and brain stimulation techniques like transcranial magnetic stimulation[175]. Additionally, there is growing recognition of the role of the gut-brain axis and microbiome in SZ[176]. Investigating these novel fields may yield new therapeutic targets.

1.1.2 Bipolar disorder

Bipolar disorder, or BiPD, is a mental illness characterized by dramatic shifts in mood with extreme periods of manic and depressive states.

1.1.2.1 Symptoms of BiPD

People in manic states are highly active, sleep less, and experience an exaggerated confidence and unusually elevated mood, which can lead to risky behavior. In contrast, individuals experiencing a depressive episode often suffer from anhedonia and extreme fatigue. BiPD can be chronic or episodic with irregular intervals. BiPD is roughly divided into two types: type one has more severe manic episodes and may include psychosis, while type two has less intense manic episodes and longer and more severe depressive episodes compared to type one[1,2,177].

1.1.2.2 Etiology of BiPD

As for the genetic component of BiPD, heritability in monozygotic twins ranges from 40 to 70%, while GWAS identified 64 genomic loci associated with BiPD[178,179]. Whole-exome sequencing (WES) studies, including the Bipolar Exome (BipEx) project, identified *AKAP11* as a risk gene for BiPD[180]. Another risk gene for BiPD is *CACNA1C*, which encodes the L-type voltage-gated calcium channel, highlighting that a disbalance in calcium signaling could play a role in BiPD[181,182]. Moreover, the *BDNF* Val66Met polymorphism and genetic alterations of the *Toll-like receptor 2* genes were identified as genetic risk factors for BPD, and the environmental effects on them was explored[183–185]. Additionally, MDD, BiPD, and SZ cluster together genomically, sharing 109 loci

enriched in genes linked to neurodevelopment, neuronal signaling, and synaptic plasticity[186].

On the other hand, environmental factors can play an essential role in BiPD, especially in the pre-and early postnatal periods. Perinatal events, including respiratory distress, abnormal growth and development, as well as maternal infection with *Toxoplasma gondii,* have been linked to increased BiPD risk[187], while postnatal factors, such as childhood trauma are strongly associated with more severe and frequent mood episodes and higher suicide risk[188,189]. Interestingly, individuals with BiPD experienced higher hospitalization and mortality rates from COVID-19[188,190]. Environmental factors can also trigger inflammatory pathways: BiPD patients show increased levels of proinflammatory cytokines, where neuroimaging studies reveal hippocampal and prefrontal cortex microglial overactivity in BiPD[191].

Moreover, mitochondrial alterations were associated with BiPD. Analysis of *post-mortem* brain samples from patients with BiPD and SZ showed changes in mitochondrial features[192], which was further explored in cell models.

Since BiPD patients experience a decreased need for sleep during manic episodes and hypersomnia in depressive episodes, the circadian rhythm is also researched for BiPD. While individual circadian *clock* genes were not confirmed to be associated with BiPD by GWAS, network analysis reveals associations between *CLOCK* variants and BiPD risk and/or responsiveness to therapy[193,194].

1.1.2.3 Diagnosis of BiPD

For diagnosis of BiPD, criteria in DSM-V include at least one manic episode or at least one hypomanic episode and one major depressive episode lasting for at least a week for BiPD[1]. However, accurate diagnosis requires testing for other disorders like SZ or thyroid disorders due to symptom overlap. In addition, the mood symptoms of BiPD can be either mimicked or worsened by the use of recreational drugs[195]. Beyond SZ, other mental health illnesses can co-exist with BiPD, for instance attention-deficit/hyperactivity disorder[196].

1.1.2.4 Epidemiology of BiPD

In 2017, the global incidence rate of BiPD was 4.53 million and accounted for 9.29 million disability-adjusted life years based on results from the Global Burden of Disease study[197]. Global lifetime prevalence was ~1% for BiPD type one and ~1.57% for BPD type two, according to a meta-analysis that included findings of 25 studies. There is variability in prevalence across countries, probably influenced by ethnic and/or cultural factors[189].

The estimated age-standardized prevalence for BiPD is around 0.61% for the USA and 0.48% for Croatia, according to the Global Burden of Disease for 2021[198]. For the European Union, the prevalence is approximately 0.55%[199,200].

BiPD appears equally distributed across sexes, with the mean age for onset being early adolescence. Socioeconomic and environmental factors, including urbanization, may play a role in risk for BiPD development, but findings remain inconsistent across studies[189].

1.1.2.5 Current treatments for BiPD

So far, most prescribed medications for BiPD are mood stabilizers like lithium and valproate. Lithium prevents mood episodes, reduces severity, and lowers suicide risk. Lithium and valproate target inositol signaling, affecting IP3-stimulated calcium release from the endoplasmic reticulum (ER) through distinct pathways[177].

Alongside mood stabilizers, atypical antipsychotics are used to manage acute symptoms whereas antidepressants are prescribed in depressive states and to prevent triggering manic episodes or rapid cycling. Additionally, BiPD therapy can include drugs targeting sleep and anxiety[177]. Several other approaches are being explored for BiPD treatment. Mitochondrial modulators like N-acetylcysteine, a glutathione precursor, have demonstrated a moderate anti-depressive effect in the treatment of BiPD[201]. Modulation of the dopaminergic and noradrenergic systems with drugs like cariprazine demonstrates efficacy in mania and mixed episodes[202], while modafinil shows promise in alleviating depressive symptoms and cognitive impairments in treatment-resistant BiPD cases[203].

A key part of BiPD therapy is psychotherapy, in order to provide emotional and behavioral support. The most commonly used types of

psychotherapy for BiPD include interpersonal and social rhythm therapy and cognitive behavioral therapy. Other treatments may consist of electroconvulsive therapy, transcranial magnetic stimulation, and light therapy for severe or treatment-resistant cases of BiPD[177].

Another example of a non-pharmacological approach to alleviate depressive symptoms comes in the form of digital therapeutics like Rejoyn. Rejoyn is a web/mobile application approved by the FDA that combines more traditional psychotherapy (cognitive behavioral therapy) with cognitive training[204].

1.1.2.6 Animal and cell models of BiPD

Based on genetic risk factors for BiPD, animal models were created, mainly in mice. Mouse models with *Akap11* knockouts exhibit abnormalities on electroencephalogram and synaptic proteomic changes, mirroring findings in SZ and BiPD subjects[205]. Mutant mice with impaired *Cacna1c* expression display abnormal brain development, increased anxiety-like behavior, and disrupted spontaneous calcium activity in neural circuits[206]. In mice with the *Bdnf* Val66Met mutation altered fear extinction behavior, anxiety-like behaviors, and disrupted GABAergic neurons in amygdala were reported [207]. Mutant mice with an impaired gene essential for circadian rhythm, *Clock*, exhibit mania-like behaviors such as hyperactivity, impulsivity, and heightened reward responses[208,209]. Knockout of other core circadian genes, like *Bmal1*, also display mood-related behaviors[210]. In addition, circadian rhythm disruption was seen in iPSC-derived neural progenitor cells (NPCs) and neurons from BiPD patients[211,212].

Other research in cell lines derived from BiPD patients showed slower proliferation rates in cells, smaller neurospheres, and abnormal migration patterns[213]. Furthermore, lymphoblastoid cell lines, NPCs, and hippocampal-like neurons derived from BiPD patients display lower mitochondrial membrane potential, reduced oxygen consumption rates, and impaired glycolytic activity, indicating significant mitochondrial dysfunction[214]. Calcium signaling was also investigated in platelets and lymphocytes from BiPD patients. Higher basal free intracellular calcium levels and an enhanced calcium response to serotonin and thrombin stimulation were detected[192,215]. Interestingly, improved oxygen consumption rates were reported in cell models

created from BiPD patients responding to lithium, while valproate had a similar effect, but only in lithium non-responders[216]. Expression analysis revealed distinct patterns between these two groups, with differences primarily linked to focal adhesion and extracellular matrix functions[217].

Additional insights come from human cortical spheroids derived from BiPD patients, which were smaller, with fewer neurons, diminished excitability, and reduced network activity compared to control individuals[218]. Similarly, fewer mitochondria-endoplasmic reticulum contact sites and upregulated expression of calcium-related genes were detected in both neurons and organoid structures of BiPD models[192,219]. Moreover, single-cell RNA sequencing of cerebral organoids derived from monozygotic twins discordant for BiPD with psychosis revealed increased GABAergic neuron specification and reduced proliferation[220].

1.1.3 Major depressive disorder

1.1.3.1 Symptoms of MDD

Major depressive disorder (MDD) is a serious chronic mental health illness characterized by emotional, cognitive, behavioral, and somatic symptoms that significantly impair patient's daily life[1]. Emotional symptoms include persistent sadness, feelings of hopelessness or emptiness, frequent crying episodes and anhedonia. Cognitively, MDD is associated with difficulties in concentration, memory impairment, indecisiveness, and pervasive negative thinking patterns. Sleep disturbances, such as insomnia or hypersomnia, are common, as well as the changes in appetite and weight. Fatigue or loss of energy is a hallmark symptom, also. In addition, MDD can manifest with psychomotor agitation or retardation, and in more severe cases, individuals may experience recurrent thoughts of death or suicide.

1.1.3.2 Diagnosis of MDD

For MDD diagnosis, at least five of these symptoms must be present during the same two-week period, and at least one of the symptoms must be either depressed mood or anhedonia[1]. Standardized rating scales are often employed to assess the severity and profile of depressive symptoms[221]. One of them is Hamilton Depression Rating Scale (HDRS), which is administrated by clinician

and is widely used in clinical trials. HDRS focuses on core depressive features such as mood, guilt, suicidal ideation, insomnia, and somatic symptoms. Another scale administrated by clinician is the Montgomery–Åsberg Depression Rating Scale (MADRS), which is preferred in pharmacological studies and when trying to track symptom reduction over time due to its high responsiveness. In contrast, the Beck Depression Inventory (BDI) is a self-report questionnaire that captures both emotional and cognitive aspects of depression, providing insight into the patient's subjective experience.

As MDD is a heterogeneous disorder, with symptom profiles varying significantly among individuals and even across different episodes in the same person, diagnosis and treatment are complicated.

1.1.3.3 Etiology of MDD

Several theories about MDD etiology and pathology have been proposed, among which the monoamine disbalance, hypothalamic-pituitary-adrenal axis dysfunction, and neuroinflammation are the most researched hypotheses, accompanied by hypotheses suggesting genetic and epigenetic anomalies and structural/functional brain remodeling[222].

The theory of monoamine disbalance in MDD is mainly focused on the lack of serotonin, dopamine, and norepinephrine. It is primarily supported by the efficacy of antidepressant medicines targeting monoamine transporters and receptors[223]. Serotonin is one of the most researched monoamines for MDD, with low levels of serotonin and its precursor, L-tryptophan, detected in patients with MDD[224]. Norepinephrine regulates the neuronal function and is another target of antidepressant medications[222]. MDD is linked to reduced dopamine signaling in regions like the striatum and hippocampus, while disrupted dopamine D2 receptor signaling can impact depressive behavior and synaptic activity[222]. Glutamate is the primary excitatory neurotransmitter implicated in MDD due to its involvement in the synaptic loss and altered neuronal-astrocyte interaction[225,226].

The hypothalamic-pituitary-adrenal (HPA) axis can be activated in response to stress factors. It results in an increased level of corticotropin-releasing hormone, which stimulates the release of adrenocorticotropic hormone and, subsequently, glucocorticoids. Elevated glucocorticoids damage neurons in brain regions like the

hippocampus and prefrontal cortex[222]. In addition, the HPA axis interacts with the hypothalamic-pituitary-thyroid axis, which produces cortisol and suppresses thyroid-releasing hormone production. The low thyroid-releasing hormone may impair neuronal and glial development and function. Another hormone, estrogen, can promote neuron proliferation and differentiation, as well as amplify the effects of antidepressants like ketamine. Leptin is a hormone that regulates the HPA axis as well as increases serotonin receptor activity and BDNF secretion, which can improve MDD symptoms[222].

Individuals with MDD exhibit lower level of BDNF in blood[227], making it a potential biomarker for MDD. Additionally, BDNF is highly regulated by genetic and environmental factors and has antidepressant actions in the hippocampus and prefrontal cortex[228]. Additionally, the Val66Met *BDNF* polymorphism, previously discussed as a genetic risk factor for BiPD, has also been implicated in MDD[229].

Moreover, a comprehensive meta-analysis examined various other biomarkers of MDD and found that elevated levels of the inflammatory marker interleukin (IL) 6, a decrease in hippocampal volume, and increased activity in the default mode brain network (thinking about oneself and dwelling on negative thoughts) were associated with a higher risk for MDD[230].

Episodes of depression characterize both BiPD and MDD, but the difference is present in symptomatology, course of the disease, and treatment approaches. While MDD involves only depressive episodes, BiPD includes both depressive and manic/hypomanic episodes. BiPD often manifests in late adolescence or early adulthood, whereas MDD can first occur at any age. As for treatment, MDD is commonly treated with antidepressants and psychotherapy, while BiPD treatment often involves mood stabilizers or antipsychotic medications. The use of antidepressants in BiPD is approached with caution due to the risk of triggering mania. Hence, correct diagnosis is essential for effective treatment[231].

MDD often co-occurs with other psychiatric and medical conditions, which can complicate diagnosis, treatment, and prognosis. Out of the psychiatric comorbidities, MDD most frequently occurs with anxiety disorders, substance abuse, attention deficit hyperactivity disorder, and post-traumatic stress disorder. In addition, medical conditions like chronic pain are commonly associated with MDD.

Neurological disorders (Parkinson's disease, multiple sclerosis, etc.), cardiovascular diseases, and chronic obstructive pulmonary disease are linked to an increased risk to develop MDD[232].

1.1.3.4 Epidemiology of MDD

The global prevalence of MDD in 2021 is approximated 3%, making it one of the leading causes of disability[233]. Treatment resistance was estimated to affect 30% of patients with MDD in the USA in 2017[234]. In the European Union, the prevalence of MDD was estimated at around 2% between 2013 and 2015[235], while clinically relevant depressive symptoms affected approximately 6% of the population in Europe from 2018 to 2020[236].

As for Croatia, 10.3% of Croatia's population experiences mild to moderate depressive symptoms, while 1.2% has moderately severe to severe symptoms of MDD, according to data from the European Health Survey conducted in 2014-2015[237]. Depressive disorders prevalence in Croatia for 2021 was 3.5%, according to Global Burden of Disease[238].

1.1.3.5 Current treatments of MDD

Medications for MDD, called antidepressants, are categorized by three different mechanisms of action: selective serotonin or serotonin/norepinephrine reuptake inhibitors (SSRIs or SNRIs), tricyclic antidepressants (TCAs), monoamine oxidase inhibitors (MAOIs), norepinephrine reuptake inhibitors (NRIs), noradrenergic and specific serotonergic antidepressants (NaSSAs) and ketamine[222].

SSRIs, like fluoxetine, are first-line treatments for severe MDD, and they primarily target serotonin transporters by blocking their ability to reabsorb serotonin from the synaptic cleft back into presynaptic neurons. After serotonin is released into the synaptic cleft, serotonin transporters recycle it, terminating the signaling activity. SSRIs bind to serotonin transporters, inhibiting the reuptake process and increasing serotonin levels in the synaptic cleft[222].

The mechanism of action for TCAs, like imipramine, is still not fully understood, but it includes inhibiting the reuptake of serotonin, norepinephrine, and, to a lesser extent, dopamine[222]. Novel research in rat models suggests additional mechanisms involving astrocytes[239].

MAOIs are one of the earliest classes of antidepressants, functioning by inhibiting the enzyme monoamine oxidase and in turn MAOIs increase the availability of serotonin, norepinephrine, and dopamine[240]. Although effective, their use is limited today due to potentially serious side effects and dietary restrictions, such as the need to avoid tyramine-rich foods to prevent hypertensive crises.

NRIs represent another pharmacological approach, selectively blocking the reuptake of norepinephrine into presynaptic neurons and enhances noradrenergic signaling[241]. While NRIs like reboxetine or atomoxetine are not as commonly used as SSRIs or SNRIs, they may be beneficial in patients whose symptoms are linked more closely to noradrenergic dysfunction.

NaSSAs such as mirtazapine, act by antagonizing presynaptic alpha-2 adrenergic receptors, hence, enhance the release of both norepinephrine and serotonin[242]. In addition, NaSSAs block specific serotonin receptors, which can reduce common side effects associated with SSRIs.

Moreover, another antidepressant is ketamine, which blocks NMDA receptors, increases BDNF levels, and enhances synaptic function, which can help in the improvement of synaptic plasticity and alleviating MDD symptoms[243]. Similarly, a ketamine enantiomer, esketamine, is highly effective in treating treatment-resistant MDD in intranasal formulations[244]. Additionally, hydroxynorketamine, a ketamine metabolite, offers antidepressant effects[245].

Boldrini et al demonstrated that antidepressants could stimulate neurogenesis in the anterior dentate gyrus, seen as an increase in neural progenitor cells, mitotic cells, and mature granule neurons in individuals treated with antidepressants compared to both untreated individuals with MDD and healthy untreated controls[246]. However, individuals receiving both antidepressants and benzodiazepines had fewer granule neurons compared to those treated with antidepressants alone[247].

Novel pharmacological therapies include psychedelic compounds, Rapastinel, nitrous oxide and GABAergic modulators. Psychedelics like psilocybin and LSD, which can produce long-lasting antidepressant effects and promote neural plasticity[248,249]. As for drugs in clinical research, a novel noncompetitive NMDA receptor antagonist,

esmethadone, improves depressive-like behaviors in animal models and provides sustained benefits for individuals unresponsive to conventional treatments[250]. Rapastinel is a glycine site partial agonist at NMDA receptors and it enhances synaptic plasticity and long-term potentiation[251]. It provides rapid antidepressant effects without the psychotomimetic or dissociative side effects seen with ketamine. For it, rapid onset of antidepressant action within 2 hours was observed with sustained effects for up to 7 days in treatment-resistant MDD. Nitrous oxide demonstrates ketamine-like rapid antidepressant effects but with a simpler administration profile and fewer long-term safety concerns. Significant antidepressant effects of nitrous oxide were observed within 24 hours of administration[252]. GABAergic modulation shows potential through agents like brexanolone, which is approved for postpartum MDD and demonstrates rapid mood stabilization, especially in depressive episodes[253]. Anti-inflammatory agents are currently in clinical trials and have shown potential to reduce depressive symptoms[254].

Novel non-pharmacological therapies, in combination with antidepressants, include electroconvulsive therapy (ECT), phototherapy, repetitive transcranial magnetic stimulation, and different types of psychosocial treatments[222]. ECT is an effective treatment for severe or treatment-resistant depression and it works by inducing controlled seizures to restore brain chemistry[255]. Modern methods have minimized side effects like memory loss, making it a safe option when rapid relief is needed. Phototherapy with bright light targets serotonin and brain circuits and rapidly improves mood. Repetitive transcranial magnetic stimulation is a non-invasive technique that stimulates certain brain regions, with optimal results when treatment is personalized based on individual brain activity patterns. As for psychological treatments, cognitive-behavioral therapy (CBT) and interpersonal therapy have significantly reduced relapse rates and improved long-term outcomes.

1.1.3.6 Animal models of MDD

Several animal models for MDD have been created, with mice models based on chronic mild stress or social defeat and learned helplessness being the most frequent models used.

In the chronic mild stress model, mice are subjected to various low-intensity stressors presented at unpredictable intervals over period of time[256,257]. Animals exposed to chronic stress display altered open-field behavior, characterized by changes in exploration and locomotion in a novel environment and reduced saccharin or sucrose consumption, indicative of anhedonia. Transcriptome analysis revealed significant expression changes in the prefrontal cortex and hippocampus, affecting mitochondrial function and neurogenesis.

The chronic social defeat model induces MDD in mice by exposing the experimental mouse to a larger, aggressive mouse for several minutes daily, then housing them on opposite sides of a transparent barrier to maintain sensory contact. Mice in this model show reduced locomotor activity, decreased enthusiasm and aggression, increased submissive behavior, and heightened anxiety[258]. Morphologically, the model shows reduced neuronal proliferation and hippocampal volume, along with disruptions to reward circuitry and dopaminergic neuron activity in the ventral tegmental area[259]. Transcriptome analysis revealed alterations in genes related to mitochondria in the prefrontal cortex and hippocampus, while RNA and ribosome-related genes showed significant changes in nucleus accumbens[256]. Interestingly, the chronic mild stress model and the chronic social defeat model exhibit decreased neurogenesis in the prefrontal cortex and nucleus accumbens, suggesting a common mechanism and location specificity.

For the learned helplessness model[256,260], mice are exposed to unpredictable, inescapable electric foot shocks over two consecutive days, leading to impaired escape behavior and the development of neurochemical and molecular changes, such as increased inflammation and the death of norepinephrine neurons in the locus coeruleus. Transcriptome analysis revealed changes related to the synapse and synapse remodeling. Unlike the other two models, the learned helplessness model exhibits distinct alterations, confirming diversity of MDD pathology.

It is important to note that *heat shock protein family B (small) member 11* was the only gene significantly changed in the prefrontal cortex across all of these models[256]. Methylation and role of small heat *shock* proteins in protein aggregation have already been investigated previously in NDs[261]. Genes like *Neuronal PAS domain protein 4* and *ATP5G1* were also detected in at least one MDD animal model[262,263].

Animal models of MDD are also characterized by peripheral biomarkers, like dysregulation of hormones in the hypothalamic-pituitary-adrenal axis, and cytokines, like IL-6 and IL-10[256].

1.1.4 Suicide

1.1.4.1 Definitions and classification of suicidal behavior

Suicidal behavior includes terms like "suicidal ideation" and "suicidal attempt". Suicidal ideation involves thinking, considering, or planning suicide, while suicide attempt is any instance of engaging in potentially self-harmful behavior with an intent to die.

Suicide is usually classified as violent or non-violent, according to Asberg's criteria[264]. Violent suicide includes hanging, use of firearms, jumping from heights or under train and deep cuts, while drug overdoses are considered non-violent. A European study found that violent suicide attempts are more common, and successful, among men. Men are also more prone to shift from non-violent attempts to violent suicides[265]. Additionally, suicidal behavior has other classifications in the literature beyond violent versus non-violent attempts: high- versus low-lethality and impulsive versus non-impulsive behavior; all of which can be assessed through scales like Beck's Suicide Intent Scale[264].

1.1.4.2 Epidemiology of suicide

Every year about 10 out of 100,000 people dies by suicide [266]. In 2021, suicide accounted for 0.9% of all deaths in the European Union[267] and in Croatia the suicide rate was approximately 16 per 100,000 people in 2021[266].

1.1.4.3 Risk factors for suicide

Several clinical, biological, and social risk factors were identified for suicide. Clinical risk factors like CMIs diagnosis and history of self-harm were strongly associated with suicide[268]. A leading contributor to suicidal behavior in USA is MDD, with 10-20% of patients with MDD attempting suicide at least once[269].

The rate of suicide-related mortality was almost ten times higher for people diagnosed with SZ, than in the general population[270,271]. Similarly, individuals with MDD also face a markedly elevated suicide

risk, especially among those with treatment-resistant forms[234]. Also, a high suicide rate is recorded among people with BiPD, mostly linked to depressive episodes[272,273].

Social determinants of suicide include factors such as experiencing suicidal attempts of close acquaintances or family members, accessibility to firearms, divorce, experience in foster care, release from incarceration, and midlife unemployment, all of which have been identified as high-risk situations[274].

As for biological risk factors for suicide, disruptions in neurotransmitters, inflammation, and stress response are intensively researched. Low cerebrospinal fluid levels of serotonin and dopamine metabolites are associated with higher suicide risk[275], while genetic studies linked polymorphisms in serotonin-related genes to suicidal behavior[276,277]. Elevated inflammatory markers and neuroinflammatory processes are implicated in suicide[278]. As for stress response, dysregulation of the HPA axis is linked to suicidal behavior[279].

As for neuroanatomical findings, Boldrini et al observed larger dentate gyrus volume in individuals with MDD who were not suicide victims compared to suicide victims with MDD. Additionally, suicide victims with MDD diagnosis had fewer granule neurons in the dentate gyrus compared to both non-suicidal individuals with MDD and healthy controls260. Both findings show a link between reduced neurogenesis and suicidal behavior.

An alternative approach for investigating risk factors is the psychological autopsy method, which involves reconstructing the life circumstances of a victim through standardized interviews with the victim's close circle, such as family, partners, friends, and co-workers, and combining collected information with traditionally collected administrative data from available medical records[268,280]. These studies showed mood and substance use disorders are at high risk for suicide, which was also highlighted in a recent meta-analysis[281].

1.1.4.4 Genetic aspects of suicide

Interestingly, death by suicide and suicidal behavior exhibited positive genetic correlations with SZ in a recent GWAS analysis[282], highlighting one locus in the *NLGN1*, a gene previously linked to suicide, autism, and SZ. *NLGN1* encodes a neuronal cell surface protein

involved in synaptogenesis through its role as a ligand for the β-neurexins.

Analysis of rare protein-coding variants yielded several genes with a higher burden of rare variants in a cohort of individuals who died by suicide, comparing the frequency of rare variants in specific genes to that in control populations. Some of these genes are *PER1, SNAPC1, TNKS1BP1, ESS2,* and *ADGRF5*, all of them previously associated with CMIs and/or suicidal behavior[283]. Variants in genes *Regulator of G Protein Signaling 7 Binding Protein (RGS7BP)*, *14-3-3 protein ε (YWHAE*), and *Actin-related protein 6 (ACTR6)* were enriched in individuals with a history of suicide attempt, after analyzing soldiers from the "Army Study to Assess Risk and Resilience in Service Members"[284]. Moreover, the genes *Butyrophilin Subfamily 3 Member A2 (BTN3A2)* and *Chemokine ligand 17 (CXCL17)* showed the most significant association of polygenic risk scores for suicide attempts, among other behavior and physical factors, in the cohort from UK Biobank[285]. The rs1800532 polymorphism in the *Solute Carrier Family 6 Member 4* (*SLC6A4*) gene, a type of the serotonin transporter, has been potentially associated with increased suicide risk and a reduced response to treatments like lithium and clozapine in a recent review[277].

1.1.5 Proteins involved in suicide

Recent research highlights the role of protein dysregulation in the neurobiology of both CMIs and suicidal behavior.

Studies analyzing brain regions in suicide victims have identified alterations in proteins related to stress response, neurogenesis, and neurotransmission. Research has shown that suicide victims without a history of early-life adversity (ELA) had lower BDNF levels in the anterior cingulate cortex compared to individuals who neither experienced ELA nor died by suicide[286]. Similarly, among those who didn't die by suicide, individuals with ELA had lower BDNF levels compared to those without ELA. Moreover, researchers were able to utilize levels for BDNF, FK506-binding protein, and glucocorticoid receptor, to predict suicide with high sensitivity and specificity for a small cohort they analyzed[287].

A study done on Brodmann area 9 (BA9) showed a dysregulation of certain protein kinase C isozymes in people with MDD, who did or did not commit suicide[288]. A small study done by Dean et al showed

possible disruption in iron transport proteins in *post-mortem* brain samples from suicide victims, specifically in BA6 and 10[289].

A bioinformatics and statistical analysis of proteomic data obtained from brain tissue identified several proteins associated with suicide. Glutaredoxin 5, GDP-mannose pyrophosphorylase, and plasma α-L-fucosidase were strongly linked to suicide attempts in glutamatergic neuronal cells[287]. However, when the same analysis was performed for blood samples, Platelet Endothelial Aggregation Receptor 1, NudE Neurodevelopment Protein 1, Eva-1 Homolog C, and β-1,4-Galactosyltransferase 2 were identified as potentially important. Still, they didn't show strong evidence of being connected to brain findings[287].

Increased immune system markers like C-reactive protein (CRP) and IL-6 were seen in individuals exhibiting suicidal behavior compared to healthy controls and/or people with MDD or psychiatric illness diagnosis[290].

An alternative approach to understanding protein changes connected to suicidal intentions comes from ketamine research. Ketamine modulates the NMDA receptor, which leads to enhanced synaptic plasticity and rapid antidepressant effect. The downstream signaling affected by ketamine involves BDNF and the mammalian target of rapamycin (mTOR). Additionally, ketamine's metabolites contribute independently to its antidepressant effect[291].

1.1.5.1 Treatment targeting suicide tendencies

So far, lithium remains the only medication proven to lower suicide rates in BiPD[292], while clozapine remains the key treatment for SZ patients with suicidal tendencies[163]. Additionally, treatment with antidepressants and CBT have shown positive results in MDD patients[264].

Novel treatments include glutamate modulation for antidepressant-like effects, out of which ketamine, Rapastinel, and nitrous oxide show the most promising effects in treating suicidal tendencies.

Ketamine has consistently shown significant reductions in depressive symptoms and suicidality within 24 to 48 hrs, with some benefits persisting for weeks after repeated doses. Additionally,

alternative administration routes, such as intranasal and oral, are under investigation to improve accessibility and convenience for diagnosed individuals[293].

Finally, the most successful prevention of suicide includes education of both primary care workers and the general public from a young age about MDD and suicide, as well as an active outreach to patients with CMIs or after suicidal attempt(s)[294].

1.1.6 Challenges in diagnosis and treatments of CMIs

Despite advances in psychiatric care, the diagnosis of CMIs relies primarily on clinical assessments rather than objective biomarkers, posing challenges for early detection and personalized treatment.

Recent research has focused on potential neuroimaging biomarkers of CMIs, with variations in brain connectivity positively correlating with cognitive functions and negatively correlating with psychopathological measures[295]. Recent diagnostic endeavors include establishing a multi-biomarker panel from serum for MDD, consisting of BDNF, plasma CRP, and cortisol[296]. A novel approach has been used to distinguish between BiPD and MDD during depressive episodes by analyzing dried blood spots: a metabolomic biomarker signature specific to BiPD was found. However, the cohort was relatively small, and more research is needed[297]. Meta-analysis highlighted DNA methylation as a promising biomarker for predicting treatment outcomes regarding SZ, BiPD, and MDD[298]. All these examples are promising; however, they need to be extensively validated before they can be utilized for early detection and personalized treatment.

Additionally, treatment efficacy remains limited, with many individuals exhibiting resistance to pharmacological and psychosocial therapies, underscoring the urgent need for innovative therapeutic approaches. Approximately 30% of individuals with SZ are considered treatment-resistant, failing to respond adequately to standard antipsychotic medications[299]. As for BiPD, research suggests treatment resistance might be even higher than in MDD. A subset of individuals with MDD diagnosis does not achieve remission with first-line antidepressant therapies and require alternative treatment strategies. Several novel therapeutic strategies are being developed, as discussed above; however, the definitions for treatment resistance across

different CMIs are still not standardized, and many traditional and novel treatments are either costly or require specialized administration.

Emerging evidence implicates a novel approach focused on disrupted protein homeostasis and aggregation as key pathological mechanisms in CMIs, providing a promising avenue for research to understand CMIs[300].

1.2 Protein aggregation

Homeostasis of proteins is called proteostasis, which is a process that regulates the concentration, interactions, and localization of proteins in a cell, all while preventing the buildup of misfolded proteins through degradation pathways [301]. Proper protein folding and structural integrity are essential for biological function[302].

Proteins can also form aggregates — abnormal clusters of misfolded or unfolded proteins that accumulate within cells[303,304]. Change in native protein structure exposes hydrophobic regions, usually hidden in the properly folded state, which can then interact with each other. Hence, proteins cluster together, and their solubility is reduced. Once formed, protein aggregates can interfere with cellular compartments, disrupt normal protein interactions, or sequester essential cellular components, impairing overall cell function. Alternative scenarios include either loss of function or gain of new, toxic properties. Moreover, proteins can form aggregates as a response to outside stress factors. Additionally, certain genetic mutations or errors during transcription or translation can make proteins more susceptible to forming aggregates[301,302]. Protein aggregates can form rigid, amyloid fibril structures with highly ordered β-strand arrangements formed through specific protein-protein interactions. On the other hand, protein aggregates can lack structural organization, referred to as amorphous aggregates[302,303].

The term "aggregate" refers to any accumulation of misfolded proteins, regardless of their size or cellular location. Aggresomes, on the other hand, are larger protein accumulations that specifically form around the centrosome[305,306]. When a single large aggregate is observed within a cell, it is likely an aggresome. Aggresomes are hypothesized to serve as a cellular containment strategy, sequestering misfolded proteins in one area to minimize their potential toxicity.

Under normal conditions, aggregated proteins are degraded through two key pathways: the ubiquitin-proteasome system and the autophagosomal-lysosomal system. The ubiquitin-proteasome system mainly targets soluble misfolded proteins, while lysosomal degradation handles larger aggregates and cellular organelles[307,308].

Nevertheless, if proteostasis in post-mitotic neurons is disrupted, it can lead to the accumulation of insoluble/aggregating (I/A) proteins — a hallmark of diseases known as "proteinopathies"[309].

Graphical summary for this Chapter can be seen in **Figure 1**.

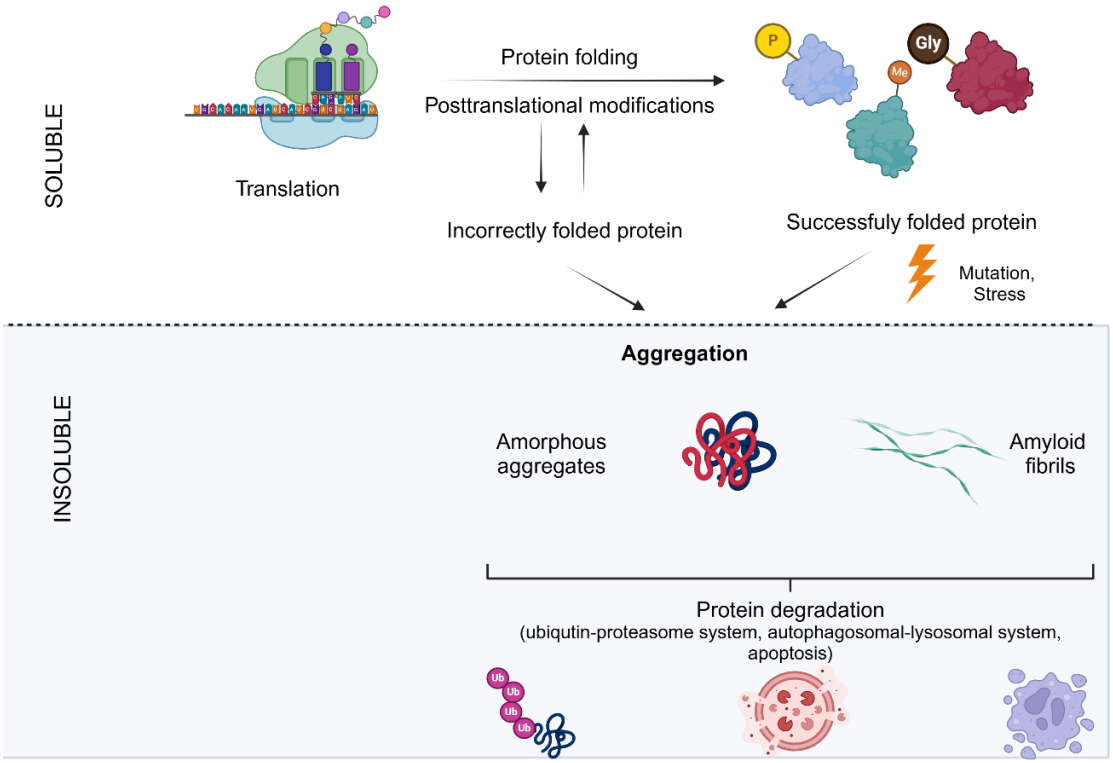

Figure 1: Maintenance and disruption of protein homeostasis. Newly synthesized proteins undergo proper folding and post-translational modifications to achieve functional conformations. However, cellular stress or genetic/environmental insults can impair folding, leading to misfolded proteins. Misfolded species may undergo aggregation into either amorphous aggregates or structured amyloid fibrils, both of which are insoluble. Alternatively, the cell may attempt to resolve aggregated proteins through degradation pathways, including the ubiquitin-proteasome system, autophagosomal-lysosomal pathway, or apoptosis. Failure in these clearance systems contributes to toxic protein accumulation and cellular dysfunction. Scheme was created in BioRender.

1.2.1 Protein aggregation in neurodegenerative disorders

Protein aggregation is well described in neurological disorders, where misfolded proteins accumulate and contribute to neurodegeneration.

In Alzheimer's disease (AD), the accumulation of tau and amyloid-beta plaques disrupts neuronal function and synaptic integrity, ultimately leading to cognitive decline[308]. The impairment of autophagy pathways plays a crucial role in the dysregulation of proteostasis and disease progression.

Frontotemporal dementia is a clinically and genetically heterogeneous disorder characterized by the accumulation of either tau or TAR DNA-binding protein 43 (TDP-43), leading to neuroinflammation and synaptic loss[310]. The molecular pathology of frontotemporal dementia varies across subtypes, with tauopathies and TDP-43 proteinopathies being distinct in clinical sense, but overlapping in mechanisms.

In Parkinson's disease, the aggregation of misfolded α-synuclein in Lewy bodies and Lewy neurites drives neuronal dysfunction, particularly affecting dopaminergic neurons in the substantia nigra [311]. The interplay between α-synuclein misfolding, mitochondrial dysfunction, and oxidative stress contributes to progressive neurodegeneration.

Huntington's disease is marked by the accumulation of mutant huntingtin protein, which forms toxic aggregates that interfere with cellular homeostasis, impair autophagy, and trigger neuronal death. The expanded polyglutamine repeats in mutant huntingtin drive aggregation, affecting multiple cellular pathways, including transcriptional dysregulation and proteasomal degradation[312].

Collectively, these disorders illustrate how protein aggregation can disrupt cellular processes and lead to neuronal loss, which in turn results in a disease.

Another interesting phenomenon in NDs is concept of co-aggregation, where different proteins interact and influence each other's misfolding and aggregation pathways. They can also come together to form complex aggregates that contribute to disease. Protein co-aggregation can occur through cross-seeding where

misfolded proteins can act as a template to induce aggregation in another protein. For instance, Aβ can enhance tau fibrillization. Different proteins can also co-aggregate to form hybrid amyloids, as observed between α-synuclein and tau. Additionally, the presence of co-aggregating proteins can alter the stability and degradation of aggregates by modifying interactions with clearance pathways.

In AD, extracellular amyloid-β (Aβ) plaques and intracellular tau neurofibrillary tangles represent hallmark pathologies. Studies show that Aβ cross-seeds tau, enhancing its phosphorylation and aggregation. This interaction likely explains why AD pathology often involves both Aβ and tau, with Aβ accumulation preceding tau pathology in disease progression[313]. ApoE is a major genetic risk factor for late-onset AD. The ApoE4 variant promotes Aβ aggregation and reduces its clearance, leading to increased neurotoxicity[314]. TDP-43 also co-aggregates with Aβ, tau, and α-synuclein[315]. Protein co-aggregation may explain why some patients develop mixed proteinopathies, complicating diagnosis and treatment.

Moreover, protein aggregation in NDs can start in one brain region and then spread to other areas[316–318]. For example, amyloid plaques can first form in an area like temporal lobe and then spread to the hippocampus and/or amygdala. However, tau neurofibrillary tangles can start in the hippocampus and then spread to the temporal or other lobes.

1.2.2 Protein aggregation in CMIs

Neurodegenerative disorders (NDs) characterized by protein aggregation in their pathology often share a wide range of cognitive, emotional, and behavioral symptoms with CMIs. These similarities are not only clinical but also biological, as these conditions frequently co-occur[319]. This overlap has spurred interest in exploring the role of protein aggregation in CMIs, prompting numerous studies investigating its potential contribution[320–324].

Research has highlighted disruptions in key cellular processes in CMIs and NDs, including endoplasmic reticulum function[325,326], autophagy [327], and the ubiquitin-proteasome system[328,329]. These disruptions may create a cellular environment conducive to forming and accumulating protein aggregates, which could impair normal cellular functions.

The hypothesis that protein aggregates might form in the brains of individuals with CMIs provides a potential explanation for these conditions' chronic and progressive nature[309]. While NDs are often marked by large protein deposits causing widespread neuronal loss, protein aggregation in CMIs appears to primarily disrupt cellular processes and recruit other proteins into aggresomes, further exacerbating cellular dysfunction. Researchers hope to uncover new therapeutic strategies for CMIs linked to protein aggregation by investigating these mechanisms.

1.2.3 Proteins implicated as aggregating in CMIs

Our theory includes the notion that aggregated or misfolded proteins in CMIs can affect key pathways governing neuronal structure, plasticity, and resilience, contributing to the chronic progression of these illnesses.

So far, several proteins have been implicated as aggregating in CMIs, which were identified by either genetic studies or hypothesis-free approaches based on samples from patients with CMIs.

1.2.3.1 Collapsin response mediator protein 1

Collapsin response mediator protein 1 (CRMP1) is essential for axon guidance, neuronal migration, and synapse formation. Disrupted CRMP1 has been linked to neurological disorders, including intellectual disability and autism spectrum disorder, and recently to CMIs.

1.2.3.1.1 CRMP family

Collapsin response mediator proteins (CRMPs) are phosphoproteins heavily involved in the reelin and Semaphorin 3A (or shorter Sema3A) pathways[330,331]. They regulate microtubule dynamics and actin cytoskeleton rearrangement[330,332]. Predominantly, CRMPs are expressed during embryonic and early brain development, with expression tapering off in adulthood[333]. CRMPs are highly conserved, with high sequence and structural homology across mammals, birds, amphibians, and even invertebrates[334].

Most CRMPs exist in short and long isoforms, produced through alternative splicing[335]. The folded CRMP structure resembles dihydropyrimidinase (DHPase), which hydrolyzes the amide bond of pyrimidine bases[336]. CRMPs form tetramers through interactions in their

central α/β barrel region. Each individual CRMP monomer has an N-terminal region rich in β-sheets and a central α/β barrel where four units link. Although the stretch of amino acids (aa) at the C-terminus is hard to map because of its flexibility, partial data suggests it helps stabilize the four-unit structure. Additionally, CRMPs can form hetero-oligomeric complexes[330].

CRMPs have phosphorylation sites at their C-terminal regions, regulated by key kinases specific to each CRMP[332]. Altered CRMP phosphorylation has been linked to shared mechanisms in neurological disorders[330,337]. Less-studied post-translational modifications of CRMPs include O-GlcNAcylation and SUMOylation. CRMP2 undergoes O-GlcNAcylation at a key site for kinase-mediated regulation in Sema3A signaling, with a mutant mouse showing short-term memory deficits[338]. SUMOylation involves the attachment of a SUMO group, upon which sodium channel trafficking and surface expression are promoted[339]. CRMPs also undergo proteolytic cleavage, where a cleavage on the N-terminus can lead to neuronal death[340]. Truncated CRMP fragments, especially in synaptosomes, influence synaptic plasticity[341,342].

CRMPs primarily regulate the depolymerization of F-actin and tubulin, leading to the collapse of growth cones. Beyond this role, CRMPs interact with various proteins, including motor proteins, kinases, and proteins involved in endocytosis and exocytosis. CRMPs act as adaptors or scaffold molecules through these interactions, playing a key role in regulating synaptic transmission[343].

So far, five CRMP family members (CRMP1–5) have been identified in mammals, all sharing over half of aa sequence identity. Among them, CRMP1 and CRMP2 have been extensively studied for their implications in neurodevelopmental and psychiatric disorders.

1.2.3.1.2 Structure, regulation, and localization of CRMP1

CRMP1, like other members of the CRMP family, is produced in two isoforms: a short (CRMP1 Sv, ~572 aa, ~65 kDa) and a long isoform (CRMP1 Lv), which includes an additional N-terminal extension (~100 aa, ~75 kDa)[332].

As for the structure of CRMP1, it is significantly similar to other CRMPs, and it is composed of two primary regions: an N-terminal β-sheet-rich domain (residues 15–69) and a central α/β barrel domain (residues 70–490)[344]. The C-terminal region (490–572) of CRMP1

remains structurally unresolved due to its flexibility. However, studies on CRMP2[345] suggest that residues 491–506 may interact with neighboring monomers, stabilizing the whole tetramer. CRMP1 is also capable of forming hetero-oligomeric complexes with CRMP2 and CRMP3. However, their biological roles remain underexplored[331]. The scheme for CRMP1 structure can be seen in **Figure 2**.

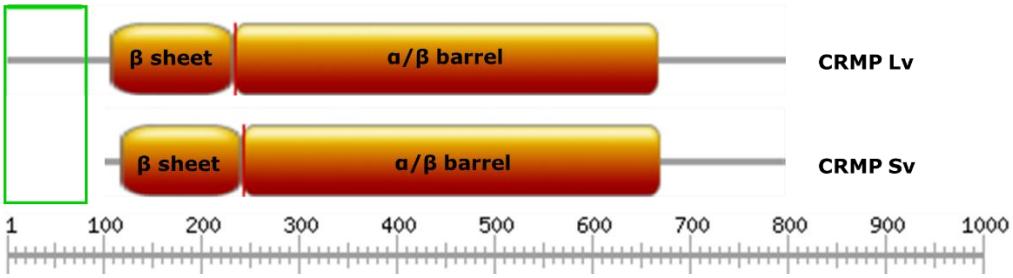

Figure 2 CRMP1 Lv and Sv structure. Green rectangle marks the N-optionally translated region which is present in CRMP1 Lv, but lacking in CRMP1 Sv. Orange rectangles show domains with known structures, while the gray line represents domains predicted to be disordered. Gray ruler which marks location of aa is shown below. Scheme was created in ProSite.

A major regulator of CRMP1 is phosphorylation, which can change the conformation of the C-terminal region. The Cyclin-dependent kinase 5 and Fyn kinase phosphorylate human CRMP1[346,347]. Also, phosphorylated CRMP1 can bind more of the Filamin-A and reduce its cross-linking, making it easier to reorganize the actin cytoskeleton[332]. As for other CRMP1 interaction partners, CRMP1 binds ena/VASP-like protein, one of the key regulators of actin filament dynamics[348]. This interaction supports the elongation of actin filaments at their growing ends. Also, CRMP1 interacts with a sodium channel and modulates sodium currents by lowering the activation threshold[349].

In cultured cortical neurons, CRMP1 localizes primarily to axons and presynaptic regions, while CRMP2 is distributed across axons and dendrites at later developmental stages[331]. In growth cones, CRMP1 localizes to both the actin-rich peripheral regions (filopodia and lamellipodia) and the tubulin-rich central domain, indicating its role in axon guidance and cytoskeletal organization[350].

1.2.3.1.3 Functional roles of CRMP1

As mentioned previously, CRMP1 plays an important role in two key signaling pathways: Sema3A signaling and Reelin signaling[330]. Sema3A binds to a Neuropilin-1/Plexin-A complex, which triggers

Cdk5-mediated phosphorylation of CRMP1. In the *Crmp1* knock-out mouse model, cortical neuron migration was delayed, a defect not seen in the *Sema3A* knock-out mouse model.

Furthermore, studies on heterozygous mice for *Sema3A* and *Crmp1* show impaired synapse formation. However, *Crmp1* and *Crmp2* appear to mediate distinct pathways, as mice heterozygous for both exhibit normal synaptic phenotypes[331]. In the reelin pathway, CRMP1 interacts with DAB1, which is essential for neuronal migration and cortical layer formation. Both CRMP1 and DAB1 show changed expression and phosphorylation in *Reelin* knockout mice[351].

Studies in *Crmp1* knock-out mice show that CRMP1 is crucial for neurite outgrowth in the adult hippocampus, with deficits in spatial learning and memory[352].

1.2.3.1.4 Other CRMPs

One of the most well-characterized CRMPs is CRMP2. CRMP2 has a highly conserved sequence across humans and mammals[334], highlighting the importance of its role in neuronal migration and differentiation. Also, it interacts with tubulin heterodimers and promotes microtubule polymerization. The activity of CRMP2 is regulated through phosphorylation, similar to CRMP1. During development, CRMP2 has been seen to move into the nucleus and inhibit neurite outgrowth[353]. *Crmp2* knock-out mice exhibit reduced dendritic spine density in cortical layer pyramidal neurons, which was also seen in *Sema3A* and *Crmp1* knock-out mouse models[331]. Furthermore, reduced CRMP2 expression was seen in the FC of patients with SZ, BiPD, or MDD[354].

CRMP3 exhibits histone deacetylase activity and contributes to neuronal death following a traumatic injury. Additionally, CRMP3 has been associated with dendritic spine maturation and long-term potentiation in the hippocampus[355].

CRMP4 directly interacts with F-actin, promoting its bundling[356] with its variants implicated in Amyotrophic lateral sclerosis[357].

CRMP5 is primarily expressed in oligodendrocytes of the olfactory bulbs, the retina, hippocampal dentate gyrus, and peripheral nerve axons[358]. It is recognized as a biomarker for paraneoplastic optic neuropathy, and it is also linked to lung cancer and thymoma. Moreover, monoallelic CRMP5 variants can cause Ritscher–Schinzel

syndrome 4, a neurodevelopmental disease with craniofacial features, cerebral and cardiovascular malformations, and cognitive dysfunction.

1.2.3.1.5 CRMPs in neurological and psychiatric disorders

CRMPs have been implicated in autism spectrum disorder[359,360], while the increased phosphorylated CRMP2 was detected in AD and amyotrophic lateral sclerosis in humans[361,362]. Co-localization of phosphorylated CRMP2 and tau was observed in transgenic AD mouse model[363]. Future researched showed CRMP2 phosphorylation promotes Aβ-induced tau phosphorylation[364].

Heterozygous *de novo* variants in *CRMP1* have been implicated in muscular hypotonia, intellectual disability, and autism spectrum disorder[365]. Those variants have been predicted *in silico* to affect the structure and are seen to impact the oligomerization of recombinant CRMP1. Moreover, overexpression of the CRMP1 variants affected the neurite outgrowth of murine cortical neurons.

CRMP-2 plays a crucial role in neuroplasticity and is significantly reduced in the hippocampus of individuals with MDD[366]. Lithium, one of major drugs for BiPD, acts as a potent inhibitor of GSK-3β and affects pathway with CRMP2 in rat models[367]. *CRMP2* variants and altered protein levels are linked to SZ risk and antipsychotic drug responses[368–370]. Decreased levels of CRMP4 levels were detected in the hippocampus of SZ patients[371].

I/A CRMP1 was detected using a specific monoclonal antibody in mice after immunization with insoluble protein fraction collected from brain samples of patients diagnosed with SZ. The follow-up verified the existence of I/A CRMP1 in patients with diagnosed SZ and/or BiPD, but not in brain samples of patients diagnosed with MDD or a control group[322]. CRMP1 Sv was seen to aggregate when co-expressed with DISC1[322] or huntingtin[372].

These findings suggest that CRMP1 aggregation may contribute to disease pathology in SZ and BiPD, aligning with broader evidence that protein misfolding and aggregation play a role in neuropsychiatric disorders.

1.2.3.2 Disrupted in Schizophrenia 1

Disrupted in Schizophrenia 1 (DISC1) is a key genetic and molecular player in the pathophysiology of SZ through its diverse

structural regions, polymorphisms, and extensive interaction network. DISC1 also serves as a multifunctional scaffolding protein, interacting with over 200 proteins, many of which are also implicated in SZ[373,374]. DISC1 interacts with key proteins involved in neurodevelopment and psychiatric disorders, including Activating Transcription Factor 4, Phosphodiesterase 4B isoform 1, Lissencephaly 1, CRMP1, and Glycogen synthase kinase-3 isoform β[375]. These interactions regulate critical cellular processes like cAMP signaling, transcription, and cytoskeletal organization.

1.2.3.2.1 Structure and function of DISC1

DISC1 encodes an 854 aa scaffold protein consisting of N-terminal and C-terminal domains, with the N-terminal domain predicted to be partially disordered and the C-terminal domain composed of α-helices and self-association domains. Advanced structural studies identified stable regions within DISC1, named D, I, S, and C regions, with unique oligomerization properties[376].

DISC1 has diverse cellular functions, including regulation of neuronal development, migration, synapse formation, mitochondrial trafficking, and cytoskeletal organization[377,378].

One of the many roles of DISC1 is regulating mitochondrial dynamics as part of the mitochondrial transport machinery. It achieves this by interacting with key adaptor proteins, TRAK1 and TRAK2, which link mitochondria to motor proteins, such as kinesin and/or dynein[379,380]. Also, well-known binding partners of DISC1, Lisencephaly protein-1, Nuclear distribution element 1 (NDE1), and NDE-like 1 (NDEL1) are the dynein regulators, also contributing to neuronal mitochondrial trafficking[381]. DISC1 has been shown to localize in mitochondria, which is critical in maintaining their morphology and proper intracellular distribution[382]. Deletion mutants of DISC1 disrupt these functions, leading to abnormal mitochondrial morphology and impaired transport[380,383]. These findings align with DISC1's established roles in regulating mitochondrial dynamics, trafficking through interactions with motor proteins, and ensuring proper neuronal energy supply.

When exposed to hydrogen peroxide (H_2O_2), cortical neurons normally show a slow rise in mitochondrial calcium levels, but this rise was much larger when DISC1 was reduced. Additionally, neurons with

lower DISC1 levels had significantly less calcium stored in the ER after H_2O_2 exposure, suggesting a disturbance in calcium balance within the cells [384]. Under normal conditions, DISC1 interacts with girdin to inhibit Akt/mTORC1 signaling, a key pathway regulating translation[385]. However, under oxidative stress, DISC1 shifts its role to support protein production by interacting with eukaryotic translation initiation factor 3, a critical component of the translation initiation machinery[386,387]. This dual functionality highlights DISC1's importance in maintaining protein synthesis and cellular integrity during stress.

Studies have shown that reducing DISC1 levels leads to stronger inhibition of protein synthesis, increased number of stress granules, and decreased cell viability, emphasizing its protective role[386]. Additionally, truncated C-terminal DISC1 has been observed to bind arsenic derivatives, further linking DISC1 to stress response pathways[388].

1.2.3.2.2 DISC1 in CMIs

DISC1 expression peaks during early brain development and decreases in adulthood. Dysregulation of DISC1 impairs neurogenesis, neuronal migration, and synaptic connectivity, aligning with structural and functional abnormalities observed in psychiatric disorders[389,390]. DISC1 was first identified in a Scottish family carrying a balanced chromosomal translocation between chromosomes 1 and 11 [t(1;11)(q42.1;q14.3)], which segregated with major psychiatric disorders, including SZ, recurrent MDD, and BiPD[70,391]. The balanced translocation disrupts the *DISC1* gene, resulting in a truncated protein lacking key C-terminal domains. This disruption compromises protein stability and impairs interactions with other proteins[376]. Common *DISC1* polymorphisms have been linked to SZ and reduced hippocampal gray matter volume[392,393], with them also affecting synaptic plasticity, cortical thickness, and neuronal migration[394,395].

1.2.3.2.3 Aggregation of DISC1

DISC1 aggregates have been identified in the cingulate cortex in a subset of patients with SZ, BiPD, or MDD, but were absent in healthy controls and patients with NDs[320,321]. Aggregated DISC1 was seen to have a disrupted interaction with NDEL1 leading to a loss-of-function phenotype [320]. DISC1 aggregates recruited dysbindin, which is critical for dendritic spine formation, disrupting neuronal function and mitochondrial transport[321,396]. Moreover, inhibition of the

autophagosomal pathway intensified DISC1 aggregation. DISC1 aggregates were observed to impair intracellular transport and contribute to neuronal dysfunction.

Elevated levels of DISC1 aggregates have been detected in the cerebrospinal fluid of patients with first-episode psychosis, specifically in subsets diagnosed with SZ or schizoaffective disorder[397]. DISC1 aggregation also caused hippocampal dysfunction, including impaired neuronal response during sleep and disrupted network synchrony, mirroring deficits observed in SZ patients[398]. In Huntington's disease, DISC1 co-aggregates with mutant huntingtin, disrupting DISC1's interaction with PDE4 and resulting in elevated PDE4 activity and reduced cAMP levels[399]. In frontotemporal dementia, DISC1 co-aggregates with TDP-43, impairing local dendritic translation and causing behavioral and cognitive deficits[400]. Restoring DISC1 expression in the FC partially alleviated these deficits.

Transgenic rat models expressing *DISC1* exhibited signs of protein aggregation and dopaminergic dysfunction, including heightened dopamine sensitivity, hyper-exploratory behavior, and motor deficits[401]. They also exhibited cognitive impairments, such as deficits in cognitive flexibility and social performance[402,403]. Elevated cytosolic dopamine levels increased DISC1 aggregation and interaction with the dopamine transporter[401]. Morphological changes included reduced dopaminergic neurons in the substantia nigra pars compacta and lower dopamine content in the dorsal striatum, impacting locomotor behavior and reward pathways[404].

DISC1 interacts with serine racemase, which modulates D-serine production and NMDA receptor function, both linked to glutamatergic signaling[405]. In cortical neurons, serine racemase co-localized with DISC1 aggresomes, with D-serine enhancing DISC1 aggregation and disrupting NMDA receptor signaling[406].

1.2.3.3 Neuronal PAS domain-containing protein 3

Neuronal PAS domain-containing protein 3 (NPAS3) is a transcription factor specific for RNA polymerase II[407]. Given its dual role in neurodevelopment and metabolic regulation, NPAS3 is implicated in mental illnesses such as SZ, where disruptions of its expression or function may contribute to disease mechanisms.

1.2.3.3.1 NPAS proteins

NPAS proteins are part of a family of transcription factors with basic helix–loop–helix (bHLH) and PAS structural protein motifs. A basic helix-loop-helix (bHLH) motif is characteristic for proteins that act as transcription factors and require dimerization for it. It contains basic aa that facilitate binding to DNA[408]. Transcription factors with this motif such as c-Myc and BMAL1-Clock, are essential for development and cell metabolism[409]. PAS is an acronym originating from the first three proteins that contain this polypeptide motif: the *period*, the aryl hydrocarbon receptor nuclear transporter, and the *single-minded* product in *Drosophila*[410].

NPAS1 is expressed in the CNS and implicated in neuronal differentiation and development[411]. It acts as a transcriptional repressor, and one of the known interaction partners is the aryl hydrocarbon receptor nuclear translocator (ARNT). ARNT guides NPAS1 into the nucleus, where NPAS1 can inhibit the transactivation functions of both ARNT and ARNT2. *Npas1* is expressed in the developing basal ganglia regions in a mouse model[412]. In the same model, lack of NPAS1 leads to increased cell growth (proliferation) and enhanced activity in ERK signaling pathways. Also, NPAS1 reduced the activity of an enhancer for *Arx* which is linked to neuron proliferation, suggesting that NPAS1 helps control the production of inhibitory neurons during brain development. Recent data detected NPAS1 in a group of basal forebrain neurons[413]. These neurons are GABAergic neurons and present in brain regions involved in sleep-wake control, motivation, and stress responses. As they are involved in sleep homeostasis, they could play a role in stress-induced insomnia and neuropsychiatric disorders, including dementia and sleep disturbances.

NPAS2 forms complexes with proteins like BMAL1 to bind to DNA, with the complex formation depending on the ratio of the oxidized and reduced forms of the nicotinamide-adenine dinucleotide (phosphate), NAD(P)+/NAD(P)H[414]. Hence, NPAS2 can be an 'environmental sensor'. The PAS domain of NPAS2 also associates with a heme cofactor and can act as a receptor for gaseous neurotransmitters, like carbon monoxide. If carbon monoxide binds to NPAS2, the BMAL1 binding and transcriptional activity are consequently inhibited[415]. Also, the NPAS2-BMAL1 complex acts like the CLOCK-BMAL1 complex within the negative transcriptional feedback loops that drive circadian rhythm[416].

Knock-out *Npas2* mouse models display circadian deficits[417], disrupted sleep homeostasis[418], and impaired memory[419].

NPAS4 is classified as one of the immediate early genes and is implicated in converting experience into long-term memory. *NPAS4* is exclusively expressed in neurons and activated selectively by neuronal activity rather than extracellular stimuli[420]. It plays a critical role in regulating many activity-dependent genes and is essential for the development of glutamatergic and GABAergic synapses[421]. Moreover, it contributes to neural circuit plasticity, helps to maintain circuit homeostasis, and is necessary for long-term memory formation, highlighting its significant role in brain function and adaptability[422].

1.2.3.3.2 NPAS3 structure

NPAS3 comprises three key subunits: a basic helix-loop-helix (bHLH) domain and two PAS domains (PAS-A and PAS-B). The bHLH domain, common in transcription factors, binds specific DNA sequences in target promoters. The PAS region regulates NPAS3's interaction capabilities, with the PAS-A domain playing a key role in its interaction with the ARNT. Meanwhile, the PAS-B domain is involved in gene regulation, ligand binding, and interactions with chaperone proteins. A transcriptional activation domain (TAD), which contains binding sites for other proteins, is also involved in transcription[423,424].

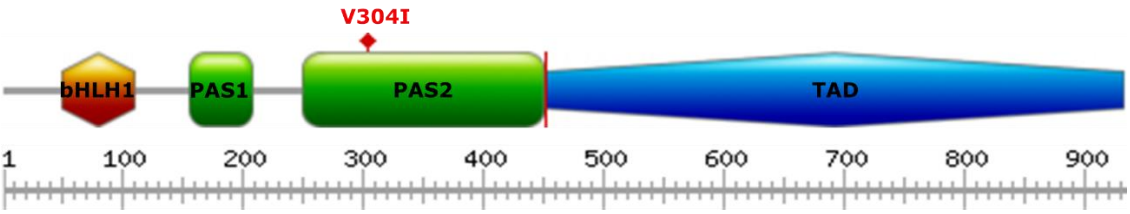

Figure 3: Major regions of NPAS3. A bHLH domain is represented as an orange hexagon, two PAS domains are depicted as green rectangles, and the TAD region is shown as a blue rhomb. The gray ruler which marks location of aa is shown below. The scheme was created with ProSite.

The *NPAS3* is located on chromosome 14, on q13, for which chromosomal abnormalities are associated with SZ and cognitive disabilities[425–427].

NPAS3 contains the largest cluster of human-accelerated regions (HARs) in the genome, with 14 elements that have undergone rapid changes compared to evolutionary ancestors. These HARs act as transcriptional enhancers, particularly within the developing nervous system, and are hypothesized to contribute to human-specific cognitive

traits[428]. Comparative analyses suggest that NPAS3-HAR202, one of these elements, has undergone functional evolution in the human brain, potentially playing a role in shaping human neurodevelopmental differences[429].

As for post-translational modifications, they include O-linked β-N acetylglucosamine (O-linked GlcNAc) and serine/threonine phosphorylation. In general, O-linked GlcNAc is a reversible modification that affects many cell processes like protein interactions, structure, activity, and stability[430]. Also, O-GlcNAc has been shown to slow protein aggregation, for example of α-synuclein and tau, but the extent of this effect remains unclear[431]. Similarly, phosphorylation can significantly affect protein structure and its local environment by introducing a large, charged group, altering the protein's activity, or creating a new binding site[432]. There is evidence of cross-talk between O-GlcNAc and serine/threonine phosphorylation since they both can occur on serine and threonine residues, modulating protein stability and degradation[433,434]. An example of the relationship between O-GlcNAc and phosphorylation is seen in the tau protein, where increased tau O-GlcNAcylation can inhibit pathological tau hyperphosphorylation[435].

The isoform investigated in this thesis is NPAS3 isoform A, here referred to as NPAS3 wt, which has 933 aa with a theoretical weight of 100.8 kDa.

1.2.3.3.3 NPAS3 function and expression

NPAS3 activity bridges neurodevelopmental processes and metabolic regulation, which may explain its contribution to mental illness etiology. As for the role of NPAS3 in transcriptional regulation, its transcriptional targets vary depending on circadian rhythm and C-terminal structure, showing its regulatory complexity[436]. NPAS3 strongly upregulates *VGF Nerve Growth Factor*[437], which is implicated in neurogenesis, MDD, and SZ, underscoring its relevance in neurodevelopment and mental health. Many NPAS3 target genes are also regulated by SRY-related HMG-box transcription factors, suggesting shared roles in neurodevelopment[436]. NPAS3 represses multiple glycolysis-related genes, indicating a significant role in glucose metabolism.

NPAS3 expression exhibits distinct developmental patterns, with mRNA levels high at birth and declining to steady-state adult levels by the second decade of life, while protein levels show an inverse trend, increasing during cortical development[438]. In SZ a significant reduction in NPAS3 was observed in females, despite no changes in mRNA or protein levels across the total cohort, suggesting post-transcriptional regulation. An SZ-associated microRNA, miR-17, was identified as a potential regulator of NPAS3 transcripts during development, with increased miR-17 expression potentially disrupting normal NPAS3 regulation. In humans, *NPAS3* is highly expressed in the brain, specifically in the amygdala, cerebral cortex, and basal ganglia[439]. Intense *Npas3* expression in the mouse is localized to the hippocampal subgranular zone, specifically in maturing neuronal precursor cells, emphasizing its role in adult neurogenesis[436].

1.2.3.3.4 NPAS3 interaction partners

NPAS3 is known to interact with 27 proteins, with several of them standing out for their relevance to brain development, neuronal function, and mental illnesses. Here several of them are mentioned, to showcase versatility of NPAS3.

ARNT2, a transcription factor, regulates genes responsive to environmental and developmental stimuli, including oxygen levels during hypoxia, and plays a role in neurogenesis, linking it to brain adaptability and function[440]. ARNT2 was also recently investigated for its interaction with NPAS4[441,442]. DDX39A, an RNA helicase, is essential for RNA processing, influencing cell growth and neural differentiation, processes critical for brain health[443]. TP53, or p53, regulates cellular stress responses such as DNA repair and apoptosis, playing a key role in brain protection and development, with mutations linked to cancer and possibly NDs[444]. AS3MT, an enzyme involved in arsenic metabolism, is important for detoxification processes that may influence neural health indirectly[445].

1.2.3.3.5 NPAS3 animal models

Animal studies have provided valuable insights into the role of NPAS3 in brain development and its potential link to SZ.

Mice lacking *Npas1* and *Npas3* exhibit behavioral abnormalities resembling SZ models, including diminished startle response, gait defects, increased open-field activity, and impaired social

recognition[446]. Further research has revealed more specific neurological changes in *Npas3* knockout mice. A follow-up study demonstrated that these mice have significantly lower levels of FGF receptor subtype 1 mRNA in the dentate gyrus of the hippocampus, along with a substantial reduction in neural precursor cell proliferation in the same region compared to normal mice[447]. This research group also reported rescuing this phenotype after prolonged administration of aminopropyl carbazole[448].

More recent studies have shown that reducing *Npas3* levels in the developing mouse brain leads to neuronal migration defects, with cells failing to reach their intended cortical layers and exhibiting incorrect layer-specific identities. This NPAS3 downregulation also results in prolonged stemness in radial glial cells and increased proliferation of neural progenitors in the ventricular and subventricular zones[449].

Npas3 knockout mice exhibit changes in key metabolites, including NAD+, glycolysis metabolites (dihydroxyacetone phosphate, fructose-1,6-bisphosphate), pentose phosphate pathway components and Krebs cycle intermediates (succinate and α-ketoglutarate)[436].

1.2.3.3.6 NPAS3 in CMIs

NPAS3 was initially implicated in SZ through a case report involving a mother and daughter diagnosed with SZ and learning disabilities, both carrying a chromosomal translocation disrupting the *NPAS3* on chromosome 14. Analysis of individual-derived lymphoblastoid cell lines revealed that the translocation directly disrupts the *NPAS3*[425,426].

Previous research also linked this chromosomal region to idiopathic basal ganglia calcification (known as Fahr's disease), characterized by motor deficits, cognitive impairments, and, in some instances, psychiatric disorders[450].

Additionally, disruptions of regions on chromosome 14 were linked to BiPD in multiple populations in scan meta-analysis[451]. Moreover, a deletion on the 14th chromosome was linked to a lack of speech development with delayed overall development in a child[452]. A follow-up study revealed three common variants of NPAS3 associated with SZ that affected protein function[427].

Additionally, the V304I mutation in NPAS3 has been identified in a family affected by SZ and major depressive disorder. This mutation results in a valine-to-isoleucine substitution, which increases the tendency of NPAS3 to be I/A[453]. In previous chapter, miR-17 was mentioned as regulator of NPAS3 synthesis. In the context of SZ, researchers have observed elevated levels of miR-17 in the prefrontal cortex of some individuals and a reduction in NPAS3 levels[454]. This finding suggests that in SZ, the issue may not be large-scale changes in *NPAS3* expression, but rather a disruption in the normal biosynthesis process of NPAS3. Also, four SNPs regions in the *NPAS3* were significantly associated with bipolar disorder and/or SZ diagnosis[455]. Near a translocation breakpoint, SNPs linked to the efficacy of iloperidone, an atypical antipsychotic, were identified, too[456].

In the review by Pickard et al[407], two possible outcomes were explored for NPAS3 affected by the translocation.

The first option is producing a truncated NPAS3 containing only the bHLH domain. Pickard et al described a similar situation with other bHLH-PAS proteins, HIF-1α, and the aryl hydrocarbon receptor. These isoforms, which lack TADs, are non-functional and act in a dominant-negative manner by occupying promoter sites or sequestering interaction partners into non-functional complexes, thereby disrupting normal cellular regulatory processes. Another example available in *Drosophila* involves the CLOCK, a regulator of circadian rhythm. A point mutation in the *Clock* gene, known as the Jrk mutation, introduces a premature stop codon, leading to the expression of a truncated CLOCK lacking its C-terminal activation domain. The truncated protein can still dimerize with its partner, CYCLE, but fails to activate transcription of target genes, thereby acting in a dominant-negative manner by occupying promoter sites without initiating transcription. This disruption leads to arrhythmic locomotor behavior in flies, underscoring the critical role of the full-length CLOCK in maintaining normal circadian rhythms. A more recent example involves the bHLH transcription factor Twist1, which plays a role in epithelial-mesenchymal transition. Deletions in Twist1's N-terminal region can cause it to misfold and form aggregates in aggresomes, potentially interfering with normal cellular functions[457].

The second option is that mRNAs for these truncated versions of NPAS3 are destroyed by cellular quality control mechanisms,

preventing the production of any truncated NPAS3[407]. This could eliminate the potential for dominant-negative effects (as described earlier). Also, truncated protein is actively degraded by the proteasome. However, the downside is that the overall level of NPAS3 in the cells would drop to about 50% of normal, as only the intact *NPAS3* from the non-disrupted chromosome 14 would contribute to protein production. Halving the NPAS3 level might impair its normal functions, which could contribute to disease mechanisms, in literature also referred to as haploinsufficiency. A similar situation is described with DISC1, affected by a translocation break on chromosomes 1 and 11, where no truncated version of DISC1 was detected. Mutations in the gene encoding *transcription factor 4 (TCF4)* provide another example. These mutations are linked to Pitt–Hopkins syndrome, a neurodevelopmental disorder characterized by intellectual disability and developmental delays. Some mutations create premature termination codons in the TCF4 mRNA, leading to its degradation. This degradation typically prevents the production of truncated TCF4 that might otherwise disrupt normal TCF4 function in a dominant-negative manner. However, the overall reduction in TCF4 levels impairs its ability to regulate expression, contributing to the symptoms of Pitt-Hopkins Syndrome[458].

Nevertheless, these alterations affect both the bHLH and PAS domains, hence disrupting the DNA-binding and dimerization functions of NPAS3, further compromising its role in transcriptional regulation.

1.2.3.4 Trio and F-actin binding protein isoform 1

Trio and F-actin binding protein isoform 1 (TRIOBP-1) is a multifunctional protein crucial for actin cytoskeleton stabilization, neurite outgrowth, and cellular adhesion. Its structural versatility and interaction network suggest broader cellular roles, including centrosomal localization, protein stability, and mitotic regulation[459].

1.2.3.4.1 Structure and function of TRIOBP-1

TRIOBP-1 (in literature also referred to as Tara) contains two primary structured regions: a Pleckstrin Homology (PH) domain near the N-terminus and Coiled-Coil (CC) domains in the C-terminal half, separated by a 100 aa intrinsically disordered mid-domain[459]. An optional disordered N-terminal region, arising from two potential start codons, produces two isoforms of TRIOBP-1: 593 or 652 aa long. The

PH domain forms a compact folded structure with two extended loops, the second of which is highly conserved across mammals and likely mediates protein-protein interactions. The C-terminal CC domains are divided into central and C-terminal regions. The central CC domain forms hexameric complexes, driving TRIOBP-1 oligomerization, while the C-terminal CC domain remains monomeric in isolation. Both of them enable interactions with other proteins, allowing TRIOBP-1 to play a role in neurite outgrowth, and cytoskeletal organization. Smaller TRIOBP-1 fragments (45–60 kDa) primarily represent portions of the CC domains and lack the PH domain. Another splice variant, TRIOBP-2, contains N-terminal and partial CC regions, though its function remains unclear.

The major known function of TRIOBP-1 is as a stabilizer of filamentous actin (F-actin) by preventing its depolymerization, which in the end is crucial for neuronal outgrowth, migration, and adhesion[459]. TRIOBP-1 has many interaction partners, with one of them being NDEL1, a neurodevelopmental protein associated with the microtubule cytoskeleton and their interaction enhances actin polymerization, neurite outgrowth, and dendritic arborization. TRIOBP-1 is regulated by the ubiquitin ligase HECTD3, which targets it for degradation, preventing excessive accumulation and aggregation in normal conditions[460].

1.2.3.4.2 TRIOBP-1 in CMIs

Although TRIOBP-1 is not a known genetic risk factor for mental illness, subtle increases in TRIOBP-1 transcripts have been observed in SZ patients[461], and its expression is affected by a polymorphism in the NDE1/miR-484 locus[462]. Moreover, the chromosomal locus containing the *TRIOBP-1*, 22q12.3 q13.3, has been investigated in a family with SZ, epilepsy, and hearing issues[463]. Additionally, I/A TRIOBP-1 has been detected in brain samples of patients with SZ and MDD, but not in healthy controls[323,464]. TRIOBP-1 aggregation is driven by its central coiled-coil domain. A critical 25 aa sequence, rich in charged residues, was identified as essential for this aggregation, later shortened to the 7 aa domain. Shorter fragments of TRIOBP-1 (45–60 kDa) containing the CC domain, but not the PH domain, can also aggregate in cells and in the brain. Aggregated TRIOBP-1 has been shown to impair neurite outgrowth, affecting the structural integrity and growth of neurons in cell culture models.

1.2.3.4.3 Other members of the TRIOBP family

TRIOBP-4 is predicted to be an intrinsically disordered protein with no fixed secondary or tertiary structure[459]. It contains two distinct repeat regions: R1 and R2, out of which R1 is critical for actin bundling. *TRIOBP-4* is highly expressed in inner ear hair cells, where it organizes actin filaments into densely packed bundles, essential for forming stereocilia rootlets. Knock-out *Triobp-4* mice show failed stereocilia rootlet formation, loss of rigidity, and subsequent deafness. Also, *TRIOBP-4* is expressed in the retina and implicated in filopodia formation in cancer cells.

TRIOBP-5 shares sequence homology with both TRIOBP-1 and -4[459]. It consists of R1 and R2 regions from TRIOBP-4 and C-terminal coiled-coil domains from TRIOBP-1. As for function, similar to TRIOBP-1 and -4, it has actin-binding and bundling properties. In the inner ear, TRIOBP-5 is found at the lower sections of stereocilia rootlets, complementing the role of TRIOBP-4. While TRIOBP-4 is crucial for rootlet formation, TRIOBP-5 contributes to rootlet widening and structural maintenance. Knock-out *Triobp-5* mice show progressive hearing loss rather than congenital deafness[465].

TRIOBP-6 is the longest isoform of the TRIOBP family, containing an R1 repeat region from TRIOBP-4, and PH and C-terminal coiled-coil domains from TRIOBP-1[459]. Additionally, TRIOBP-6 has unique isoform-specific N-terminal sequences and unstructured regions. They are largely predicted to be disordered, except for short stretches of α-helices near the N-terminus and central region. Like *TRIOBP-4* and *-5*, *TRIOBP-6* is expressed in the inner ear hair cells and plays a significant role in stereocilia rootlet stability and maintenance. *TRIOBP-6* is expressed in multiple tissues, including the inner ear, brain, and cancerous tissues, alongside *TRIOBP-1*. Due to its structural similarity to TRIOBP-1, TRIOBP-6 may also aggregate.

Mutations in *TRIOBP-4, -5,* and *-6* cause autosomal recessive hearing loss, while both TRIOBP-4 and TRIOBP-5 are implicated in pancreatic cancer and glioblastoma[459].

1.3 Brain regions investigated in this thesis

The first brain region used for this thesis is the insular cortex (IC). IC is a brain region hidden beneath the frontal, temporal, and parietal lobes involved in emotion, self-awareness, pain perception, and

interoception (body awareness). It plays a key role in mood regulation, decision-making, and cognitive functions, linking it to CMIs[466].

Brain samples used in this thesis were primarily from the cerebral cortex. The frontal lobe, also known as the FC, is the largest lobe of the cerebral cortex[466]. It is responsible for functions such as movement, speech, reasoning, emotional expression, and socially appropriate behavior, and it also plays a vital role in the integration of memories. The second major part of the cerebral cortex is the temporal lobe (here referred to as temporal cortex or TC), which is involved in processing sensory input for memory, language, and emotion[466]. The third major region of the cerebral cortex is the parietal lobe (here referred to as parietal cortex or PC), which integrates sensory information, processes touch, spatial awareness, and navigation, and plays a role in language processing, with the somatosensory cortex mapping the body based on sensory input[466].

The last major lobe of the cerebral cortex, the occipital lobe, is represented here by Brodmann area 17 (BA17). BA are regions of the cerebral cortex, defined by their histological structure and cell organization. BA3, 1, and 2 overlap with the primary somatosensory cortex, which is responsible for receiving and integrating sensory stimuli related to the sense of touch[467]. The primary motor cortex, or BA4 is involved in planning and executing voluntary movements, together with other motor areas[467]. BA6 is part of the premotor cortex and supplementary motor cortex, and it is essential for sensory-guided movement and aiding in the planning of complex actions[467]. BA9 is part of FC and plays an important role in memory, attention, reasoning, and intention[467]. The primary visual cortex, striate cortex, or BA17, processes visual information about static and moving objects, their orientation, and color. It integrates all data for further processing in higher-order visual areas[467]. BA36 and BA37 are important for the formation and retrieval of memory, including memory and recognition of faces[467].

The piriform cortex (PiFC) is involved in the sense of smell and contains a key epileptogenic trigger zone where chemical and electrical seizures can be induced[468]. The superior frontal gyrus (SFG), which makes up about a third of the frontal lobe, is involved in self-awareness and sensory coordination[469]. In one case, electrical stimulation of a specific area in a left SFG consistently triggered laughter, with

increasing stimulation intensifying the response. The individuals associated the laughter with external stimuli, even though it was caused by the stimulation. The lateral orbitofrontal gyrus (LOG) processes punishments, and non-rewards, and helps regulate emotional behavior[470].

Some of the brain regions mentioned overlap with each other, for example, the FC includes the primary motor cortex, while BA37 is part of the temporal region[467]. Described brain regions are marked in **Figure 4**.

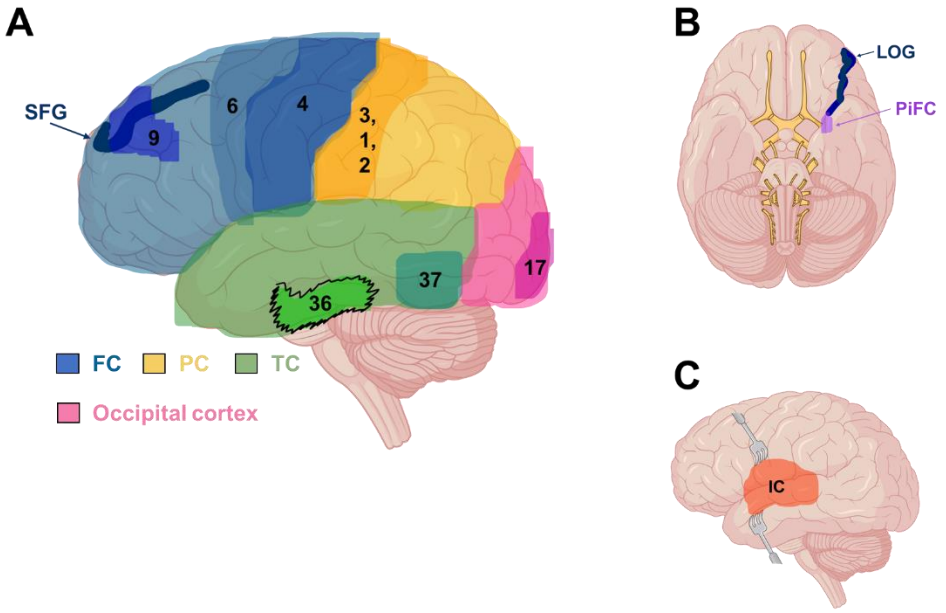

Figure 4: Approximate location of the brain regions examined in this thesis. A) Frontal cortex (FC), parietal (PC), temporal (TC) and occipital cortex are shown in shades of blue, yellow, green and pink, respectively. BA are marked with numbers and corresponding color, while SFG is shown as a line. Notably, BA36 is marked as a shape with sketched line, to indicate location deep in the brain. B) On bottom view of the brain, lateral orbital gyrus (LOG, blue) and piriform cortex (PiFC, purple) are shown as a line and a dot, respectively. C) Insular cortex (IC, red) is located deep within lateral sulcus and shown with retractors on the scheme. The scheme was created with BioRender.

1.3.1 Previously investigated human brain regions in MDD and suicide

Brain regions investigated for MDD in humans include the hippocampus, prefrontal cortex, mesolimbic pathway, and striatum.

The hippocampus is essential for memory and stress regulation and observed abnormalities included elevated glucocorticoids from

hypothalamic-pituitary-adrenal axis dysfunction[222], decreased hippocampal volume[230], and antidepressant effect of BDNF[251].

Post-mortem studies of patients with MDD have shown reduced densities of glial cells in the prefrontal cortex, hippocampus, and amygdala[471]. The amygdala is associated with emotional reactivity and changes in the amygdala were also observed in a recent meta-analysis of structural and functional abnormalities in the brains of patients with MDD[472]. In the same analysis, several other brain regions were implicated in MDD. In the left hemisphere, beyond the hippocampus, the subgenual cingulate cortex, which is important for emotional regulation and mood processing, was also implicated. Furthermore, the left retrosplenial cortex demonstrated significant changes in MDD. That region includes BA29 and BA30, both important for self-referential thought and memory retrieval. The right hemisphere also exhibited changes, particularly in the putamen, which is linked to motor and reward processing. Lastly, the right middle occipital gyrus and inferior temporal gyrus were identified as areas of abnormality, both involved in visual and perceptual processing.

Similar brain regions were investigated for suicide and suicidal behavior, with decreased BDNF levels correlating with suicide risk and smaller dentate gyrus volume in suicide victims with MDD compared to non-suicidal individuals was reported in the hippocampus[473]. Also, decreased BDNF levels and protein dysregulation[286], and alterations in small heat shock protein expression[261] were reported in the prefrontal cortex.

Interestingly, several other brain regions were investigated for suicide, compared to MDD: anterior cingulate cortex, BA6 and BA10, dentate gyrus, and locus coeruleus. Alterations in BDNF, FK506-binding protein, and glucocorticoid receptor were reported in the anterior cingulate cortex[286], while disruption in iron transport proteins was seen in BA6 and BA10 collected from suicide victims[289]. In the dentate gyrus, reduced neurogenesis was observed[473].

1.3.2 Previously investigated brain regions in SZ

Post-mortem and neuroimaging studies have shown differences in dopamine-related markers in the midbrain region substantia nigra and striatum, connected to SZ diagnosis[474]. As discussed in previous sections, both the striatum and mesolimbic system have been

repeatedly implicated in SZ, MDD, and TRS through alterations in dopamine signaling, receptor activity, and regional connectivity. The midbrain houses the dopamine-producing neurons that project to the striatum[475]. The midbrain region substantia nigra sends dopamine to the dorsal striatum, influencing movement and motor control. The other midbrain region, the ventral tegmental area, sends dopamine to the ventral striatum (part of the limbic system), influencing motivation and reward-related behaviors. The striatum is a brain region where signals related to dopamine are processed, and it is divided into the dorsal striatum (involved in decision-making and planning), ventral striatum (part of the limbic system, linked to emotions and rewards), and associative striatum (connected to the higher-level brain areas like the FC, crucial for problem-solving and cognition).

Individuals with diagnosed SZ or with a high risk for it have shown higher dopamine synthesis and release in the striatum than controls [476]. Contrary to earlier theories, the dorsal striatum, not the ventral, shows the most significant dopamine overactivity in SZ.

1.4 *Drosophila* as a transgenic model

Creating an animal model of SZ is challenging, due to complexity of behavioral symptoms and methods to measure specific endophenotypes. Inserting a SZ risk gene in an animal model can contribute to understanding molecular mechanisms, but also indicate behavior changes caused by expression.

Drosophila melanogaster later called fly or just *Drosophila*, is a powerful model organism for dissecting mechanisms of brain circuit dysfunction. This is possible because of its similarity to mammals in neurotransmitters, and monoamines transporters and receptors on the cellular level[477]. *Drosophila* has been used in the research of various mental illnesses, including SZ[478–480].

Although the binary expression system from yeast GAL4-UAS was initially used in the cell cultures, later it was utilized in *Drosophila*[481]. GAL4 is a yeast transcription activator protein that specifically recognizes and binds to the upstream activation sequence (UAS) promotor and activates transcription. However, the GAL4 alone has little to no effect on cells. The *GAL4* is inserted downstream of a native promoter in the *Drosophila* genome, such as the *elav* promoter, which stands for the embryonic lethal abnormal visual system. The *elav* is expressed pan-neurally (in the entire nervous system) during

Drosophila development[482]. An analysis of *elav*-GAL4 showed that *elav* is expressed in neural progenitor cells and nearly all embryonic glial cells[483].

To utilize this system, the gene of interest needs to be located behind the UAS (upstream activation sequence) promotor[482]. In the transgenic line used in this thesis, the full-length human *DISC1*, *hflDISC1* was balanced on the second or third chromosome to maintain the heterozygous state of the line, resulting in UAS-*hflDISC1*-2nd or UAS-*hflDISC1*-3rd line. Balancer chromosomes are specially modified chromosomes used in *Drosophila* with dominant visible markers and lethal mutations in homozygosity, ensuring that only heterozygous flies survive. In this case, balancing was used to stably maintain the UAS-*hflDISC1* insertion in a heterozygous state, preventing potential lethality or artifacts from overexpression in homozygotes.

UAS lines should not express *hflDISC* without the GAL4 enhancer, which binds to UAS and initiates transcription. To activate the target gene in a specific cell, flies carrying the target gene (e.g., UAS-*hflDISC1*) are crossed with flies expressing GAL4 (e.g., *elav*-GAL4). The result of the cross is a line (e.g., *elav*-GAL4-UAS-*hflDISC1*-2nd) that expresses the target gene (*hflDISC1*) in cells where the driver gene is present (e.g. *elav* in all neuronal cells).

To investigate psychiatric disorders in *Drosophila*, it is important to address how neurotransmitters are processed in the brain of *Drosophila*. The mushroom body is a brain region central to olfactory associative learning, processes sensory information from dopaminergic, octopaminergic, cholinergic, serotonergic, and GABAergic neurons [484–486]. Within the mushroom body, Kenyon cells play a key role in responding to odors by generating specific activity patterns. These patterns are passed to output neurons (MBONs), which drive behavioral responses like attraction or avoidance. The primary neurotransmitters in this system are glutamate, acetylcholine, and GABA. Kenyon cells are primarily activated by acetylcholine, which is released by cholinergic neurons that deliver sensory input. MBONs use glutamate to transmit excitatory signals, typically influencing behaviors associated with attraction or repulsion. GABAergic neurons provide inhibitory signals, either regulating Kenyon cell activity or modulating MBONs, thereby balancing the network and refining behavioral responses. Dopamine plays a crucial role in learning by inducing plasticity at synapses between odor-responsive Kenyon cells and

MBONs. Specific subsets of dopaminergic neurons encode positive or negative valence and target distinct compartments of the mushroom body, aligning precisely with MBON dendritic fields. This dopamine release alters the strength of Kenyon-MBON connections, biasing the network towards approach or avoidance behaviors. Beyond forming memories, dopamine regulates their expression, influenced by factors like hunger or internal states. This dual role allows the mushroom body to integrate sensory inputs, context, and internal conditions, optimizing behavior based on past experiences and current needs.

1.4.1 Overview of previous transgenic *DISC1 Drosophila* models

Transgenic rat and mouse models with *DISC1* are used more. However, it is hard to distinguish if the effect is primarily led by the introduced human *DISC1* or by the expression of the endogenous animal *DISC1*. Since there is no endogenous homolog for the human *DISC1* in *Drosophila*, it can serve as an excellent model organism for describing the mechanisms of *DISC1*. However, many genes for DISC1 interaction partners are conserved in *Drosophila*, like *Phosphodiesterase 4B1* and *dysbindin*[487]. So far, few research groups have investigated the human *DISC1* in *Drosophila*.

The initial studies done by Sawamura et al. showed disrupted sleep homeostasis in flies expressing the full-length human *DISC1*[488]. Flies normally have a circadian activity pattern with more frequent and longer rest periods at night than during the daytime, referred to in the literature as sleep bouts[489]. Beyond providing information about sleep homeostasis, quantitative assessment of sleep bouts can give insight into the arousal of flies. Sawamura et al observed that transgenic *DISC1* male flies had longer sleep periods with reduced arousal states during the day[488]. However, the circadian rhythm and frequency of sleep periods were similar to the controls. The same effect was not observed for the truncated version of the gene, *DISC1* 1-597 aa (a variant which occurs after translocation described in the Scottish family), nor in female flies with either DISC1 version. Since ATF4 is a known DISC1 interaction partner, they suggest DISC1 regulates sleep homeostasis in flies with CRE-mediated gene transcription.

During brain development, over-expressing the *DISC1* in *Drosophila* was seen to suppress axonal and dendritic neuronal branching, affecting associative olfactory memory. Using the GAL4-

UAS system, *hflDISC1* was expressed in mushroom body neurons of *Drosophila* larvae, an area of *Drosophila* brain critical for memory formation after neuronal signaling of olfactory information[484]. After appetitive larvae training with sucrose, controls (wt *Drosophila*, UAS flies carrying the *DISC1* gene, and flies with only GAL4 driver) showed normal olfactory memory. At the same time, the flies expressing the human *DISC1* failed to exhibit olfactory memory. Lack of olfactory memory was reported in flies expressing truncated *DISC1*, 1-597 aa.

Sawamura et al observed full-length *DISC1* localized in the nucleus of adult flies upon expression[488]. In a study done by Furukobo-Tokunaga et al, the truncated version mimicking the Scottish translocation (DISC1 1–597 aa) localized to the nucleus in adult flies but not to dendrites or axons. In contrast, it showed weak expression in axons and dendrites of larval neurons, indicating developmentally regulated subcellular dynamics[490], consistent with observations in mammalian cells and mouse cortical neurons[488,491]. I/A DISC1 was isolated, but without neuronal cell death in the fly's compound eyes, a highly sensitive area of the fly to neurodegeneration[490].

Another study in flies with truncated *DISC1* expressed pan-neuronally showed a significant reversal learning deficit compared to flies expressing full-length *DISC1* or controls[492]. The learning deficit was seen only in glutamatergic neurons and neurons expressing rutabaga-adenylyl cyclase when the expression was more focused. Truncated DISC1 can affect synaptic transmission and nerve terminal organization in transgenic larval neuromuscular junctions, which was not observed with full-length DISC1 or control lines. Moreover, interactions between DISC1 and *Drosophila's* homolog genes for human *dysbindin*[490] and *Neurexin*[493] were observed in the development of glutamatergic synapses of *Drosophila*. Aberrant glutamine and dopamine neurotransmission[476] are strongly implicated in SZ pathology, leading to the importance of investigating human *DISC1* in the *Drosophila* model.

In *Chapter 1.2.3.2.1* connection between DISC1 and mitochondria was mentioned. Briefly, Phosphodiesterase 4B1, one of many DISC1 interaction partners, is involved in mitochondrial trafficking and mutations of *DISC1* lead to impairment of mitochondria. Additionally, reactive oxidative species and glutathione antioxidant

levels were also associated with SZ. Hence, the influence DISC1 on mitochondria should be investigated

As mentioned in *Chapter 1.1.1.3*, one of the early behavioral sings in the onset of SZ pathology is social isolation. Analysis of social interaction networks (SINs) is a novel aspect of research using *Drosophila*[494]. SIN analysis examines interaction patterns and structures among flies in a circular arena, quantifying social bond strength by interaction frequency or duration. Parameters like degree centrality can measure each fly's social activity, while the clustering coefficient indicates the tendency to form close-knit groups[495–497].

1.5 Unanswered questions

Despite significant progress in understanding protein aggregation in CMIs, several fundamental questions remain unanswered.

Research confirms that proteins aggregate in individuals with CMIs, but it is unclear whether they do so independently or through direct interactions. In NDs, co-aggregation is documented (*Chapter 1.2.1*), but its role in CMIs remains uncertain. Proteins may aggregate in response to common stressors like oxidative stress or form large complexes through direct interactions. Clarifying if protein aggregation is independent event is crucial for understanding its role in CMIs.

Moreover, protein aggregation in CMIs has been observed in several brain regions through different studies (*Chapter 1.2.2*). However, the distribution of these aggregates appears to be inconsistent across studies. In NDs protein aggregation follows a progressive, region-specific pattern (*Chapter 1.2.1*), the same question for in CMIs remains unanswered.

Additionally, genetic factors and environmental stressors may influence protein aggregation. If protein aggregation is widespread in CMIs, it could indicate a novel disease pathway. However, if it occurs only due specific genetic events, it may represent a specific mechanism rather than a general pathology.

Future research addressing these gaps will provide valuable insights into disease pathogenesis and may open new avenues for diagnosis and therapy.

2 Hypotheses and thesis aims

CMIs have complex etiologies involving different genetic and environmental factors. Emerging evidence implicates protein aggregation in CMIs but remains poorly understood. This study investigates the potential for aggregation and co-aggregation of several proteins implicated in CMIs.

Hypotheses

1. NPAS3, DISC1, TRIOBP-1, and CRMP1 can aggregate and become increasingly insoluble in specific brain regions affected by CMIs in suicide victims, patients with SZ, MDD and AD and individuals without prior ND or CMI diagnosis (controls).
2. Their aggregation patterns differ across brain regions.
3. The aggregation of one protein may influence another, potentially through co-aggregation.
4. Genetic mutations, such as NPAS3 V304I, can promote aggregation and alter subcellular localization compared to the wild-type form.
5. Expression of human genes in *Drosophila* induces biochemical and behavioral changes resembling CMIs symptoms.

Thesis Aims

1. Determine whether NPAS3, DISC1, TRIOBP-1, and CRMP1 aggregate and exhibit increased insolubility in the brain.
2. Evaluate the extent and regional distribution of protein I/A to determine whether these patterns are consistent across different brain regions within the same individuals.
3. Investigate whether the aggregation of one protein in the cell can influence another through mechanisms like co-aggregation.
4. Determine whether the NPAS3 V304I mutation alters protein aggregation properties and subcellular localization, and assess how these changes are affected by cellular stress.
5. Develop and analyze a transgenic *Drosophila* model expressing human *DISC1* to determine whether it induces changes relevant to SZ.

3 Materials and methods

If not mentioned differently, all solutions written in this chapter were prepared by dissolving in distilled water.

3.1 Human brain samples collection

Our collaboration partners at Semmelweis University, Budapest collected samples of the human brain. The samples were obtained shortly after death (*post-mortem* interval, PMI, was from 1 to 10 hrs), as part of the Hungary-wide Lenhossék Program, using a micropunch technique, followed by freezing in liquid nitrogen[498,499]. Sample collection was done after obtaining consent from the family or legal permission. Before the analysis, samples were stored at −80°C.

For the initial analysis of I/A proteins, the insular cortex (IC) was collected from 40 individuals (16 from victims of suicide, 18 from control individuals, 6 from patients with diagnosed MDD, and 6 from patients with AD diagnosis) and analyzed. For the follow-up study, samples from the previously mentioned patients were analyzed from other brain regions. To be precise, 70 regions from 19 patients were analyzed: 4 victims of suicide (minimum 3 regions, maximum 6 regions), 1 patient with SZ diagnosis (4 regions), 8 control individuals (minimum 2 regions, maximum 7 regions), 4 patients with diagnosed MDD (minimum 2 regions, maximum 5 regions) and 2 patients with AD diagnosis (2 and 6 regions). For additional experiment, 20 tissue samples (10 regions from each hemisphere) from a patient with diagnosed SZ and AD were used. Additionally, 3 patients with diagnosed SZ (1 region each) were included. Controls were samples from 4 control individuals (minimum 4, maximum 8 regions) and 5 patients with AD (minimum 3, maximum 8 regions), totaling 72 regions. More information about samples can be found in **Tables 1-3**.

Table 1: Demographic data for samples used in *Chapter 4.1* Analysis was done with one-way ANOVA in GraphPad.

	n	Sex (number, percent)		Age (years)			PMI (hrs)	
		Male	Female	Average	SEM	p_{tukey} vs control	Average	SEM
Suicide	16	11 (69%)	5 (31%)	47	4	0.023	4*	0.4*
Control	18	11 (61%)	7 (39%)	63	3		4	0.5
MDD	6	2 (33%)	4 (67%)	77	8	<.001	7	0.7
AD	6	2 (33%)	4 (67%)	81	6	<.001	5	0.3

Table 2: Demographic data for samples used in *Chapter 4.1.7* Analysis was done with one-way ANOVA in GraphPad.

	n	Sex (number, percent)		Age (years)		PMI (hrs)	
		Male	Female	Average	SEM	Average	SEM
SZ	1	0 (0%)	1 (100%)	79	0	6	0
SZ/AD	1	1 (100%)	0 (0%)	74	0	6	0
Control	4	3 (75%)	1 (25%)	55	3	6	0.9
AD	5	3 (60%)	2 (40%)	74	5	5	0.6

Table 3: List of brain regions used in *Chapter 4.1*

AD			
Patient Code	**Region**	**Patient Code**	**Region**
A1	IC	A4	IC
	BA17		BA17
	LOG		LOG
	FC		FC
	BA4		TC
	BA 3, 1, 2		PiFC
	PC		PC
A2	IC		PiFC
	BA4	A5, A1	IC
	BA 3, 1, 2		FC

C					
Patient Code	**Region**	**Patient Code**	**Region**	**Patient Code**	**Region**
C1	IC	C7	IC	C11	IC
C2	IC		LOG	C12	IC
C3	IC		BA4	C13	TC
	TC		PiFC		BA9
C4	IC		BA 3, 1, 2		PiFC
	LOG		PC		SFG
	BA4		BA17		BA36, 37
	TC	C8	IC		BA9
	BA 3, 1, 2		LOG		FC
	BA17		BA4		SFG

	BA17		IC
	FC		BA17
	PC		TC
	LOG		BA4
A2	BA6a		BA6a
	BA6a		BA21
	BA36, 37		BA36, 37
	BA36, 37		PC
	BA21		BA4
	BA21		BA6a
	BA4		BA21
	BA4		BA36, 37
	TC		PC
	TC	A6	BA 3, 1, 2
A3	IC		BA17
	LOG		TC
	BA4		PiFC
	PiiFC		
	BA 3, 1, 2		
	BA17		
	PC		

	FC		BA 3, 1, 2		BA36, 37
C5	IC		BA17	C14	IC
	FC		PiFC		LOG
	BA17	C9	IC		BA6a
	PiFC		BA 3, 1, 2		PC
	BA4		BA4		TC
	BA 3, 1, 2		BA17		PiFC
C6	IC		FC	C15	IC
	LOG		PC		LOG
	BA17	C10, C4	IC		FC
	FC		BA6a		BA6a
	BA4		BA6a		PC
	PC		BA36, 37	C16	IC
	BA 3, 1, 2		BA36, 37	C17	IC
	TC		BA21	C18	IC
	PiFC		BA21		
			BA4		
			BA4		
			PC		
			PC		

SZ		MDD	
Patient Code	**Region**	**Patient Code**	**Region**
R	BA9	D1	BA4
	BA36, 37		BA 3, 1, 2
	SFG		BA17
	BA6a		TC
	TC	D2	IC
	FC		TC
	LOG		BA17
	BA21		PC
	BA4		BA 3, 1, 2

S			
Patient Code	**Region**	**Patient Code**	**Region**
S1	IC	S10	IC
	BA4	S11	IC
	BA 3, 1, 2		FC
	TC		LOG
	BA17		PiFC
	PiFC		BA17
S2	IC		BA 3, 1, 2
S3	IC		BA4
S4	IC	S12	IC

	BA4		BA4
	BA17		LOG
	PC		FC
	BA9	D3	IC
	BA6a		TC
	BA36, 37		BA4
	SFG		BA17
	TC		FC
	LOG		PC
	FC		BA 3, 1, 2
	BA4		PiFC
	BA21		BA6a
	PC		TC
	BA 3, 1, 2	D4	IC
	BA17		TC
	PC		PC
	TC		BA17
SZ1	FC	D5	IC
	BA4		LOG
	BA 3, 1, 2		PiFC
	LOG		BA17
		D6	IC
			LOG
			PiFC

S5	IC	S13	IC
	BA17		BA4
	BA4		TC
	BA 3, 1, 2		FC
	PiFC		PC
	TC		BA 3, 1, 2
S6	IC		LOG
	FC		BA17
S7	IC	S14	IC
S8	IC		TC
	FC		PiFC
S9	IC		LOG
	BA 3, 1, 2		PC
	BA4	S15	IC
	PiFC	S16	IC
	TC		
	PC		
	BA17		
	LOG		

Samples were matched according to age and sex, if possible. All data was anonymized and further encoded during all experiments; only after quantification was data decoded.

Ethical approval for collecting brain samples was granted by the Committee of Science and Research Ethics of the Ministry of Health of Hungary (6008/8/2002/ETT) and the Semmelweis University Regional Committee of Science & Research Ethics (31/1992/TUKEB). The analysis of brain samples was approved by The Ethical Committee of the University of Rijeka, Faculty of Biotechnology and Drug Development (18.02.2022-Bradshaw).

3.2 I/A protein fraction purification from brain samples

The optimized version of method was used to isolate I/A protein fraction, which includes aggregating proteins, as previously published [320,464]. The diagnostic status of samples was blinded.

Specifically, obtained brain tissue was homogenized to a 10% (w/v) concentration in Buffer A (50mM HEPES pH 7.5 H3375, Sigma-Aldrich; 250mM sucrose, S9378, Sigma-Aldrich; 5mM magnesium chloride; 100mM potassium acetate; 2mM PMSF), with the addition of 1%Triton (X100, Sigma-Aldrich) and 1xProtease Inhibitor Cocktail (11873580001, Sigma-Aldrich). A small fraction of the sample (100µL was taken and labeled as "homogenates," representing the whole protein fraction of samples.

The 400µL of the sample was transferred to an ultracentrifugation tube (S5007, Science Services or 343777, Beckman Coulter) and centrifuged at 20000× g for 20 min at 4°C in Sorvall MTX ultracentrifuge equipped with an S140-AT fixed-angle rotor or S80-AT2 (Thermo Fisher Scientific).

The supernatant was discarded, and the pellet was resuspended in buffer B: 50mM HEPES pH 7.5, 250mM sucrose, 5mM magnesium chloride, 100mM potassium acetate, 2mM PMSF, 1%Triton, followed by a second centrifugation in the same conditions.

The pellet was resuspended in Buffer C: 50 mM HEPES pH 7,5, 1,6M sucrose, 5mM magnesium chloride, 100mM potassium acetate, 2mM PMSF, 1%Triton, followed by centrifugation at 130000× g for 45 min at 4°C.

The buffer D: 1.5mM HEPES pH7.5, 7.5mM sucrose, 0.15mM magnesium chloride, 1.33mM potassium acetate, 0.06mM PMSF, 1M sodium chloride, 100U/mL DNaseI, was used for resuspension of the pellet. The solution was transferred from the ultracentrifuge tube to the microcentrifuge tube, laid on its side, and incubated for the night in the fridge at 4 °C.

The following day, the solution was transferred to previously used ultracentrifugation tubes and centrifuged at 130000× g for 45 min at 4°C. The pellet was washed in buffer E: 10mM HEPES pH 7.5, 5mM EDTA, 0.5% sarkosyl, and centrifuged, again at 130000× g for 45 min

at 4°C. The removal of the supernatant, washing of the pellet, and centrifugation were repeated.

After the final centrifugation, the remaining pellet ("I/A protein fraction") was transferred to a microcentrifuge tube and resuspended in 2×Protein loading buffer: 4% (w/v) sodium dodecyl sulfate (SDS, 74255, Sigma-Aldrich), 20% glycerol (15523, Merck), 120mM Tris-Cl pH 6.8, 0.02% (w/v) bromophenol blue (114391, Sigma-Aldrich), and 1M DTT for subsequent Western blot analysis. This process is summarized in **Figure 5**.

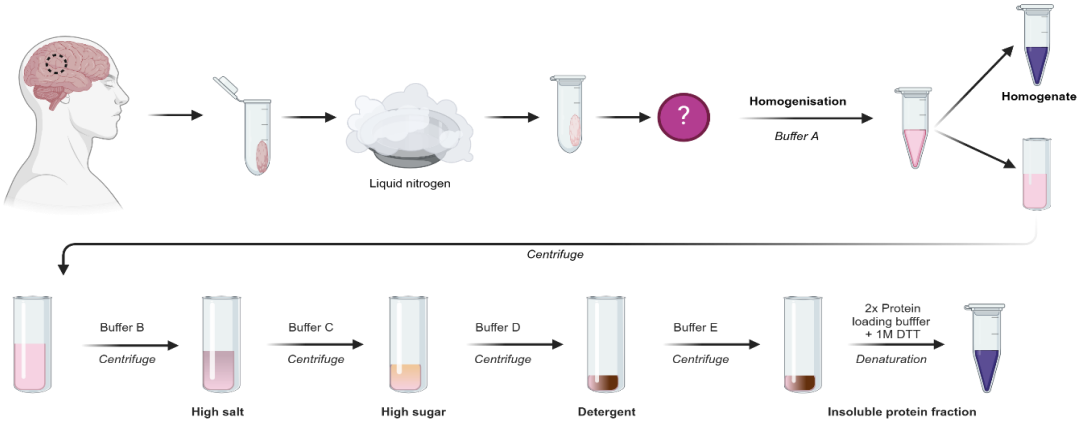

Figure 5: Purification of I/A protein fraction from brain tissue samples protocol. The scheme was created with BioRender. DTT – dithiothreitol.

3.3 Bacterial transformation

Competent NEB5α *E.coli* bacterial cells (C2987I, New England Biolabs) were transformed with plasmids containing the gene of interest. For each transformation, 1µL of plasmid DNA was added to the 50µL of freshly thawed NEB5α cells in a 1.5mL microcentrifuge tube and incubated on ice for 30 min. This amounts of plasmid DNA and bacteria have been empirically optimized for reliable transformation efficiency in our lab.

A heat shock facilitated the transformation at 42°C for 30 sec, followed by a 5 min recovery period on ice. The transformed cells were then plated on Luria—Bertani (LB) agar: 10g/L tryptone (95039, BioChemika), 5g/L yeast extract (92144, Sigma-Aldrich), 10g/L sodium chloride (P148590, GramMol), supplemented with 100µg/mL ampicillin (K029.4, Carl Roth).

Plates with bacterial cells were incubated overnight at 37°C in the incubator (Gallenkamp). The following day, a single colony was

selected and grown overnight in 3 mL LB media: 10 g/L tryptone, 5 g/L yeast extract, 10g/L sodium chloride, 20g/L agar (92144, Sigma-Aldrich) containing 100µg/mL ampicillin in an incubator with orbital shaker SI600C Stuart, set at 37°C and 150 rpm.

Post-cultivation, the bacterial culture was centrifuged at 3700 rpm for 10 min in the 5920 R centrifuge (5948, Eppendorf). The pellet was processed for plasmid DNA extraction. This process is summarized in **Figure 6**.

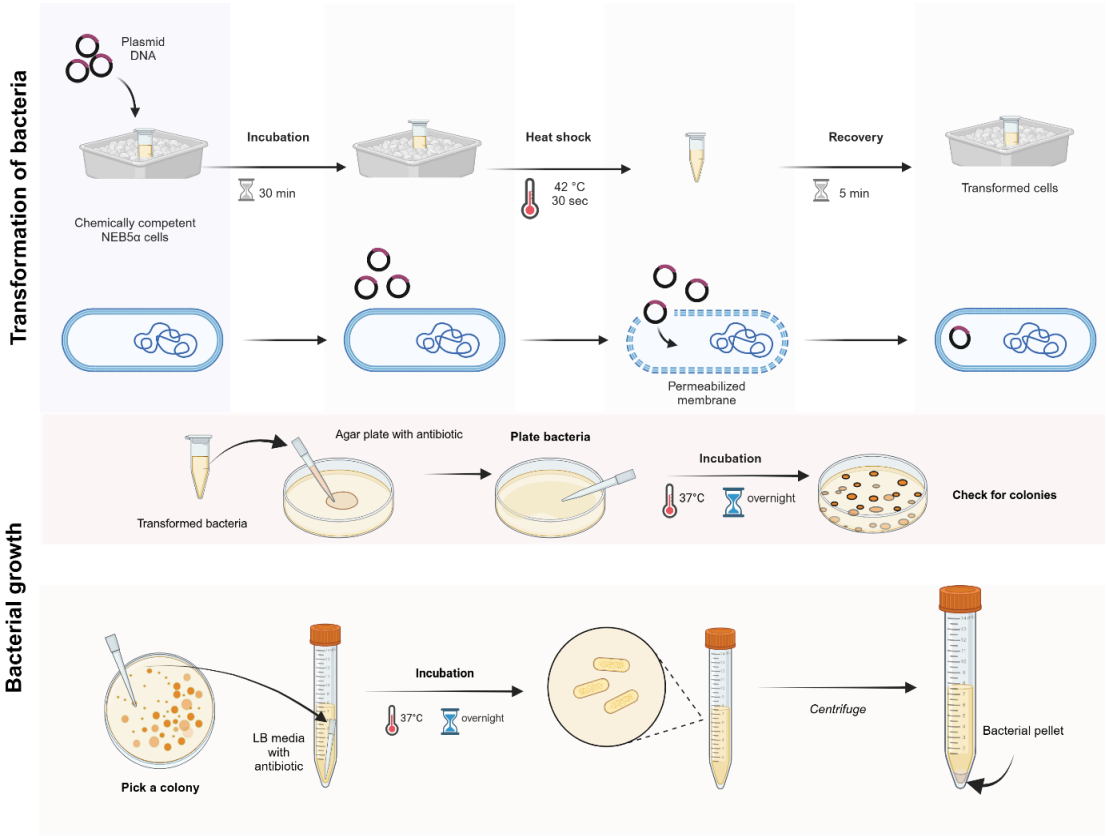

Figure 6: Bacterial transformation protocol. The scheme was created with BioRender. sec – seconds, min – minutes, LB media - Luria—Bertani media

3.4 Plasmid DNA extraction

Plasmid DNA extraction was done using the QIAprep Spin Miniprep Kit (27106, Qiagen) in accordance with the manufacturer's instructions.

Briefly, pelleted bacterial cells were resuspended in 250µL Buffer P1 and transferred to a microcentrifuge tube, followed by the addition of 250µL Buffer P2 and thorough mixing by inversion. After adding 350µL Buffer N3, the solution was inverted again and centrifuged at 13000 rpm for 10 min. The supernatant was applied to a QIAprep Spin

Column and centrifuged, followed by washing with Buffer PE and a final spin to remove residual wash buffer. Finally, DNA was eluted by adding 50µL Buffer EB: 10mM Tris-Cl, pH8.5 to the column and centrifuging for 1 min.

The concentration of the extracted plasmid DNA was quantified using a BioDropDuo spectrophotometer (BD1607, BioDrop, software version 7144 V1.0.4), with absorbance measured at 230, 260, and 280nm. Elution buffer (Buffer EB) served as the blank, and plasmid DNA concentrations were reported in µg/mL. This process is summarized in **Figure 7**.

3.5 DNA agarose gel electrophoresis

Plasmid integrity was confirmed by size determination after agarose gel electrophoresis. The buffer used for agarose gel electrophoresis was 1xTAE buffer: 40mM Tris-Cl pH6.8 (93362, Sigma-Aldrich), 1mM ethylenediamine tetraacetic acid (EDTA, 20301.186, Sigma-Aldrich) and 200mM acetic acid (607-002-006, Honeywell).

1% agarose gel was cast with electrophoresis apparatus (13-55-1094, Edulab). Gel was prepared by stirring with heat and by dissolving agarose (10-35-1010, Bio-Budget) in a 1xTAE buffer. After the cooldown, myBudget DNA Stain Green (87-1000-G, Bio-Budget) was added. Samples were diluted with 10x FastDigest Green Buffer (B72, Thermo Scientific) and loaded on the gel, along with myBudget 1kb DNA-Ladder (85-1000-250, Bio-Budget).

The gel electrophoresis was performed with PowerPac (1645070, BioRad) at 120V for 20 min, while the DNA bands on the gel were visualized with ChemiDoc MP Imaging System Universal Hood III (170-8280, BioRad) on the software ImageLab 5.2 with setting Nucleic Acid Gels-SYBR Green. This process is summarized in **Figure 7**.

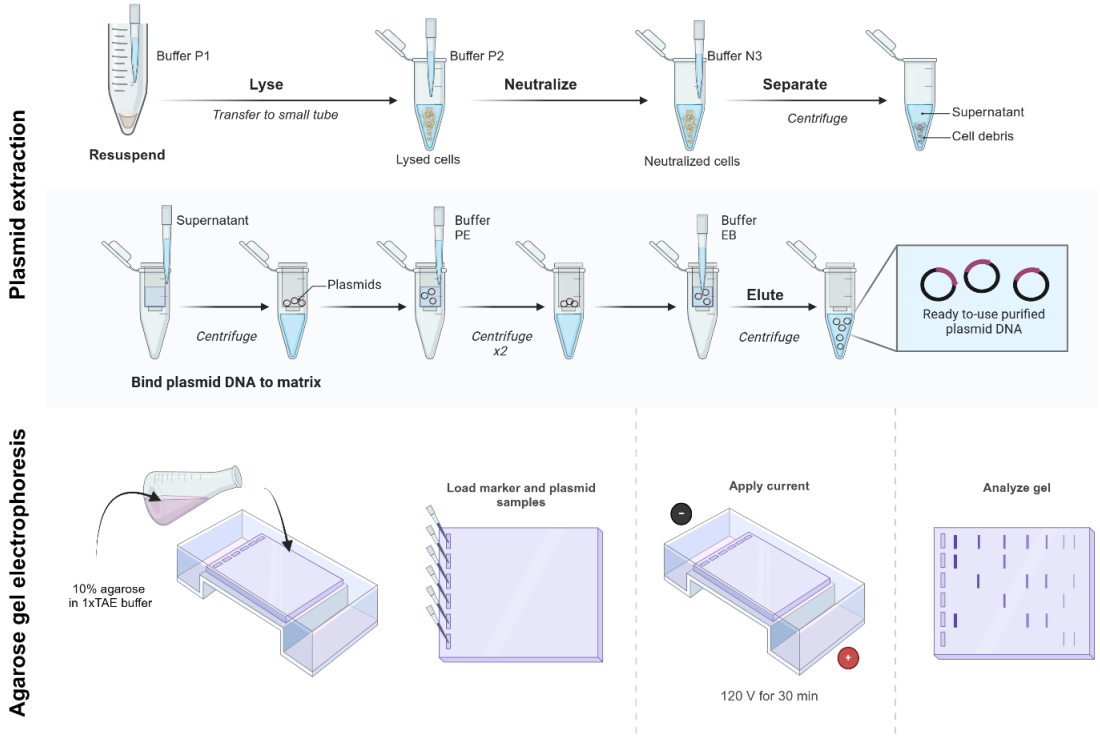

Figure 7: Plasmid DNA extraction and agarose gel electrophoresis protocol. The scheme was created with BioRender. V – volt, min - minutes

3.6 Mammalian cell culture maintenance

The HEK293 (human kidney, CRL-1573, American Type Culture Collection) and the SH-SY5Y (human neuroblastoma, ACC 209 Deutsche Sammlung von Microorganism und Zellkulturen) cell lines were both grown in cell culture flask T-25 (83.3910.002, Sarstedt) in the incubator at 37°C and 5% CO_2 (Z10.EC 160, NUVE).

For HEK293 cells, media D-MEM (41965039, Thermo Fisher Scientific) was used, supplemented with 10%Fetal Bovine Serum (F7524, Sigma-Aldrich) and 1xPenicillin-Streptomycin (P06-07100, PAN Biotech).

For SH-SY5Y cells, media DMEM:F12 (31330038, Thermo Fisher Scientific) was used with the addition of 1xMEM non-essential aa w/o L-Glutamine (P08-32100PAN, Biotech), 10%Fetal Bovine Serum and 1xPenicillin-Streptomycin.

The cells were split when the confluency reached 90% or more with Trypsin (P10-019500, PAN Biotech, 0.25%EDTA, 0.02%, in PBS w/o: Ca^{2+} and Mg^{2+}). For experiments, the cells were grown in either 6-, 12- or 24-well plates (83.3920-2, Sarstedt).

3.7 Mammalian cell transfection

For cell transfection with constructs, two types of solutions per well were prepared: one containing 0.5µg per plasmid DNA and 100µL of media (without serum or antibiotics), other containing 100µL media with 2µL of transfection reagent. SH-SY5Y cells were transfected using Metafectene Pro (T040-2.0, Biontex), while HEK293 cells were transfected with Metafectene (T020-1.0, Biontex). The DNA and transfection reagent solutions were incubated separately for 5 min, then mixed and incubated for an additional 30 min at 37°C.

The mixtures were subsequently added to plates and incubated for 6 hrs. After 6 hrs, the media were replaced with fresh media containing serum and antibiotics. Additionally, some transfections of HEK293 or SH-SY5Y cells included treatment with the 1µM proteasome inhibitor MG-132 (282T2154, TargetMol) for 30 min after the initial 6 hrs transfection period. After incubation, cells were either lysed or fixed. For co-aggregation experiments, two different plasmids with two different genes and different tags were included. Plasmids were also tested against plasmids containing tags only as a control and all used plasmids are listed in **Table 4**. This process is summarized in **Figure 8**.

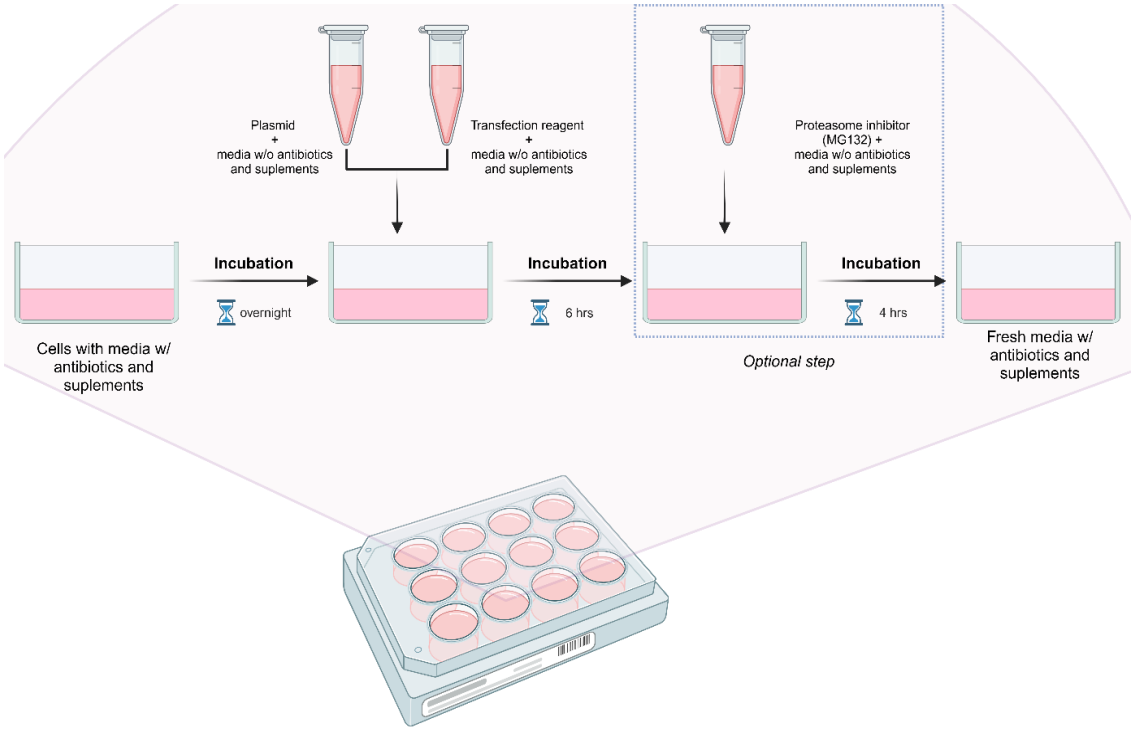

Figure 8: Mammalian cell transfection. w/o – without, w/ - with, hrs – hours, The scheme was created with BioRender.

Table 4: Plasmids used for cell transfection of mammalian cells

Vector	Gene	Source
pCI-HA	none	Gift by Fred Berry[423]
pCI-HA	NPAS3 wt	Gift by Fred Berry[423]
pCI-HA	NPAS3 mt (V304I)	Gift by Fred Berry[423]
pCI-HA	NPAS3 (116-450 aa, PAS)	Gift by Fred Berry[423]
pCI-HA	NPAS3 (116 – 933 aa, PAS-TAD)	Gift by Fred Berry[423]
pdcDNA-Flag	NPAS3 (1-111 aa)	Rijeka[500]
pdcDNA-Flag	NPAS3 (1-156 aa)	Rijeka[500]
pdcDNA-Flag	NPAS3 (1-208 aa)	Rijeka[500]
pdcDNA-Flag	NPAS3 (1-354 aa)	Rijeka[500]
pdcDNA-Flag	DISC1 full-length	Rijeka[501]
pdcDNA-Flag	DISC1 (257- 655 aa)	Rijeka[502]
pDEST-CMV-N-mCherry	(Gateway cassette)	Addgene,clone 123215[503]
pDEST-CMV-N-mCherry	NPAS3 wt	Rijeka[500]
pDEST-CMV-N-EGFP	(Empty control)	Rijeka[501]
pDEST-CMV-N-EGFP	CRMP1 Sv	Rijeka[501]
pDEST-CMV-N-EGFP	CRMP1 Lv	Rijeka[501]
pDEST-CMV-N-EGFP	DISC1	Rijeka[501]
pDEST-CMV-N-EGFP	NPAS3	Rijeka[501]
pDEST-CMV-N-EGFP	TRIOBP-1	Rijeka[501]
pdcDNA-Flag	CRMP1 Sv	Rijeka[501]
pdcDNA-Flag	CRMP1 Lv	Rijeka[501]
pdcDNA-Flag	DISC1	Rijeka[501]
pdcDNA-Flag	NPAS3	Rijeka[501]
pdcDNA-Flag	TRIOBP-1	Rijeka[501]

3.8 Sodium arsenite cellular stress test

Cells were treated with sodium arsenite (5μM) after a minimum of 14 hrs since the end of the transfection. A sodium arsenite solution was prepared in fresh media (containing serum and antibiotics). The cells were treated for 30 min in the incubator at 37°C and 5% CO_2, after which the cells were fixed according to the protocol described in *Chapter 3.14.*

3.9 I/A protein fraction purification from mammalian cell lysates

The method for purification of I/A protein fraction from mammalian cell lysates was previously published[320].

Lysis of transfected HEK293 cells was done in the lysis buffer: 50mM HEPES pH 7.5, 250mM sucrose, 5mM magnesium chloride, 100mM potassium acetate (P1147, Sigma-Aldrich), 2mM Phenylmethylsulfonyl fluoride (PMSF, PMSF-RO, Roche), 1xProtease Inhibitor Cocktail, 1%Triton, followed by 30 min incubation on a rotary wheel at room temperature.

A portion of the lysate was preserved (later called "lysate"), while the remaining lysate was used to purify the I/A protein fraction. Samples were transferred to ultracentrifugation tubes (11x34mm, S5007, Science Services) and centrifuged for 20 min at 20000×g and 4°C (S140-AT fixed-angle rotor in MTX 150 Micro-Ultracentrifuge, Sorvall). The supernatant was discarded, and the previous step was repeated with the pellet.

After the second centrifugation, the pellet was resuspended in new buffer A1 (50 HEPES, pH 7.5, 1.6M sucrose, 100mM potassium acetate, 1%Triton, 1mM PMSF) and centrifuged for 45 min at 130000×g and 4°C. The supernatant was discarded, and the previous step was repeated with the pellet.

After the second centrifugation, the pellet was transferred to a sterile microcentrifuge tube, where it was resuspended in buffer B1 (50mM HEPES, pH7.5, 1M sodium chloride, 20mM magnesium chloride; 30mM calcium chloride (C1016, Sigma-Aldrich), 2U/mL DNaseI, 1xProtease Inhibitor Cocktail and incubated over the night at 4°C.

The following day, samples were returned to their original ultracentrifuge tubes and centrifuged for 45 min at 130000×g and 4°C. The supernatant was removed, and the pellet was resuspended in buffer B1, previously described, but this time without DNaseI, once again followed by centrifugation for 45 min at 130000×g and 4°C.

The pellet was then dissolved in a buffer C1 (50mM HEPES, pH7.5, 0.5% sarkosyl) using an insulin syringe and needle 0.4mm, followed by 1h incubation on ice and on the shaking tray. After incubation, samples were centrifuged for 45 min at 112000× g and 4°C. Once again, the previous step was repeated but this time without incubation on ice.

Finally, the pellet ("I/A protein fraction") was resuspended in 2xProtein Loading Buffer. Also, the 1M dithiothreitol, DTT (D0632, Sigma-Aldrich), was added to each sample, followed by denaturation at 95°C for 5min. This process is summarized in **Figure 9.**

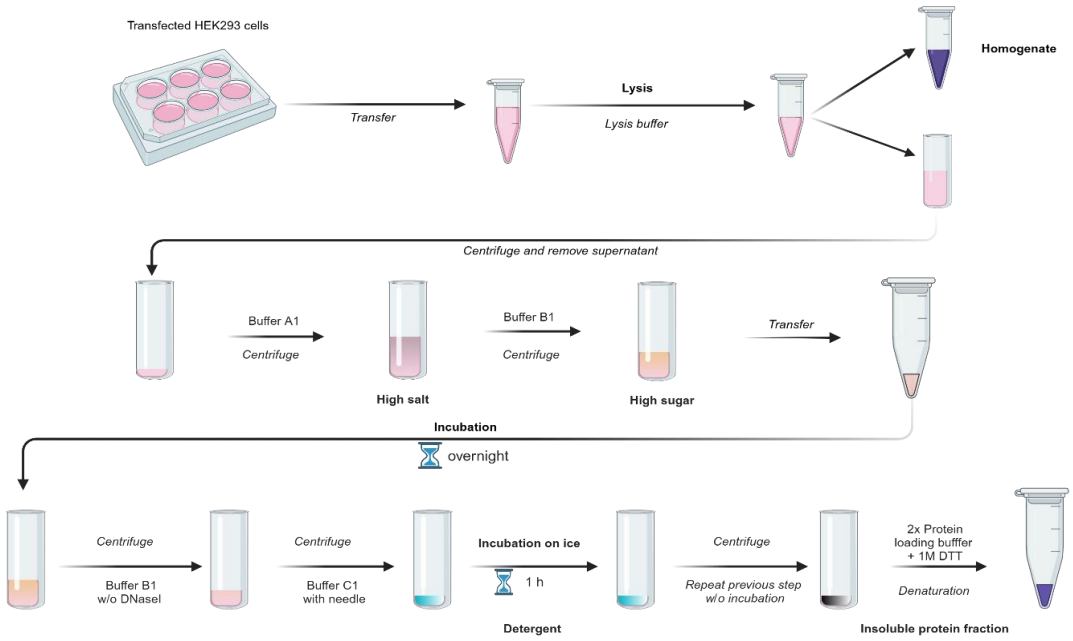

Figure 9: Purification of I/A protein fraction from cells protocol. The scheme was created with BioRender. h – hour, w/o – without, DTT – dithiothreitol.

3.10 Cell lysis

The day following transfection, HEK293 cells were washed twice with 1xPhosphate-Buffered Saline, PBS: 137mM sodium chloride, 2.7mM potassium chloride (P9333, Sigma-Aldrich), 10mM disodium

hydrogen phosphate (7164, Sigma-Aldrich), 1.8mM potassium dihydrogen phosphate (26936.293, VWR Chemicals).

Subsequently, 100 µL of Cell Lysis Buffer: 1xPBS, 1%Triton, 20mM magnesium chloride (P139120, Grammol), 2U/mL DNaseI (M0303L, New England Biolabs), 1xcOmplete (TM), EDTA-free, 1xProtease Inhibitor Cocktail, was added per well and incubated for 5 min.

The lysed cell suspensions were then scraped from the plates, transferred to 1.5 mL microcentrifuge tubes, and incubated on ice for 30 min with gentle rotation. The samples were prepared for SDS-PAGE analysis as previously described. This process is summarized in **Figure 10**.

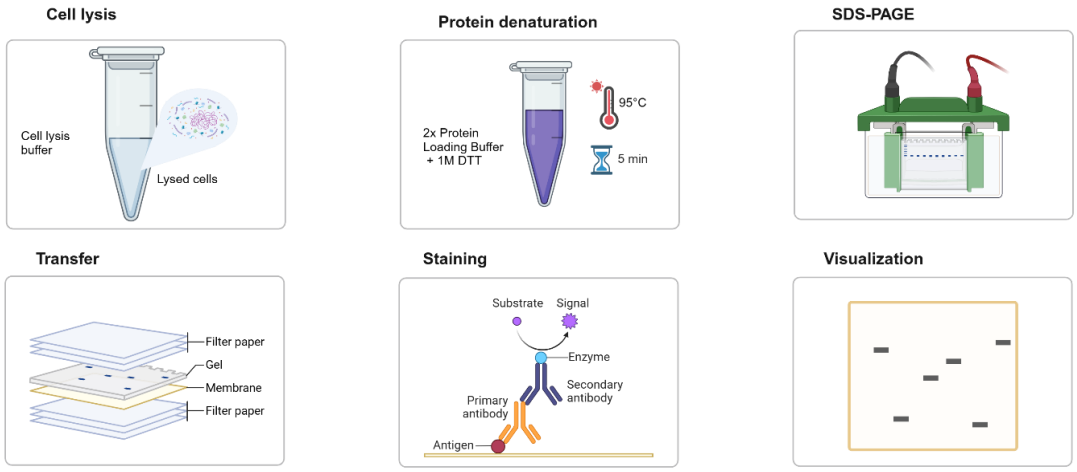

Figure 10: Cell lysis, SDS-PAGE and Western blot protocol. The scheme was created with BioRender. M – mol/L, DTT – dithiothreitol

3.11 Sodium Dodecyl Sulfate Polyacrylamide Gel Electrophoresis

Bis-acrylamide gels were cast using Mini-PROTEAN® Tetra Cell Casting Stand with Clamp Kit (1658051, BioRad). The percentage of acrylamide in resolving gel depended on the protein size, usually 8-12%. Besides the acrylamide mix (30% w/v acrylamide A8887, Sigma-Aldrich and 1% w/v N, N-Metylenbisacrylamide, 43701.14, Alfa Aesar), resolving gel contained: Tris-Cl 1.5 M pH 8.8, 1% SDS, 1% ammonium persulfate (APS, A3678, Sigma-Aldrich) and N,N,N′,N′-Tetramethylethylenediamine (TEMED, T7024, Sigma-Aldrich). 2,2,2 trichloroethanol (TCE, T54801, Sigma-Aldrich) was added to the resolving gel when total protein was analyzed in the samples. Resolving

gel was followed by the stacking gel (5% acrylamide, Tris-Cl 1.0M, pH 6.8, 1% SDS, 1% APS and TEMED). The samples were loaded onto the acrylamide gels and a my-Budget Prestained Protein Ladder (10 kDa - 180 kDa, 86-1000, Bio-Budget). Sodium Dodecyl Sulfate Polyacrylamide Gel Electrophoresis (SDS-PAGE) was run in Mini-PROTEAN Tetra cell with PowerPac (1645070, BioRad) at 140V for 1.5 hrs using 1xTris-glycine buffer: 25mM Tris-Cl, 250mM glycine (33226, Sigma-Aldrich), 0.1% SDS. This procedure facilitated the separation of protein samples based on their molecular weight. After electrophoresis, the gels were washed once with distilled water. If gels were prepared with the addition of 2,2,2-Trichloroethanol (TCE, T54801, Sigma-Aldrich), the proteins were visualized on ChemiDoc MP Imaging System (170-8280, Bio-Rad), using StainFree Blot option in software ImageLab 5.2. This process is summarized in **Figure 10**.

3.12 Western blot

Following SDS-PAGE, the gels were transferred to a Parablot PVDF membrane (0.2µm pore, 741260, Macherey-Nagel) using a Transblot Turbo Transfer system (1704151, Bio-Rad) with the default Bio-Rad settings for 30 min. The membrane was then stained with 0.5% Ponceau S (5938.2, Roth)/2% acetic acid to verify sample transfer.

To block non-specific binding, the membrane was incubated with 5% non-fat dried milk powder (A0830, PanReac AppliChem) in 1xPBS-T: 1xPBS with 0.05% Tween (P1379, Sigma-Aldrich) for a minimum of 1 h on a shaker at room temperature, or overnight at 4°C in most cases. Exceptionally, membranes used in *4.1.2 Figure 19* and *Figure 23*, were blocked with Aqua Block (ab166952, Abcam). Subsequently, the membrane was incubated overnight at 4°C with the primary antibody (as detailed in **Table 5**) diluted in 1xPBS-T. The next day after washing in the 1xPBS-T buffer, the membrane was incubated with secondary antibodies (listed in **Table 5**) for 1 hour at room temperature with shaking. After each incubation step, the membrane was washed three times with PBS-T over a 20 min period.

Protein bands were visualized using Pierce ECL Western Blotting Substrate (32209, Thermo Fisher Scientific) or ECL Prime Western Blotting Detection Reagent (RPN2236, Cytiva) on a ChemiDoc MP Imaging System (170-8280, Bio-Rad), with the Chemi High Sensitivity setting in software ImageLab 5.2. This process is summarized in **Figure 10**.

Table 5: List of antibodies used for Western blot

Name with catalogue number	Antigen	Type	Supplier	Concentration	Dilution
Anti-Flag M2 (F1804)	FLAG® peptide sequence at the N-terminus, Met-N-terminus, C-terminus, or internal sites of a fusion protein	Monoclonal mouse primary antibody	Sigma-Aldrich	1 mg/mL	1:2000
Anti-HA Antibody Clone HA-7	synthetic peptide corresponding to aa residues YPYDVPDYA (98-106) of the human influenza virus hemagglutinin (HA)	Monoclonal mouse primary antibody	Sigma-Aldrich	1 mg/mL	1:1000
Anti-NPAS3 antibody (PK-AB718-4107)	N-terminus of NPAS3	Monoclonal rabbit primary antibody	PromoKine	1 mg/mL	1:1000
Anti-NPAS3 antibody (4107)	N-terminus of NPAS3	Polyclonal rabbit primary antibody	ProSci	1 mg/mL	1:1000
Anti-TRIOBP Antibody (HPA019769)	Recombinant Protein Epitope Signature Tag (PrEST)for TRIOBP	Polyclonal rabbit primary antibody	Atlas Antibodies	0.2 mg/mL	1:1000
Anti-DISC1 Polyclonal Antibody (40-6800)	synthetic peptide derived from the C-terminal region of the mouse DISC1	Polyclonal rabbit primary antibody	Invitrogen	0.25 mg/mL	1:1000

CRMP1 Antibody (3625)	aa 290 - 340 of CRMP1	Polyclonal rabbit primary antibody	ProSci	1 mg/mL	1:1000
Anti-β actin, clone OTI1 (TA811000)	synthetic peptide corresponding to the N terminal of human beta-actin	Monoclonal mouse primary antibody	OriGene	1 mg/mL	1:1000
Anti-Actin Antibody, clone C4 (MAB1501)	chicken gizzard muscles actin	Monoclonal mouse primary antibody	Sigma	2 mg/mL	1:10000
Anti-β-Actin−Peroxidase antibody, clone AC-15 (A3854)	epitope located on the N-terminal end of the β-isoform of actin	Monoclonal mouse primary antibody Peroxidase Conjugated	Sigma-Aldrich	2 mg/mL	1:10000
Peroxidase Conjugated Affinity Purified Goat anti-Mouse IgG (31430)	Mouse IgG	Polyclonal goat secondary antibody	Thermo Fisher	1 mg/mL	1:2000 – 1:1000
Peroxidase Conjugated Affinity Purified Goat anti-Rabbit IgG (65-6120)	Rabbit IgG	Polyclonal goat secondary antibody	Invitrogen	1 mg/mL	1:2000 – 1:10000

3.13 Gels and Western blot quantitative analysis

The Band Analysis tools of ImageLab software (5.2, Bio-Rad) were used to select and determine the volume of the bands in all the gels and blots. Background signal was subtracted by default settings (referred to in the software as "Adjusted Volumes"). The signal from the protein of interest was normalized either to actin level or total protein level (after stain-free imaging using TCE). If possible, membranes were normalized among themselves based on a common sample.

3.14 Immunocytochemistry and microscopy

Transfected SH-SY5Y cells growing on glass coverslips were gently washed with 0.5mL 1xPBS, fixed with 4%formaldehyde solution, buffered pH 6.9 (1.00496.0700, Merck) for 15 min, and permeabilized with 1%Triton in 1xPBS for 10 min at room temperature. Coverslips were then washed three times with 1xPBS and blocked with 10% goat serum (G9023, Sigma-Aldrich) in 1xPBS for a minimum of 30 min, usually for 45 min, at room temperature with shaking. The blocking medium was removed, and the fixed cells were stained with primary antibody (listed in **Table 6**) diluted 1000-fold in 10% goat serum/1xPBS for a minimum of 3 hrs at room temperature with shaking. Cells were washed three times with 1xPBS over a period of 15min and incubated with the secondary antibody (also listed in **Table 6**) and nuclear stain in 10% goat serum/1xPBS for 1h in the dark at room temperature with shaking. For single plasmid transfections, F-actin binding probe (Acti-stain™ 488 Fluorescent Phalloidin, PHDG1-A, Cytoskeleton) was also used. The cells were washed three times with PBS and once distilled water and attached to slides with commercial mounting medium Fluoroshield (F6182, Sigma-Aldrich).

The coverslips were observed on an Olympus IX83 fluorescent microscope with 20x and 60x objective. Images were taken using an Orca R2 CCD camera (Hamamatsu Photonics, C10600-10B) and CellSens software (Olympus, 1.18), while further analysis was done on ImageJ 1.52p (National Institute of Health) or Fiji 2.15.1 (National Institute of Health). This process is summarized in **Figure 11**.

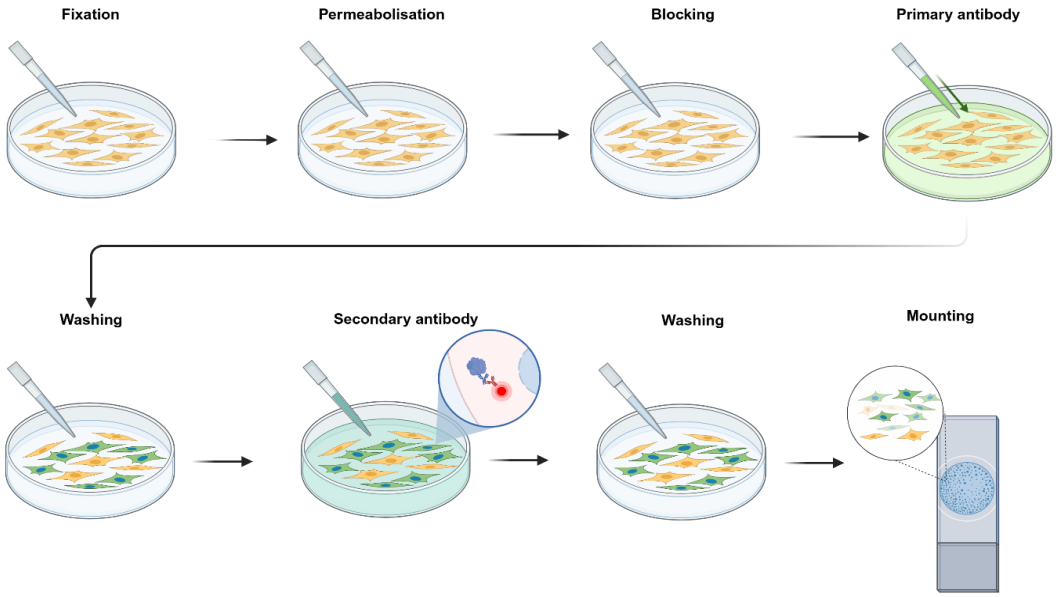

Figure 11: Immunocytochemistry protocol. The scheme was created with BioRender.

3.15 Quantitative blinded immunocytochemistry assay

During quantitative blinded immunocytochemistry assays, samples used for transfection of cells were coded and randomized, ensuring that I remained blinded to the specific plasmid present in each tube. The samples stayed blinded during the immunocytochemistry and image acquisition until quantitative analysis was done. Images of the first 10 (or as many as could be found if 10 were not available) transfected cells per coverslip were taken and analyzed. For the purposes of quantification, an "aggregate" was defined as any compact area of intense signal larger than 1 µm in diameter. All obtained quantitative data was statistically analyzed after decoding, either by JASP (0.19.0, JASP Team) or Prism (10.2.3, GraphPad), for comparisons between two or more groups with a single variable, a one-way ANOVA with Brown-Forsythe correction for homogeneity was applied, with statistical significance defined as $p<0.05$. When three or more groups were compared, Tukey's post hoc test was used, with statistical significance set at $p<0.05$. In the analysis of quantitative blinded immunocytochemistry assays, a nominal value of 0.1% was assigned to a sample if all sample replicates were zero. Comparisons between two groups involving two variables were conducted using multivariate or two-way ANOVA, with statistical significance criteria of $p<0.05$.

Table 6: List of antibodies, probes, and dyes used for immunocytochemistry

Name (catalogue number)	Type	Antigen or specificity	Host	Supplier	Concentration	Dilution
Anti-Flag M2 (F1804)	Monoclonal primary antibody	FLAG® peptide sequence at the N-terminus, Met-N-terminus, C-terminus, or internal sites of a fusion protein	Mouse	Sigma-Aldrich	1 mg/mL	1:1000
Alexa Fluor Plus 555 (A32727)	Polyclonal secondary antibody	Mouse IgG	Goat	Thermo Fisher	2 mg/mL	1:500
Alexa Fluor Plus 594 (A32742)	Polyclonal secondary antibody	Mouse IgG	Goat	Thermo Fisher	2 mg/mL	1:500
Acti-stain™ 488 Fluorescent Phalloidin (PHDG1-A)	Fluorescent marker	actin filaments	N/A	Cytoskeleton	2 mg/mL	1:500
4',6-Diamidino-2-phenylindole (DAPI, D9542)	Fluorescent marker	double-stranded DNA	N/A	Sigma-Aldrich	1 mg/mL	1:500

3.16 Fly lines and maintenance

A plasmid containing the human full-length *DISC1* (*hflDISC1*) gene sequence was sourced from the DNASU Plasmid Repository (clone HsCD00516321, Arizona State University).

In order to transfer this reading frame into the pPRW vector (RRID, Indiana University, funded by NIH Grant 2P40OD010949), LR clonase II was used (11791020, Thermo Fisher Scientific). During P-element transgenesis, the pPRW-hflDISC1 vector, along with a P-element helper plasmid, was injected into white (w^{1118}) embryos (injection service provided by the Department of Genetics, University of Cambridge). The resulting transformants were balanced using *SM6a* (for the 2nd chromosome) in flies w[1118][iso]/y[+]Y; Sco/SM6a; 3[iso], and *TM6C* (for the 3rd chromosome) in flies w[1118][iso]/y[+]Y; 2[iso]; TM2/TM6C, Sb. Hemizygous flies carrying a transgenic construct with UAS promoter fused to the *hflDISC1* gene, balanced on either the 2nd chromosome (UAS-*hflDISC1*-2nd) or the 3rd chromosome (UAS-*hflDISC1*-3rd) were generated. The graphical summary is shown in **Figure 12**. As a control, the w^{1118} line from the Bloomington Stock Center (5905) was used.

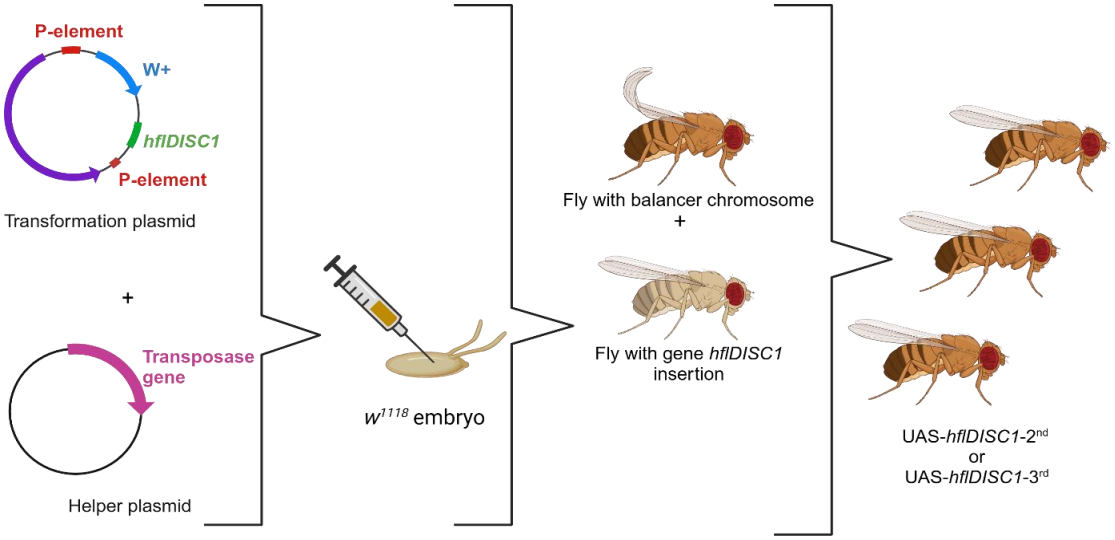

Figure 12: Creation of hemizygous flies carrying a transgenic construct with UAS promoter fused to the *hflDISC1* gene. P-element transgenesis was performed by injecting a pPRW vector and P-element helper plasmid in w^{1118} embryos, which were later crossed with flies carrying balancer chromosome for: *SM6a* (2nd chromosome) or *TM6C* (3rd chromosome. Finally, the generated flies were hemizygous for the *hflDISC1* gene, balanced on the 2nd or 3rd chromosome (UAS-*hflDISC1*-2nd or UAS-*hflDISC1*-3rd). The scheme was adapted from the original created by dr. sc. Lara Saftić Martinović and created in BioRender.

Flies were raised on a standard cornmeal-based medium: sugar, agar, corn flour, and yeast dissolved in water, with added 4-hydroxybenzoic acid methyl ester (nipagin, 3646.4, Carl Roth, dissolved in ethanol) and propionic acid (87062.290, GPR RECTAPUR) to prevent fungal growth. The environmental conditions were maintained at 25 °C, with 70% humidity, and a 12 h light/dark cycle (lights on at 08:00, lights off at 20:00).

The next chapters will describe biochemical and behavioral analyses done for fly lines, with graphical overview shown in **Figure 13**.

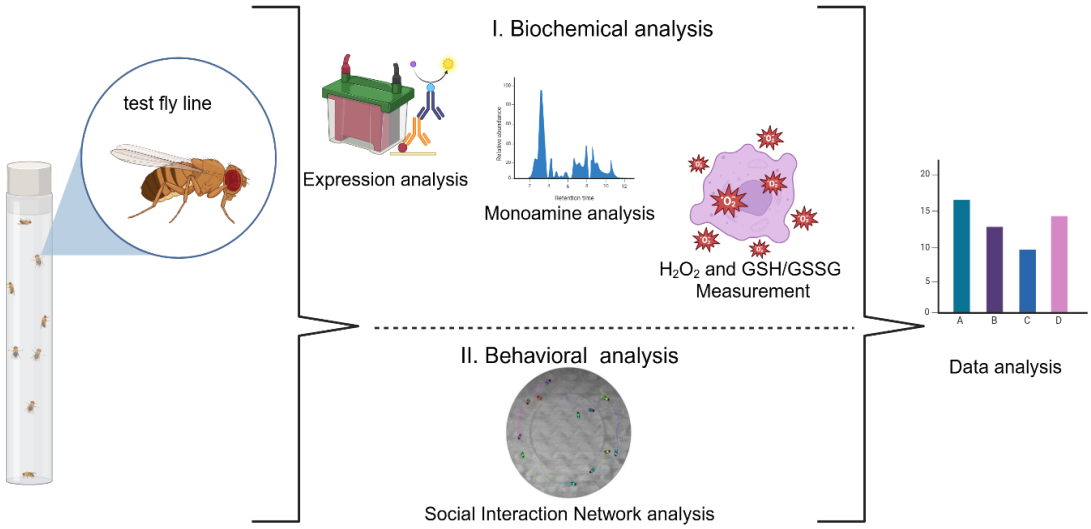

Figure 13: Workflow of analyses done for *hflDISC1* transgenic *Drosophila* model. Adapted from the original figure created by dr. sc. Lara Saftić Martinović in BioRender.

3.17 Biochemical analysis

3.17.1 Gene expression analysis in selected fly lines

Fly homogenates were prepared from 5 headless fly bodies or 20 fly heads per genotype. Samples were lysed on ice for 10min using RIPA buffer: 50mM Tris-HCl, 150mM sodium chloride, 0.1%NP-40, 0.5%sodium deoxycholate, 0.1% SDS, pH 8, supplemented with 1xProtease Inhibitor Cocktail. After centrifugation at 10000 rpm for 45 min at 4 °C in FA-24x2 rotor for 5425R centrifuge (Eppendorf), the protein was precipitated by adding cold acetone, followed by overnight incubation at 4 °C. Protein concentrations were determined using a BioDrop Touch Duo (BD1607).

Precipitated proteins were resuspended and denatured in 2xProtein Loading Buffer and 1M DTT at 95 °C for 4 minutes. Protein samples were analyzed using Western blot, as previously described. Used primary and secondary antibodies are listed in **Table 2**. Visualization was achieved using ECL (Thermo Fisher Scientific) and the ChemiDoc MP Imaging System with ImageLab 5.2 software (Bio-Rad).

3.17.2 Monoamine analysis with Liquid chromatography-tandem mass spectrometry

Fly homogenates prepared from 15 heads per sample were homogenized in 0.1M perchloric acid. Samples were analyzed by Liquid Chromatography-Tandem Mass Spectrometry (LC-MS/MS) composed from an Agilent 1260 HPLC system integrated with an Agilent 6460 triple quadrupole mass spectrometer (QQQ) equipped with an AJS ESI source.

The chromatography was carried out using a Purospher STAR RP-18 Hibar HR column (50 mm × 2.1 mm, 1.7 µm, Merck) for separation. The mobile phase consisted of (A) 1% formic acid in Milli-Q water and (B) acetonitrile, with gradient elution set as follows: 1% to 10% B from 0 to 0.9 min, 10% to 20% B from 0.9 to 3 min, 20% to 25% B from 3 to 4.5 min, 25% to 30% B from 4.5 to 6 min, 30% to 99% B from 6 to 6.1 min, 99% to 1% B from 6.1 to 6.2 min, and maintained at 1% B from 6.2 to 10 min. The flow rate was set to 0.33 mL/min, and the column temperature was held at 25°C. Samples were injected in triplicate, with an injection volume of 2.5µL per sample.

The MS/MS analysis was performed using the AJS-ESI-QQQ source with the following settings: a capillary voltage of 3.5 kV for both positive and negative ion modes, nozzle voltage of 0.5 kV, ion source temperature at 300°C, 5 L/min gas flow, 45 psi nebulizer pressure, 250°C drying gas temperature, and 11 L/min sheath gas flow. Nitrogen served as the collision gas.

Dopamine (DA), octopamine (OA), and tyramine (TA) were analyzed quantitatively. Glutamine (GLU), acetyl-chole (ACh), and γ-aminobutyric acid (GABA) were analyzed semi-quantitatively by using extracted ion chromatograms of deprotonated ions and processing data with MassHunter Qualitative Analysis software version B.07.00 (Agilent Technologies). The method is previously described [504].

3.17.3 Hydrogen peroxide concentration measurement

Hydrogen peroxide concentrations were determined in homogenates of 5 headless bodies and 32 fly heads using 1×PBS with 0.1% Triton. After mechanical homogenization, samples were centrifuged for 45 min at 13.600 rpm and 4 °C in an FA-24x2 rotor for 5425R centrifuge, and the supernatant was used for further analysis. Samples were incubated for 30 minutes at 37 °C in the dark using a fluorescent probe dihydroethidium (DHE, 3791, Sigma-Aldrich).

The amount of hydrogen peroxide is measured as a percentage of the formation of the fluorescently active dye ethidium (E^+) or 2-hydroxyetidium (2-E^+OH), the reaction shown in **Figure 13a**. Fluorescence was measured on a microplate reader (Infinite M200PRO, 30050303, Tecan, with Tecan i-control software, 3.7.3.0), with excitation and emission wavelengths set to 480 nm for E^+ and 625 nm for 2-E^+OH. To account for the environmental oxidation of DHE, the relative fluorescence units (RFU) of each measured sample were adjusted for dilution, and the RFU of DHE was subtracted from the sample's RFU.

Hydrogen peroxide concentration was determined using a calibration curve for known H_2O_2 concentration relative to measured DHE fluorescence. This experiment was done following previously described methods [505].

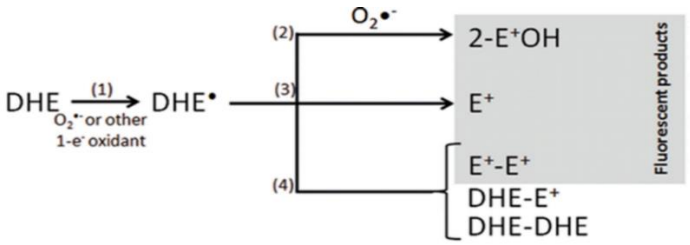

a)

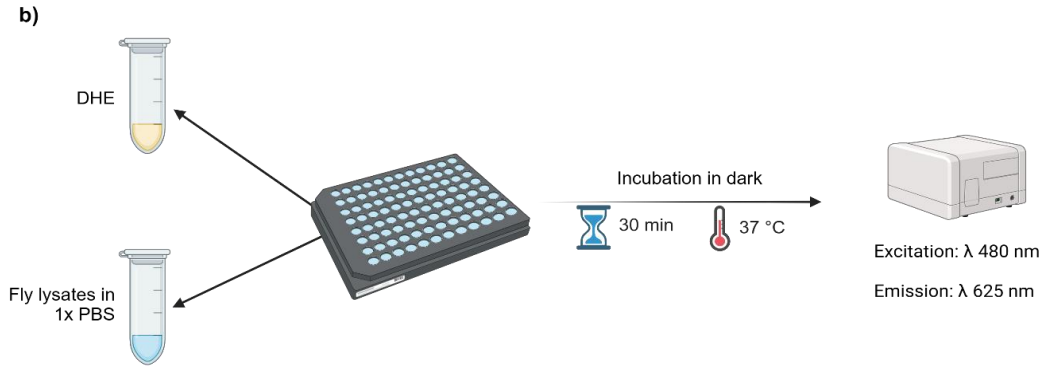

Figure 14: Protocol for measuring H_2O_2 levels in *Drosophila*. The transformation of inactive DHE into fluorescent products[506] (**a**) and protocol scheme created with BioRender (**b**).

3.18 Glutathione concentration measurement

For measuring glutathione levels, samples of 5 headless bodies and 32 heads were homogenized in PBS with 5% trichloroacetic acid (TCA, 20742.236, AnalaR NORMAPUR), followed by centrifugation for 45 min at 13600 rpm and 4 °C in FA-24x2 rotor for 5425R centrifuge. For the following steps, supernatant was used. Ellman's method was employed to measure reduced (GSH), oxidized (GSSG), and total glutathione levels[507].

To measure free GSH, R1 solution (10mM EDTA in 500mM Tris buffer pH 8.2) and R2 solution (10.0mM 5,5'-dithiobis(2-nitrobenzoic acid), DTNB, A14331.06, Alfa Aesar, dissolved in methanol) were added to the samples, and absorbance at 415 nm was measured using a microplate reader (Infinite M200PRO).

For GSSG determination, samples were reduced to GSH using sodium borohydride ($NaBH_4$, 35788, Thermo Scientific) and sodium hydroxide (NaOH, P147010, GramMol), followed by neutralization with concentrated hydrochloric acid (HCl, P133901, GramMol). Total GSH was measured after the reduction process, and GSSG was calculated by subtracting free GSH from total GSH and dividing by two. GSH concentration in samples was determined using a calibration curve for known GSH concentrations. This process is summarized in **Figure 14**.

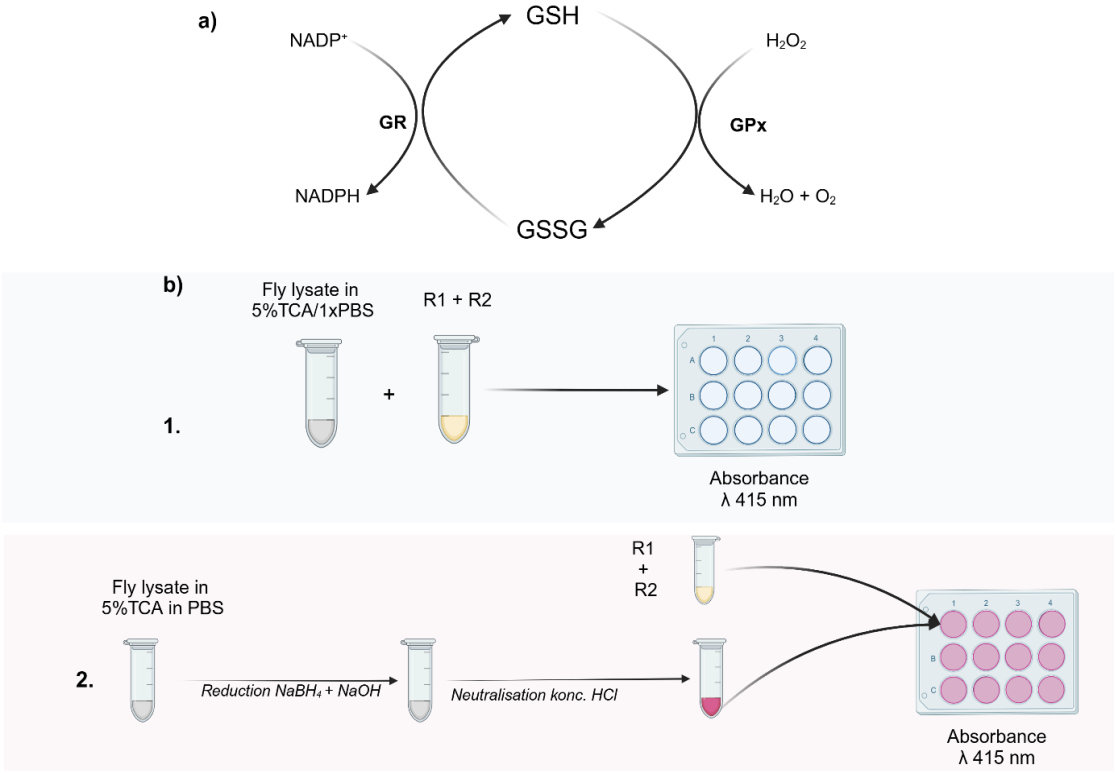

Figure 15: GSH reduction mechanism and protocol scheme. Glutathione reductase (GR) reduces GSSG in GSH and vice versa for glutathione peroxidase (GPx) (**a**). A scheme for the protocol of measuring GSH levels in fly lysates was created with BioRender (**b**).

3.19 Behavioral analysis

3.19.1 Social interaction network analysis

Male flies 3–5 days old were selected using CO_2 the day before video recording and grouped into sets of 12. The recording was performed in a circular arena while files were transferred from cultivation vials using an aspirator. The bottom of the arena used for recording was made of white translucent Plexiglas (61 mm diameter and 3 mm height), while the top of the arena was clear Plexiglas, coated with Sigmacote (SLCM2185, Sigma-Aldrich), restraining fly movement to 2D.

Simultaneously, four arenas were recorded in light conditions (on a luminous LED surface) with an ACA3800-10GM Basler industrial camera with 3856 x 2764 pixels video resolution, complemented by Basler software. Following a 10-minute acclimation period after aspiration, video recordings were made for 25 min. All recordings were performed between 10.00-12.00 in the morning when flies are naturally active. For each recording, the arena was cleaned with

ethanol and wiped, to avoid interference of olfactory clues from the previous fly group.

The described method for video recording was previously established[494]. FlyTracker software[508], running on MATLAB, was utilized to identify each fly, determine its spatial position (x and y coordinates), and establish orientation. Each video was checked for errors like identity swaps. Social interaction networks (SINs) were defined based on the following parameters for interaction: distance between two flies in interaction is within a 2.5-body length (approx. 5 mm), interacting flies facing each other at an angle of less than 160 degrees, and duration of interaction had a minimum of 0.6 sec, as per standardized protocols[497,509].

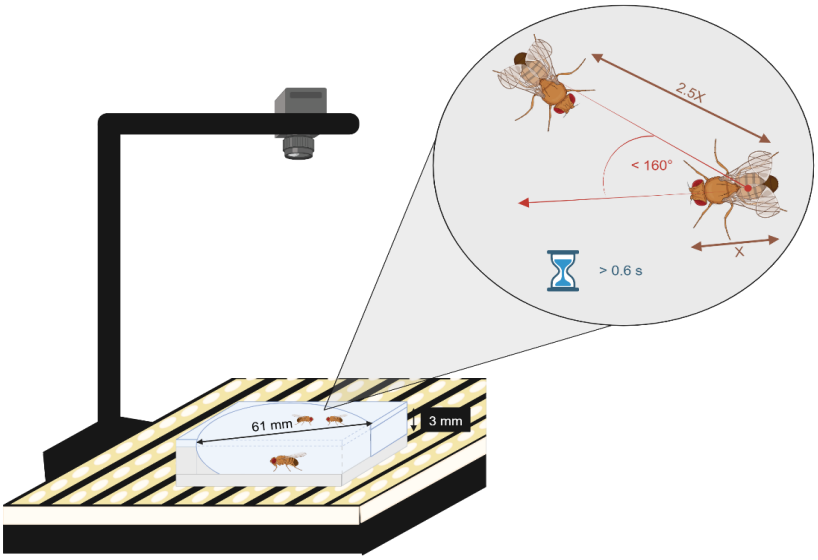

Figure 16: Video recording station for SIN experiment. Criteria for interaction between flies are marked on the scheme. The scheme was created with BioRender. mm – millimeters, s – seconds, ° - degree.

Analysis of SIN parameters (trajectory data) was performed using a Python script, as detailed previously [510]. The resulting SINs were represented as directed graphs with two types of data: nodes (individual flies) and edges (links between two nodes, e.g., interactions between flies). Directionality in these graphs indicated which fly initiated the interaction. Network analysis included two types of weights: interaction count and duration per fly.

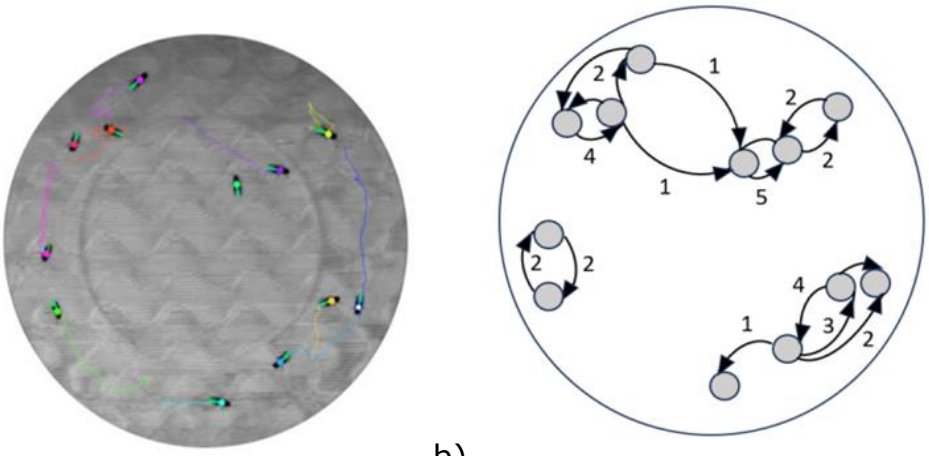

a) b)

Figure 17: Screenshot from FlyTracker software (a) and scheme of SINs (b).

SIN parameters were examined at both the global network level and the local level (focusing on the behavior of individual flies). Global metrics were efficiency (a measure of fly group connectivity based on distance) and clustering coefficient (a measure of how closely connected flies are within a local network and the likelihood that their neighboring flies will also form connections with one another).

The local metrics were betweenness (a measure of the importance of each fly for maintaining group cohesion) and closeness (a measure of the shortest paths between each fly, on average) centrality. The mentioned SIN parameters were previously established[494].

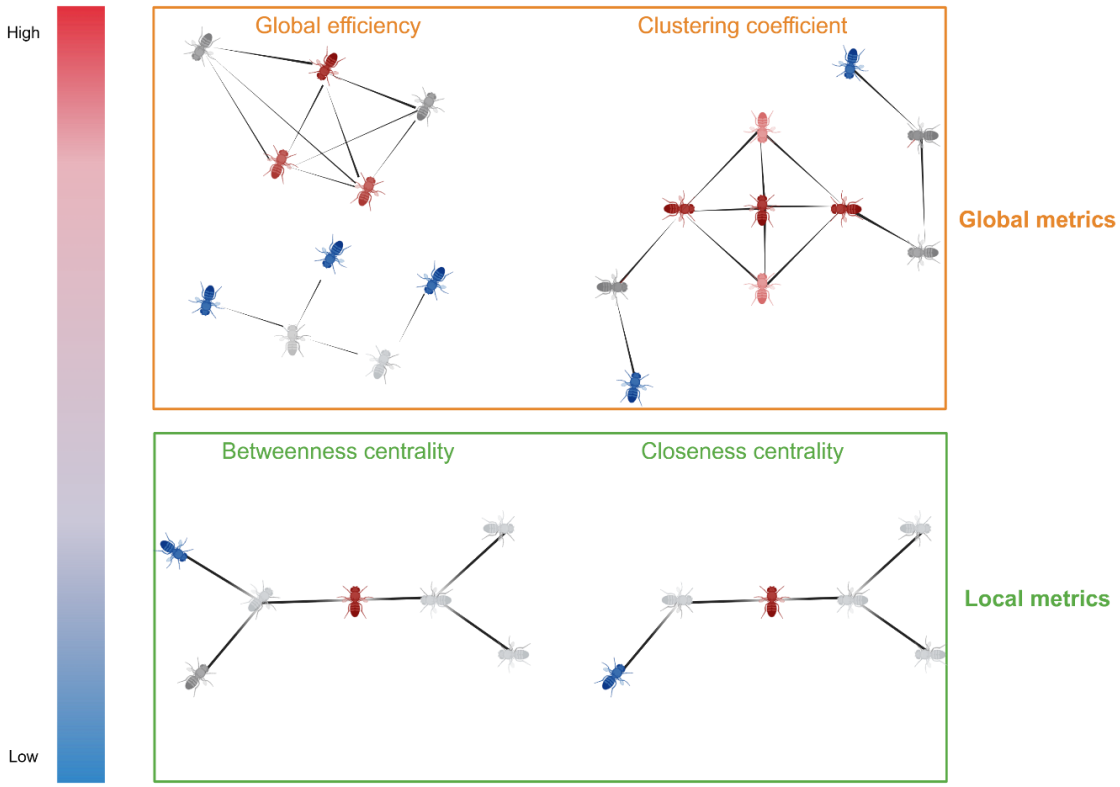

Figure 18: Global and local metrics from SINs. The scheme was created with BioRender.

All SIN data were normalized using z-scores derived from comparing observed and randomly generated networks. Random networks (n=10000) were generated by sampling 12 random flies from the same experimental group and analyzing them as a single group.

3.19.2 Statistical analysis

Data analysis was performed using Prism (10.2.3, GraphPad). Normality was assessed using Bartlett's test or Brown-Forsythe's test. Group comparisons were conducted using either one-way ANOVA or Kruskal-Wallis ANOVA, followed by Tukey's post-hoc test as appropriate. A p-value <0.05 was considered statistically significant.

4 Results

4.1 Analysis of human *post-mortem* samples

Protein aggregation was investigated in *post-mortem* brain samples across different patient groups. The initial study was done in one brain region, the IC, across many suicide victims compared to control individuals or patients with diagnosed MDD or AD. Additionally, for some patients, additional brain regions were investigated. Finally, the protein DISC1 was investigated in more detail in multiple brain regions collected from patients with SZ diagnosis, compared to control individuals or patients with AD diagnosis.

4.1.1 Antibody validation

All antibodies used to test samples were validated previously; however, some of them were further checked by Western blot. Anti-TRIOBP antibody and anti-NPAS3 antibody (PromoKine) were validated simultaneously by Beti Zaharija[500].

Anti-NPAS3 antibody used in this thesis (PromoKine) was validated against another anti-NPAS3 antibody (ProSci). Additionally, an anti-NPAS3 antibody (PromoKine) was tested on Flag-tagged N-terminal fragments of NPAS3 expressed in HEK293 cells, along with anti-Flag M2 antibody[500]. Anti-DISC1 antibody was tested in lysates from HEK293 cells expressing human DISC1: full-length and aa 257-655 of human DISC1 (D and I domain only). The samples were also stained with anti-Flag antibody. All of these antibodies were detected by peroxidase-conjugated affinity purified goat anti-rabbit IgG antibody. As loading control, all mentioned samples were stained with anti-β actin (OriGene or Merck), detected by peroxidase-conjugated goat anti-mouse IgG antibody.

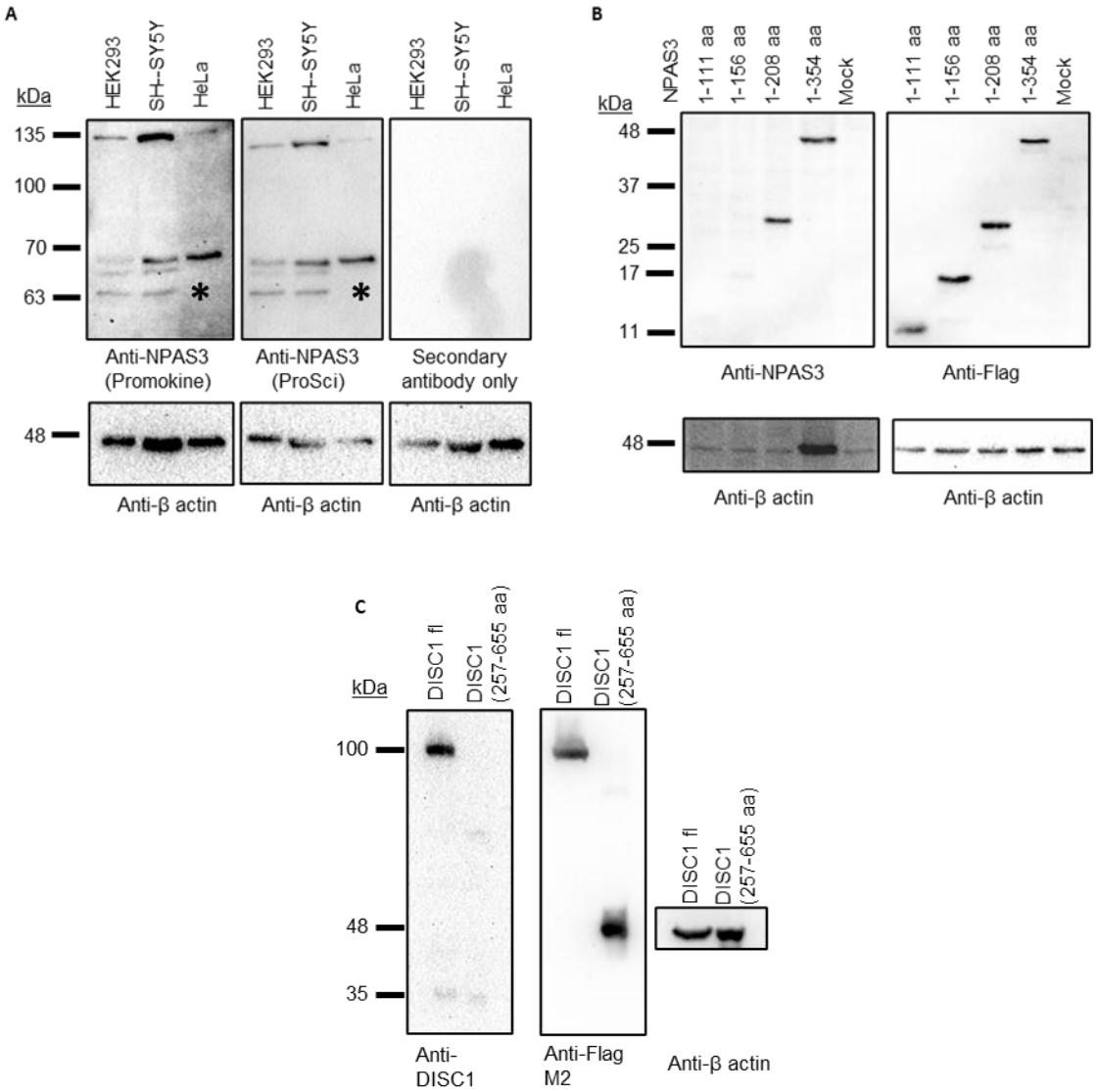

Figure 19: DISC1 and NPAS3 antibodies were validated by Western blot in cell lines. In all images, vertically arranged blots show re-staining of the same membrane, while horizontally arranged blots represent identical samples that were run and stained simultaneously. Two variants of the anti-NPAS3 antibody (PromoKine and ProSci) were tested for validation against endogenous NPAS3 in lysates from three cell lines: HEK293, SH-SY5Y, and HeLa. Smaller bands are marked with asterix (*). (**A**). NPAS3 (PromoKine) was also tested against four N-terminal NPAS3 fragments expressed in HEK293 cells (**B**). DISC1 antibody and anti-Flag were tested against lysates from HEK293 cells expressing human DISC1: full-length and 257-655 aa, expressed in HEK293 cells (**C**). Loading control was confirmed by anti-β actin in all three cases.

Both anti-NPAS3 antibodies (PromoKine and ProSci) recognized similar bands of endogenous NPAS3 in the following cell line lysates: HEK293, SH-SY5Y, and HeLa (**Figure 18 A**). Smaller bands were detected at 70 and 63 kDa, marked with * on the figure. This does not match the predicted molecular weight of full-length NPAS3 (~100.8

kDa), but may represent an alternatively spliced isoform, a truncated NPAS3[407], or a degradation fragment.

While the anti-Flag antibody recognized all four NPAS3 fragments, anti-NPAS3 antibodies showed intense bands in lysates expressing NPAS3 fragments 1-208 and 1-354 aa, but none for fragments 1-111 and 1-156 aa (**Figure 18 B**). This suggests that the epitope for the antibody is located within aa 156-208, which is consistent with the supplier's statement that the epitope is near the N-terminus.

The anti-DISC1 antibody recognized only full-length human DISC1, and the anti-Flag recognized both versions, locating epitope near the C-terminus, which is in line with data about synthetic peptides used in creating this antibody (**Figure 18 C**).

Other antibodies used in this thesis were previously confirmed by other research groups, as mentioned in data.

4.1.2 Investigation of key proteins in *post-mortem* human brain samples, with a focus on suicide victims

Four proteins implicated as aggregating in CMIs, NPAS3, DISC1, CRMP1, and TRIOBP-1, were detected in the IC of suicide victims, control individuals, and patients with MDD or AD. The IC is a key brain region for processing information[467]. Analysis was done on brain samples collected from suicide victims, patients with MDD or AD who did not die by suicide but by different causes, and control individuals which died by other cause of death than suicide and did not have a diagnosis of AD or MDD. The sex and intervals between death and sample collections did not significantly differ between the diagnostic categories. At the same time, the suicide victims were younger than other individuals at the time of death.

Firstly, the presence of NPAS3, a brain-specific transcription factor involved in neurodevelopment, neuronal function, and synaptic plasticity, was investigated across all samples.

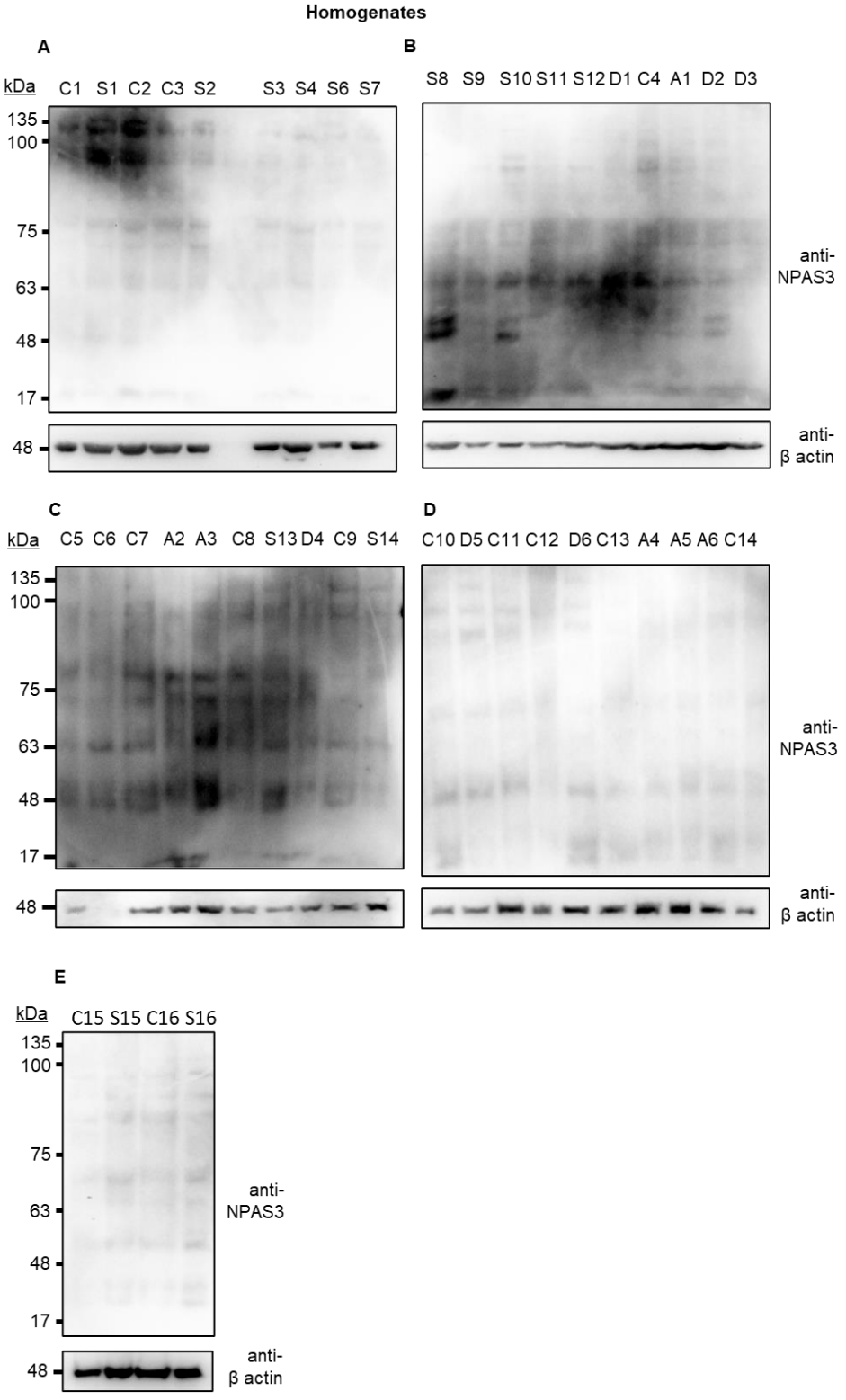

Figure 20: Low levels of NPAS3 are present in "homogenate" (total protein) brain samples across all diagnoses and in control individuals. The samples were collected from suicide victims (S), control individuals (C), and patients with either AD (A) or MDD (D) diagnosis. Analysis of samples included Western blot with either anti-NPAS3 or anti-β actin antibodies and appropriate secondary antibody for visualization (**A-E**). Samples were anonymized and randomly loaded on acrylamide

gels. Visualization was performed with an ECL kit and on a ChemiDoc MP Imaging System.

No clear, specific band corresponding to NPAS3 was detected in IC samples from suicide victims, control individuals, or patients with MDD or AD (**Figure 20 A-E**). Additionally, the signal was only visible using high exposures, and did not match the expected molecular weight of NPAS3, suggesting it may represent non-specific binding rather than true NPAS3 detection.

Secondly, the presence of DISC1, a multifunctional scaffold protein strongly linked to psychiatric disorders, was investigated.

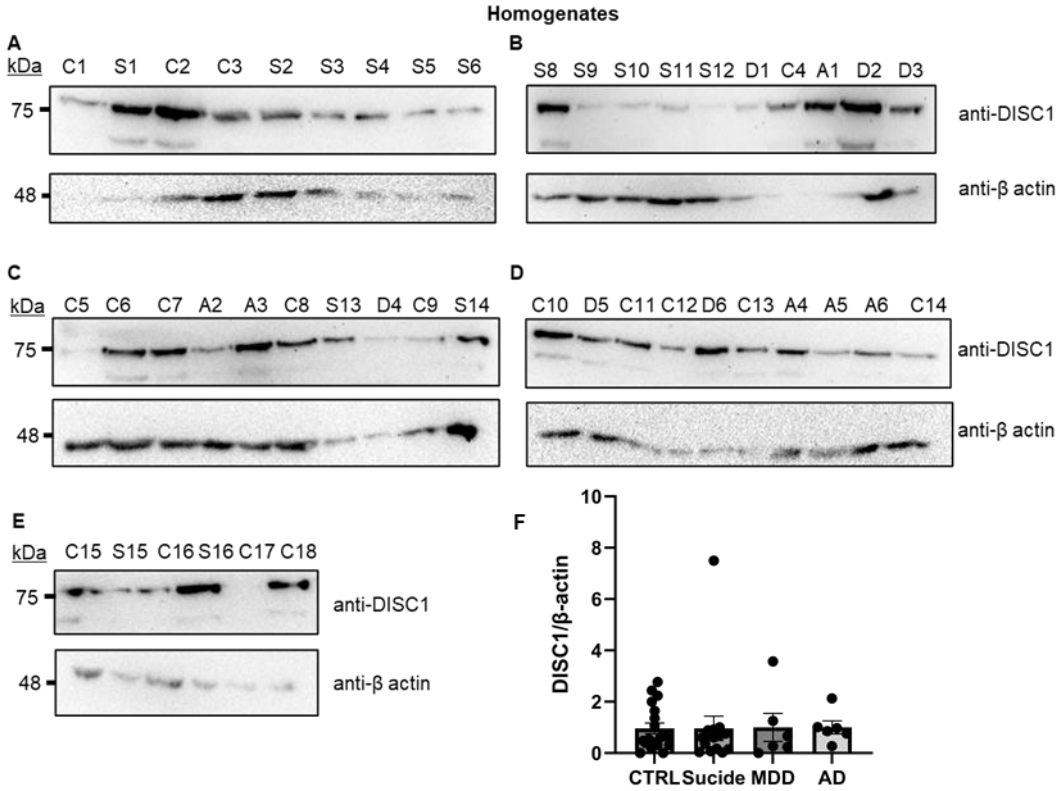

Figure 21: Levels of DISC1 in total protein samples vary between individuals. The samples were collected from suicide victims (S), control individuals (C), and patients with either AD (A) or MDD (D) diagnosis. Analysis of samples included Western blot with either anti-DISC1 or anti-β actin antibodies and appropriate secondary antibody for visualization (**A-E**). Samples were anonymized and randomly loaded on acrylamide gels. Visualization was performed with an ECL kit and on a ChemiDoc MP Imaging System. **F** Intensity of DISC1-specific bands was quantified with Image Lab software (Bio-Rad) and normalized to β-actin bands. Additionally, the value of DISC1/β-actin for each sample was normalized to an average value of diagnosis group or control. Data on the graphs is presented as AVE +/- SEM and statistically analyzed with one-way ANOVA with Tukey's multiple comparisons test. All sample groups were compared, but only the pairs with significant differences are shown on the graph.

DISC1 was detectable across all samples, with no obvious correlation to diagnosis status after normalization to actin level in each sample (**Figure 21 A-E**). Since DISC1 has many functions in neuronal cells, it is likely to persist even in pathological states. However, no statistical difference between diagnosis was detected upon quantification (**Figure 21 F**).

The next protein investigated was CRMP1, a cytosolic phosphoprotein that regulates neuronal differentiation and cytoskeletal dynamics. CRMP1 exists in humans in the form of two variants: long variant, marked as CRMP1 Lv and short variant, marked as CRMP1 Sv. CRMP1 Lv has been described as aggregating in cell systems[322], while the CRMP1 Sv is more expressed than CRMP1 Lv in the human brain[332].

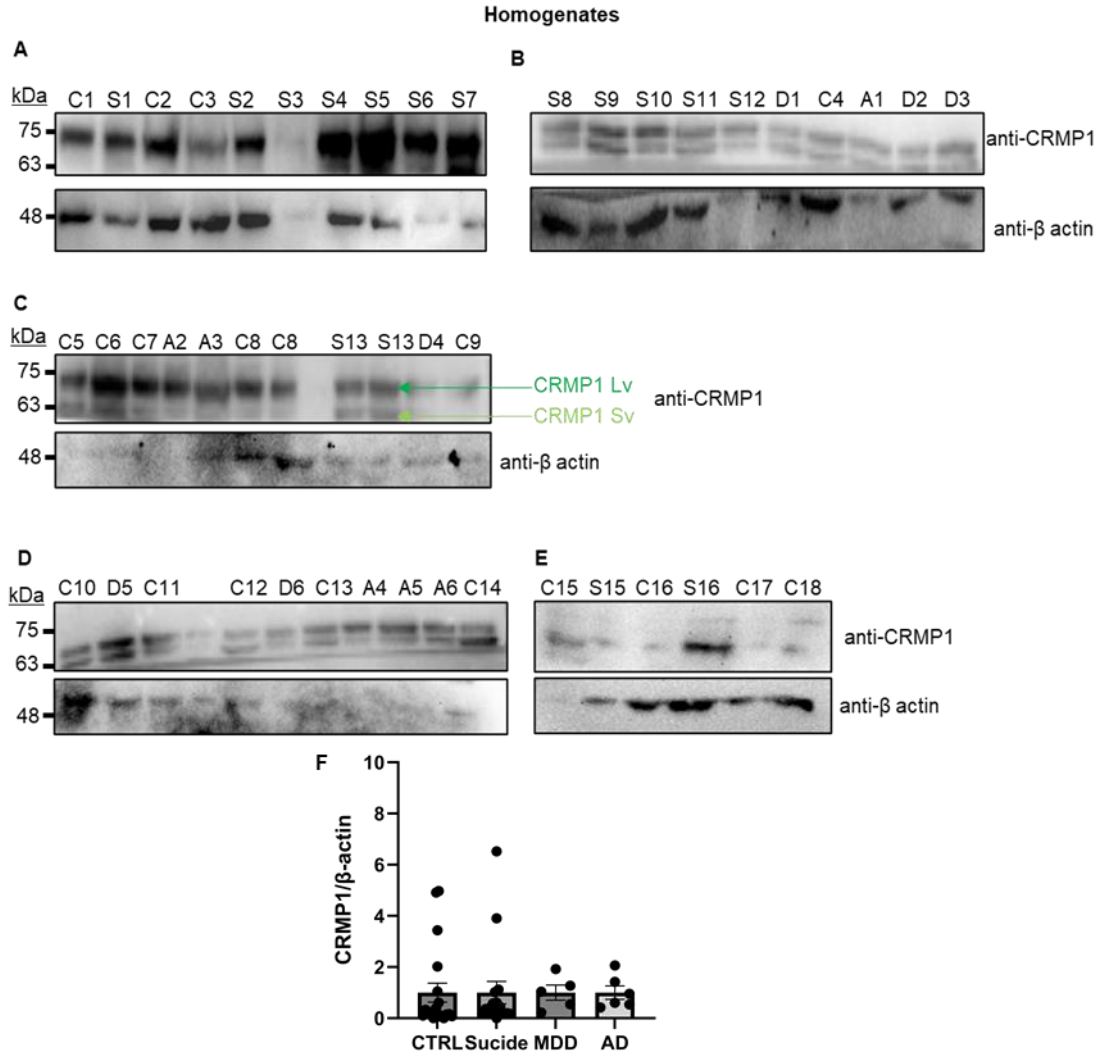

Figure 22: Both variants of CRMP1 were present in high abundance across all samples. The samples were collected from suicide victims (S), control individuals (C), and patients with either AD (A) or MDD (D) diagnosis. Long variant CRMP1

(CRMP1 Lv, marked dark green) can be observed as a higher band, closer to 75 kDa, while the short variant (CRMP1 Sv, marked as light green) is seen below, closer to 63 kDa (C). Analysis of samples included Western blot with either anti-CRMP1 or anti-β actin antibodies and appropriate secondary antibody for visualization (**A-E**). Samples were anonymized and randomly loaded on acrylamide gels. Visualization was performed with an ECL kit and on a ChemiDoc MP Imaging System. **F** Intensity of CRMP1-specific bands was quantified with Image Lab software (Bio-Rad) and normalized to β-actin bands. Additionally, the value of CRMP1/β-actin for each sample was normalized to an average value of diagnosis group or control. Data on the graphs is presented as AVE +/- SEM and statistically analyzed with one-way ANOVA with Tukey's multiple comparisons test. All sample groups were compared, but only the pairs with significant differences are shown on the graph.

CRMP1 was detected in whole protein samples as a double band between 75 and 63 kDa, indicating the presence of both CRMP1 Sv and CRMP1 Lv (**Figure 22 A-E**). The bands were prominent in control and suicide samples, with variability between individuals, but no statistical difference between diagnosis was detected upon quantification (**Figure 22 F**).

Last analyzed protein was TRIOBP-1, which supports actin stabilization, neurite outgrowth, and cell adhesion, and has additional roles in centrosome function and mitosis.

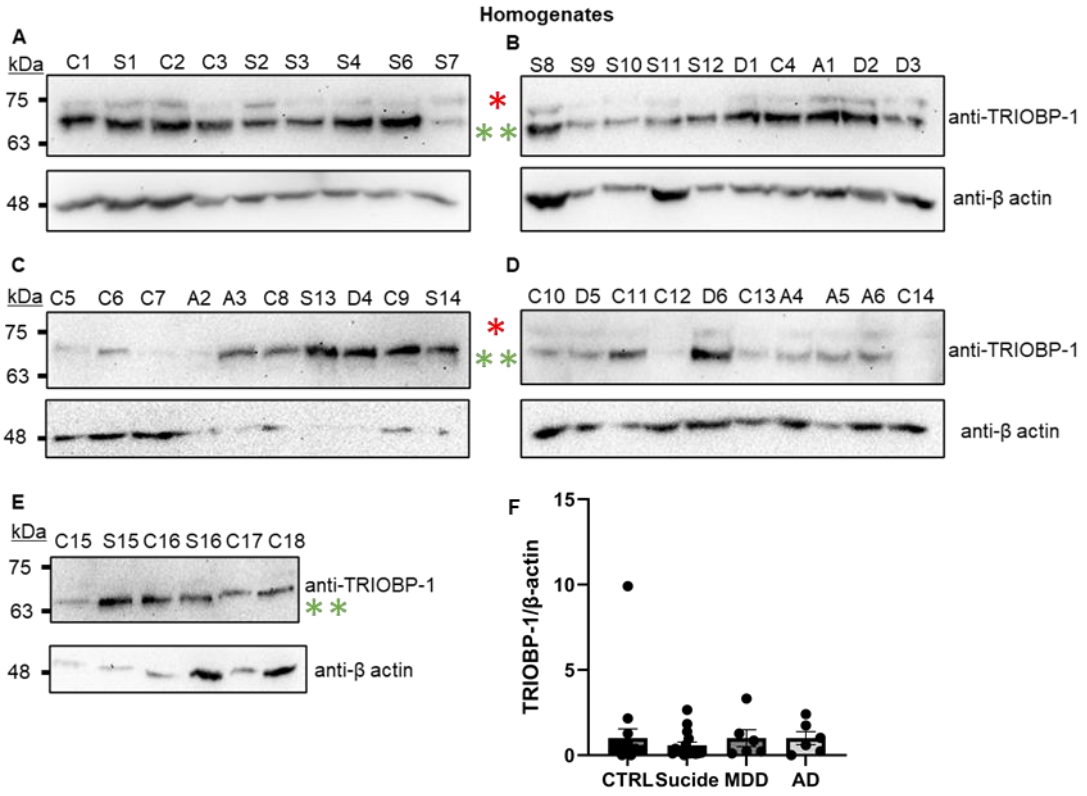

Figure 23: TRIOBP-1 is present across all samples, with no correlation to diagnosis status. The samples were collected from suicide victims (S), control

individuals (C), and patients with either AD (A) or MDD (D) diagnosis. Analysis of samples included Western blot with either anti-TRIOBP-1 or anti-β actin antibodies and appropriate secondary antibody for visualization (**A-E**). There are two specific TRIOBP-1 bands: one at 75 kDa representing a full-length protein (marked with red asterix *) and one at 63 kDa which is probably a variant of protein without its optionally translated N-terminal domain (marked with green asterix *). Samples were anonymized and randomly loaded on acrylamide gels. Visualization was performed with an ECL kit and on a ChemiDoc MP Imaging System. **F** Intensity of TRIOBP-1-specific bands was quantified with Image Lab software (Bio-Rad) and normalized to β-actin bands. Additionally, the value of TRIOBP-1/β-actin for each sample was normalized to an average value of diagnosis group or control. Data on the graphs is presented as AVE +/- SEM and statistically analyzed with one-way ANOVA with Tukey's multiple comparisons test. All sample groups were compared, but only the pairs with significant differences are shown on the graph.

The levels of total TRIOBP-1 vary between individuals in the same or different diagnosis group, as shown in **Figure 23 A-E**. However, it is worth noting that the β-actin signal was not detected for samples A3- S14, shown in **Figure 23 C,** and their signal was normalized to the average β-actin signal on that membrane. In some samples (**Figure 23 A-C**), there are two specific TRIOBP-1 bands, one closer to 75 kDa and one lower, closer to 63 kDa, likely representing a full-length protein and a variant of protein without its optionally translated N-terminal domain[323,459]. However, no statistical difference between diagnosis was detected upon quantification (**Figure 23 F**).

In summary, no significant correlation exists between the levels or presence of NPAS3, DISC1, CRMP1, or TRIOBP-1 and the specific diagnosis and controls across all analyzed samples from the IC. Hence, their insolubility was investigated further.

4.1.3 Aggregation of key proteins in *post-mortem* human brain samples, with a focus on suicide victims

The I/A protein fraction was purified from the IC of suicide victims, patients with diagnosed MDD or AD and control individuals. The used protocol is described in more detail in *Chapter 3.2*.

After purification, both "aggregates" (representing I/A protein fraction, heavily composed of aggregating proteins) and "homogenates" (representing total protein levels) were analyzed with Western blot. Normalization of the total protein content was performed by using an identical mass of starting material before purification (protein content in 10% w/v brain homogenates), as in previous research[320–322]. Initially these samples were investigated for NPAS3.

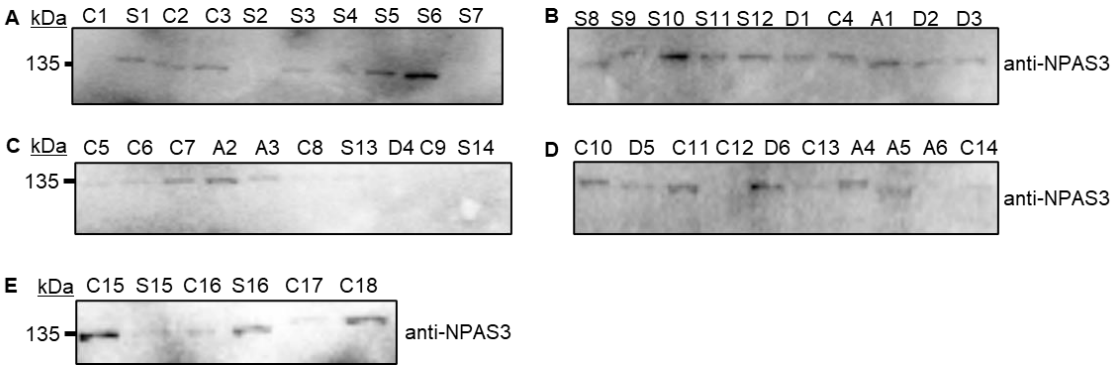

Figure 24: Specific NPAS3 bands were detected in I/A protein fraction across all diagnoses. The samples were collected from suicide victims (S), control individuals (C), and patients with either AD (A) or MDD (D) diagnosis. The I/A NPAS3 protein in samples marked as aggregates. Analysis of samples included Western blot with either anti-NPAS3 or anti-β actin antibodies and appropriate secondary antibody for visualization. Samples were anonymized and randomly loaded on acrylamide gels. Visualization was performed with an ECL kit and on a ChemiDoc MP Imaging System.

A major NPAS3 band was observed in the I/A protein fraction at 135 kDa (**Figure 24 A-E**), similar to a band observed in cell lines (**Figure 19 A**), which is higher than the expected size for full-length protein (approx. 100 kDa). Also, bands specific to NPAS3 were detected across all tested groups. Unfortunately, as there was no quantification of total proteins in I/A protein fraction and no loading control, the quantification of these samples was not possible.

Similar to the previously described experiment, the insolubility of DISC1, a known risk factor for SZ, was investigated in the same set of patients with the same protocol.

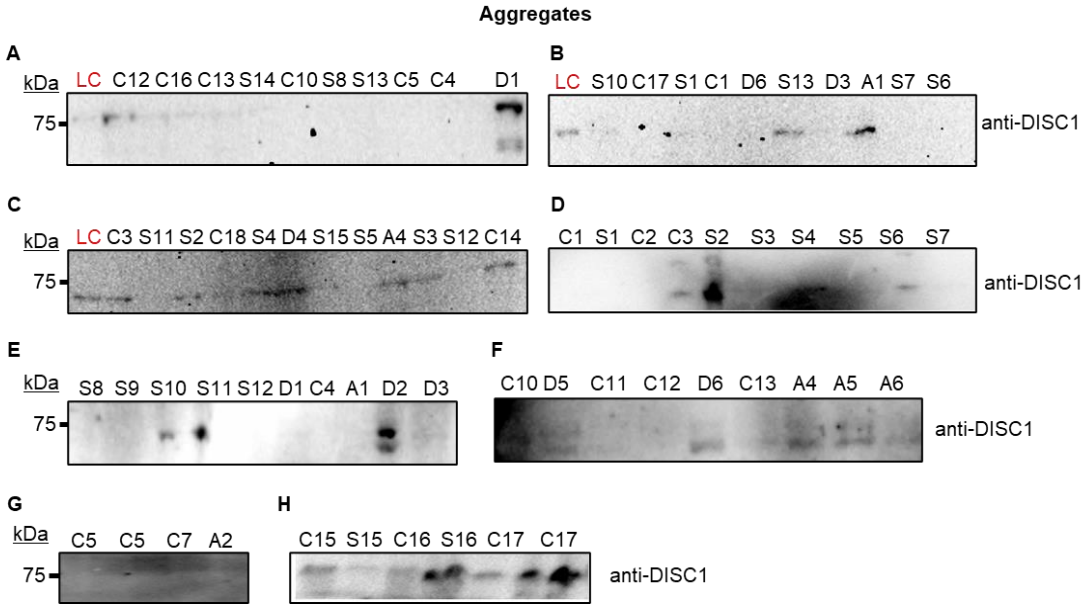

Figure 25: The level of I/A DISC1 varies between individuals. The samples were collected from suicide victims (S), control individuals (C), and patients with either AD (A) or MDD (D) diagnosis. The I/A DISC1 was detected in a purified protein fraction marked as "aggregates." Some samples were run twice, and in some cases a homogenate sample from the control individual C14 was run as a loading control (LC). Analysis of samples included Western blot with either anti-DISC1 or anti-β actin antibodies and appropriate secondary antibody for visualization (**A-H**). Samples were anonymized and randomly loaded on acrylamide gels. Visualization was performed with an ECL kit and on a ChemiDoc MP Imaging System.

The detected DISC1 band at 75 kDa corresponds to previously described bands [320]. Detectable levels of I/A DISC1 vary for each individual in the same diagnosis group (**Figure 25 A-G**). However, two suicide victims, one patient previously diagnosed with MDD and one control individual, had detectable DISC1 bands with particularly high intensity (marked as D2, S16, S11, and C17 in **Figure 25 E** and **H**). The patient with MDD marked as D2 was female, 87 years old, and had a PMI of 6 hrs. Suicide victim S16 was male, 58 years old, and had PMI over 24 hrs, while suicide victim S11 was male, 35 years old, and had PMI of 2 hrs. Control individual C17 was male, 68 years old, and had a PMI of 2 hrs. There were other patients with similar age and PMI without intense DISC1 band in "aggregate" (I/A proteins) samples, ruling out a simple effect of these factors on increased DISC1 aggregating signal.

As in previous chapters, the "aggregate" (I/A protein) was purified and analyzed in pairs with "homogenate" (total protein) with specific anti-CRMP1 staining during Western blot. A similar protocol

was used to identify CRMP1 as an aggregating protein in samples collected *post-mortem* from patients with diagnosed SZ[322].

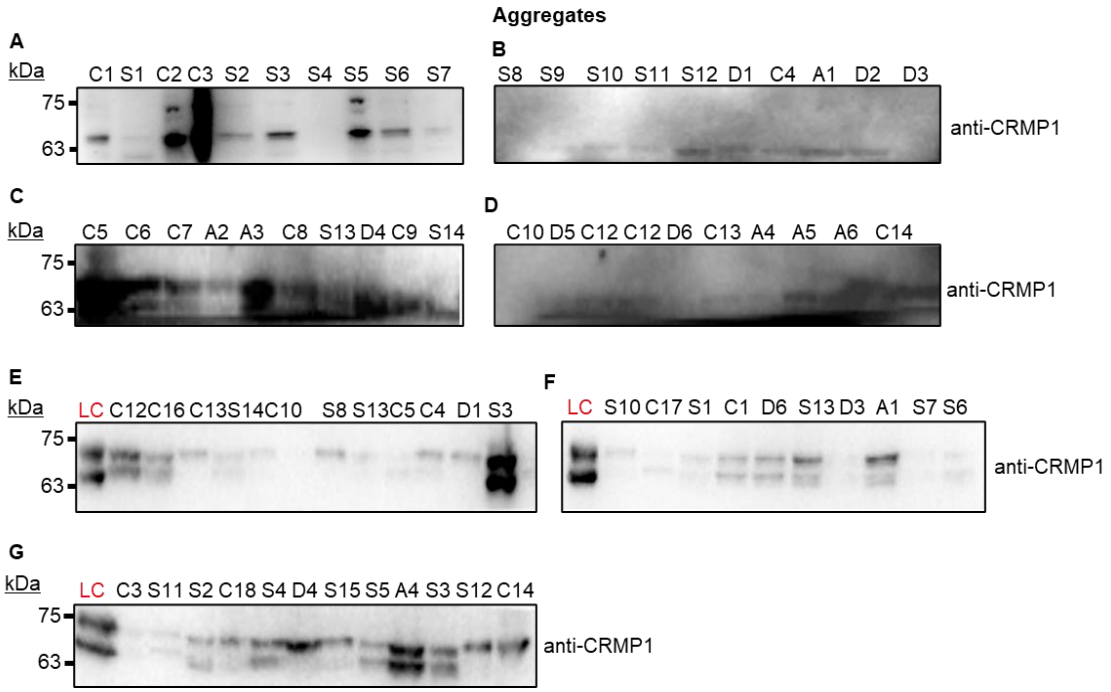

Figure 26: Both variants of CRMP1 show signs of aggregation across all samples. The samples were collected from suicide victims (S), control individuals (C), and patients with either AD (A) or MDD (D) diagnosis. Aggregates (I/A protein fraction) were purified from *post-mortem* brain samples, which included the IC. Analysis of samples included Western blot with either anti-CRMP1 or anti-β actin antibodies and appropriate secondary antibody for visualization (**A-G**). Long variant CRMP1 (CRMP1 Lv, marked dark green) can be observed as a higher band, closer to 75 kDa, while the short variant (CRMP1 Sv, marked as light green) is seen below, closer to 63 kDa. Samples were anonymized and randomly loaded on acrylamide gels. Visualization was performed with an ECL kit and on a ChemiDoc MP Imaging System.

Intense bands were detected for both CRMP1 Sv and CRMP1 Lv in I/A protein fractions collected from several individuals, with no clear connection to diagnosis status (**Figure 26 A-G**). A portion of samples showed only one intense band, more corresponding to CRMP1 Lv than CRMP1 Sv based on expected size.

Finally, the last protein analyzed in this set of experiments was TRIOBP-1. It was identified as an aggregating protein in CMIs through a hypothesis-free approach, using purified I/A fractions following a protocol similar to the one applied in my experiments.

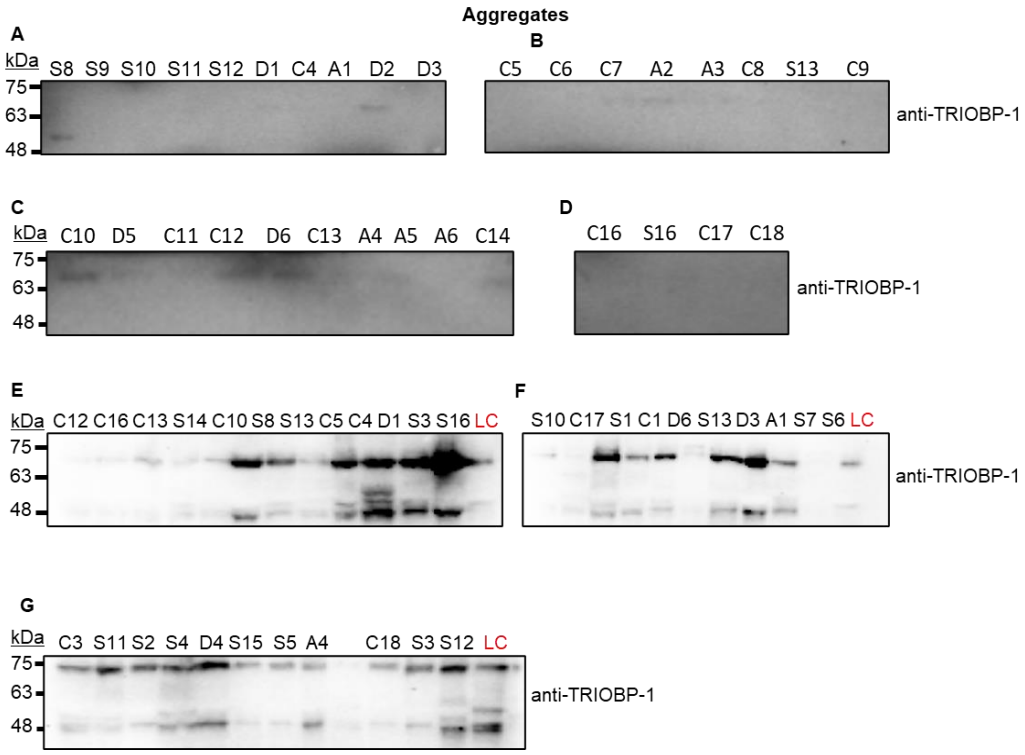

Figure 27: I/A TRIOBP-1 is detected in all samples, with no correlation to diagnosis status. "Aggregates" "represent purified I/A protein fraction from the IC region of *post-mortem* brain samples. The samples were collected from suicide victims (S), control individuals (C), and patients with either AD (A) or MDD (D) diagnosis. Analysis of samples included Western blot with either anti-TRIOBP-1 or anti-β actin antibodies and appropriate secondary antibody for visualization (**A-G**). Samples were anonymized and randomly loaded on acrylamide gels. Visualization was performed with an ECL kit and on a ChemiDoc MP Imaging System.

The initial round of Western blot staining showed low levels of TRIOBP-1 aggregation (**Figure 27 A-D**). However, samples were run twice if there was enough sample (**Figure 27 E-G**). The higher band, closer to 75 kDa, corresponds to the expected size for full-length protein and matches the bands observed previously in "homogenates" (total protein) (**Figure 23**). The smaller band, closer to 48 kDa, is more likely either a processed version of TRIOBP-1 (post-translational modifications) or a protein from the same family (for example, TRIOBP-2), which also contains an epitope for the anti-TRIOBP-1 antibody used.

In summary, the insolubility and aggregation of NPAS3, DISC1, CRMP1, and TRIOBP-1 in the IC did not consistently correlate with diagnostic categories. There is a variability among individuals, suggesting that protein aggregation may occur in subsets of individuals rather than being a universal marker of these conditions. However, I

noticed that multiple proteins are I/A in the same individuals, so we further analyzed it.

4.1.4 Aggregation of multiple proteins in the same individuals

The concept of multiple proteins aggregating in the same patient has been poorly studied so far, with the focus usually on one protein at a time[320,321]. However, assessing the aggregation of four proteins in the same patient(s) is possible in these samples. The exact number of patients with this pattern has been visualized in **Figure 28**.

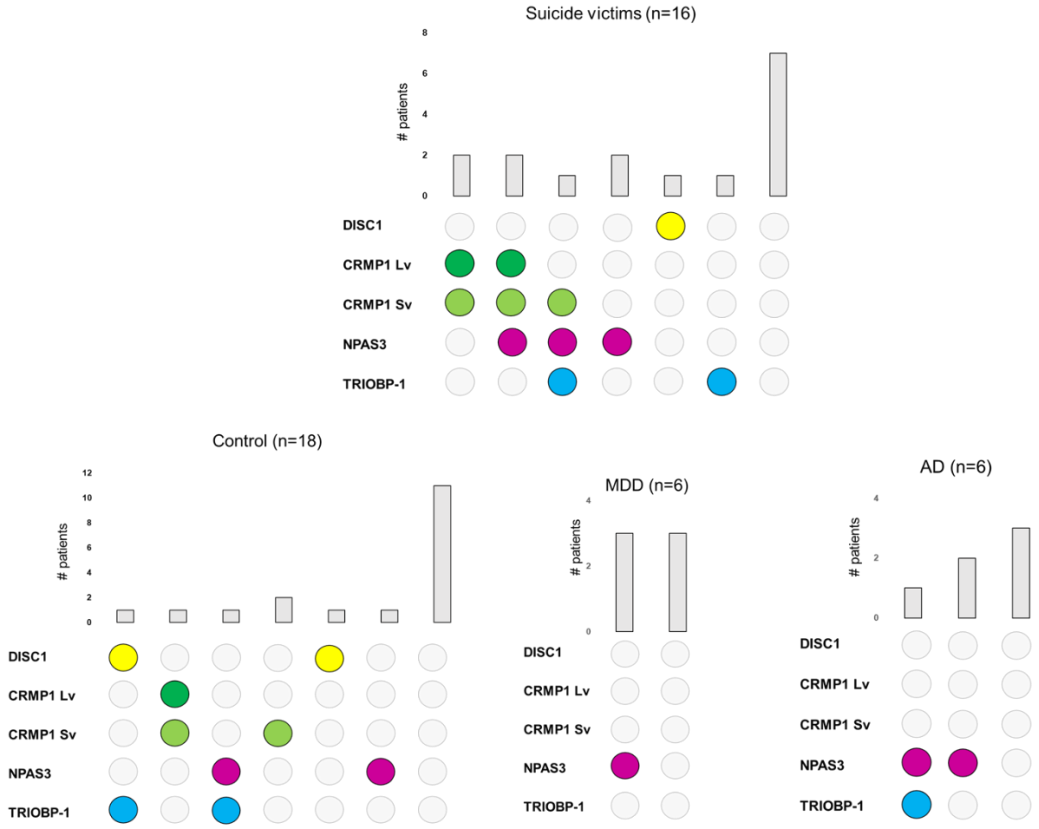

Figure 28: Graphic representation of possible combinations of aggregating proteins and the number of patients in which they were detected. Each analyzed protein is color-coded (DISC1 yellow, CRMP1 Lv dark green, CRMP1 Sv light green, TRIOBP-1 blue, NPAS3 purple). Each category of diagnosis has a separate part.

The presence of multiple aggregating proteins alone is not correlated to diagnosis, but certain combinations seem to overlap.

Combination of CRMP1 Sv with CRMP1 Lv is present suicide victims and controls, while combination of CRMP1 Sv with either NPAS3 or TRIOBP-1 is present only in suicide victims. So far, co-aggregation of CRMP1 with DISC1 has been investigated previously[322]. Also, in

suicide victims two individuals had intense NPAS3-specific bands, one had DISC1 and one had TRIOBP-1, while the rest (7 out of 16 total) had no intense bands for proteins of interest. As for controls, three individuals had combination of proteins: DISC1 with TRIOBP1, CRMP1 Sv with CRMP1 Lv, and NPAS3 with TRIOBP-1. Also, two control individuals had CRMP1 Sv-specific bands, one had DISC1 and one had NPAS3, while majority of samples (11 out of 18 total) had no intense bands for proteins of interest. Interestingly, there was no combination of proteins present in patients with MDD. Three MDD patients had intense bands specific for NPAS3 and three had no intense bands for other proteins. Finally, in patients with AD diagnosis there was one individual with combination of NPAS3 with TRIOBP-1 and two individuals with only NPAS3, while the rest (3 out of 6) had no no intense bands for proteins of interest.

Nevertheless, it is important to note that this is a small set of patients, and conclusions need to be drawn after processing a larger set of samples. The most interesting protein combinations were also assessed for signs of co-aggregation in cell culture assays, described in *Chapter 4.2.4*.

4.1.5 Investigation of key proteins across different brain regions, with a focus on suicide victims

To further analyze the presence of the proteins of interest — DISC1, CRMP1, and TRIOBP-1 — additional brain regions from the same patients used in the previous set of experiments were investigated. Brain samples were mainly collected from the cerebral cortex, focusing on key regions. As a reminder, key functions of analyzed brain regions are included in **Table 7**.

Table 7: Brain regions analyzed in this thesis and their key function

Brain region	Key function
IC	integrating sensory, emotional, and cognitive information
FC	Central for movement, speech, reasoning, and integrating memories
TC	processing sensory input for memory, language, and emotion
PC	integrating sensory information and aids spatial awareness and navigation

BA 3, 1 and 2 (somatosensory cortex)	processing touch
BA4 (motor cortex)	aids voluntary movement
BA6 (the premotor cortex and supplementary motor cortex)	sensory-guided movement and aiding in the planning of complex actions
BA9 (frontal cortex)	supports memory and reasoning
BA17 (occipital lobe)	handles visual processing
BA36 and BA37	support memory and facial recognition
PiFC	smell and epileptogenic activity
SFG, LOG	self-awareness, laughter, and emotional regulation

Compared to previous research for this thesis, these experiments included adding TCE in acrylamide gels, which allowed quantification of total proteins after electrophoresis under UV light. The total protein staining is shown in *Appendix Figure 65-68*. Also, a loading control across different membranes was introduced. It was the pooled sample (PC and TC region from the right hemisphere of patient R, FC, and BA17 from patients with AD diagnosis (A1 and A2), and BA17 from the control individual (C5). The samples were analyzed with anti-DISC1, anti-CRMP1 antibodies, and anti-β actin antibodies, with normalization according to the loading control.

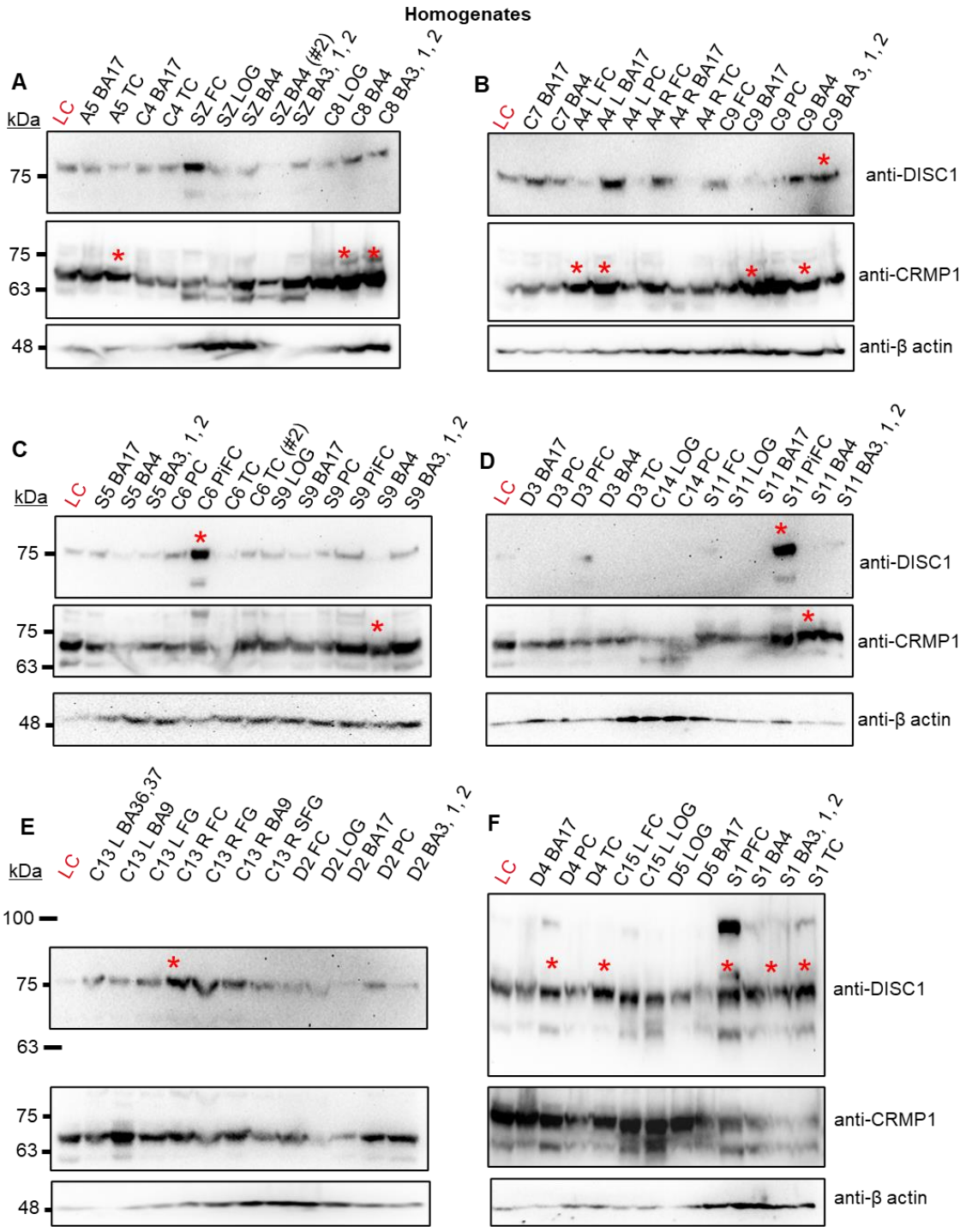
Homogenates
A
kDa
LC
A5 BA17
A5 TC
C4 BA17
C4 TC
SZ FC
SZ LOG
SZ BA4
SZ BA4 (#2)
SZ BA3, 1, 2
C8 LOG
C8 BA4
C8 BA3, 1, 2
75
75
63
48
B
LC
C7 BA17
C7 BA4
A4 L FC
A4 L BA17
A4 L PC
A4 R FC
A4 R BA17
A4 R TC
C9 FC
C9 BA17
C9 PC
C9 BA4
C9 BA 3, 1, 2
anti-DISC1
anti-CRMP1
anti-β actin
C
kDa
LC
S5 BA17
S5 BA4
S5 BA3, 1, 2
C6 PC
C6 PiFC
C6 TC
C6 TC (#2)
S9 LOG
S9 BA17
S9 PC
S9 PiFC
S9 BA4
S9 BA3, 1, 2
75
75
63
48
D
LC
D3 BA17
D3 PC
D3 PFC
D3 BA4
D3 TC
C14 LOG
C14 PC
S11 FC
S11 LOG
S11 BA17
S11 PiFC
S11 BA4
S11 BA3, 1, 2
anti-DISC1
anti-CRMP1
anti-β actin
E
kDa
LC
C13 L BA36,37
C13 L BA9
C13 L FG
C13 R FC
C13 R FG
C13 R BA9
C13 R SFG
D2 FC
D2 LOG
D2 BA17
D2 PC
D2 BA3, 1, 2
100
75
63
75
63
48
F
LC
D4 BA17
D4 PC
D4 TC
C15 L FC
C15 L LOG
D5 LOG
D5 BA17
S1 PFC
S1 BA4
S1 BA3, 1, 2
S1 TC
anti-DISC1
anti-CRMP1
anti-β actin

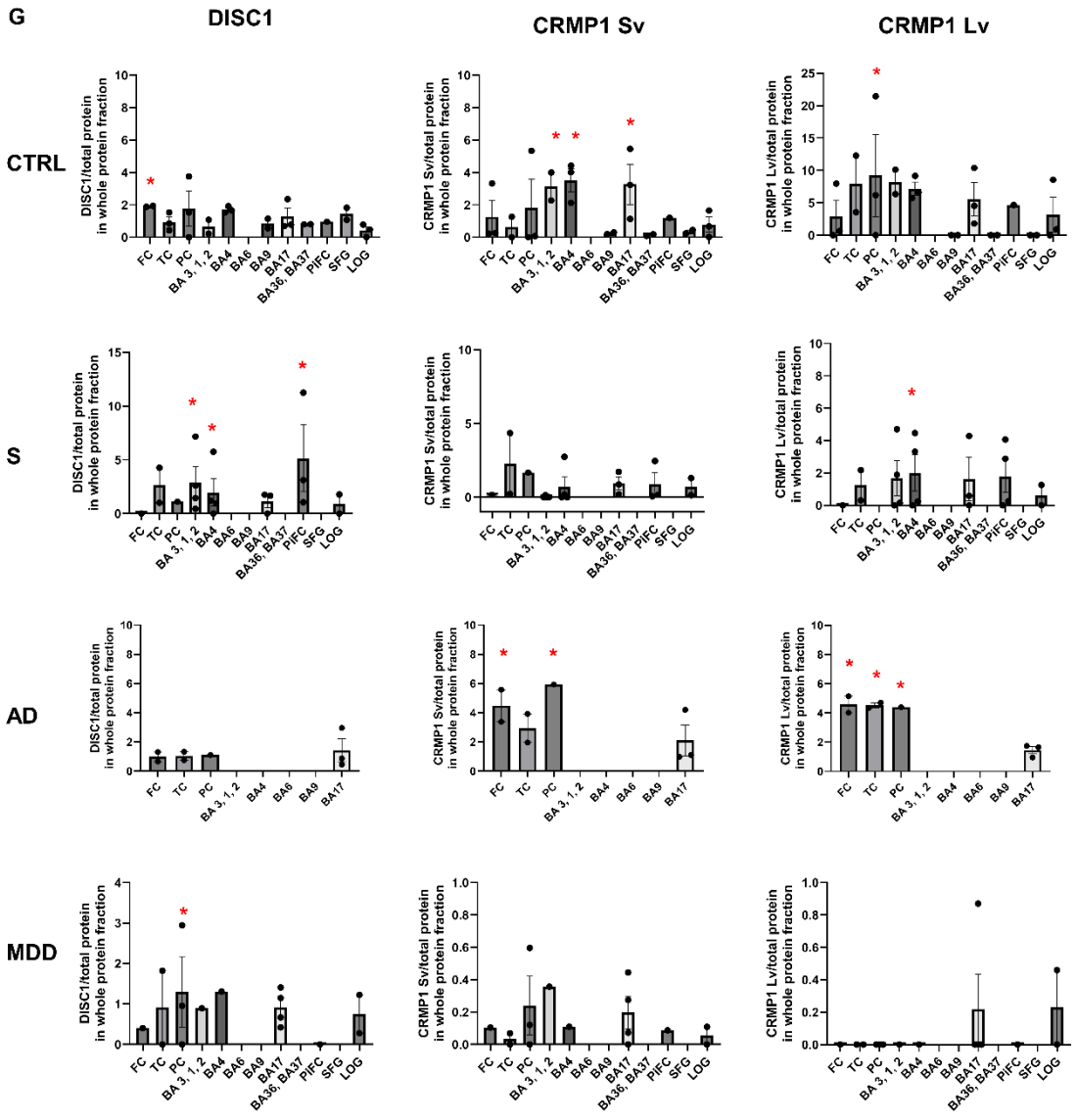

Figure 29: Intense bands were observed for CRMP1 and DISC1 in different brain regions, not correlating to diagnosis status. The samples were collected from suicide victims (S), control individuals (C), and patients with either AD (A), SZ, or MDD (D) diagnosis. Analysis of samples included Western blot with either anti-CRMP1, anti-DISC1, or anti-β actin antibodies and appropriate secondary antibody for visualization (**A-E**). Samples were anonymized and randomly loaded on acrylamide gels. Visualization was performed with an ECL kit and on a ChemiDoc MP Imaging System. Intensity of DISC1- and CRMP1-specific bands was quantified with Image Lab software (Bio-Rad) and normalized to total protein (**G**). Additionally, the value of protein of interest/total protein for each sample was normalized to loading control. Samples were grouped based on the diagnosis status, and regions. Columns represent different proteins (DISC1, CRMP1 Sv or CRMP1 Lv), while rows represent different diagnosis status or control: control (CTRL), suicide victims (S), and patients with AD or MDD diagnosis. Data on the graphs is presented as AVE +/- SEM and statistically analyzed with one-way ANOVA with Tukey's multiple comparisons test. All sample groups were compared, but only the pairs with significant differences are shown on the graph, with p values marked as follows. Abbreviations: L: left hemisphere or R: right hemisphere, BAx: Brodmann area number x, FC: frontal

cortex, LOG: lateral orbitofrontal gyrus, PC: parietal cortex, SFG: superior frontal gyrus, TC: temporal cortex, PiFC: piriform cortex.

A high DISC1 level in whole protein fraction was detected in at least one individual in all investigated diagnosis groups (marked as a red asterisk in **Figure 29 A-F**), however no statistically significant difference was observed. In control group, FC region showed an intense DISC1-specific bands in whole protein fraction (**Figure 29 E, F, G**). Increase for DISC1 bands was also seen in samples of PiFC, TC and BA 3, 1,2 collected from suicide victims (**Figure 29 C, D, F, G**). PC had increased level of DISC1 in patients with MDD diagnosis (**Figure 29 F**), while no region showed an increase in DISC1 level in patients with AD.

Regions BA3, 1, 2, BA4, BA 17 and PC showed increased CRMP1 in whole protein samples collected from control individuals (**Figure 29 A, B, G**). As PC region showed increased CRMP1 in patients with AD diagnosis (**Figure 29 B, G**), these elevations may reflect normal physiological expression. In contrast, CRMP1 increases in the FC and TC were specific to patients with Alzheimer's disease (**Figure 29 A, B, G**). Given that both FC and TC are regions critical for cognitive and emotional functioning, elevated CRMP1 in these areas may contribute to the cognitive decline and emotional dysregulation observed in AD. Levels of CRMP1 were generally low in whole protein samples from patients with MDD diagnosis.

Similarly, a second set of membranes was prepared for specific staining with anti-TRIOBP-1 antibody, followed by anti-β actin stain.

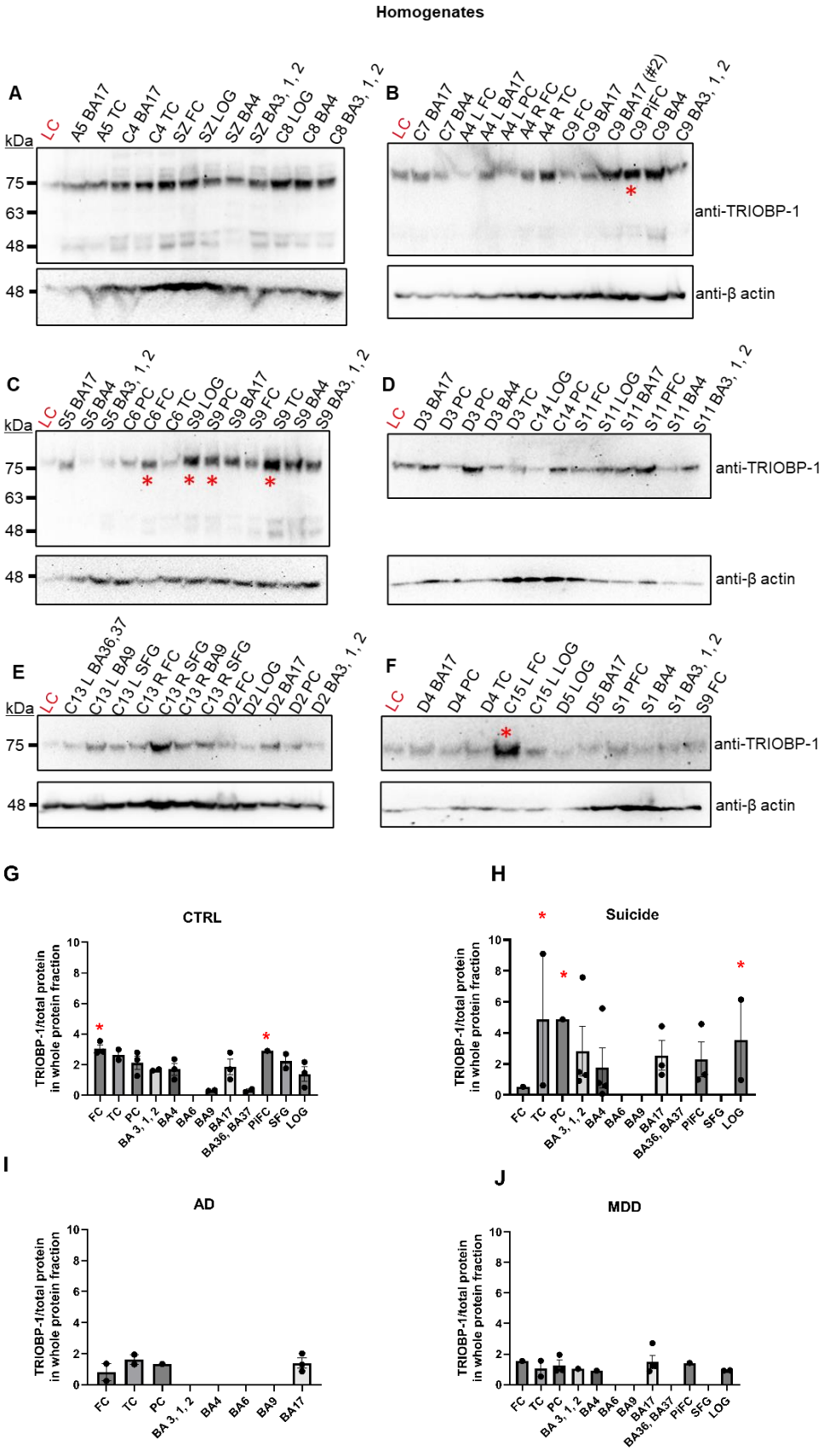
Homogenates
A
kDa
LC
A5 BA17
A5 TC
C4 BA17
C4 TC
SZ FC
SZ LOG
SZ BA4
SZ BA3, 1, 2
C8 LOG
C8 BA4
C8 BA3, 1, 2
75
63
48
48
B
LC
C7 BA17
C7 BA4
A4 L FC
A4 L BA17
A4 L PC
A4 R FC
A4 R TC
C9 FC
C9 BA17
C9 BA17 (#2)
C9 PIFC
C9 BA4
C9 BA3, 1, 2
anti-TRIOBP-1
anti-β actin
C
kDa
LC
S5 BA17
S5 BA4
S5 BA3, 1, 2
C6 PC
C6 FC
C6 TC
S9 LOG
S9 PC
S9 BA17
S9 FC
S9 TC
S9 BA4
S9 BA3, 1, 2
75
63
48
48
D
LC
D3 BA17
D3 PC
D3 PC
D3 BA4
D3 TC
C14 LOG
C14 PC
S11 FC
S11 LOG
S11 BA17
S11 PFC
S11 BA4
S11 BA3, 1, 2
anti-TRIOBP-1
anti-β actin
E
kDa
LC
C13 L BA36,37
C13 L BA9
C13 L SFG
C13 R FC
C13 R SFG
C13 R BA9
C13 R SFG
D2 FC
D2 LOG
D2 BA17
D2 PC
D2 BA3, 1, 2
75
48
F
LC
D4 BA17
D4 PC
D4 TC
C15 L FC
C15 L LOG
D5 LOG
D5 BA17
S1 PFC
S1 BA4
S1 BA3, 1, 2
S9 FC
anti-TRIOBP-1
anti-β actin
G
CTRL
TRIOBP-1/total protein in whole protein fraction
FC
TC
PC
BA 3, 1, 2
BA4
BA6
BA9
BA17
BA36, BA37
PIFC
SFG
LOG
H
Suicide
I
AD
J
MDD

Figure 30: Intense bands were observed for TRIOBP-1 in different brain regions, not correlating to diagnosis status. The samples were collected from suicide victims (S), control individuals (C), and patients with either AD (A), SZ, or MDD (D) diagnosis. Analysis of samples included Western blot with anti-TRIOBP-1 and anti-β actin antibodies and appropriate secondary antibody for visualization (**A-E**). Samples were anonymized and randomly loaded on acrylamide gels. Visualization was performed with an ECL kit and on a ChemiDoc MP Imaging System. Intensity of TRIOBP-1-specific bands was quantified with Image Lab software (Bio-Rad) and normalized to total protein (**F**). Additionally, the value of TRIOBP-1/total protein for each sample was normalized to loading control. Samples were grouped based on the diagnosis status, and regions. Data on the graphs is presented as AVE +/- SEM and statistically analyzed with one-way ANOVA with Tukey's multiple comparisons test. All sample groups were compared, but only the pairs with significant differences are shown on the graph. Abbreviations: L: left hemisphere or R: right hemisphere, BAx: Brodmann area number x, FC: frontal cortex, LOG: lateral orbitofrontal gyrus, PC: parietal cortex, SFG: superior frontal gyrus, TC: temporal cortex, PiFC: piriform cortex.

Total TRIOBP-1 levels were detected in at least one individual in all investigated diagnosis groups and bands with high intensity are marked with red asterisk in **Figure 30 A-J**). In some membranes, two bands were identified by the anti-TRIOBP-1 antibody (**Figure 30 A-C**), one at 75 kDa, corresponding to full-length TRIOBP-1 previously described in the literature[323,464] and other double bands at lower molecular weight, at 48 kDa, which could correspond to other proteins from the TRIOBP family, like TRIOBP-2, due to size and location of the region against which this antibody was raised. For this analysis, the focus was only on bands detected at 75 kDa. In control group, high level of TRIOBP-1 was detected in regions FC and PiFC (**Figure 30 B,C, F,** and **G**). In suicide victims, regions with high TRIOBP-1 levels were FC, TC and LOG (**Figure 30 C** and **H**).

The analysis of multiple brain regions highlights significant individual variability, with elevated levels of DISC1, CRMP1 and TRIOBP-1 in specific regions for certain individuals, no consistent diagnostic patterns.

4.1.6 Aggregation of key proteins across different brain regions, with a focus on suicide victims

To better understand the role of these proteins, the analysis was extended to investigate the insolubility of DISC1, CRMP1, and TRIOBP-1 across multiple brain regions. This is built on earlier results from I/A proteins in the IC, providing a broader perspective on how these proteins behave in diverse brain regions.

DISC1 insolubility was tested by staining purified protein fraction with an anti-DISC1 antibody. Like the homogenates (total proteins), the total protein level in the 'aggregate' (I/A proteins) samples was checked using stain-free imaging. The band intensity was quantified after visualization and used for later normalization of specific protein bands. After visualization, the samples were transferred from gel to membrane and specifically stained with anti-DISC1 and anti-CRMP1 antibodies.

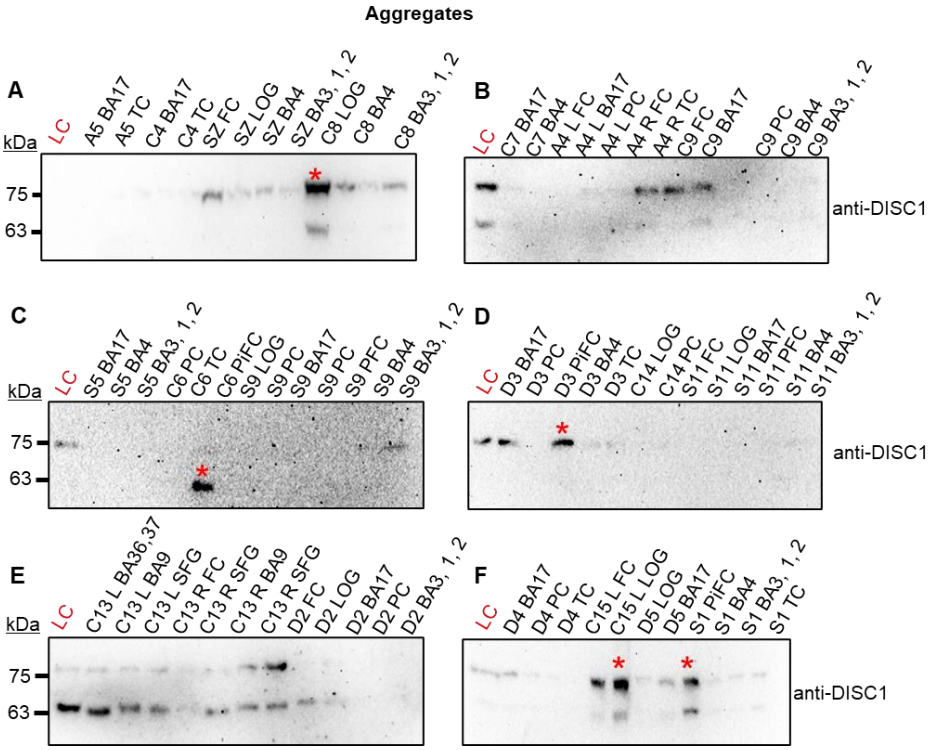

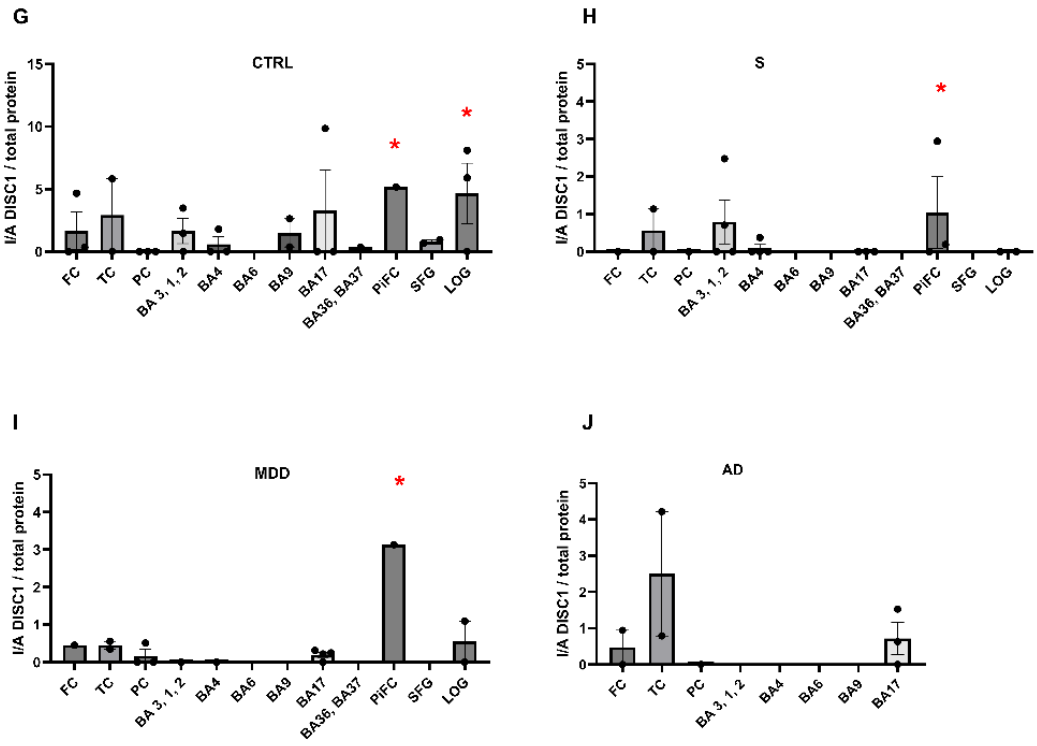

Figure 31: Intense bands were observed for DISC1 in different brain regions in I/A protein fraction, not correlating to diagnosis status. The samples were collected from suicide victims (S), control individuals (C), and patients with either AD (A), SZ, or MDD (D) diagnosis. Analysis of samples included Western blot with anti-DISC1 antibody and appropriate secondary antibody for visualization (**A-F**). Samples were anonymized and randomly loaded on acrylamide gels. Visualization was performed with an ECL kit and on a ChemiDoc MP Imaging System, while the band signal intensity was quantified with Image Lab software (Bio-Rad). Additionally, the samples were normalized to a loading control (LC) containing pooled samples. The samples with highly intense bands are marked with a red asterisk (*). Intensity of DISC1-specific bands was quantified with Image Lab software (Bio-Rad) and normalized to total protein (**G-J**). Additionally, the value of DISC1/total protein for each sample was normalized to loading control. Samples were grouped based on the diagnosis status, and regions with high intensity are marked with a red asterisk (*). Data on the graphs is presented as AVE +/- SEM and statistically analyzed with one-way ANOVA with Tukey's multiple comparisons test. All sample groups were compared, but only the pairs with significant differences are shown on the graph. Abbreviations: L: left hemisphere or R: right hemisphere, BAx: Brodmann area number x, FC: frontal cortex, LOG: lateral orbitofrontal gyrus, PC: parietal cortex, SFG: superior frontal gyrus, TC: temporal cortex, PiFC: piriform cortex.

When DISC1 aggregation/insolubility was assessed in the IC region, high-intensity 75 kDa DISC1 bands were detected in two suicide victims, one MDD patient, and one control, independent of age or postmortem interval, suggesting individual variability in DISC1 aggregation unrelated to these factors. Similarly, the detected I/A

DISC1 signal shows far more inter-sample variability than the total proteins in the same, I/A protein, fraction (**Figure 31 A-F**), indicating that variability in the detected protein signal is not solely a result of changes in total protein insolubility.

Specific DISC1 bands with high intensity were detected in I/A protein fraction collected from PiFC region in both a suicide victims and controls (**Figure 31 A, C, F, G**). However, it is important to note how values for I/A DISC1 in control group are higher than in suicide group. Since PiFC connects to brain areas involved in emotion and impulse control, this may reflect dysregulation linked to mood disorders and suicidality. However, since there is a high level of DISC1 in controls as well, it is more likely that region has naturally high expression DISC1. Additionally, LOG region showed high level of I/A DISC1 in control group. However, there were no statistically significant changes.

In this analysis, all quantified protein signals, both from the whole protein fraction (homogenates) and the insoluble/aggregated (I/A) fraction, were normalized to total protein levels, allowing for the calculation of aggregation levels as the ratio between I/A and whole protein fractions.

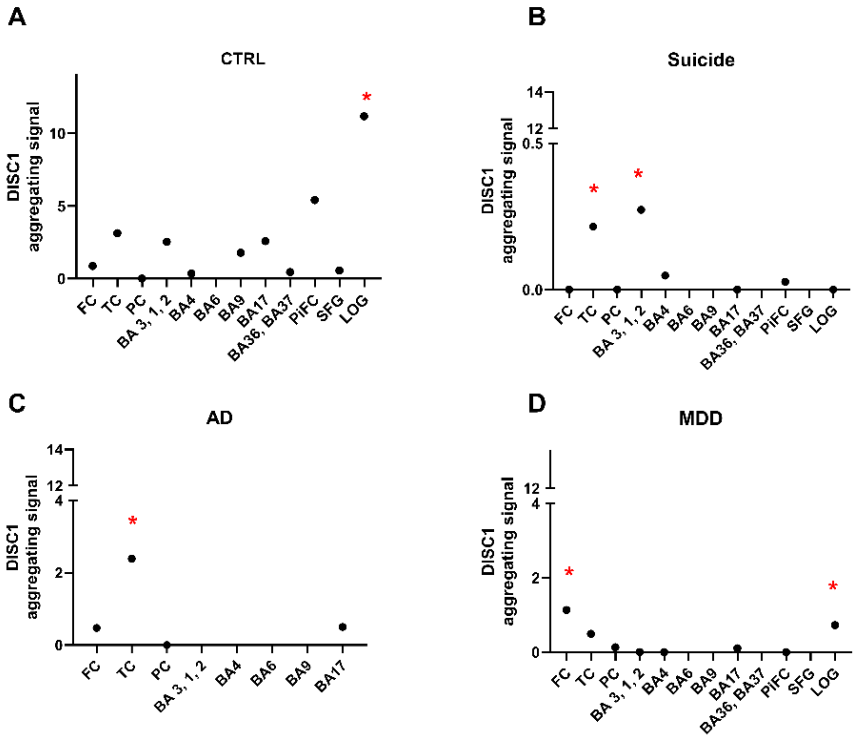

Figure 32: DISC1 aggregating signal varies by diagnosis. Data on the graphs represents average aggregating signal (ratio between I/A and whole protein fraction)

for protein DISC1. The values are grouped by diagnosis: suicide victims, controls (CTRL), patients with previous MDD and AD diagnosis (**A-D**). High values are marked with a red asterisk (*). Increased aggregating signal is detected in LOG region collected from control individuals and distinct regional patterns in suicide victims, patients with MDD and AD diagnosis.

Unexpectedly, the highest DISC1 aggregation signals is seen in previously healthy control individuals, particularly in the LOG, as indicated by the red asterisk in (**Figure 32 A)**. In comparison, suicide victims and patients diagnosed with MDD show similar levels of DISC1 aggregation, with the highest signals in the TC and BA 3, 1, and 2 for suicide victims (**Figure 32 B**), and in the FC and LOG for MDD patients (**Figure 32 D**). In contrast, individuals diagnosed with AD exhibit overall low DISC1 aggregation, with the TC region showing the highest signal among them (**Figure 32 C**).

In summary, DISC1 protein was detected in the whole protein fraction across all diagnostic groups, but no statistically significant differences were observed. In control individuals, strong DISC1 bands were most prominent in the FC, while suicide victims showed increased levels in the PiFC, TC, and somatosensory cortex (BA 3, 1, 2). In patients with MDD, elevated DISC1 levels were observed in the PC, whereas no regional increases were detected in patients with AD. In the I/A protein fraction, high-intensity 75 kDa DISC1 bands were found in two suicide victims, one MDD patient, and one control in the IC, with variability not attributable to age or *post-mortem* interval. Notably, high I/A DISC1 levels were also observed in the PiFC of both controls and suicide victims, and in the LOG of controls. Overall, controls exhibited higher I/A DISC1 levels than suicide victims, though differences were not statistically significant, suggesting that regions like PiFC may naturally express high DISC1 irrespective of pathology. When examining the DISC1 aggregation signal (ratio of I/A to total DISC1), controls displayed the highest values, particularly in the LOG. Suicide victims and MDD patients had similar overall aggregation levels, but with distinct regional peaks: suicide victims in TC and BA 3, 1, 2, and MDD patients in FC and LOG. AD patients exhibited the lowest DISC1 aggregation overall, with the TC showing relatively higher values among them.

To conclude, these findings indicate that DISC1 aggregation depends on region and analyzed individual. The unexpectedly high levels observed in healthy controls underscore the importance of interpreting protein aggregation in context, as presence alone may not indicate pathology. Nevertheless, distinct regional patterns in suicide

victims and MDD patients suggest potential roles for DISC1 in emotion, impulse control, and sensory integration.

The insolubility of CRMP1 was assessed next, as it showed interesting results in samples from the IC region, especially regarding possible co-aggregation with DISC1.

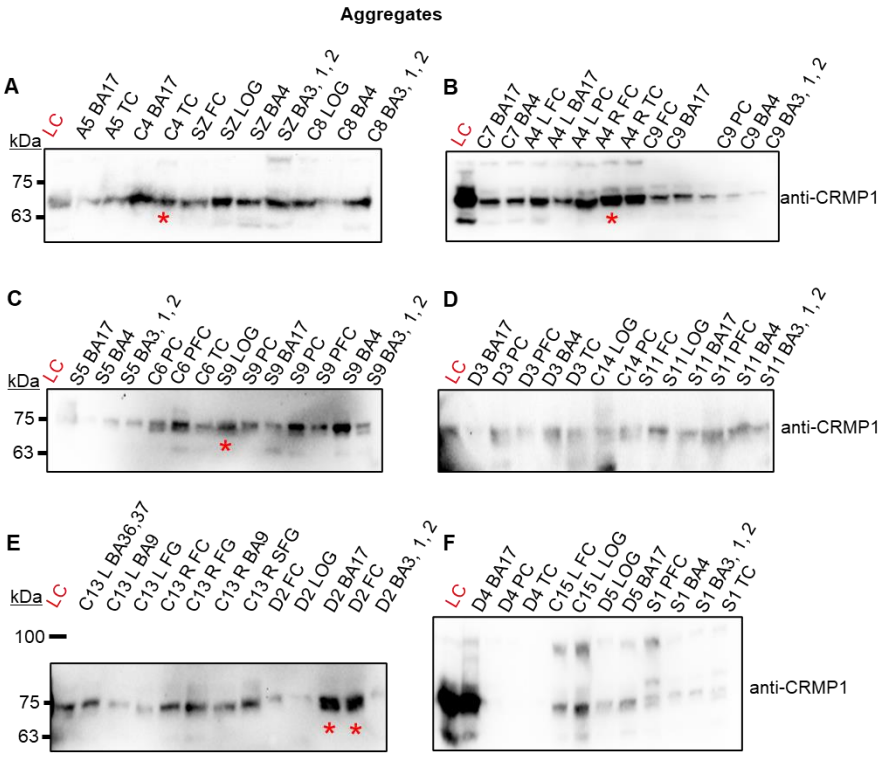

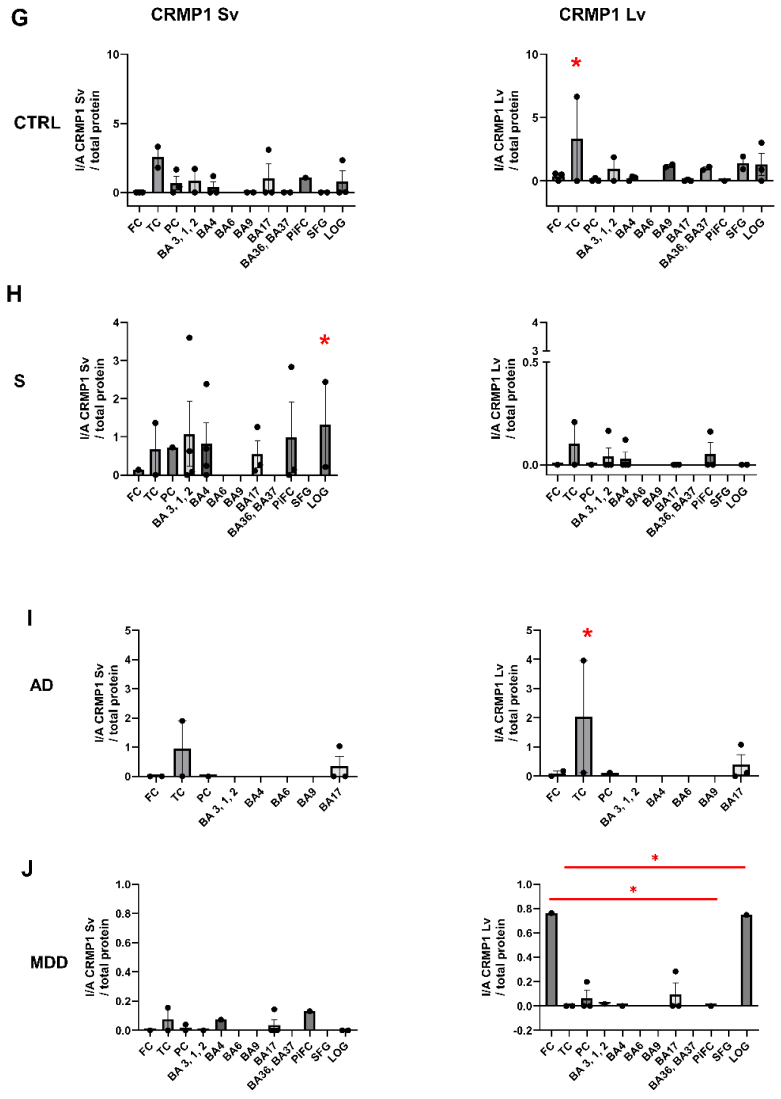

Figure 33: Intense bands were observed for both CRMP1 variants in different brain regions in I/A protein fraction, not correlating to diagnosis status. The samples were collected from suicide victims (S), control individuals (C), and patients with either AD (A), SZ, or MDD (D) diagnosis. Analysis of samples included Western blot with anti-CRMP1 antibody and appropriate secondary antibody for visualization (**A-F**). Samples were anonymized and randomly loaded on acrylamide gels. Visualization was performed with an ECL kit and on a ChemiDoc MP Imaging System. Additionally, the samples were normalized to a loading control (LC) containing pooled samples. The samples with highly intense bands are marked with a red asterisk (*). Intensity of CRMP1-specific bands was quantified with Image Lab software (Bio-Rad) and normalized to total protein (**G - J**). Additionally, the value of CRMP1/total protein for each sample was normalized to LC. Samples were grouped based on the diagnosis status and brain region. Columns represent different proteins (CRMP1 Sv or CRMP1 Lv), while rows represent different diagnosis status or control: control (CTRL), suicide victims (S), and patients with AD or MDD diagnosis. The samples with highly intense bands are marked with a red asterisk (*). Data on the graphs is presented as AVE +/- SEM and statistically analyzed with one-way ANOVA with Tukey's multiple

comparisons test. All sample groups were compared, but only the pairs with significant differences are shown on the graph, with p values marked as follows: p < .05 (*) and red line, p <.001 (**), p <.001 (***). Abbreviations: L: left hemisphere or R: right hemisphere, BAx: Brodmann area number x, FC: frontal cortex, LOG: lateral orbitofrontal gyrus, PC: parietal cortex, SFG: superior frontal gyrus, TC: temporal cortex, PiFC: piriform cortex.

Highly intense CRMP1 Lv bands are detected in I/A protein fraction collected from TC region of control samples (**Figure 37 A** and **G, right**), while highly intense CRMP1 Sv bands are detected in LOG region of suicide victims (**Figure 37 C** and **H, left**). In patients with AD diagnosis, TC region has high level of I/A CRMP1 Lv (**Figure 37 B** and **I, right**). Interestingly, regions FC and LOG from patients with MDD had more I/A CRMP1 Lv compared to other brain regions, with statistical significance (p < .05, **Figure 37 E** and **J, right**). Abnormal CRMP1 Lv accumulation in areas responsible for emotional regulation and self-awareness (LOG) and cognitive functions (FC) is interesting as, both regions were previously reported as impaired in MDD [354,470]. However, it is important to note how values of I/A CRMP1 Lv and Sv are lower in patients with MDD (**Figure 37 J**) than other tested groups, with control samples having the highest values (**Figure 37 G**), indicating that CRMP1 aggregation probably is not a primary feature of MDD pathology compared to other disorders.

As previously, the relative amount of I/A CRMP1 Sv and Lv was quantified by normalizing CRMP1 band intensity from aggregating samples to CRMP1 band intensity detected in "homogenate" (total protein) samples, grouped by diagnosis and shown as on the graphs (**Figure 34** and **35**).

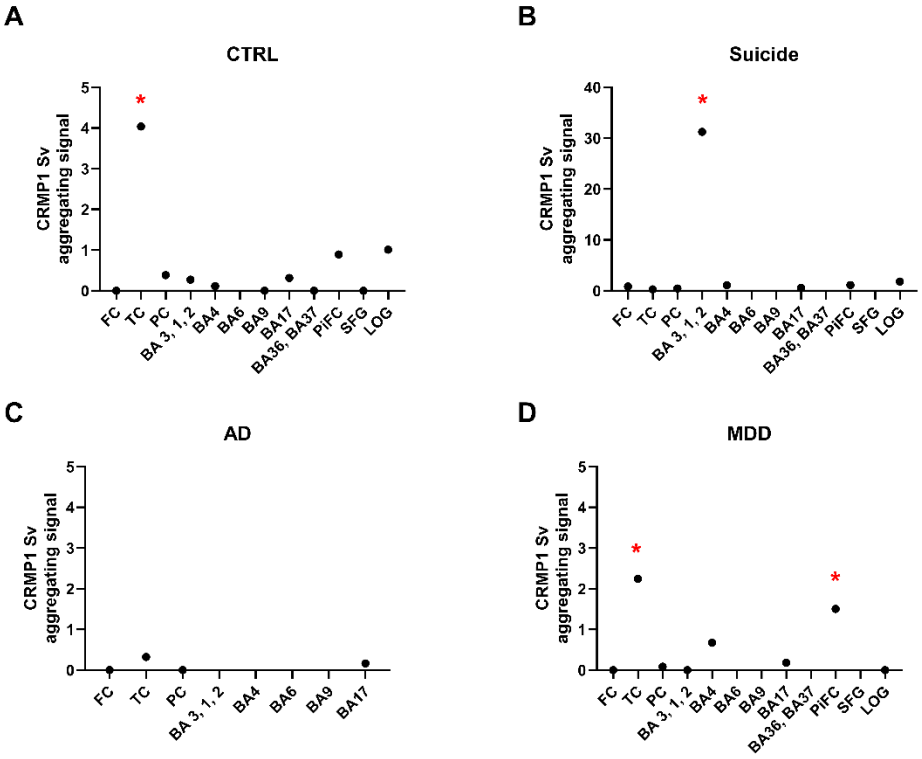

Figure 34: CRMP1 Sv aggregation patterns highlight somatosensory elevation in suicide. Data on the graphs represents average aggregating signal (ratio between I/A and whole protein fraction) for protein CRMP1 Sv. The values are grouped by diagnosis: suicide victims, controls (CTRL), patients with previous MDD and AD diagnosis (**A-D**). High values are marked with a red asterisk (*).

High CRMP1 Sv aggregation signals are observed in the TC of both control individuals (**Figure 38 A**) and patients diagnosed with MDD (**Figure 38 D**). Additionally, the PiFC shows elevated aggregation in MDD patients (**Figure 38 D**). Interestingly, values of CRMP1 Sv aggregating signal are higher in suicide victims, with region BA 3, 1, 2 having the highest signal (**Figure 38 B**), suggesting a possible link between CRMP1 aggregation and altered sensory processing in suicide victims, which was also referenced in previous research[289,511]. Patients with AD diagnosis have no high values for aggregating signal of CRMP1 Sv.

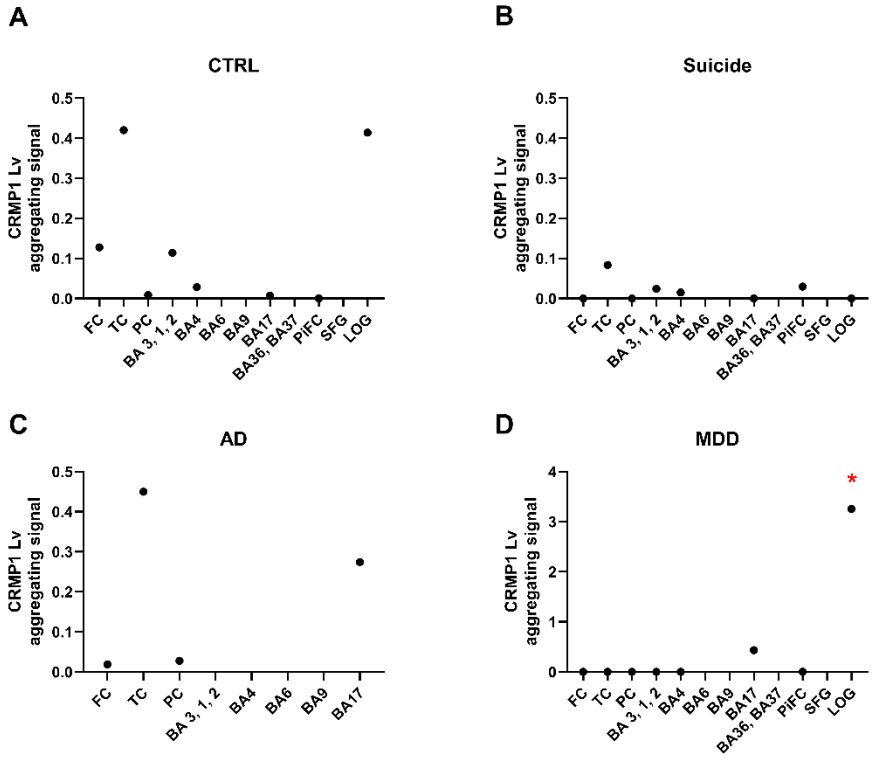

Figure 35: CRMP1 Lv aggregation signal peaks in LOG of MDD patients. Data on the graphs represents average aggregating signal (ratio between I/A and whole protein fraction) for protein CRMP1 Lv. The values are grouped by diagnosis: suicide victims, controls (CTRL), patients with previous MDD and AD diagnosis (**A-D**). High values are marked with a red asterisk (*).

Patients diagnosed with MDD exhibited the highest CRMP1 Lv aggregation signal compared to other diagnostic groups. Within this group, the LOG showed the most prominent signal (**Figure 35 D**). Elevated CRMP1 Lv aggregation was also observed in the TC and BA17 in both control and AD groups (**Figure 35 A and C**). In contrast, no brain regions from suicide victims showed increased CRMP1 Lv aggregation signal (**Figure 35 B**).

In summary, CRMP1 levels in the whole protein fraction were elevated in several brain regions of control individuals, including the somatosensory cortex (BA 3, 1, 2), motor cortex (BA 4), visual cortex (BA 17), and PC, with the PC also showing increased levels in AD patients, which could suggest a physiologically high expression. In contrast, elevated CRMP1 in the FC and TC was specific to AD and may relate to cognitive and emotional decline. MDD samples showed generally low CRMP1 in this fraction. In the I/A fraction, intense CRMP1 Lv bands were detected in the TC of controls and AD patients, while suicide victims showed high CRMP1 Sv in the LOG. MDD patients had

significantly elevated I/A CRMP1 Lv in the FC and LOG, but overall lower values compared to other groups, suggesting aggregation may not be central to MDD pathology. Aggregation signal analysis revealed high CRMP1 Sv in the TC of controls and MDD patients, and in the PiFC of MDD. Suicide victims showed the strongest CRMP1 Sv aggregation in the somatosensory cortex, possibly linking CRMP1 aggregation to altered sensory processing.

Overall, CRMP1 expression and aggregation show specific patterns depending on regions. Elevated levels of CRMP1 in control and AD samples likely reflect normal physiological expression, while increased aggregation in the frontal and orbital regions of MDD patients may relate to emotional and cognitive dysfunction. Notably, high CRMP1 Sv aggregation in the somatosensory cortex of suicide victims may point to altered sensory processing. These findings suggest CRMP1 aggregation is not a core feature of MDD but may contribute to specific symptom domains across disorders.

Besides the CRMP1 and DISC1, insolubility/aggregation of TRIOBP-1 was tested in other brain regions from the same patients used in previous experiments. The pooled sample was used as a loading control across different membranes (BA3, 1, 2 from a control individual C9 and suicide victim S9, BA17 from a control individual C7, BA4 region from a patient with SZ and S13). As with “homogenates” (total protein), the level of total protein in “aggregate” (I/A protein fraction) samples was checked with a TCE stain.

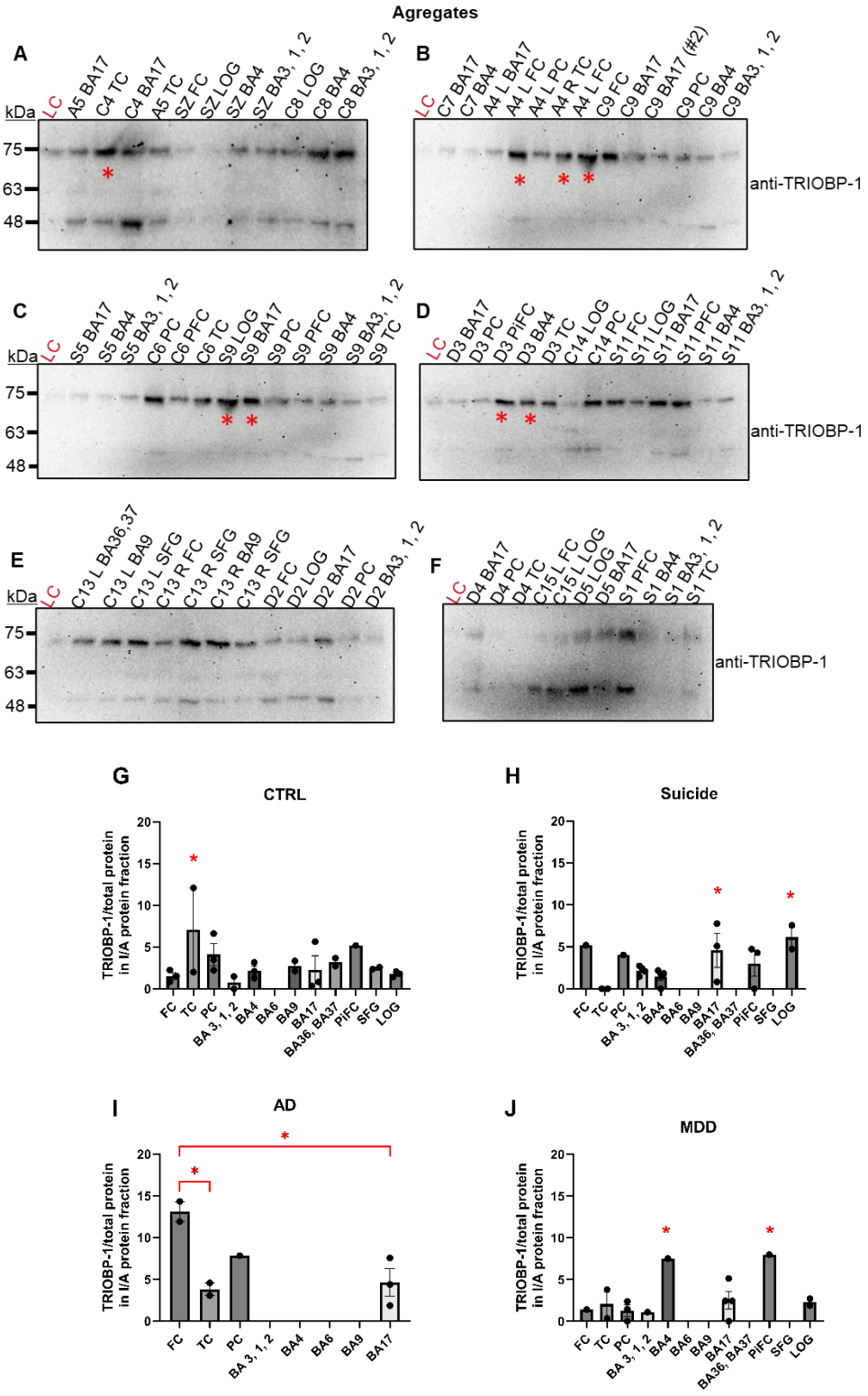

Figure 36: Significant I/A TRIOBP-1 accumulation in FC of AD patients. The samples were collected from suicide victims (S), control individuals (C), and patients with either AD (A), SZ, or MDD (D) diagnosis. Analysis of samples included Western blot with anti-TRIOBP-1 antibody and appropriate secondary antibody for visualization (**A – F**). Samples were anonymized and randomly loaded on acrylamide

gels. Visualization was performed with an ECL kit and on a ChemiDoc MP Imaging System. Intensity of TRIOBP-1-specific bands was quantified with Image Lab software (Bio-Rad) and normalized to total protein (**G - J**). Additionally, the value of CRMP1/total protein for each sample was normalized to LC. Samples were grouped based on the diagnosis status and brain region: control (CTRL), suicide victims (S), and patients with AD or MDD diagnosis. The samples with highly intense bands are marked with a red asterisk (*). Data on the graphs is presented as AVE +/- SEM and statistically analyzed with one-way ANOVA with Tukey's multiple comparisons test. All sample groups were compared, but only the pairs with significant differences are shown on the graph, with p values marked as follows: $p < .05$ (*) and red line, $p < .001$ (**), $p < .001$ (***). Abbreviations: L: left hemisphere or R: right hemisphere, BAx: Brodmann area number x, FC: frontal cortex, LOG: lateral orbitofrontal gyrus, PC: parietal cortex, SFG: superior frontal gyrus, TC: temporal cortex, PiFC: piriform cortex.

Elevated levels of I/A TRIOBP-1 were observed in the BA17 and LOG of suicide victims (**Figure 36 C** and **H**), and in the primary motor cortex (BA4) and PiFC of patients with MDD (**Figure 36 D** and **J**). In control samples, the TC showed the highest I/A TRIOBP-1 levels (**Figure 36 A** and **G**). Notably, a statistically significant increase in I/A TRIOBP-1 was found in the FC of AD patients when compared to their TC and BA17 regions (**Figure 36 B** and **I**), highlighting region-specific aggregation in AD.

As in previous examples, the aggregating signal of protein TRIOBP-1 was quantified by normalizing TRIOBP-1 band intensity from I/A protein fraction to TRIOBP-1 band intensity detected in "homogenate" (total protein) samples, grouped by diagnosis and shown as on the graph (**Figure 37**).

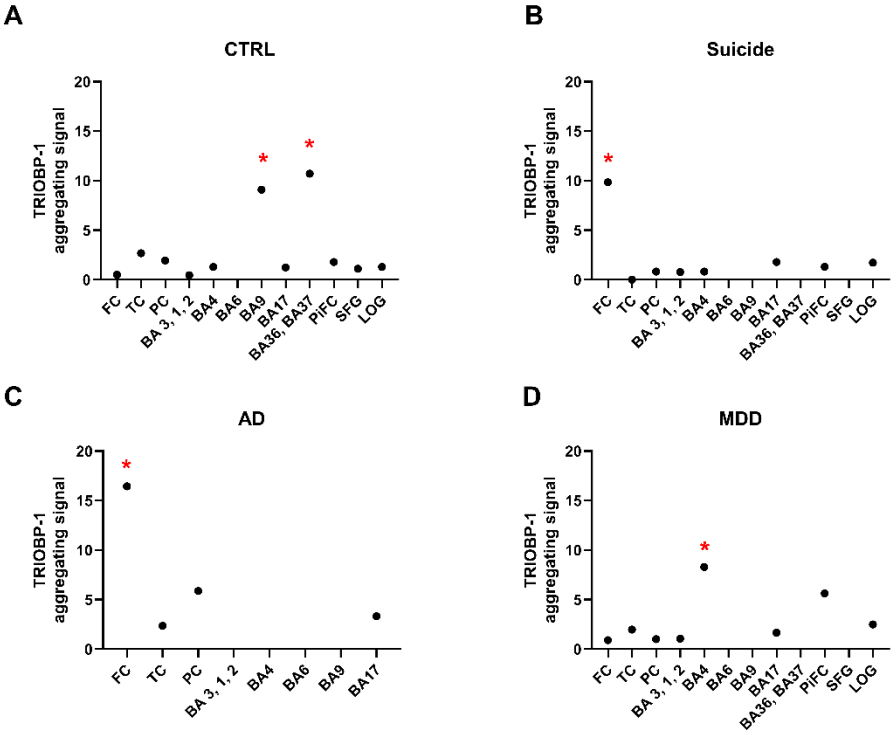

Figure 37: Region-specific TRIOBP-1 aggregation patterns across diagnostic groups, with elevated signal in the FC of AD patients. Data on the graphs represents average aggregating signal (ratio between I/A and whole protein fraction) for protein TRIOBP-1. The values are grouped by diagnosis: suicide victims, controls (CTRL), patients with previous MDD and AD diagnosis (**A-D**). High values are marked with a red asterisk (*).

A strong TRIOBP-1 aggregation signal was observed in BA9, BA36, and BA37 regions in control samples (**Figure 37 A**); in the FC of suicide victims (**Figure 37 B**); and in BA3, BA1, and BA2 of patients with MDD (**Figure 37 D**). Notably, the FC of AD patients showed the highest TRIOBP-1 aggregation signal (**Figure 37 C**), not only compared to other brain regions within the AD group, but also relative to all other groups analyzed. Given the critical role FC plays in executive function, working memory, and decision-making, the accumulation of aggregated TRIOBP-1 in this region may interfere with cytoskeletal integrity or intracellular trafficking, contributing to the disruption of neuronal function and accelerating cognitive decline.

In summary, TRIOBP-1 was detected across all diagnostic groups, with strong signals in the FC and PiFC of controls, and in the FC, TC, and LOG of suicide victims. In the I/A fraction, elevated TRIOBP-1 was observed in BA17 and LOG of suicide victims, and in BA4 and PiFC of MDD patients. Controls showed the highest I/A TRIOBP-1 levels in the TC, while AD patients exhibited a significant increase in

I/A TRIOBP-1 in the FC compared to their own TC and BA17. Aggregation-specific analysis revealed strong TRIOBP-1 signals in BA9, BA36, and BA37 of controls; the FC of suicide victims; BA3, BA1, and BA2 of MDD patients; and most prominently, in the FC of AD patients, where levels surpassed all other regions and groups. These results align with the role FC has in cognitive decline in AD [470], TC and occipital regions in emotional processing and suicide [96,470], and sensorimotor areas in MDD [48]. Moreover, strong aggregation TRIOBP-1 in the FC in AD suggests a disrupted cytoskeletal or intracellular function of TRIOBP-1, which can lead to cognitive impairment.

It is important to note that the first exposure that consistently revealed proteins in data analysis was chosen. As a result, the different antibodies are not directly comparable; comparisons can only be made within the same membrane. For instance, some proteins can show more I/A in specific samples than in others, which leads us to categorize these as aggregating. In contrast, the levels of other proteins can be more consistent across the samples. However, it is hard to conclude if this indicates that all samples exhibit protein aggregation or if they are merely at background levels.

The insolubility profiles of DISC1, CRMP1, and TRIOBP-1 reveal significant inter-individual variability and region-specific differences. As all tested proteins exhibit some aggregation in healthy controls, highlighting the need for better methods to screen participants in the analysis. Nevertheless, results from these additional regions provide a clearer picture of pathology per individual than results from the IC region only.

4.1.7 Insolubility of proteins in the human brain affected by SZ and AD, with a focus on DISC1

Previous studies of DISC1 insolubility in brain samples from patients diagnosed with SZ focused on one, or three at most, regions from the same patients due to limited availability of samples. As part of this project, 20 regions from different parts of a single patient's brain with diagnosis of SZ and AD (later referred to as patient R) were investigated. Samples from previously healthy individuals (C) and patients with AD were also collected and analyzed as control samples. The samples were blinded for me during the experiment. There was no significant difference in sex, age or PMI for analyzed individuals.

The I/A protein fraction, referred to in the figures as "aggregates," was purified. Portions from each region of the same patient were combined to create a "pooled" sample, resulting in a standardized control sample likely to contain all the proteins of interest. The hypothesis was that patient R would exhibit one or more aggregating proteins in his brain; therefore, the sample was tested against comparable pools of individuals to determine if any I/A protein was over-represented in patient R compared to the controls. Each pooled sample was stained for DISC1, CRMP1, and TRIOBP-1 proteins, previously implicated in SZ, while the loading control was β-actin.

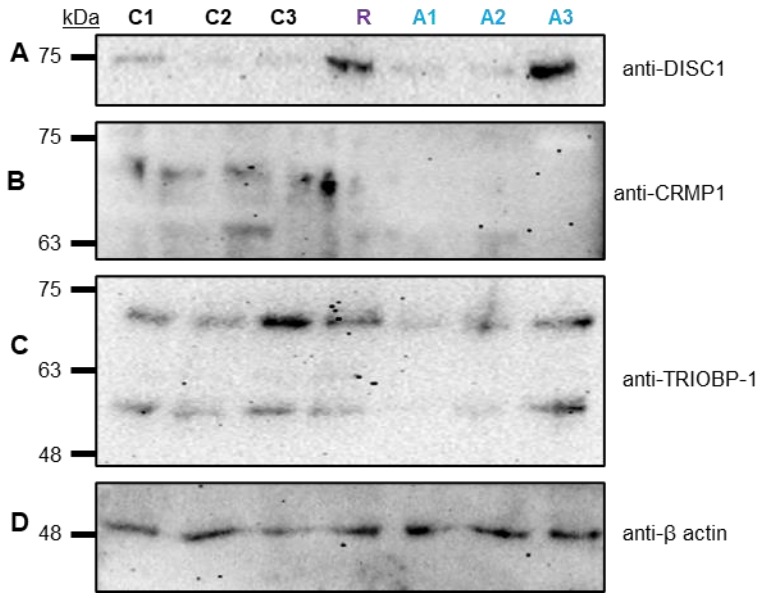

Figure 38: DISC1 shows increased insolubility in the SZ sample and one AD case, while CRMP1 is most insoluble in SZ. TRIOBP-1 remains consistent across samples, except in the control. I/A protein fractions were purified from various *post-mortem* brain tissue samples. Pooled I/A fractions from five regions of patient R's brain (the FC, LOG, OC, primary motor cortex, and the somatosensory cortex) were then compared to equivalent I/A protein pools from six other individuals: three with AD (A1-A3), and three control individuals (C1-C3). Samples were stained with anti-DISC1 (**A**), -CRMP1 (B), -TRIOBP-1 (**C**), and -β-actin (**D**) antibodies.

Among the three proteins of interest, patient R exhibited an intense band for DISC1, which was not observed in other samples except for one patient with AD (marked as A3, **Figure 38 A**).

CRMP1 was represented in all samples, with the band in the sample from patient R being the most intense (**Figure 38 B**). The isoform of TRIOBP-1 close to 75 kDa was detected in all samples, with the most intense band in the C3 sample. The isoform between 63 and

48 kDa was present in almost all samples, missing in only one patient with AD, A1 (**Figure 38 C**).

DISC1 was further analyzed in "homogenates" (total protein) from all regions available for patient R, 1 sample from the control, and 1 from the AD group. β-actin was used as a loading control.

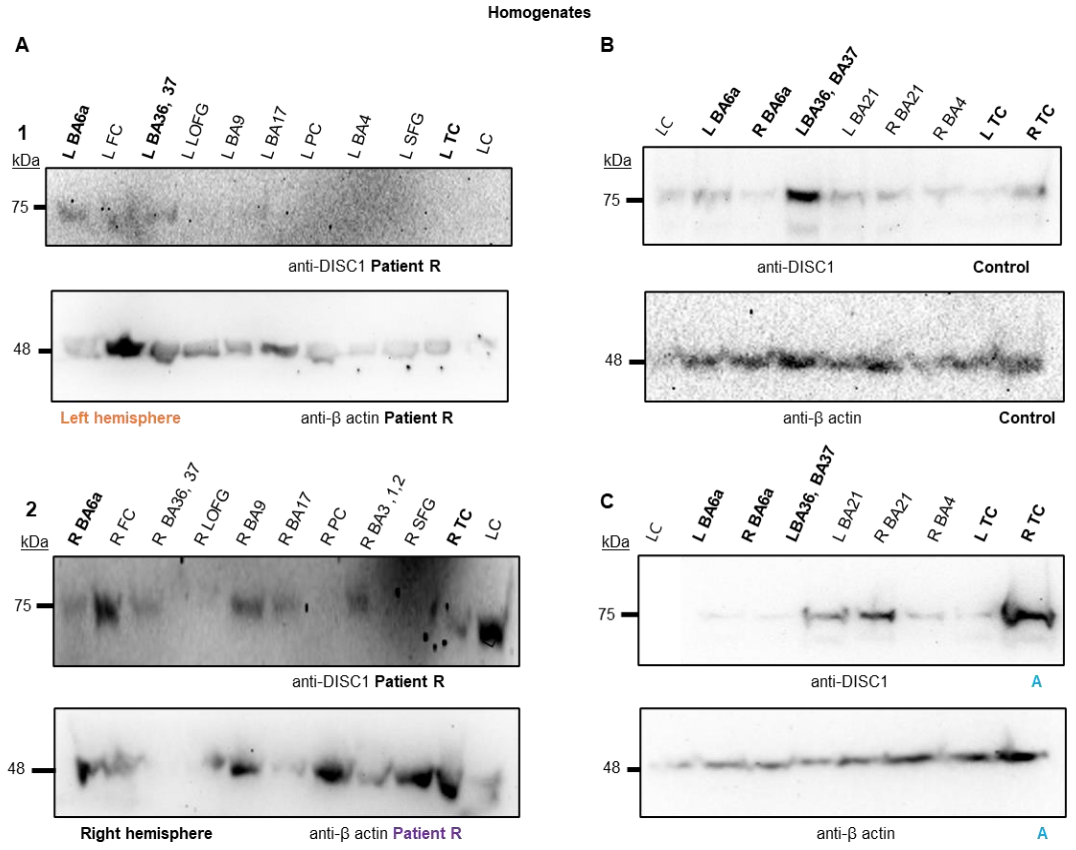

Figure 39: Total level of DISC1 varies across 20 regions from the SZ patient, AD patient, and in the control. Samples from the left and right hemispheres (**A1** and **A2**) were collected from patient R, who had SZ and AD diagnoses. Samples were also collected from control patient (**B**) and AD patient (**C**). The total protein level was analyzed in original, unpurified "homogenates" (total protein) of each brain sample with anti-DISC1 and anti-β actin antibodies during Western blot. Additionally, the samples were normalized to a loading control (LC), which contains pooled samples used in previous figure 40, which is also shown in the images. Abbreviations: L: left hemisphere or R: right hemisphere, BAx: Brodmann area number x, FC: frontal cortex, LOG: lateral orbitofrontal gyrus, PC: parietal cortex, SFG: superior frontal gyrus, TC: temporal cortex, R – SZ patient, C – control, A – AD patient.

In the left hemisphere of patient R, bands specific for DISC1 were detected only in BA6a, FC, and BA36, 37. At the same time, the loading control was consistent except for a highly intense band in the FC (**Figure 39 A1**). As for his right hemisphere, the DISC1 presence was variable, with the most intense band for DISC1 seen in the FC, BA9,

and PC, and notably, the bands for β-actin had variable intensity (**Figure 39 A2**). In samples obtained from the control group, DISC1 bands were detected in all samples, with the most intense band found in BA36 BA37 in the left hemisphere, and the loading control remained consistent (**Figure 39 B**). In the AD patient, intense DISC1 bands were detected in BA21 from both hemispheres and the TC of the right hemisphere, with lower intensity in BA4 from the right hemisphere and the TC from the left hemisphere (**Figure 39 C**). The loading control was consistent, except for a highly intense band in the TC from the right hemisphere. The relative total level of DISC1 from these samples was calculated by quantifying DISC1 band intensity and normalizing it to the band intensity of β-actin.

All regions from patient R's brain were further investigated for DISC1 insolubility using the previously described process. As controls, the available regions for one C and one AD were also investigated.

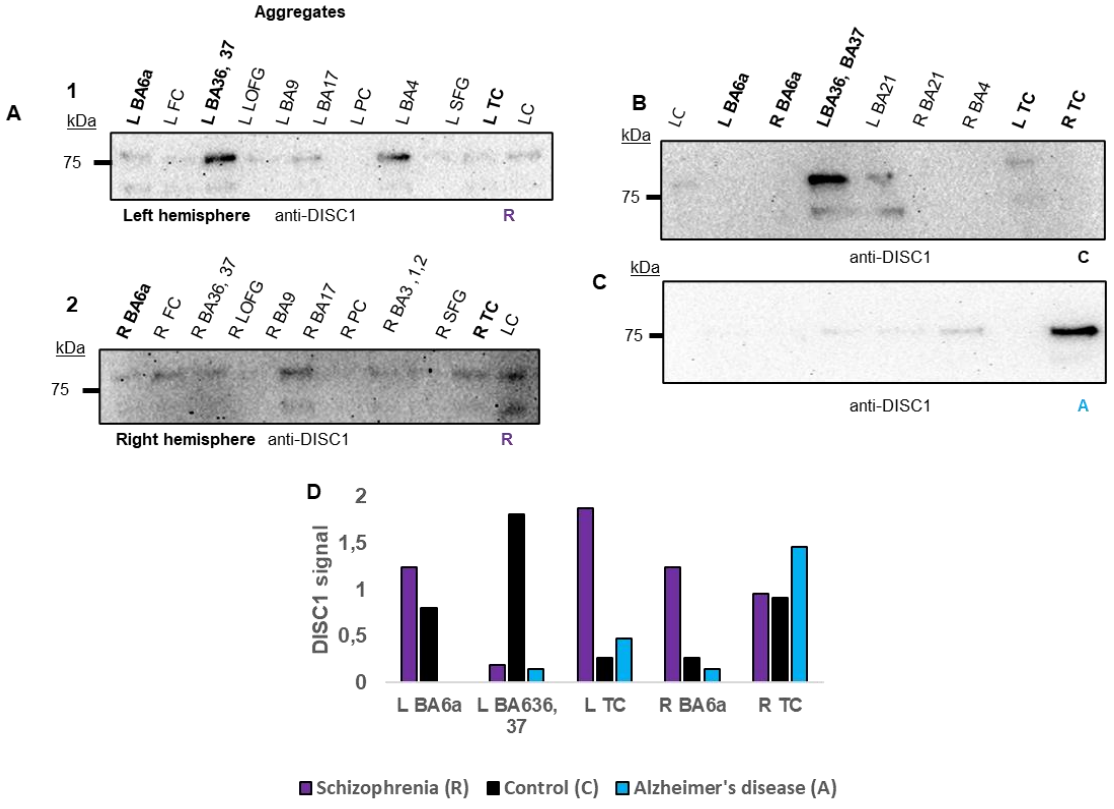

Figure 40: I/A DISC1 varies across different brain regions, regardless of diagnosis. Samples from the left and right hemispheres (**A1** and **A2**) were collected from patient R, who had SZ and AD diagnoses. Samples were also collected from control patient (**B**) and AD patient (**C**). The DISC1 signal from regions available for all three analyzed individuals (purple – SZ patient R, black – control, blue – AD patient A) was compared and shown in graph D. I/A protein fractions were purified

from each tissue sample and stained with anti-DISC1 antibody during Western blot analysis. Additionally, the samples were normalized to a LC, which contains pooled samples used in the previous figure (**Figure 41**). Abbreviations: L: left hemisphere or R: right hemisphere, BAx: Brodmann area number x, FC: frontal cortex, LOG: lateral orbitofrontal gyrus, PC: parietal cortex, SFG: superior frontal gyrus, TC: temporal cortex, R – SZ patient, C – control, A – AD patient.

DISC1 was detected in almost all samples, except for the PC in both hemispheres, BA9 and SFG in the right hemisphere **(Figure 40 A1-2**). Interestingly, the band intensity varied between the regions, with the most intense bands being in the BA 36,37, and 4 in the left hemisphere **(Figure 40 A1**). As for controls, samples from a previously healthy individual had the most intense band specific for DISC1 in BA36,37, and BA21 (**Figure 40 B**). The patient with AD had the most intense band in the TC from the right hemisphere (**Figure 40 C**). Out of all samples, there were 5 regions present in all three patients: BA36, 37 from the left hemisphere, BA6a, and TC from both hemispheres. Band intensity for DISC1 from I/A protein fraction was normalized to the total level of DISC1 in those samples (described in the previous paragraph), and a relative DISC1 signal was obtained (**Figure 40 D**). The DISC1 signal was higher in samples from patient R for BA6a in both hemispheres and the TC in the left hemisphere compared to C and AD. C had the highest DISC1 signal for BA36, 37 in the left hemisphere. As for AD, the highest DISC1 signal was in the TC from the right hemisphere.

As DISC1 variability was observed in SZ patient R, the samples from different brain regions of individuals from control and AD groups were also analyzed for DISC1. New individuals were included: control C4 and a patient SZ2 with only SZ diagnosis. As previously described, for each patient, a "pooled" sample was created and stained not only for DISC1 but for CRMP1 and TRIOBP-1, while β-actin remained as loading control.

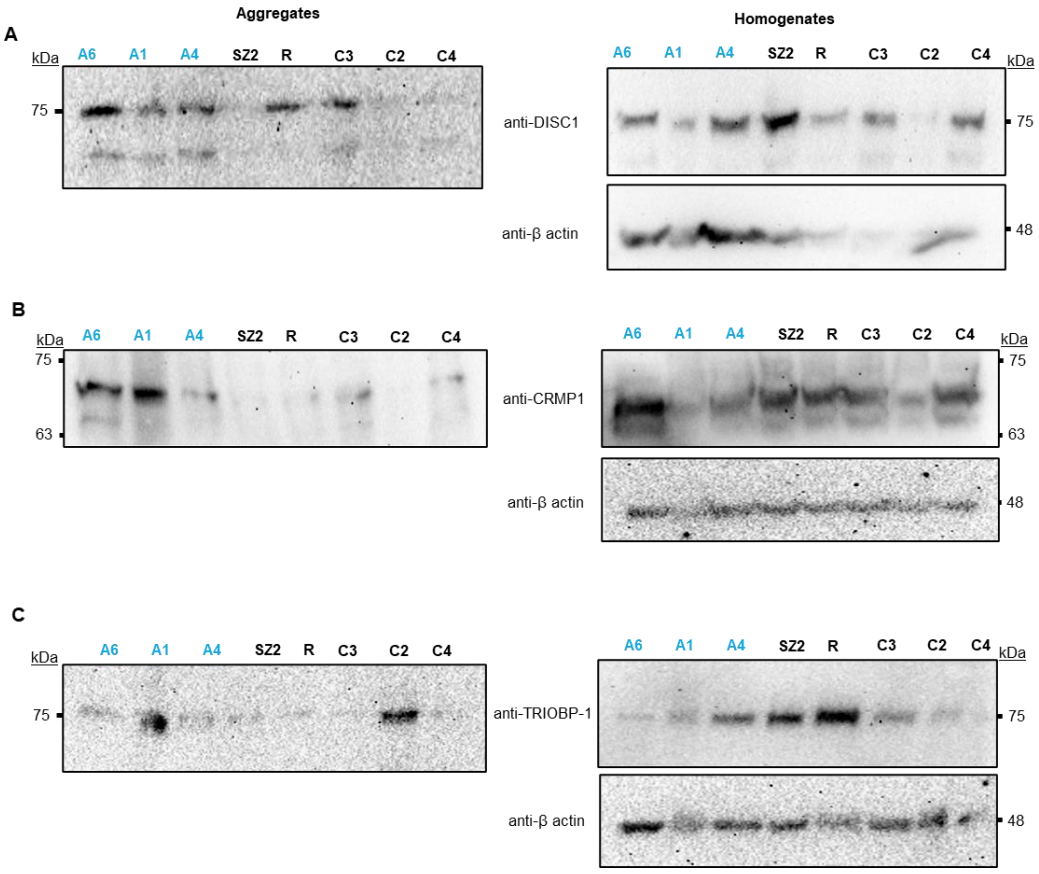

Figure 41: Pooled samples of control, AD, and SZ patients show variable levels of I/A and total protein DISC1, CRMP1, and TRIOBP-1. Samples were pooled to represent a homogenous sample of control individuals C3 and C4, patient R, SZ2 patient, and patients with AD diagnosis A1-3. Homogenate (total protein fraction) and aggregate (I/A proteins) samples were stained with anti-DISC1 (**A**), -CRMP1 (**B**), -TRIOBP-1 (**C**), and -β actin.

DISC1 bands varied across samples in I/A fraction, with the highest intensity observed in A6 and C3, while low intensity was detected in sample A1 and A4 (**Figure 41 A left**). Surprisingly, DISC1 band in SZ2 samples was low intensity. However, DISC1 bands in "homogenates" (total protein) were detected in all samples, with the most intense band in a sample from an SZ2 patient. The loading control was also inconsistent, with low-intensity bands detected in the C4 sample (**Figure 41 A right**). Variability was also observed in the intensity of bands specific to CRMP1. A6 and A1 had the most intense bands for CRMP1 in the "aggregate" (I/A proteins) fraction **(Figure 41 B left)**, while the bands in "homogenates" (total proteins) had high intensity for almost all samples, except for A1, A4, and C2, and loading control was consistent (**Figure 43 1 right**). Meanwhile, the bands with high intensity were detected in aggregate fraction from A1 and C2 samples after TRIOBP-1 stain (**Figure 41 C left**). In homogenates,

TRIOBP-1 bands were detected in all samples, with highly prominent bands in samples A4, SZ2 and R, and the loading control was consistent (**Figure 41 C right**).

4.2 Protein aggregation in cell models

Besides investigating protein aggregation with purifying I/A protein fraction from human brain tissue, the proteins of interest were encoded in plasmids with tags and over-expressed in SH-SY5Y cells. The cells were investigated by immunocytochemistry and fluorescent microscopy. Protein insolubility was investigated with a modified protocol for purifying I/A protein fraction and Western blot after overexpression of proteins in HEK293.

The first set of experiments focused on investigating the role of the V304I mutation in the aggregation of NPAS3 under normal and stressed conditions. Additionally, the tendency for aggregation of NPAS3 regions was also investigated.

The second set of experiments was based on work done with human brain samples, where multiple proteins were seen to aggregate in the same individuals, with or without diagnosis. Therefore, specific combinations of proteins of interest were further investigated in a cell system after co-transfection with fluorescent microscopy.

4.2.1 Quantification of NPAS3 wt and NPAS3 V304I under normal and stress conditions

To investigate the aggregation propensity of wild-type (wt) and V304I NPAS3, they were over-expressed in SH-SY5Y cells and their cellular localization was analyzed with fluorescent microscopy. The cells were analyzed in normal conditions and under oxidative stress caused by treatment with sodium arsenite (50 μM). The plasmid expression was verified in HEK293 cell lysates with Western blot.

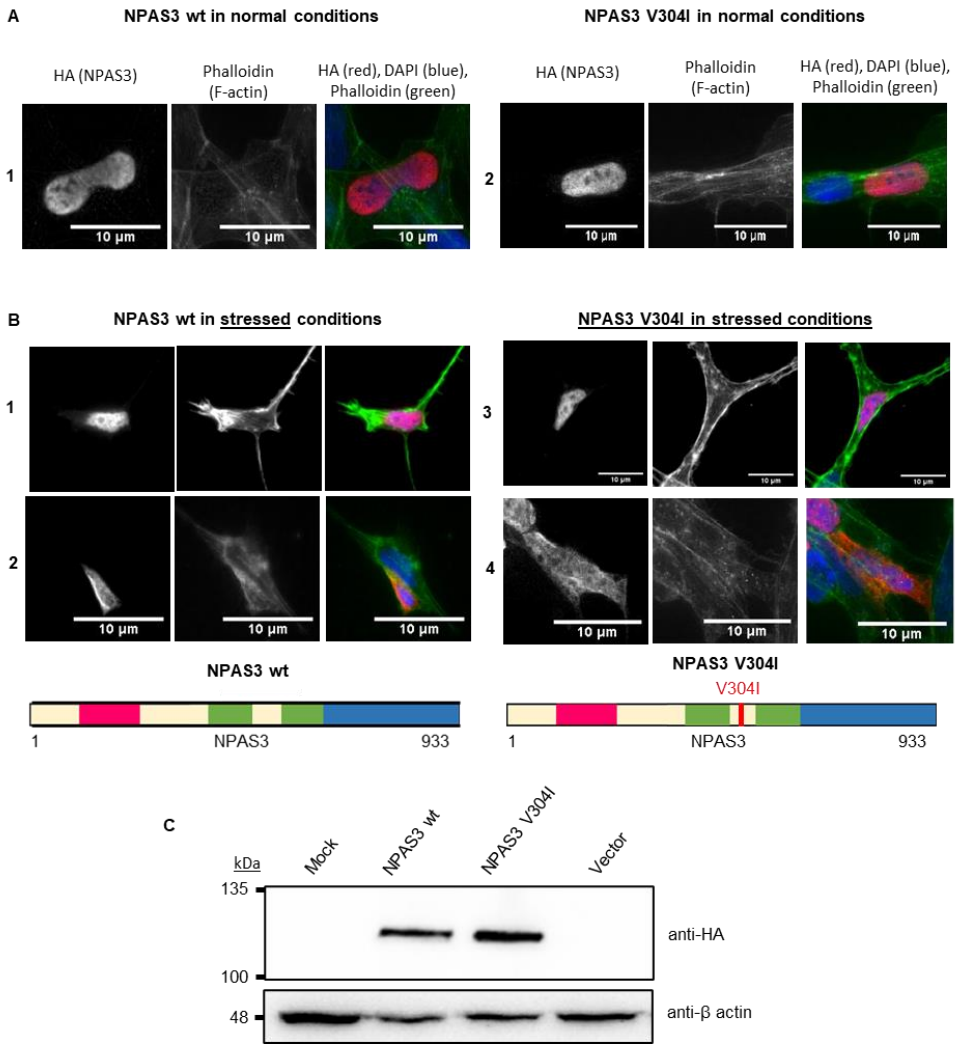

Figure 42: Both versions of NPAS3 can localize in the cytoplasm of SH-SY5Y cells under normal and stressed conditions. Plasmids with wt and V304I NPAS3 versions were overexpressed in SH-SY5Y cells containing the 933 aa of NPAS3 and HA tag. Each plasmid was imaged in normal (**A1** for NPAS3 wt and **A2** for NPAS3 V304I) conditions, without any treatment. The plasmids were then treated with 50 µM sodium arsenite to induce oxidative stress in cells (**B1** and **B2** show NPAS3 wt under stress conditions, while **B3** and **B4** show NPAS3 V304I under stress conditions). For each row of fluorescent images, there is a schematic of the expressed NPAS3 variant, with significant regions marked only by color (pink: bHLH1, basic helix-loop-helix domain, green: PAS1 and PAS2 domains, Per-Amt-Sim domain, blue: TAD, C-terminal activator domain). Both NPAS3 wt and mutated version NPAS3 V304I are primarily localized in the nucleus in normal (**A1** for NPAS3 wt and **A2** for NPAS3 V304I) and stressed conditions (**B1** for NPAS3 wt and **B3** for NPAS3 V304I). However, they can both be found in the cytoplasm under stress conditions (**B2** for NPAS3 wt and **B4** for NPAS3 V304I). The staining of actin cytoskeleton (phalloidin) and DAPI (nucleus) are also shown and all images are taken at 60x. The shown images are representative of 10 photos for each plasmid under each condition. Expression of the NPAS3 wt and V304I plasmids is confirmed in lysates from HEK293 cells by Western blot with specific anti-HA antibody (C). A mock transfection with no plasmid and cells transfected with only a vector were used as a negative control, while the loading control was β-actin.

Both wt and V304I NPAS3 inserted in the pCI vector with HA tag were primarily localized in the nucleus (**Figure 42 A** for normal conditions: **A1** for NPAS3 wt and **A2** for NPAS3 V304I; **Figure 42 B** for stressed conditions: **B1** and **B2** for NPAS3 wt, **B3** and **B4** for NPAS3 V304I), regardless of treatment, as expected based on its function as a transcription factor. Under stress conditions, NPAS3 wt and V304I were observed in the cytoplasm (**Figure 42 B2** and **A4**). Similarly, when observed in the cytoplasm, other aggregating proteins usually localized in the nucleus (e.g. TDP-43 in ALS[310]) are assumed to be in an early stage of aggregation.

The plasmids express correct proteins, as the bands in the Western blot match the expected size (~103 kDa). No specific bands for NPAS3 were observed for transfected cells or cells transfected only with the empty vector pCI (**Figure 42 C**).

To further analyze NPAS3 cytoplasmic localization, the quantitative blinded assay in SH-SY5Y cells assessed the localization. Briefly, the plasmids for transfection (6-8 tubes with NPAS3 wt and 6-8 tubes with NPAS3 V304I) were blinded for me by another researcher in our lab, and they remained coded throughout the entire process, including transfection, immunocytochemistry, fluorescent microscopy, and data analysis. After the quantification of protein localization was done (8-10 cells per plasmid and condition) and submitted, the samples were decoded. As previously, the cells were analyzed under both normal and stress conditions.

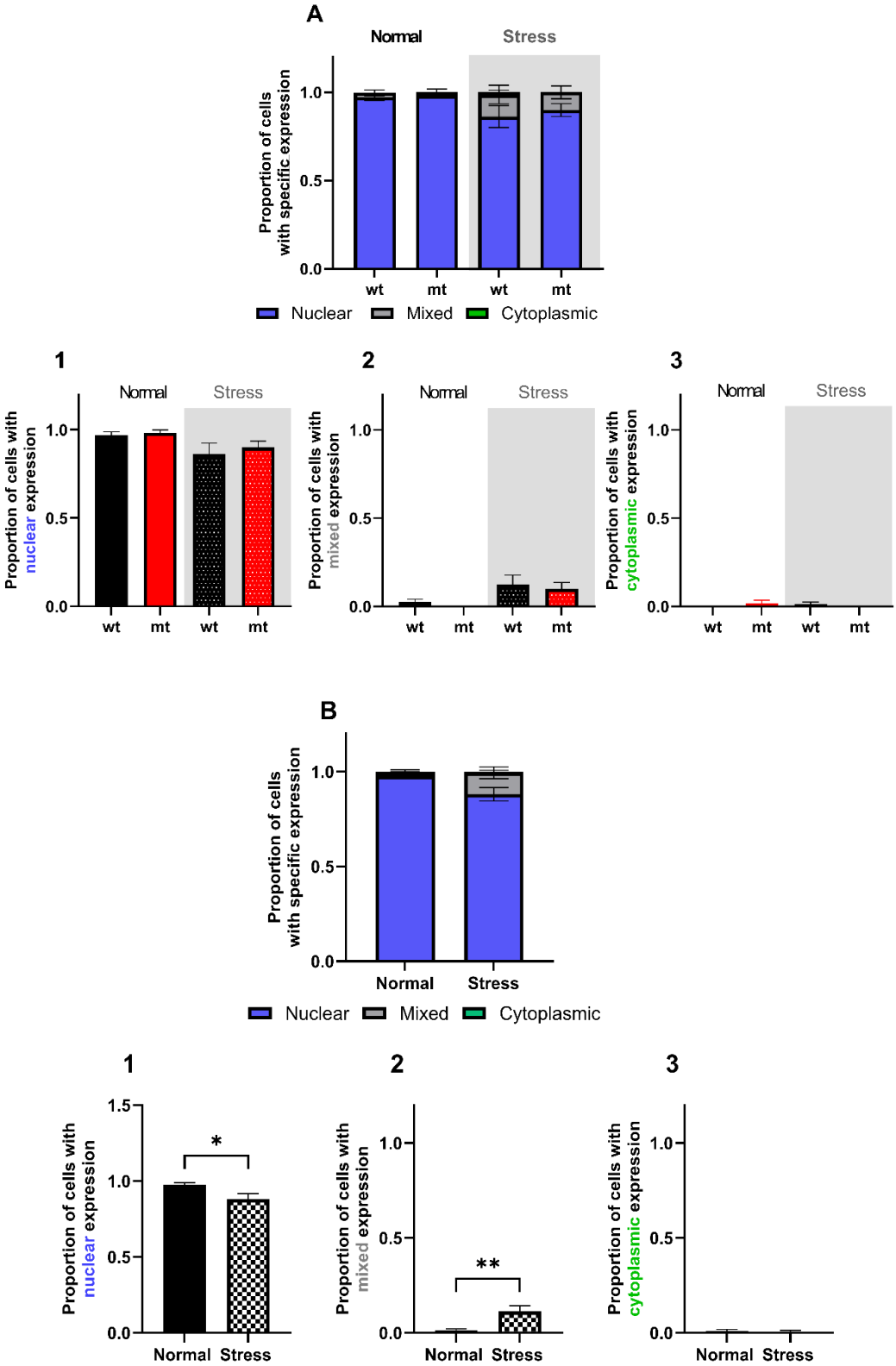

Figure 43: No significant differences are observed between NPAS3 wt and V304I localization, either under normal circumstances or when stressed. Stress conditions were evoked by 50 µM sodium arsenite treatment and 8-10 cells of each plasmid were quantified, for each condition separately. The untreated

experiment was run in parallel as a control. Both versions of NPAS3, with and without mutation, show a slight decline in nuclear localization (**A1**) and an increase in mixed phenotype (**A2**) under stress. Cytoplasmic localization remains similar (**A3**). Data for both versions of NPAS3 were combined to show the general effect of stress (**B**). Compared to controls, there is a significant decrease in nuclear localization and an increase in the mixed phenotype of both NPAS3 variants under stress conditions. Data on graphs present the proportion of cells showing specific localizations (nuclear, cytoplasmic, or a mix of both). They are presented as AVE +/- SEM (n=2 plasmids with approximately 8-10 cells each, 2 experiments) and analyzed by one-way ANOVA with Tukey's multiple comparisons test. $p < .05$ (*), $p < .001$ (**), $p < .001$ (***), ns non-significant.

While the majority cells showed clear nuclear or cytoplasmic localization, there was a portion of analyzed cells where NPAS3 wt or V304I was expressed both in nucleus and cytoplasmic, what is referred to in the analysis as "mixed" phenotype. There was no difference in localization for either wt or V304I NPAS3 in both conditions (**Figure 43 A1-3**). However, there is a significant decrease in nuclear localization (**Figure 43 B1**) and an increase in mixed phenotype (**Figure 43 B2**) when cells are under stress conditions.

4.2.2 Assessment of NPAS3 wt and V304I aggregation over long time periods

In addition to visual analysis, the aggregation propensity of NPAS3 wt and V304I can be assessed using an insolubility assay and Western blot similar to the brain samples. As HEK293 cells grew faster than SH-SY5Y cells and I needed a high number of cells for follow up analysis, HEK293 were transfected with either NPAS3 wt or NPAS3 V304I and then cultured under normal conditions for 24, 48, and 72 hrs. The NPAS3 signal from the I/A fraction was normalized to the total protein level in lysates.

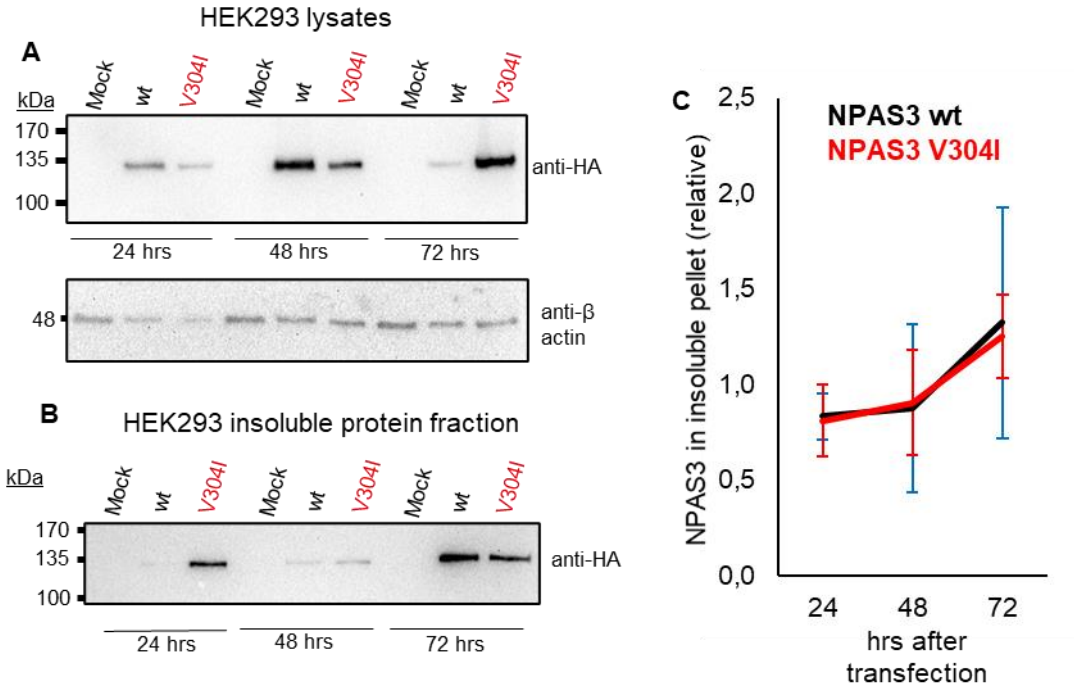

Figure 44: NPAS3 wt and V304I show similar increases in aggregation 48 and 72 hrs after transfection. HEK293 cells were transfected with HA-tagged wt or V304I NPAS3 plasmid or left untransfected as a control. Cells were lysed 24, 48, or 72 hours after transfection. Cell lysates were stained with anti-HA and anti-β actin antibodies to determine the total level of NPAS3. The level of total wt NPAS3 was highest after 48 hrs, while the total level of V304I NPAS3 was the highest after 72 hrs (**A**). The I/A protein fraction was stained with anti-HA to determine the level of I/A NPAS3. The highest level of I/A NPAS3 wt was detected after 72 hrs, while the level of I/A NPAS3 V304I was high after 24 and 72 hrs (**B**). All bands were quantified and normalized to the total NPAS3 level in cell lysates. There were no constant differences between the NPAS3 wt and V304I over three independent experiments (**C**).

The total level of both proteins varied in samples from different time points. The band for wt NPAS3 was the most intense in cells lysed after 48 hrs, while V304I had the most intense band after 72 hrs, but the band after 48 hrs was also intense, both compared to the band in samples after 24 hrs. The loading control, β-actin, remained the same in all samples (**Figure 44 A**).

Meanwhile, in the I/A fraction, NPAS3 wt had the most intense band in cells lysed after 72 hrs. The I/A V304I had prominent bands in cells lysed after 24 and 72 hrs (**Figure 44 B**), however when the level of NPAS3 in the I/A protein fraction was normalized to the total protein level from cell lysates (**Figure 44 B**), there was no difference between NPAS3 wt and V304I. Both NPAS3 wt and V304I showed an increase in insolubility after 72 hrs.

The analysis with insolubility assay was followed with fluorescent microscopy analysis. This time SH-SY5Y cells were used as they are more similar to neurons than HEK293. Cells were transfected with either NPAS3 wt or V304I and fixed at 24, 48, and 72 hrs, followed by immunocytochemistry and fluorescent microscopy.

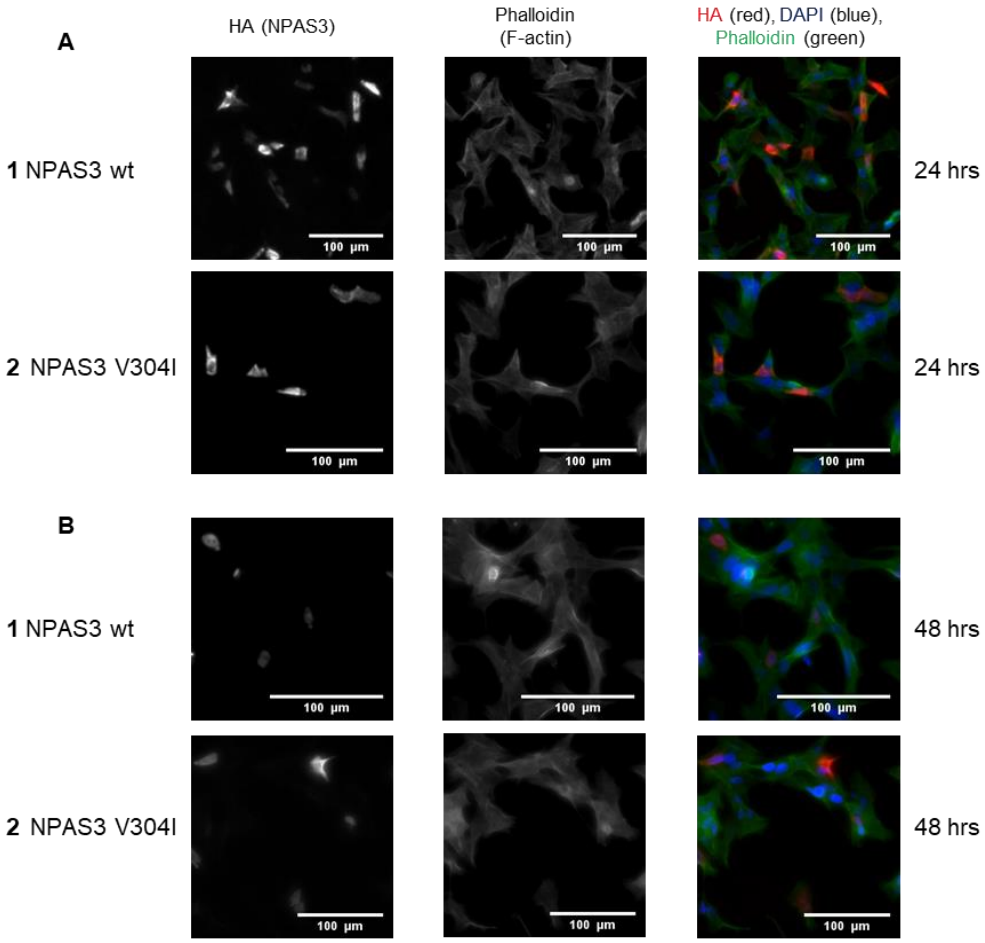

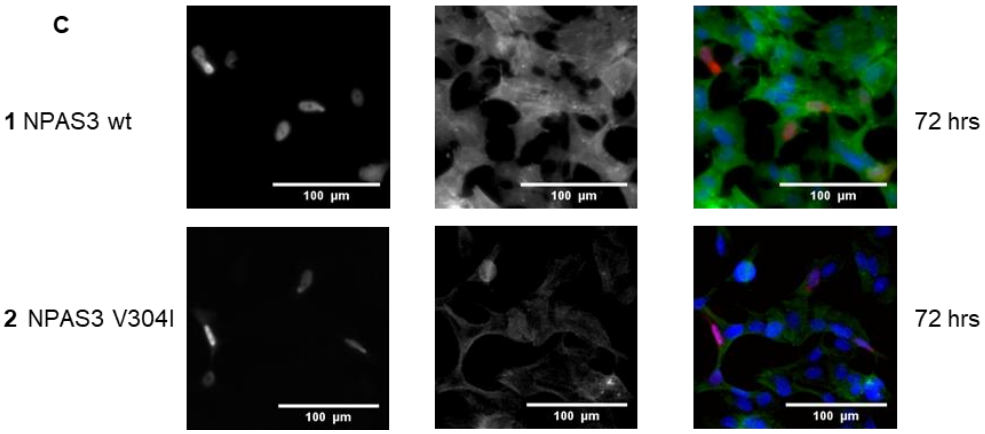

Figure 45: No constant difference in cell localization for NPAS3 wt and V304I was observed in SH-SY5Y cells after 24, 48, or 72 hrs. Plasmids for either full-length NPAS3 wt or V304I with HA tag were transfected in SH-SY5Y cells and fixed 24, 48, and 72 hrs after transfection (A-C, respectively). NPAS3 wt after 24 hrs (A1), 48 hrs (B1), and 72 hrs (C1) are shown, as well as NPAS3 V304I after 24 hrs (A2), 48 hrs (B2) and 72 hrs (C2). The cells were stained with anti-HA primary antibody and goat anti-mouse 594 nm secondary antibody, while actin cytoskeleton (phalloidin) and DAPI (nucleus) are also shown. The images were taken with 20x objective; the white bar represents 100 µm.

Both wt and V304I NPAS3 showed nuclear or cytoplasmic localization after 24 (**Figure 45 A1** and **A2,** respectively), 48 (**Figure 45 B1** and **B2,** respectively), and 72 hrs (**Figure 45 C1** and **C2,** respectively).

While no visible aggregates were observed in any of the analyzed cells, the increased cytoplasmic localization of both NPAS3 wt and V304I under stress conditions suggests that external stressors may have a greater impact on protein stability than the V304I mutation alone, as previously reported[453]. To further investigate this, I focused on dissecting individual NPAS3 regions to identify domains that may influence localization or contribute to destabilization.

4.2.3 Aggregation assessment of each major NPAS3 region

Plasmids containing different NPAS3 regions tagged with either HA or Flag tag were over-expressed in SH-SY5Y cells. The cells were analyzed with fluorescent microscopy, and the cellular localization was quantified using a blinded assay. The expression of NPAS3 wt and V304I was also confirmed in HEK293 cell lysates through Western blot analysis. The regions closer to the N-terminus (bHLH1, bHLH1-linker, bHLH1-PAS1, and bHLH1-PAS1-linker) in HA-tagged plasmids were analyzed first.

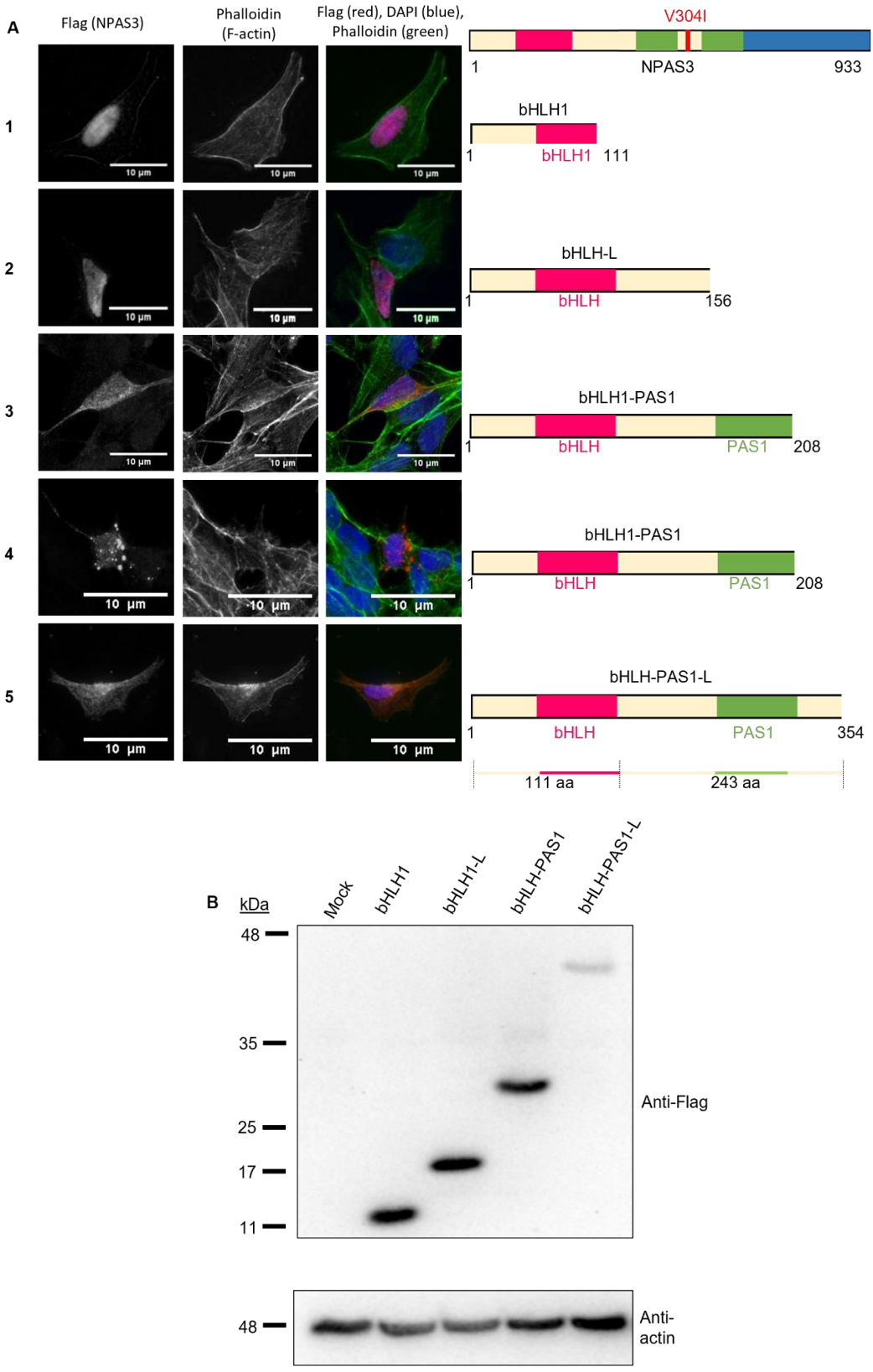

Figure 46: The PAS1 domain proves critical for NPAS3 cytoplasmic localization. Plasmids with N-terminal NPAS3 regions were overexpressed in SH-SY5Y cells. Plasmids included the following domains and linkers (L) with aa range:

bHLH (1-111 aa), bHLH-L (1-156 aa), bHLH-PAS1 (1-208 aa), bHLH-PAS1-L (1-354 aa). For each row of fluorescent images, there is a schematic of the expressed NPAS3 region, compared to the scheme of full-length NPAS3. Plasmid with bHLH region (**A1** and **A2**) both localize in the nucleus. The addition of only the PAS1 domain results in both nuclear (**A3**) and cytoplasmic (**A4**) localization, while the addition of PAS1 followed by the linker region shows cytoplasmic localization (**A5**). The cells were stained with anti-HA primary antibody and goat anti-mouse 594 nm secondary antibody, while actin cytoskeleton (phalloidin) and DAPI (nucleus) are also shown. The images were taken with 60x objective, and the white bar represents 10 μm. Images shown here are representative of at least 10 cells per tested plasmid. Expression of the NPAS3 fragments is confirmed in lysates from HEK293 cells by Western blot with specific anti-Flag antibody (**B**). A mock transfection with no plasmid is used as a negative control, while the loading control is β-actin.

After fluorescent microscopy, the plasmids containing the bHLH1 region (bHLH1 and bHLH1-linker, **Figure 46 A1-2**) were primarily observed in the cell nuclei, while the plasmids with added PAS1 domain (bHLH1-PAS1 and bHLH1-PAS1-linker **Figure 46 A3-4**) showed more cytoplasmic localization. The bHLH1-PAS1 region showed perinuclear aggregates (**Figure 46 A5**) and may have a propensity to misfold or aggregate under certain conditions. The Western blot of HEK293 cell lysates, over-expressing previously mentioned plasmids, showed bands matching the expected protein size (bHLH1 ~13, bHLH1-linker ~17, bHLH1-PAS1 23 and bHLH1-PAS1-linker 40 kDa) (**Figure 46 B**).

To further analyze the effect of the PAS1 region on NPAS3 localization, the SH-SY5Y cells over-expressing previously mentioned plasmids (5-6 replicates) were analyzed with a quantitative blinded assay.

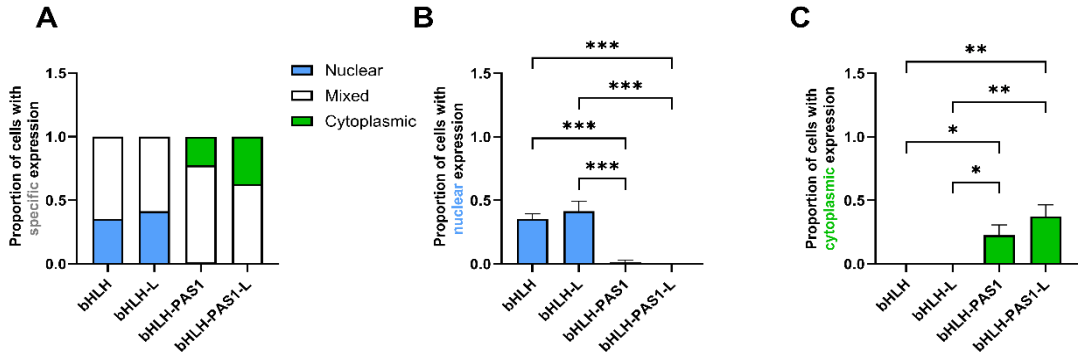

Figure 47: Quantitative analysis of localization patterns reveals distinctiveness for each N-terminal region of NPAS3 in SH-SY5Y cells. The shift between specific expression patterns is visible for N-terminal NPAS3 fragments (**A**). Regions, including the bHLH region, are primarily expressed in the nucleus (**B**). On the other hand, introducing the PAS1 domain leads to higher cytoplasmic expression (**C**). Data are presented as AVE +/- SEM (n=5-6 plasmids with

approximately 8 cells each) and analyzed by one-way ANOVA with Tukey's multiple comparisons test. p < .05 (*), p <.001 (**), p <.001 (***).

The N-terminal NPAS3 plasmids are differently localized in SH-SY5Y cells after over-expression, as shown in (**Figure 47 A)**. The plasmids containing the bHLH1 region (bHLH1 and bHLH1-linker) are significantly more localized in the nucleus (**Figure 47 B)**. In contrast, the plasmids with the PAS1 domain (bHLH1-PAS1 and bHLH1-PAS1-linker) are considerably more present in the cytoplasm (**Figure 47 C)**, suggesting that the PAS1 domain may play a role in retaining NPAS3 in the cytoplasm or interfering with its nuclear import. The presence or absence of the linker regions flanking PAS1 did not appear to influence this localization pattern.

Given the apparent instability of the bHLH1-PAS1 region, I aimed to determine whether this domain alone could influence the stability and subcellular localization of the full-length NPAS3 protein. The regions bHLH1-PAS1 and bHLH1-PAS1-linker in Flag-tagged plasmid were co-expressed in SH-SY5Y cells with full-length wt NPAS3 in mCherry plasmid and analyzed with fluorescent microscopy.

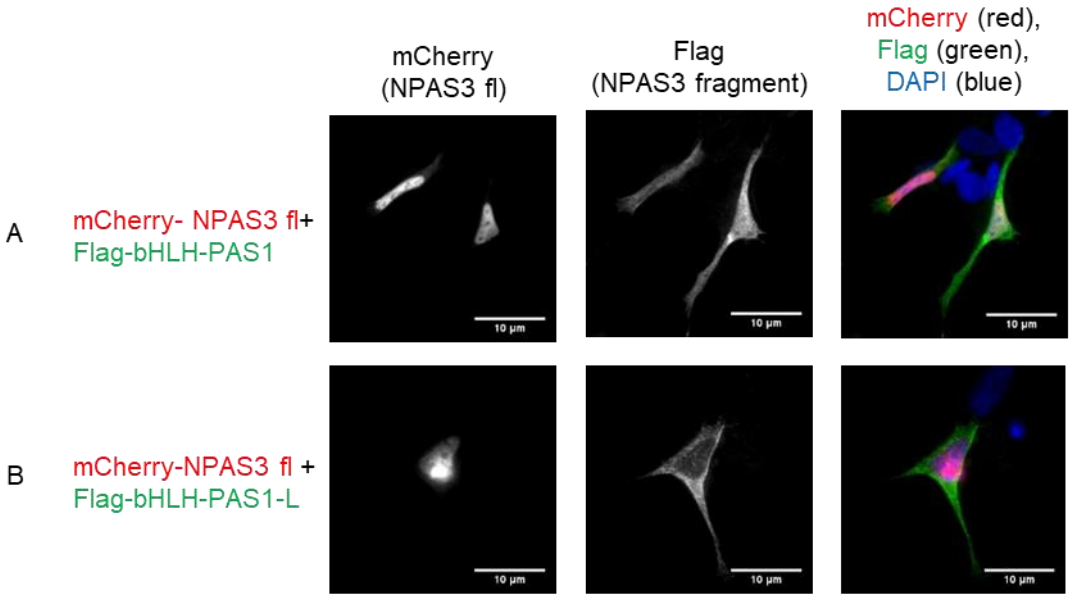

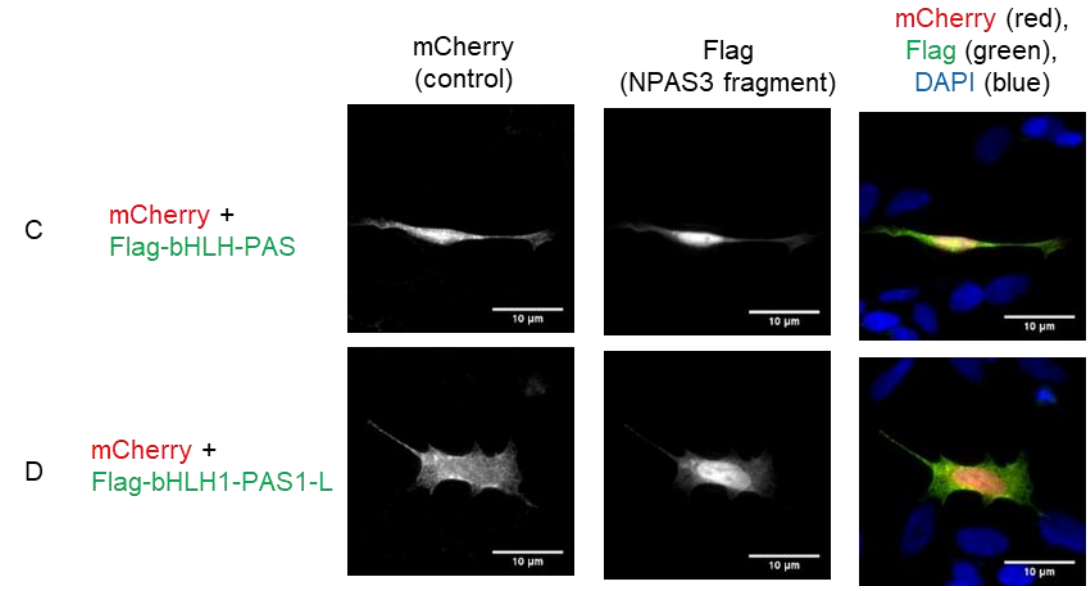

Figure 48: PAS1 domain does not affect nuclear localization of full-length NPAS3 in SH-SY5Y cells. Flag-tagged constructs with PAS1 domain (NPAS3 208) and PAS1 domain with linker (NPAS3 354) were co-expressed with full-length NPAS3 (NPAS3 fl), fused to mCherry (A and B) or mCherry plasmid alone, as control (C and D). NPAS3 and NPAS3 354 showed cellular expression, with NPAS3 fl or control. NPAS3 fl overlapped with nuclear stain (DAPI), as usual. The images were taken with 60x objective, and the white bar represents 10 µm.

The full-length NPAS3 maintains its nuclear localization when co-expressed with bHLH1-PAS1 (**Figure 50 A**) and bHLH1-PAS1-linker (**Figure 50 B)** regions. As a control, the full-length NPAS3 was co-expressed with the mCherry vector, which lacks significant gene insertion, and this did not affect bHLH1-PAS1 (**Figure 50 C**) and bHLH1-PAS1-linker (**Figure 50 D)** cytoplasmic localization.

The C-terminal regions (PAS-TAD and TAD) in plasmids with HA tag were over-expressed in SH-SY5Y cells, and their localization in cells was analyzed with fluorescent microscopy. The plasmid expression was validated in HEK293 cell lysates with Western blot.

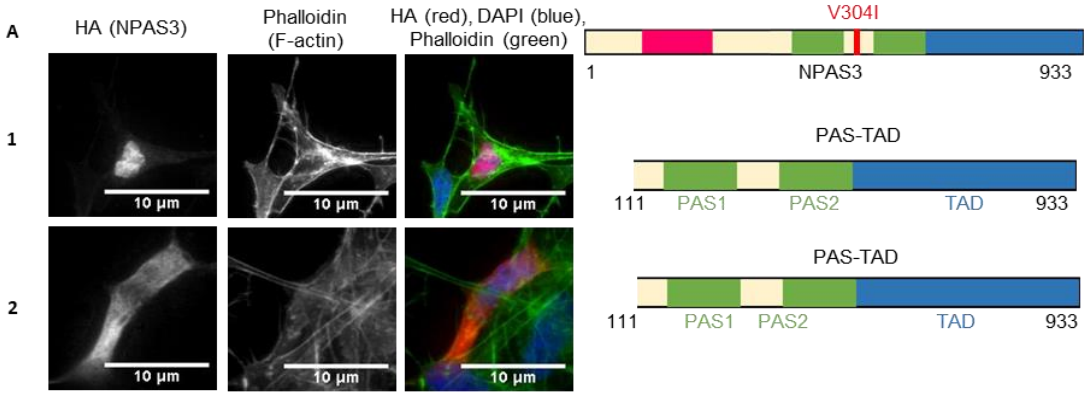

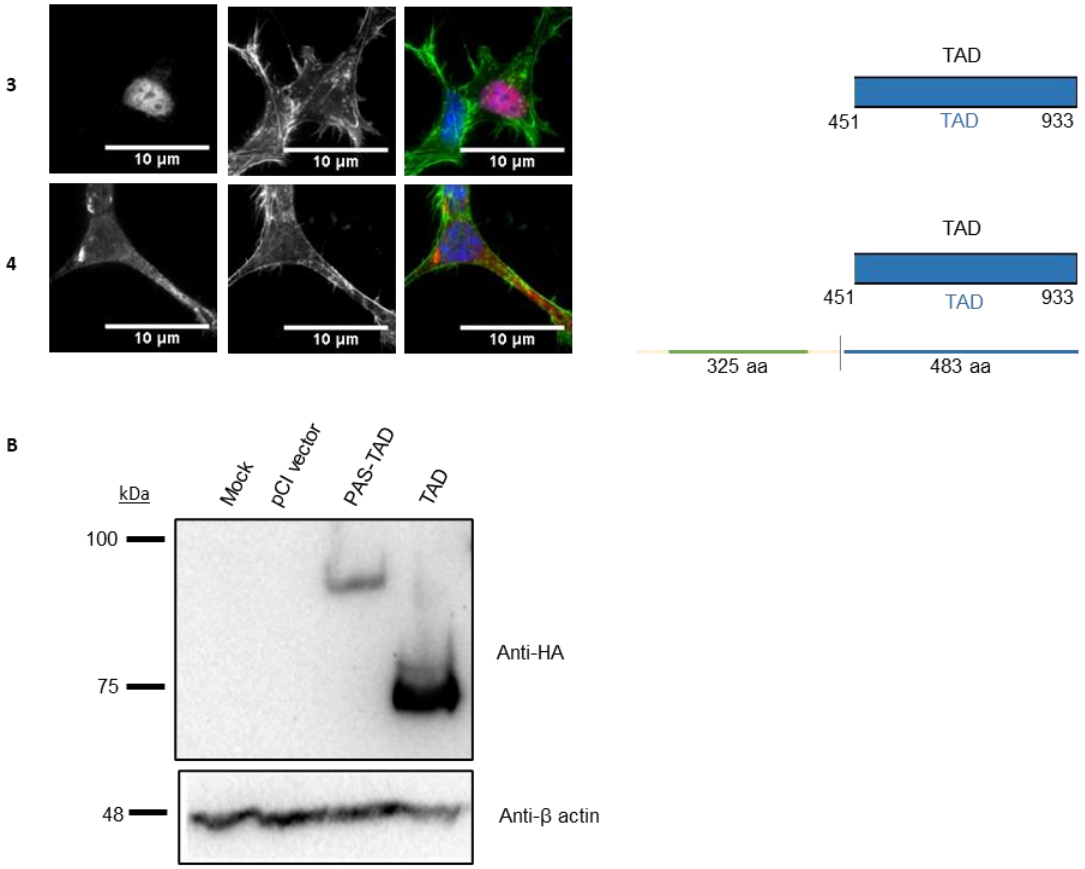

Figure 49: The PAS and TAD domains show nuclear localization, typical for NPAS3. Plasmids with C-terminal NPAS3 regions were overexpressed in SH-SY5Y cells. Plasmids included the following domains and linker (L) with aa range: PAS-TAD (111-933) and TAD (451-933 aa). For each row of fluorescent images, there is a schematic of the expressed NPAS3 region, compared to the scheme of full-length NPAS3. With (A1-2) or without (A3-4) PAS1 and PAS2 domains, there is a nuclear localization of over-expressed plasmids in SH-S5Y5, typical for full-length NPAS3 described previously. The cells were stained with anti-HA primary antibody and goat anti-mouse 594 nm secondary antibody, while actin cytoskeleton (phalloidin) and DAPI (nucleus) are also shown. The images were taken with 60x objective, and the white bar represents 10 µm. B Expression of the C-terminal NPAS3 fragments is confirmed in lysates from HEK293 cells by Western blot with specific anti-HA antibodies. A mock transfection and a pCI vector with no plasmid are used as a negative control, while the loading control is β-actin.

PAS-TAD and TAD region were primarily observed in the nucleus (**Figure 49 A1 and A3,** respectively) of SH-SY5Y cells when over-expressed. Still, in some cases, they localized in the cytoplasm (**Figure 49 A2 and A4,** respectively). The bands detected for these plasmids by Western blot of HEK293 cell lysates (**Figure 49 B**) matched expected sizes (~90 kDa PAS-TAD and ~54 kDa for TAD).

The cytoplasmic localization of PAS-TAD and TAD was further investigated in the quantitative blinded assay in SH-SY5Y cells.

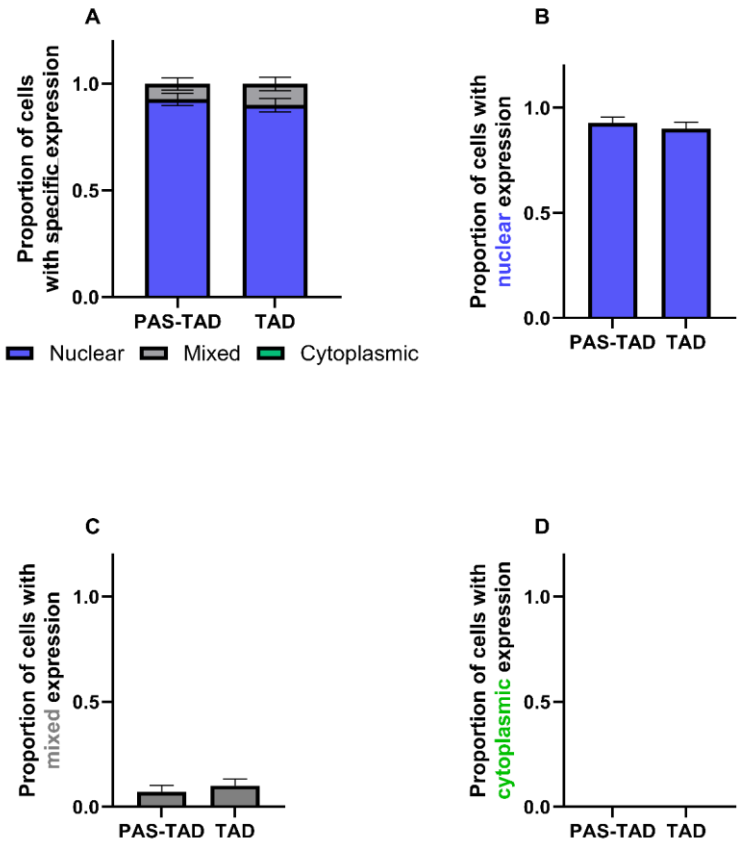

Figure 50: Quantitative analysis of localization NPAS3 C-terminal region in SH-SY5Y cells shows no significant differences among regions. Plasmids with C-terminal NPAS3 regions were overexpressed in SH-SY5Y cells and analyzed with fluorescent microscopy. The number of cells showing specific localization was quantified (**A**). No change in the localization of plasmids with NPAS3 PAS-TAD or TAD regions was observed. Specific localization is also shown separately: **B** Nuclear localization, **C** Mixed phenotype and **D** Cytoplasmic localization. Data are presented as AVE +/- SEM (n=5 for PAS-TAD and 7 for TAD with approximately 10 cells each) and analyzed by one-way ANOVA with Tukey's multiple comparisons test. $p < .05$ (*), $p < .001$ (**), $p < .001$ (***).

Both regions, PAS-TAD and TAD, showed nuclear localization in SH-SY5Y cells (**Figure 50 A and B**). The mixed phenotype was rarely observed (**Figure 50 C**), and very few cells exhibited cytoplasmic localization (**Figure 50 D**).

In summary, change in NPAS3 localization from nuclear to cytoplasmic in cells increases over time, with no major differences between wt and V304I variants. The PAS1 domain plays a crucial role in cytoplasmic localization, while the C-terminal PAS-TAD and TAD regions remain predominantly nuclear, mirroring full-length NPAS3 behavior.

4.2.4 Protein co-aggregation *in vitro* analysis

The presence of multiple I/A proteins was detected in *post-mortem* brain samples from suicide victims, patients with diagnosed SZ, MDD, and AD, as well as in control samples. The hypothesis is that these proteins either aggregate independently, without any physical connection between their aggregates (here referred to as "parallel aggregation"), or they are aggregating together, creating bigger aggregates (here referred to as "co-aggregation").

4.2.4.1 Validation of eGFP tagged-plasmids

To test the co-aggregation tendencies of proteins, they were expressed by themselves with different tags in HEK293 cells and investigated with Western blot in cell lysates. The tested vectors were also published [501], and the plasmids in eGFP plasmid were checked for this thesis.

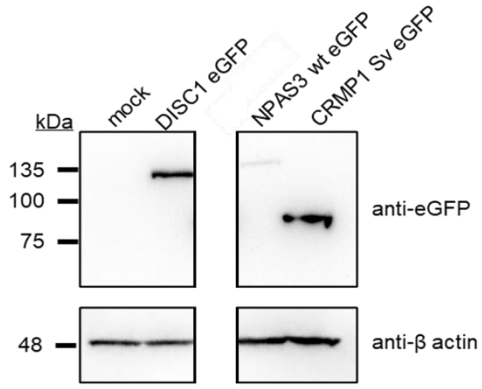

Figure 51: DISC1, NPAS3, and CRMP1 Sv can be over-expressed in cells with an eGFP tag. HEK293 cells were transfected with eGFP plasmids and analyzed with anti-eGFP antibody and appropriate secondary antibody in Western blot after cell lysis. A mock transfection with no plasmid is used as a negative control, while the loading control is β-actin.

The bands for each interest protein were detected and matched the expected protein size. Notably, NPAS3 showed low expression when tagged with eGFP.

Moreover, their expression was tested after transfection of SH-SY5Y cells and immunocytochemistry, firstly as single transfections of either Flag and eGFP plasmids, and then later in co-transfection of protein of interest in Flag-tagged plasmids with control eGFP fusion protein. Control eGFP fusion protein is expressed from a plasmid that encodes for an eGFP tag and less than 20 aa from the entry vector.

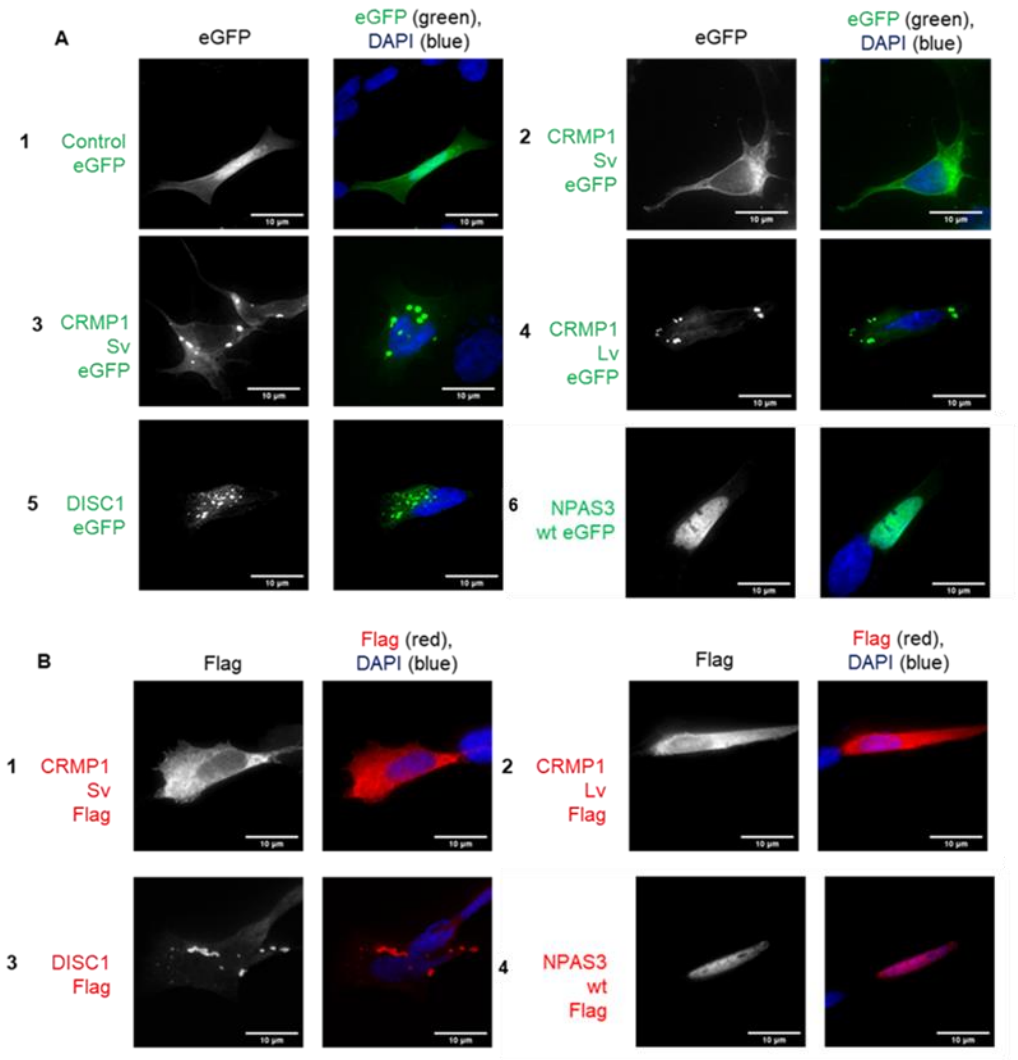
A
eGFP
eGFP (green), DAPI (blue)
eGFP
eGFP (green), DAPI (blue)
1 Control eGFP
2 CRMP1 Sv eGFP
3 CRMP1 Sv eGFP
4 CRMP1 Lv eGFP
5 DISC1 eGFP
6 NPAS3 wt eGFP
B
Flag
Flag (red), DAPI (blue)
Flag
Flag (red), DAPI (blue)
1 CRMP1 Sv Flag
2 CRMP1 Lv Flag
3 DISC1 Flag
4 NPAS3 wt Flag

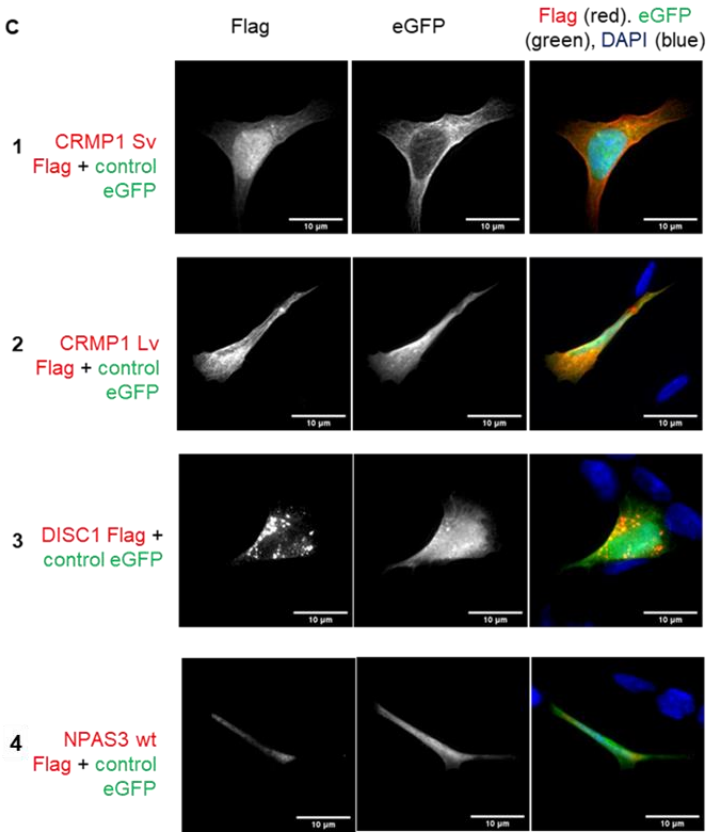

Figure 52: CRMP1 Sv and CRMP1 Lv show a higher tendency to aggregation when expressed with the eGFP tag, while other proteins show the same expression patterns unrelated to the tag. CRMP1 Sv and Lv, DISC1, and NPAS3 wt with either Flag or eGFP tag were over-expressed in SH-SY5Y cells. Only CRMP1 Sv and Lv showed normal cellular localization and aggregation signs when expressed with an eGFP tag. This effect was not observed with a Flag tag, in single transfection, or when co-transfected. The remaining proteins kept their expression pattern across single transfections regardless of tag and in co-transfections. The cells were stained with anti-Flag primary antibody and goat anti-mouse 594 nm secondary antibody, while DAPI (nucleus) is also shown. The images were taken with 60x objective, and the white bar represents 10 µm. Images shown here are representative of minimum of 10 cells per plasmid combination.

When over-expressed in SH-SY5Y cells after a single transfection, a control eGFP plasmid was seen in the cytoplasm across all tested cells. Interestingly, CRMP1 Sv with eGFP tag showed both typical cytoplasmic localization (**Figure 52 A2**), previously described, and, in some cases, signs of aggregation, shown on a representative image on **Figure 52 A3**. However, CRMP1 SV was observed in the cytoplasm only when the tag was switched to Flag (**Figure 52 B1**) or co-expressed with the control eGFP plasmid (**Figure 52 C1**). A similar effect was seen with CRMP1 Lv, which shows signs of aggregation when expressed with eGFP tag (**Figure 52 A4**), which are gone when Flag tag is introduced, without (**Figure 52 B2**) or with control eGFP (**Figure**

52 C2). DISC1 maintained the same aggregation pattern across all tested tags (**Figure 52 A5** and **B3)** and co-transformed with the control eGFP plasmid (**Figure 52 C3**). NPAS3 keeps expressing in the nucleus, regardless of tag (**Figure 52 A6,** and **B4)** and when co-transfected with control eGFP plasmid (**Figure 52 C4**).

In these experiments, the eGFP tag can associated with reduced expression (e.g., NPAS3) and increased cytoplasmic aggregation (e.g., CRMP1 variants), effects I tried to mitigate by co-expression of tested proteins with a control eGFP plasmid. In contrast, some proteins like DISC1 and NPAS3 maintained consistent localization patterns regardless of tag, emphasizing that tag impact can be protein-dependent.

4.2.4.2 Co-aggregation of DISC1 and CRMP1

After testing the expression of Flag- and eGFP-tagged plasmids in single transfections, the proteins of interest were co-transfected in SH-SY5Y cells and analyzed by fluorescent microscopy. The first combination investigated was DISC1 with the variants of CRMP1, one of the most prominent combinations observed in human brain samples, after purifying the I/A protein fraction.

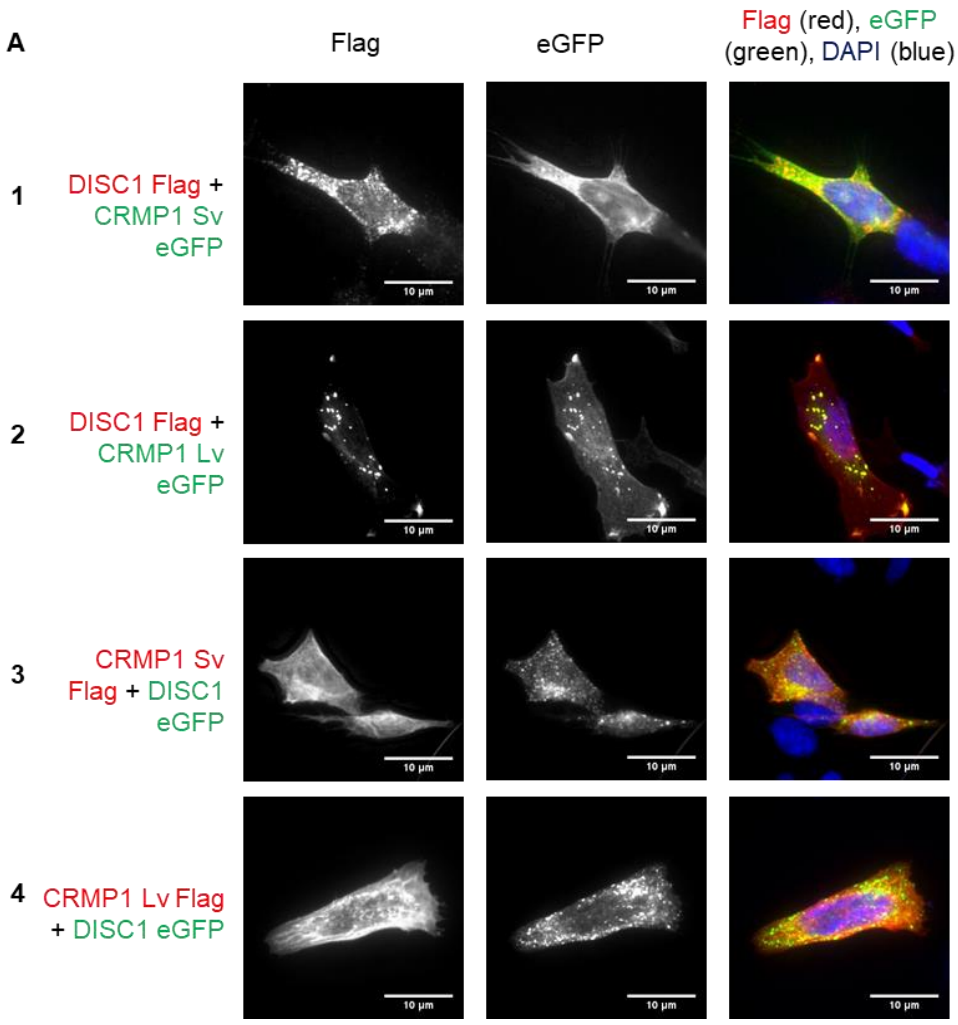

Figure 53: CRMP1 Lv is more prone to aggregation when co-expressed with DISC1, unlike CRMP1 Sv, which ceases aggregation upon co-expression with DISC1. DISC1 and CRMP1 Sv or Lv were over-expressed with either Flag or eGFP tag in SH-SY5Y cells. When DISC1-Flag is expressed with eGFP-tagged CRMP1 variants, only CRMP1 Lv shows signs of aggregation and possible co-aggregation. The effect is also observed after tags are switched. The cells were stained with anti-Flag primary antibody and goat anti-mouse 594 nm secondary antibody (red), while DAPI (nucleus, blue) is also shown, and the signal from eGFP is shown in green. The images were taken with 60x objective, and the white bar represents 10 µm.

Only CRMP1 Lv showed a punctate pattern across cytoplasm when co-expressed with DISC1, with Flag and eGFP tag (**Figure 53 A2** and **A4)**. CRMP1 Lv proved unstable with only the addition of the eGFP tag (previous **Figure 53 A4**) but remained stable with the Flag tag (previous **Figure 53 B2**). The higher aggregation tendency of CRMP1 Lv may be triggered by aggregation of DISC1, making it more unstable and prone to aggregation. CRMP1 Sv kept cytoplasmic localization after co-transfection with DISC1, regardless of tags (**Figure 53 A1** and **A3**).

The co-aggregation of DISC1 with variants of CRMP1, or control eGFP plasmid, was also tested quantitatively by fluorescent microscopy in SH-SY5Y cells.

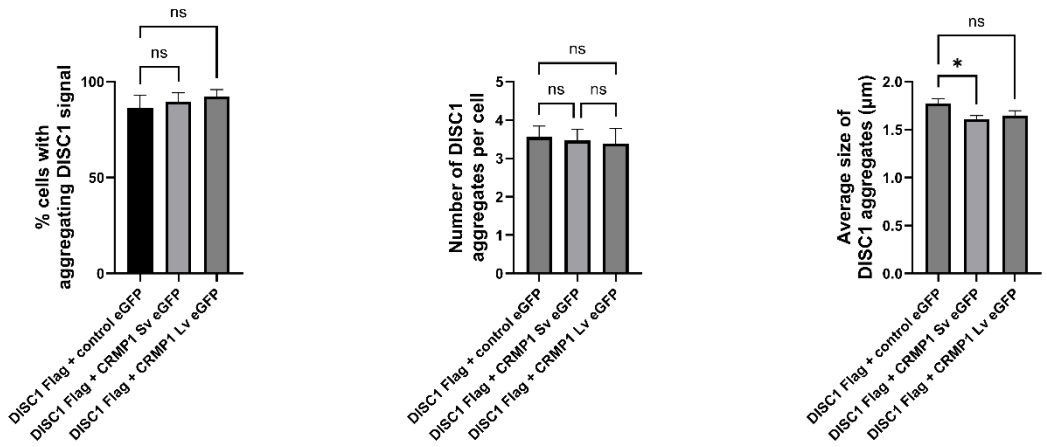

Figure 54: The size of DISC1 aggregates can be reduced upon co-expression with CRMP1, specifically CRMP1 Sv. Flag-tagged DISC1 was co-transfected with a control vector containing only an eGFP tag or either CRMP1 Sv or CRMP1 Lv, also eGFP-tagged, in SH-SY5Y cells. The cells were then analyzed by immunofluorescent microscopy in a blinded, quantified manner. The results show an average of 10 coverslips per plasmid combination of 10 transfected cells examined per coverslip. A percentage (%) of cells showing DISC1 aggregation out of the total observed transfected cells was determined (A). Also, the mean number of DISC1 aggregates per cell and their mean size were determined. *: $p < 0.05$, ns: not significant, according to one-way ANOVA.

The percentage of cells with DISC1 aggregates (**Figure 54 A**) and number of DISC1 aggregates per cell (**Figure 54 B**) remained the same across all tested options. However, a drop in the average size of DISC1 aggregates was seen when DISC1 was co-expressed with CRMP1 Sv, unlike the control eGFP or CRMP1 Lv (**Figure 54 C**), implicating CRMP1 Sv can reduce the size of DISC1 aggregates.

Insolubility/aggregation of DISC1 in Flag-tag vector, with or without CRMP1 variants eGFP tagged, was also tested with a protein insolubility assay combined with Western blot after over-expression in HEK293 cells. Tested parameters included the percentage of cells showing DISC1 aggregation patterns, the amount of DISC1 aggregates per cell, the average size of DISC1 aggregates (in µm), the rate of cells showing signs of co-aggregation between DISC1 and CRMP1 variants, the number of co-aggregates and the average size of co-aggregates (in µm).

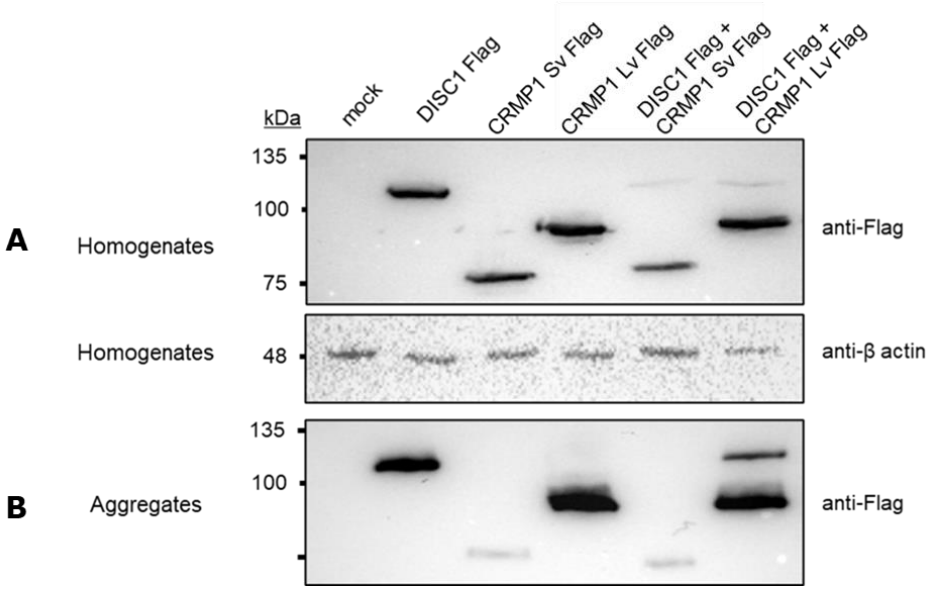

Figure 55: CRMP1 Lv shows signs of aggregation, with and without DISC1, when overexpressed in HEK293 cells, in contrast to CRMP1 Sv. HEK293 cells were transfected with Flag-tagged full-length human DISC1 and CRMP1 Sv or Lv variants or left untransfected as a control. The whole protein fraction (homogenates) is normalized to β-actin (**A**), while the fraction with I/A proteins was purified too (**B**). DISC1 and CRMP1 showed high insolubility when compared to CRMP1 Sv.

When DISC1 or variants of CRMP1 were over-expressed in HEK293 cells, there was no significant difference in the intensity of corresponding bands (**Figure 55 A**). As for their I/A, DISC1 and CRMP1 Lv showed bands with higher intensity when compared to bands corresponding to CRMP1 Sv (**Figure 55 B**), also described in previous research[321,322].

However, once the co-transfection was done, e.g., two plasmids were simultaneously transfected in the same cell, there was a significant drop in the intensity of the DISC1 band in the homogenate fraction. Interestingly, the band for DISC1 was not detected in the I/A protein fraction when expressed with CRMP1 Sv, unlike when the co-transfection happened with CRMP1 Lv. Levels of loading control, β-actin, remained the same across all samples (**Figure 55 A**). In the I/A fraction, the DISC1, CRMP1 Sv, and Lv levels remained the same after co-transfection (**Figure 55 B**).

4.2.4.3 Co-aggregation of NPAS3 with other proteins

The next set of experiments investigated the localization of NPAS3 when co-expressed with proteins that aggregate significantly (DISC1) or proteins seen to co-aggregate (CRMP1 Sv or Lv). NPAS3 is

a transcription factor that mainly localizes in the nucleus. However, after introducing external stress factors like sodium arsenite, it shows nuclear and cytoplasmic localization. In this set of experiments, the focus was on a full-length version of human NPAS3, referred to here as NPAS3 wt, and the experiments were done in standard conditions, without external stress factors.

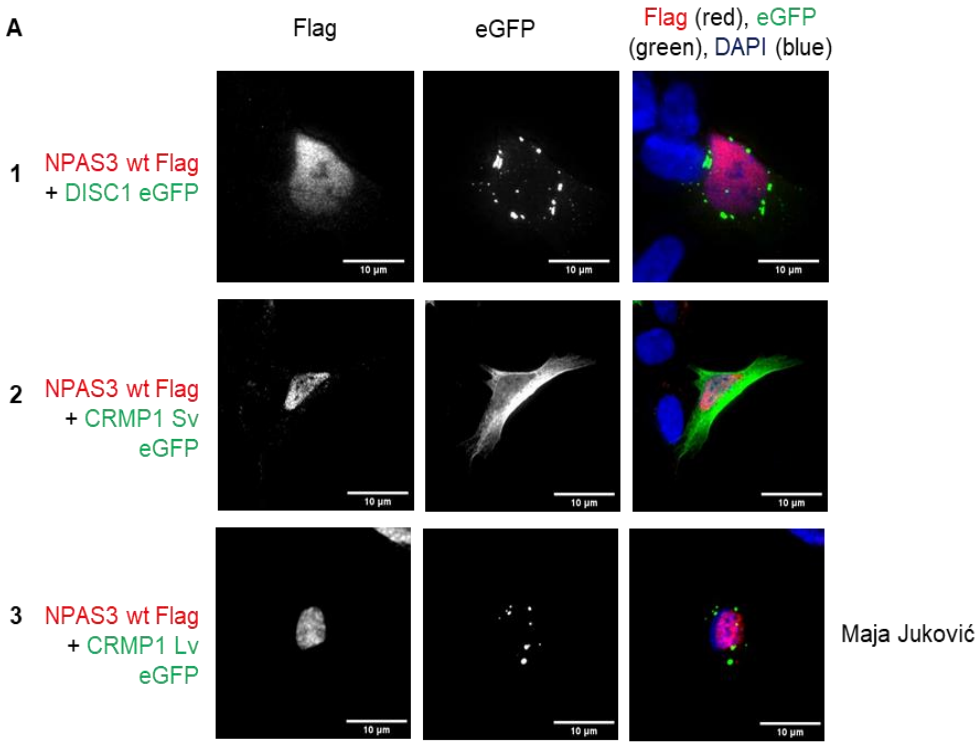

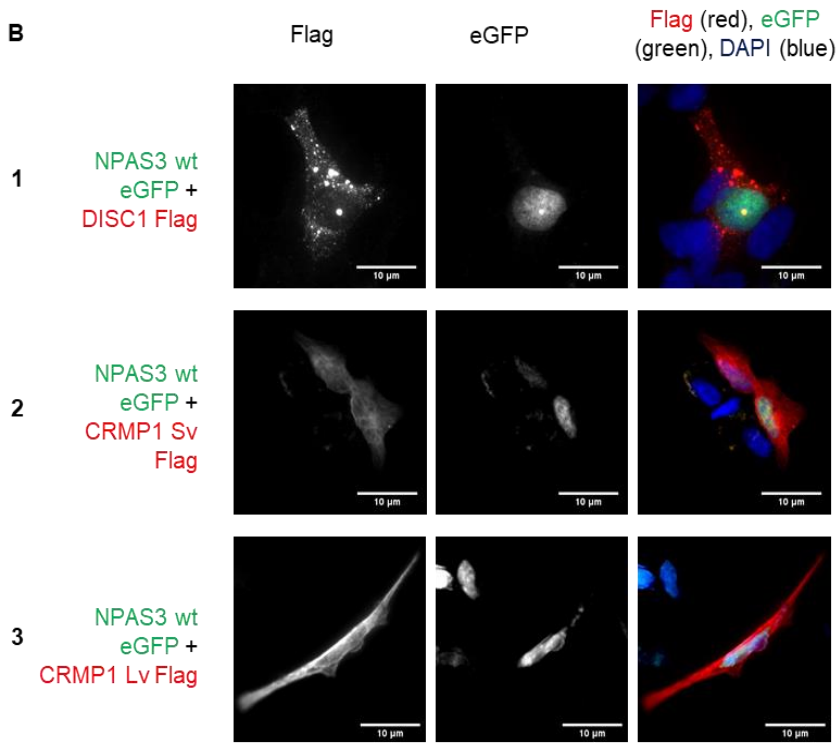

Figure 56: NPAS3-Flag maintains nuclear localization following co-expression with DISC1, CRMP1 Lv, and Sv in SH-SY5Y cells, independent of the tag. When full-length wt NPAS3-Flag (seen as red) was co-expressed with DISC1 and CRMP1 Sv or Lv -eGFP (seen as green), NPAS3 was observed in the nucleus (**A1-4**). The same effect was observed when the tags were switched, with NPAS3-eGFP (green) and DISC1, CRMP1 Sv, or Lv -Flag (red) (**B1-4**). The cells were stained with anti-Flag primary antibody and goat anti-mouse 594 nm secondary antibody (red), while DAPI (nucleus, blue) is also shown. The images were taken with 60x objective, and the white bar represents 10 µm.

NPAS3-Flag is observed in the nucleus of SH-SY5Y cells after co-transfection with proteins with eGFP tag (DISC1 and CRMP1 Lv and Sv, **Figure 56 A1-4**). DISC1-eGFP and CRMP1 Lv-eGFP show clear signs of aggregation (**Figure 56 A1,3,4**), as seen previously in single transfections (**Figure 56 A2-6**). In contrast, CRMP1 Sv was seen in the cytoplasm without clear signs of aggregation (**Figure 56 A2**). When tags were switched, NPAS3-eGFP was observed in the nucleus (**Figure 56 B1-4**), and DISC1- showed signs of aggregation (**Figure 56 B1** and **B4**), while CRMP1 Sv and Lv were observed in the cytoplasm (**Figure 56 B2** and **B3**).

In summary, DISC1, CRMP1 Sv, and Lv did not affect the nuclear localization of NPAS3 in normal conditions.

4.3 Analysis of transgenic *DISC1 Drosophila* model

4.3.1 Analysis *DISC1* expression in *Drosophila* model

The *hflDISC1* was inserted in *w*^{1118} *Drosophila melanogaster* flies and balanced on the 2nd (UAS-*hflDISC1*-2nd) or 3rd (UAS-*hflDISC1*-3rd) chromosome. Expression in all neurons was facilitated after crossing UAS lines with flies carrying pan-neuronal driver *elav-GAL4*. Western blot was used to investigate expression in uncrossed UAS lines; lines crossed with driver, driver *elav-GAL4* line, and *w*^{1118} (CTRL). The body and head homogenates were prepared from young (3-5 days old) male flies and investigated separately. The bands specific to DISC1 were quantified and normalized according to levels of β-actin in each sample, giving out a relative value of DISC1 signal per sample.

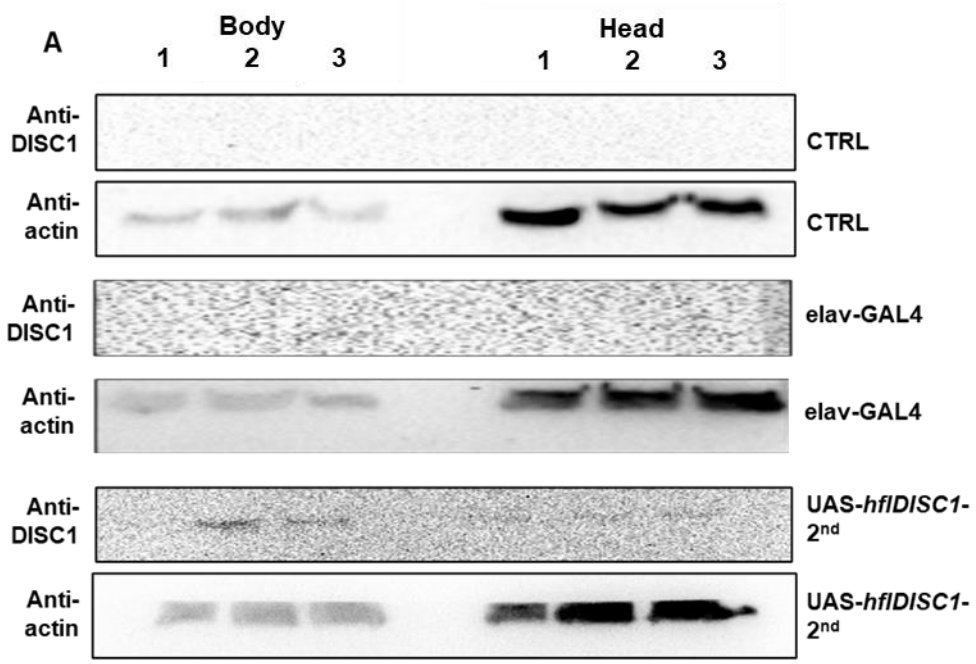

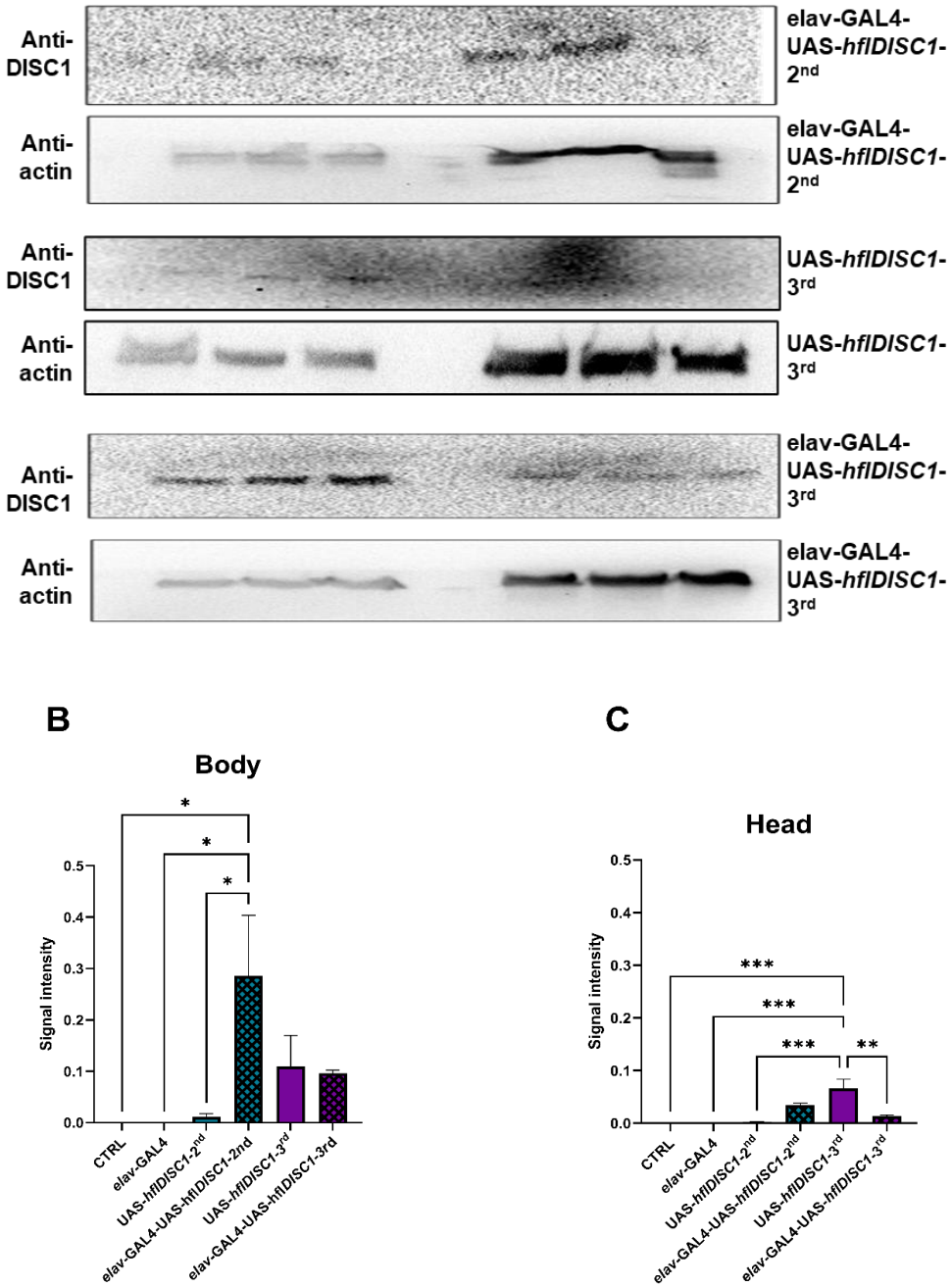

Figure 57: In both chromosomes, *hflDISC1* is expressed with or without elav-GAL4 driver in body and head homogenates. Homogenates of body (5 bodies without heads) and head (20 heads) samples were prepared from 3-5 days of adult male flies. The following fly lines were investigated: w^{1118} (CTRL), driver line *elav*-GAL4, fly line with the *hflDISC1* insertion on 2nd (UAS-*hflDISC1*-2nd) or 3rd (UAS-*hflDISC1*-3rd) chromosome, and fly lines with induced expression in crosses (elav-GAL4-UAS-*hflDISC1*-2nd and elav-GAL4-*hflDISC1*-3rd). Each sample had three technical replicates and all shown images are representative of three different experiments. During Western blot analysis, samples were stained with anti-DISC1 and anti-β actin antibody (A). Band intensity was quantified, and specific DISC1 data was normalized to β actin signal, providing a relative DISC1 signal shown on the graph. DISC1 signal data are presented as AVE +/- SEM (n=9) for body (B) and head

(C) samples. One-way ANOVA with Tukey's multiple comparisons test. All sample groups were compared, but only the pairs with significant differences are shown on the graph, with p values marked as follows: p < .05 (*), p <.001 (**), p <.001 (***).

hflDISC1 expression was detected in both UAS lines, in the body and head samples (**Figure 57 A**). Relative *hflDISC1* signal in the samples from the body was the highest in elav-GAL4-UAS-*hflDISC1*-2nd, while UAS-*hflDISC1*-3rd and their cross elav-GAL4-*hflDISC1*-3rd had the same *hflDISC1* expression levels (**Figure 57 B**). This suggests that the UAS-*hflDISC1*-3rd line may exhibit leaky expression, which can happen due to a promiscuous promoter element near the insertion site, and in turn allows transcription without GAL4. While UAS constructs typically require GAL4 for activation, such background expression has been previously reported[482,483].

In the head samples, flies carrying the *hflDISC1* on the 3rd chromosome had the highest *hflDISC1* expression even without the driver, suggesting strong leaky expression likely due to insertion site effects. Interestingly, after the driver was introduced (elav-GAL4-UAS-*hflDISC1*-3rd), the signal lowered (**Figure 57 C**), possibly due to transcriptional interference or titration of the transcriptional machinery. In contrast, elav-GAL4-UAS-*hflDISC1*-2nd line had higher expression of *hflDISC1* than UAS-*hflDISC1*-2nd, which indicates a clear GAL4-dependent upregulation. In conclusion, 2nd chromosome insertion is more suitable for controlled, GAL4-dependent expression.

4.3.2 *hflDISC1* insertion and expression influence on neurotransmitters concentration

After noticing the difference in *hflDISC1* expression, with and without activation of localized expression induced by elav-GAL4 driver, the hypothesis was that altered *hflDISC1* levels in the nervous system could impact monoaminergic signaling. To test this, the monoamine concentrations in head samples were measured using liquid chromatography with tandem mass spectrometry (LC-MS/MS).

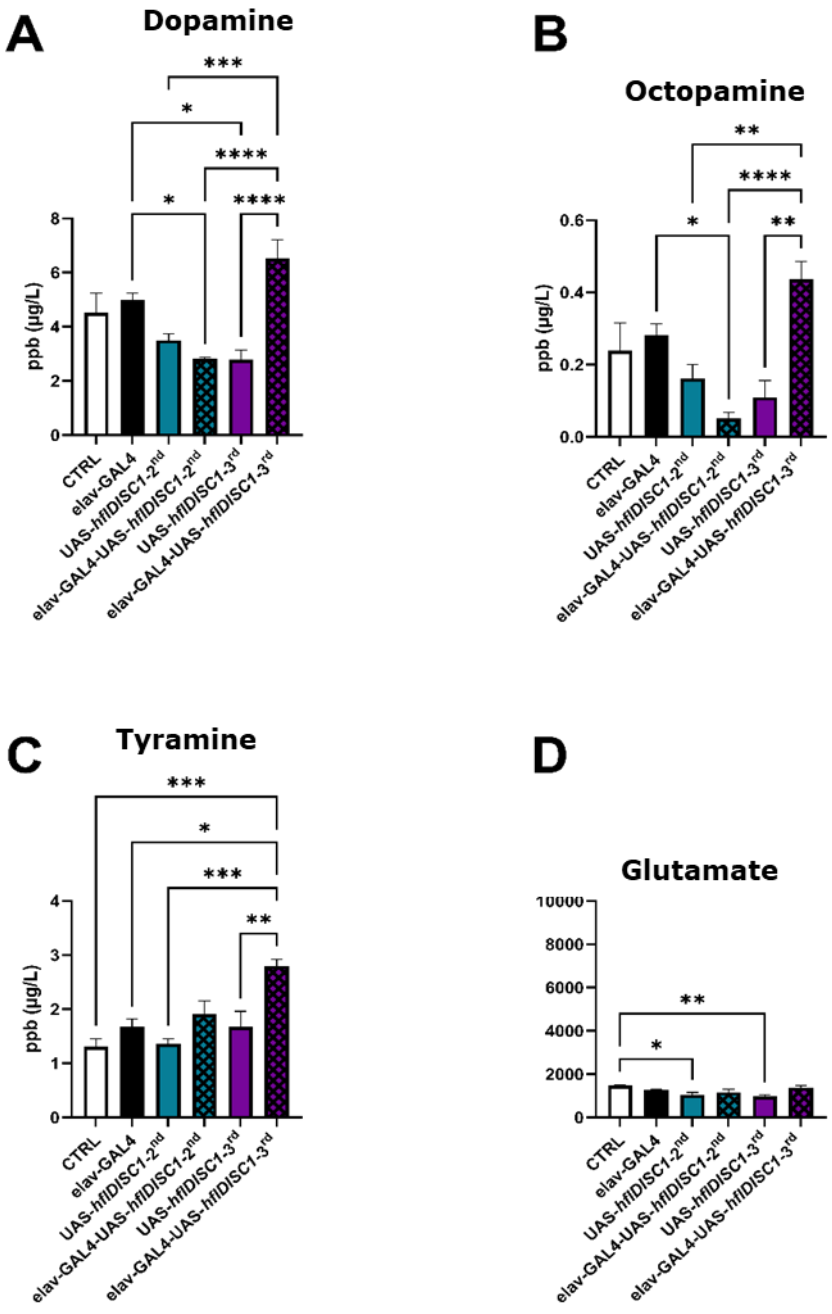
A
Dopamine
ppb (µg/L)
B
Octopamine
ppb (µg/L)
C
Tyramine
ppb (µg/L)
D
Glutamate
CTRL
elav-GAL4
UAS-hflDISC1-2nd
elav-GAL4-UAS-hflDISC1-2nd
UAS-hflDISC1-3rd
elav-GAL4-UAS-hflDISC1-3rd

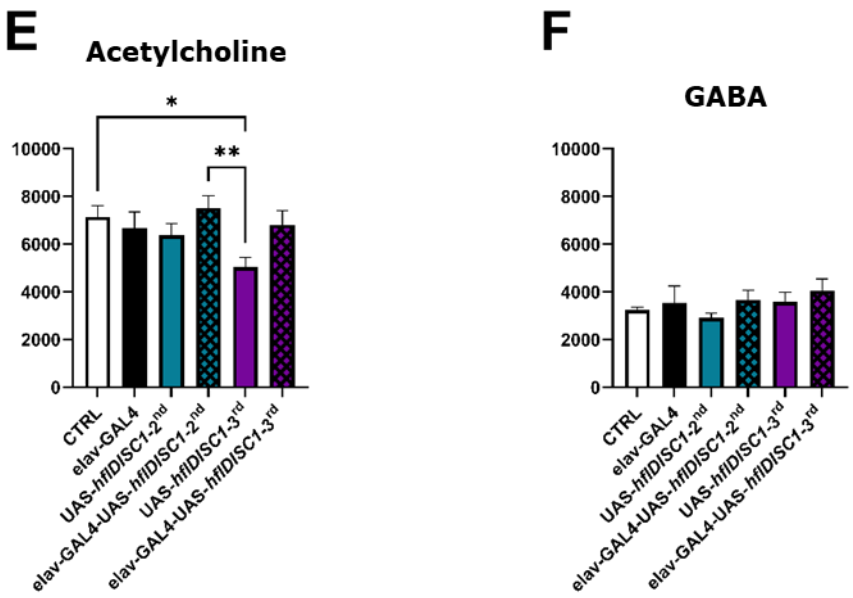

Figure 58: *hflDISC1* driver lines on both chromosomes decrease monoamines concertation: dopamine (DA), octopamine (OA), tyramine (TA), glutamate (GLU), gamma-aminobutyric acid (GABA), and acetylcholine (ACh), with increase in elav-GAL4-UAS-hflDISC1-3rd flies. The concentration of DA, OA, and TA, was determined using quantitative analysis, while the analysis for GABA, GLU, and ACh was semi-quantitative. Samples were prepared from 16 heads in triplicates (n=9) collected at 09:00 in the morning from 3-5 days old adult male flies. UAS lines had *hflDISC1* balanced on the 2nd (elav-GAL4-UAS-*hflDISC1*-2nd) or 3rd (UAS-*hflDISC1*-3rd) chromosome. The driver elav-GAL4 was introduced in lines carrying the gene: elav-GAL4-UAS-*hflDISC1*-2nd and elav-GAL4-UAS-*hflDISC1*-3rd. The controls were w^{1118} and fly lines with only driver (elav-GAL4). Data on the graphs is presented as AVE +/- SEM and statistically analyzed with one-way ANOVA with Tukey's multiple comparisons test. All sample groups were compared, but only the pairs with significant differences are shown on the graph, with p values marked as follows: $p < .05$ (*), $p < .001$ (**), $p < .001$ (***).

Dopamine and octopamine levels (**Figure 58 A** and **B**) were highest in flies expressing the *hflDISC1* on the 3rd chromosome after crossing with the driver line (elav-GAL4-UAS-*hflDISC1*-3rd), compared to flies with only the gene insertion (UAS-*hflDISC1*-3rd) and other *hflDISC1 Drosophila* models. Flies expressing *hflDISC1* on the 2nd chromosome (elav-GAL4-UAS-*hflDISC1*-2nd) also exhibited higher dopamine and octopamine levels than those expressing *hflDISC1* on the 2nd chromosome (elav-GAL4-UAS-*hflDISC1*-2nd). Interestingly, the driver line alone (elav-GAL4) also showed elevated levels compared to the *hflDISC1* models.

Tyramine levels (**Figure 58 C**) were elevated in flies expressing *hflDISC1* with the driver line, regardless of whether the gene was

balanced on the 2nd or 3rd chromosome (elav-GAL4-UAS-*hflDISC1*-2nd and elav-GAL4-UAS-*hflDISC1*-3rd), compared to flies carrying only the gene insertion (UAS-*hflDISC1*-2nd and UAS-*hflDISC1*-3rd). Flies expressing *hflDISC1* on the 3rd chromosome (elav-GAL4-UAS-*hflDISC1*-3rd) also exhibited higher tyramine levels than controls.

Glutamate levels (**Figure 58 D**) remained consistent across samples, except in the UAS lines (UAS-*hflDISC1*-2nd and UAS-*hflDISC1*-3rd), which had lower glutamate compared to CTRL.

Acetylcholine levels (**Figure 58 E**) were generally similar among groups, except for flies carrying *hflDISC1* on the 3rd chromosome (UAS-*hflDISC1*-3rd), which exhibited lower acetylcholine levels than CTRL and flies expressing *hflDISC1* on 2nd chromosome (elav-GAL4-UAS-*hflDISC1*-2nd).

Although GABA levels (**Figure 58 F**) did not show statistically significant differences, DISC1-expressing flies (elav-GAL4-UAS-*hflDISC1*-2nd and elav-GAL4-UAS-*hflDISC1*-3rd) had higher GABA concentrations compared to flies with only the gene insertion (UAS-*hflDISC1*-2nd and UAS-*hflDISC1*-3rd).

In conclusion, these results demonstrate that expression of *hflDISC1* in *Drosophila* neurons alters levels of several neurotransmitters, with the strongest effects observed when the transgene is expressed from the 3rd chromosome.

4.3.3 Effect of *hflDISC1* expression on redox parameters

Given the role of DISC1 in mitochondrial trafficking, the redox status was investigated in flies with *hflDISC1* balanced on 2nd or 3rd chromosome, before and after the expression was induced. Hydrogen peroxide (H_2O_2) is a byproduct of cellular metabolism that, while harmful at high levels due to oxidative stress, also contributes to cell signaling and immune defense at lower concentrations. As controls, the wt w^{1118} (CTRL) flies were used, and the driver line by itself (elav-GAL4). Using headless body or head extracts, H_2O_2 concentration was indirectly measured. The stain used in this assay, DHE, mainly detects superoxide, but by measuring total oxidation levels and comparing with standard curve of DHE fluorescence with known H_2O_2 concentrations, it can indirectly estimate H_2O_2 levels.

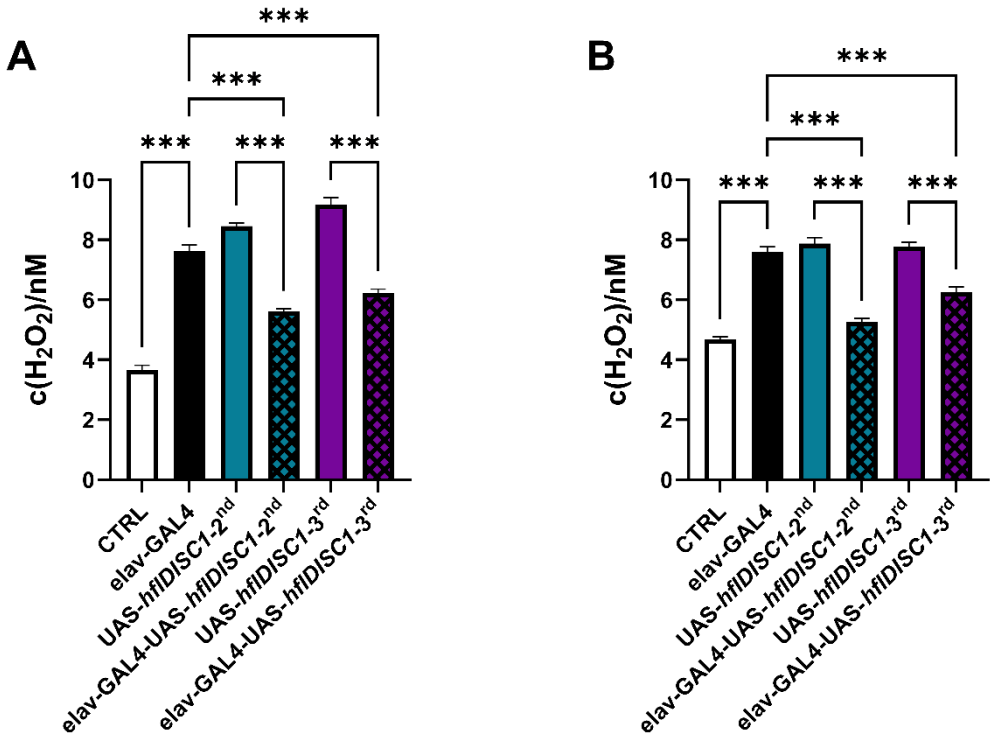

Figure 59: *hflDISC1* insertion elevates H_2O_2 levels while crossing reduces them. Samples were prepared from 32 heads (A) and 5 headless bodies (B) in triplicates (n=9) from 3-5 days-old adult male flies. UAS lines without driver had hfl*DISC1* balanced on 2nd (elav-GAL4-UAS-*hflDISC1*-2nd) or 3rd (UAS-*hflDISC1*-3rd) chromosome. The driver elav-GAL4 was introduced in lines carrying the gene: elav-GAL4-UAS-*hflDISC1*-2nd and elav-GAL4-UAS-*hflDISC1*-3rd. The controls were w^{1118} (CTRL) flies and lines with only driver (elav-GAL4). Data on the graphs is presented as AVE +/- SEM and statistically analyzed with one-way ANOVA with Tukey's multiple comparisons test. All sample groups were compared, but only the pairs with significant differences are shown on the graph, with p values marked as follows: p < .05 (*), p <.001 (**), p <.001 (***).

H_2O_2 levels were similar in the driver fly line (elav-GAL4), UAS-*hflDISC1*-2nd, and UAS-*hflDISC1*-3rd flies. However, it significantly increased compared to crossed (elav-GAL4-UAS-*hflDISC1*-2nd or UAS-*hflDISC1*-3rd) or CTRL flies. The same phenomenon was observed in the headless body (**Figure 59 A**) and head (**Figure 59 B**) samples.

Cells regulate and degrade H_2O_2 through antioxidant enzymes like catalase, glutathione peroxidase, and peroxiredoxins, whose activity is influenced by oxidative conditions. Therefore, the non-enzymatic glutathione (GSH) levels were measured, assessing both its active form (GSH) and its oxidized, inactive form (GSSG).

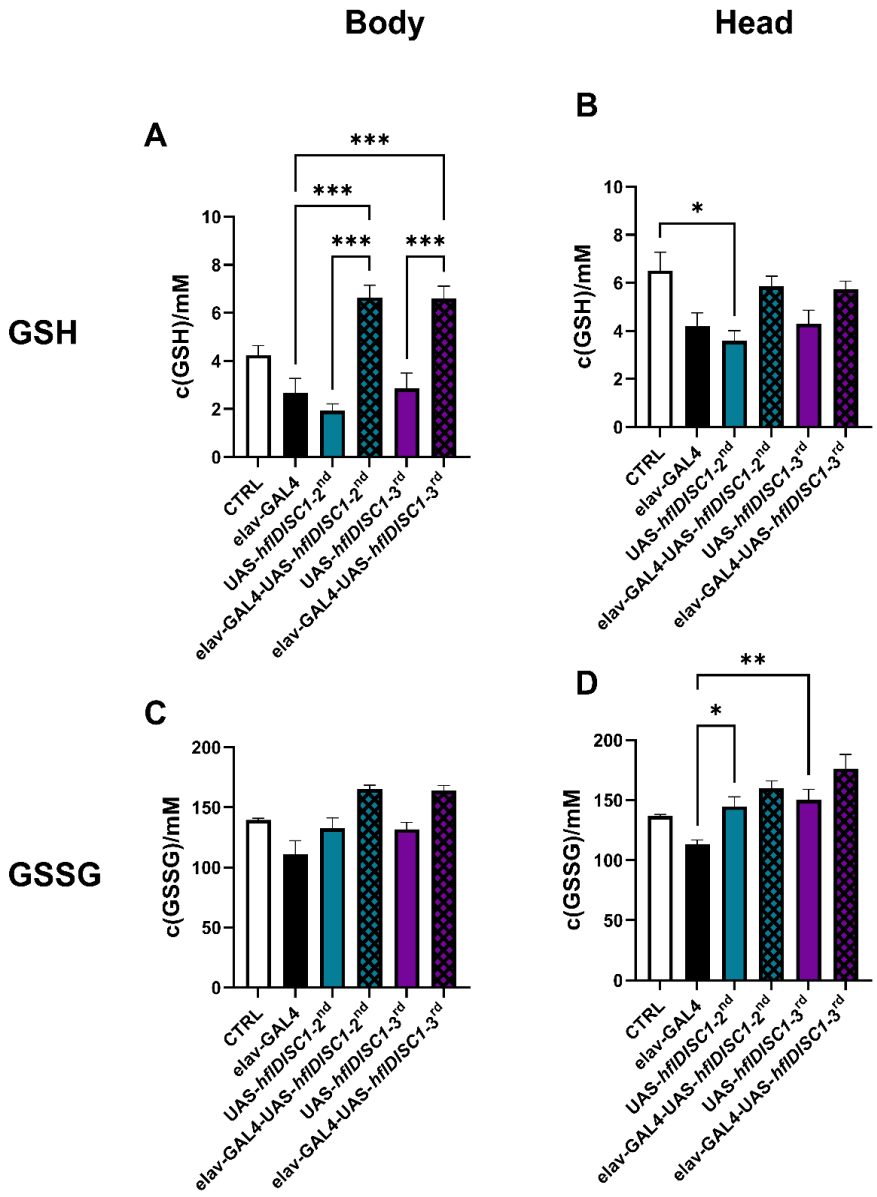

Figure 60: GSH and GSSG levels in flies expressing the *hflDISC1* after crossing with the driver line were higher than in other groups in both body and head samples. Samples were prepared from 32 heads (**B** and **D**) and 5 headless bodies (**A** and **C**) in triplicates (n=9) from 3-5 days-old adult male flies. Samples from the body are shown under A and C, while the samples from the head are shown under B and D. UAS lines without driver had *hflDISC1* balanced on 2nd (elav-GAL4-UAS-*hflDISC1*-2nd) or 3rd (UAS-*hflDISC1*-3rd) chromosome. The driver elav-GAL4 was introduced in fly lines carrying the gene: elav-GAL4-UAS-*hflDISC1*-2nd and elav-GAL4-UAS-*hflDISC1*-3rd. The controls were w^{1118} (CTRL) flies and lines with only driver (elav-GAL4). Data on the graphs is presented as AVE +/- SEM and statistically analyzed with one-way ANOVA with Tukey's multiple comparisons test. All sample groups were compared, but only the pairs with significant differences are shown on the graph, with p values marked as follows: p < .05 (*), p <.001 (**), p <.001 (***).

GSH levels in body samples (**Figure 60 A**) of elav-GAL4-UAS-*hflDISC1*-2nd and elav-GAL4-UAS-*hflDISC1*-3rd lines were significantly higher compared to w^{1118} (CTRL), driver (elav-GAL4) or gene insertion (UAS-*hflDISC1*-2nd and UAS-*hflDISC1*-3rd) lines. GSH levels in the head samples (**Figure 60 B**) followed a similar trend but without statistical significance. GSSG levels in body samples (**Figure 60 C**) varied, with it being the highest in flies with insertion of the *hflDISC1* on the 2nd or 3rd chromosome crossed out with driver line (elav-GAL4-UAS-*hflDISC1*-2nd and elav-GAL4-UAS-*hflDISC1*-3rd). There was a significant decrease in levels of GSSG in head samples (**Figure 60 D**) from the driver line (elav-GAL4) when compared to flies with gene insertion (UAS-*hflDISC1*-2nd and UAS-*hflDISC1*-3rd), suggesting that GSH/GSSG could be as a compensatory mechanism to counteract the redox imbalance induced by *hflDISC1* expression.

As this aligns with the known role of DISC1 in mitochondrial function, it is possible that dysregulation of DISC1 in neurons could disrupt cellular redox homeostasis enough to result in SZ phenotypes.

4.3.4 Social interaction network for *hflDISC1 Drosophila* models

Since CMIs, such as SZ, heavily affect the interpersonal relationships of patients with other people and *hflDISC1* has been implicated in development of these illnesses, the effect of *hflDISC1* insertion in flies on social phenotypes was investigated.

For this, the arena assay was implemented where SIN can be created based on a video recording of 12 flies per fly line, with over 20 recording for each fly line. Parameters of SINs were determined at global and at local level.

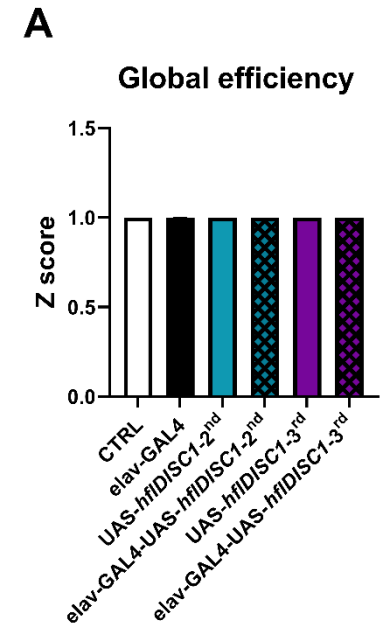
A
Global efficiency
Z score
1.5
1.0
0.5
0.0
CTRL
elav-GAL4
UAS-hflDISC1-2nd
elav-GAL4-UAS-hflDISC1-2nd
UAS-hflDISC1-3rd
elav-GAL4-UAS-hflDISC1-3rd

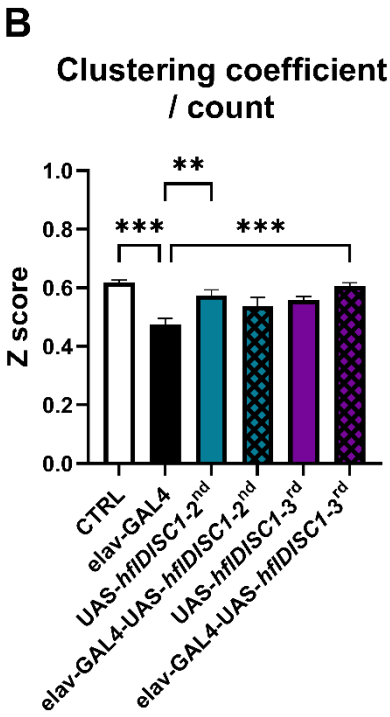
B
Clustering coefficient / count
Z score
1.0
0.8
0.6
0.4
0.2
0.0
**
***
***
CTRL
elav-GAL4
UAS-hflDISC1-2nd
elav-GAL4-UAS-hflDISC1-2nd
UAS-hflDISC1-3rd
elav-GAL4-UAS-hflDISC1-3rd

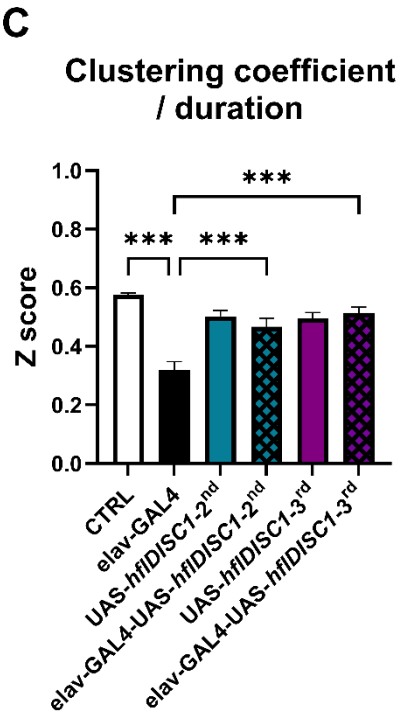
C
Clustering coefficient / duration
Z score
1.0
0.8
0.6
0.4
0.2
0.0
***
***
***
CTRL
elav-GAL4
UAS-hflDISC1-2nd
elav-GAL4-UAS-hflDISC1-2nd
UAS-hflDISC1-3rd
elav-GAL4-UAS-hflDISC1-3rd

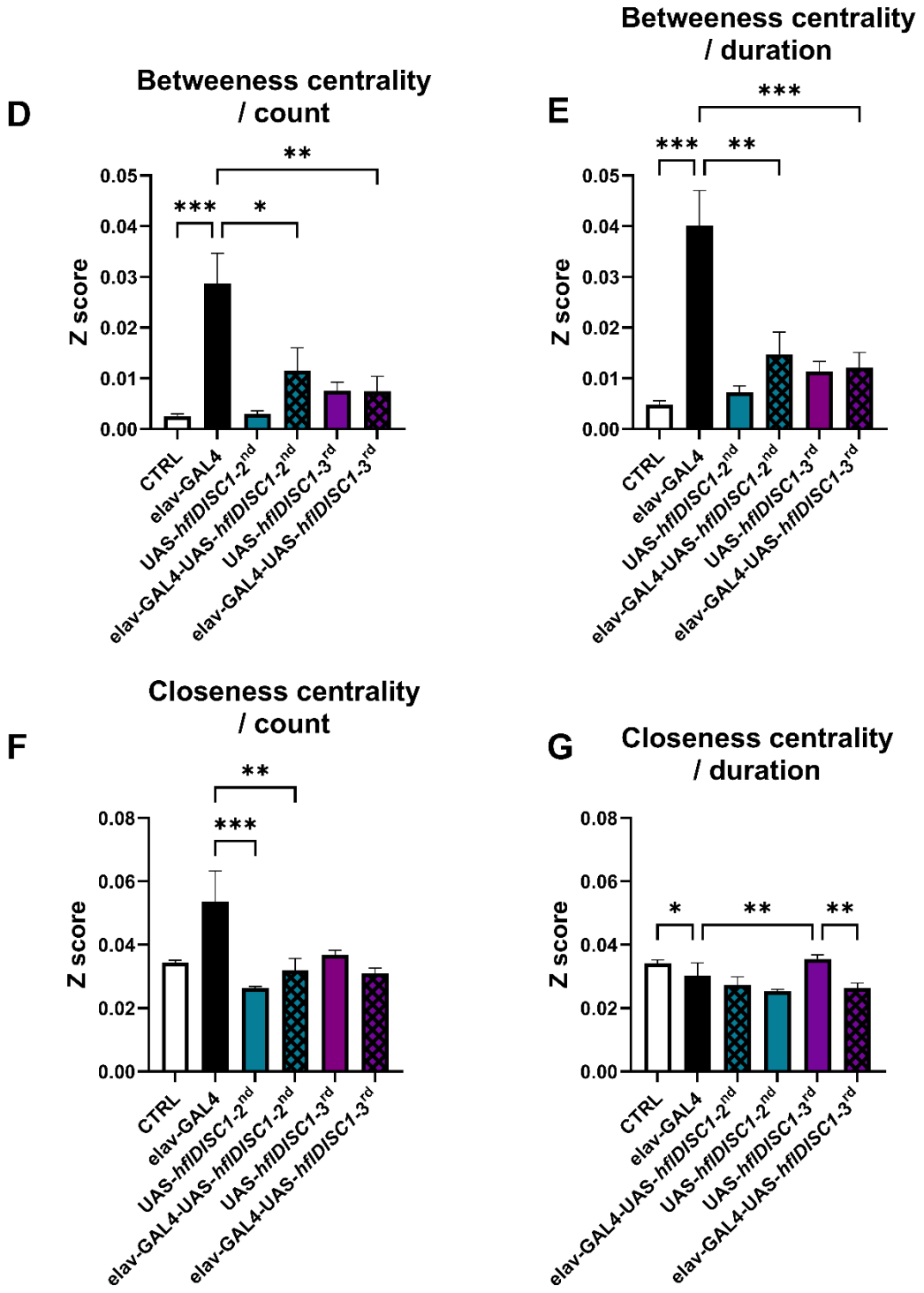

Figure 61: SIN in flies expressing *hflDISC1* have lower centrality measures. All measurements were performed in replicates (n>15) using elav-GAL4, UAS-*hflDISC1*-2nd and UAS-*hflDISC1*-3rd male flies and flies from crosses elav-GAL4-hflDISC1-UAS-*hflDISC1*-2nd and elav-GAL4-hflDISC1-UAS-*hflDISC1*-3rd. The controls were w^{1118} (CTRL) flies. Parameters global efficiency (**A**) and clustering coefficient, weighted either by count (number) (**B**) or duration (sec) (**C**), were statistically analyzed using one-way ANOVA with Tukey's multiple comparison post hoc test.

Parameters betweenness centrality (**D, E**) and closeness centrality (**F, G**), weighted either by count (number) or duration (sec), were statistically analyzed with Kruskal-Wallis. $p < .05$ (*), $p < .001$ (**), $p < .001$ (***).

In all tested fly lines, the observed global efficiency, a measure of fly group connectivity based on distance, was high (**Figure 61 A**).

The control group of flies with w^{1118} background (CTRL) had the highest clustering coefficient, indicating the degree of connectivity among flies within a local network and the probability that their neighboring flies will also establish connections. The clustering coefficient for elav-GAL4 was lower compared to flies with gene insertion (UAS-*hflDISC1*-3rd and UAS-*hflDISC1*-3rd) or when the gene was expressed in elav-GAL4-UAS-*hflDISC1*-3rd flies. The effect is more pronounced if the duration of the interaction is taken as a weight than it is for the number of interactions (**Figure 61 B** and **C**), suggesting that GAL4 expression alone may influence neuronal network properties and should be considered when interpreting results.

Betweenness centrality, a metric assessing each fly's significance in preserving group cohesion, was the highest for elav-GAL4, regardless of weights (count and duration) compared to other groups. When flies were expressing *hflDISC1*, the betweenness centrality was higher than in flies with only gene insertion, the same for both weights (**Figure 61 D** and **E**).

Closeness centrality, a metric quantifying the average shortest paths between flies in the network, was highest in the control group (CTRL) and driver line (elav-GAL4). In UAS-*hflDISC1*-2^{nd,} closeness centrality was lower than in elav-GAL4-UAS-*hflDISC1*-2nd. However, with the 3rd chromosome, the effect was reversed, flies expressing the *hflDISC1* after crossing with the driver line (elav-GAL4-UAS-*hflDISC1*-3rd) had lower closeness centrality than flies with only gene insertion (UAS-*hflDISC1*-3rd). With count as weight (**Figure 61 F**), these results are more obvious than with duration as weight (**Figure 61 G)**.

5 Discussion

Throughout this thesis, the aggregation of specific proteins implicated in CMIs and their potential for co-aggregation was assessed by *post-mortem* human brain samples, *in vitro* in mammalian cell culture*,* and *in vivo* fly models.

5.1 Co-aggregation in human brain and cell models

Protein aggregation has been extensively studied in NDs, but its role in CMIs remains poorly understood. Several studies have suggested that abnormal protein aggregation in the human brain may disrupt neuronal function, impair synaptic signaling, and induce cellular stress responses[308–323,453].

As first part of this thesis, aggregation patterns of CRMP1, DISC1, NPAS3 and TRIOBP-1 were investigated in IC brain region. The IC plays a key role in emotional regulation and cognitive processing, making it relevant for CMIs[466]. Moreover, the IC is less prone to severe structural changes than other regions, such as the hippocampus or prefrontal cortex, in conditions like AD or MDD. The samples were collected from suicide victims, MDD and AD patients, and controls to assess whether aggregation is disease-specific.

DISC1, CRMP1, and TRIOBP-1 were consistently detected in total protein fraction, while NPAS3 was largely absent, likely due to its developmental expression pattern[333,389,390,439,459]. Although NPAS3 was detected in I/A fractions across all groups, the signal was variable and could not be quantified due to lack of protein loading control, making it unclear whether group differences exist. DISC1 insolubility also showed high inter-individual variability, with prominent bands detected in specific cases across diagnostic groups, including controls, meaning that aggregation levels may not be solely dependent on diagnosis. Similarly, prominent CRMP1 Lv and Sv bands appeared I/A protein fraction collected from several individuals without a clear diagnostic pattern, and TRIOBP-1 insolubility remained generally low. In conclusion, while protein aggregation can occur in CMIs, it may be influenced by individual-specific factors rather than serving as a consistent biomarker of diagnosis.

Based on the intensity of specific bands in I/A fractions versus the bands in whole protein fraction, aggregation signal was determined for each protein.

Interestingly, NPAS3 aggregating signal appeared elevated in individuals diagnosed with AD, compared to controls, suicide victims, and patients with MDD. A slight increase was also observed in MDD samples. However, these changes did not achieve statistical significance. DISC1 aggregation signals were unexpectedly highest in controls, particularly in the LOG, while suicide victims and MDD patients showed region-specific increases. AD patients had the lowest aggregation overall, which was different than previous findings [320,321]. Importantly, whereas earlier studies combined data from all patients with CMIs and compared it to the controls, my thesis acknowledges that this pathology is not present in every patient with CMIs, but is more specific to a subset of individuals. CRMP1 variants also showed differential patterns of insolubility, where CRMP1 Sv aggregation was highest in suicide victims (notably in BA 3,1,2), while CRMP1 Lv aggregation peaked in MDD patients, particularly in the LOG and FC. Controls also showed high aggregation across several regions, suggesting a possible baseline level of aggregation or age-related changes not necessarily linked to pathology. Likewise, TRIOBP-1 aggregation was variable and region-specific. Highest levels were detected in the FC of AD patients, while suicide victims showed elevations in LOG and BA17. Notably, several control subjects and two individuals with MDD also exhibited high TRIOBP-1 aggregation signals. To conclude, the insolubility and potential aggregation of mentioned proteins in the IC does not align consistently with tested diagnosis and it appears to occur in a subset of individuals. Moreover, it reinforces the idea that protein insolubility may represent a shared pathological mechanism in a biologically defined subgroup rather than a hallmark of any single disorder.

Another major result shown in this part of thesis is that one protein rarely aggregates alone in brain. Multiple co-aggregation events occurred in suicide victims, controls, and AD patients, but not MDD. For example, CRMP1 Sv co-aggregated with NPAS3 or TRIOBP-1 only in suicide victims. Given CRMP1's critical role in axon guidance, neuronal migration, and synapse formation[351], its aggregation alongside NPAS3 or TRIOBP-1 suggests a potential disruption in cytoskeletal organization and intracellular signaling pathways. Since CRMP1 forms hetero-oligomeric complexes with other CRMPs[351] and undergoes phosphorylation[332,337], disease-specific modifications may influence its aggregation propensity. DISC1 alone in SH-SY5Y or HEK

cells exhibited robust aggregation tendencies, consistent with its known propensity to form pathological aggregates in CMIs[320,321,383,396–401,404,502]. When co-expressed with CRMP1 Sv, DISC1 aggregation was unaffected. However, CRMP1 Lv co-aggregated with DISC1. The difference is likely due to structural differences between CRMP1 Sv and Lv, as CRMP1 Lv has an N-terminal extension[332]. The aggregation-prone nature of CRMP1 Lv, particularly when co-expressed with DISC1, aligns with prior findings of CRMP1 aggregation propensity[322] and its involvement in axon guidance and cytoskeletal dynamics[332]. Observed CRMP1 Lv's instability with the eGFP tag further emphasizes its structural sensitivity. There may be a synergistic relationship between DISC1 and CRMP1 Lv, where DISC1 aggregates may serve as nucleation sites for CRMP1 Lv aggregation, which could impair cytoskeletal dynamics and synaptic plasticity. On the other hand, the reduced size of DISC1 aggregates was observed after co-transfection with CRMP1 Sv. It is possible CRMP1 Sv can exert a stabilizing effect, which has strong therapeutic implications.

Another significant result is DISC1 co-aggregation with TRIOBP-1, which reflects their shared involvement in cytoskeletal organization and neuronal integrity[389,390,459]. Aggregation of TRIOBP-1 has been shown to impair neurite outgrowth[323,464], and its interaction with DISC1 may exacerbate this effect, contributing to neuronal dysfunction. Separately, NPAS3 maintained its nuclear localization when co-expressed with DISC1, CRMP1, or TRIOBP-1. As NPAS3 has a critical role in transcriptional regulation and is conserved across different species[407,428,429], it is probably more resilient to aggregation-mediated dysfunction. Interestingly, previous studies[446,453] and our results have shown that oxidative stress or mutations can alter NPAS3 localization and aggregation propensity, suggesting that extensive combined genetic factors may trigger its aggregation in CMIs.

In summary, it is possible that a combination of proteins aggregating severely contributes to CMIs, emphasizing the need for future research in this field. Limitations of this experiment and proposals for future experiments will be discussed later.

5.2 Protein aggregation in CMIs varies across the brain regions

Research in this thesis was expanded to other brain regions, beyond IC region, from the same individuals, if available.

Levels of DISC1, CRMP1 Sv and Lv, and TRIOBP-1 in whole protein fractions across different brain region were variable and not correlating with diagnosis. However, when the I/A protein fraction was analyzed, it was obvious how protein aggregation is not uniform but rather varies across brain regions. CRMP1 aggregation was observed in controls (BA17, TC, PC), suicide victims (LOG), and AD patients (TC). In MDD, elevated CRMP1 Lv was seen in LOG and FC, though overall CRMP1 aggregation was lower.

Furthermore, multiple brain regions showed high levels of DISC1 and TRIOBP-1 aggregation, especially in control samples. Interestingly, high levels of TRIOBP-1 aggregation were detected in LOG from suicide victims, same as CRMP1. Accumulation of aggregates LOG could heighten emotional reactivity and impulsivity, contributing to suicidal behavior.

Additionally, for this part of project, multiple regions from one patient with SZ were investigated. In the SZ patient, high DISC1 and CRMP1 were found in BA3, 1, 2 and LOG, but this was not consistent across SZ cases. A second SZ patient (SZ2) showed high DISC1 expression in total protein but no aggregation in I/A fraction. While impairments in LOG are more connected to emotions, impairments in BA3, 1, 2 could lead to sensory dysfunction, tactile hallucinations, and impaired motor processing. For TRIOBP-1, none of the analyzed brain regions showed high levels of aggregation. However, all shown aggregation signals were at least 10 times higher in samples from patients with diagnosed SZ compared to other tested groups, especially for DISC1. Hence, protein aggregation probably fits better in the pathology of SZ than MDD or suicide. Nevertheless, across all investigated samples, there were high levels of aggregating proteins in control, which future research needs to answer. Region specificity was also tested in a separate experiment, where 20 tissue samples (10 regions from each hemisphere) from a patient R with diagnosed SZ and AD were analyzed. As a reference, multiple brain regions from one control and one AD patient were used. Initially insolubility of DISC1 was tested, followed up with CRMP1 and TRIOBP-1. Among the three proteins of interest, representative sample of patient R exhibited an intense band for DISC1 in I/A protein fraction. Region BA36, 37 showed high DISC1 aggregation signal for both patient R and control, while in TC aggregation signal for DISC1 was high both of patient R and AD patient. Hence, the observed aggregation pattern suggests that while

DISC1 accumulation in BA36, 37 may not be disease-specific and its presence in TC could be associated with pathological processes linked to neurodegeneration. However, high DISC1 aggregation signal was observed in region BA6a in both hemispheres. Based on this, DISC1 aggregation may not be restricted to regions traditionally associated with cognitive and emotional processing but could also impact motor-related cortical areas.

However, I/A DISC1 was not detected in new SZ patients (SZ2), even though high levels of DISC1 were seen in total protein fraction. This means that DISC1 expression may remain elevated, but its propensity to aggregate varies between patients or disease stages. The absence of detectable aggregation in SZ2 could indicate differences in post-translational modifications, chaperone activity, or cellular mechanisms regulating protein solubility.

As protein aggregation was observed to be region-specific for both suicide and SZ, it may also be resemble the patterns observed in NDs, where aggregation tends to follow specific pathways rather than occurring ubiquitously[316,318,319]. Moreover, the co-occurrence of previously mentioned proteins and their insolubility in specific brain regions shows a potential interplay between these proteins in CMIs.

5.2.1 Limitations in *post-mortem* human brain analysis with implications for future research

A notable limitation of this approach is the absence of systematic validation for brain tissue integrity. The brain tissue used in this study was collected relatively quickly after death, with an average PMI of 5 hrs, and subsequently cryo-frozen. Usually, low PMI is correlated to high quality of brain tissue. However, tissue degradation can occur at any point during collection, transfer, or storage. Many brain banks perform pH measurements on fresh and frozen brain tissue, as pH levels correlate with RNA integrity. Also, RNA integrity itself is assessed by human brain banks using the RNA Integrity Number (RIN), which ranges from 1 to 10 and is typically determined via capillary electrophoresis with instruments such as the Agilent Bioanalyzer[512]. A high RIN score (e.g., greater than 7) is essential for transcriptomics and expression analyses. Additionally, ensuring a high RIN score could indicate that the tissue was well-preserved prior to protein purification. Hence, in future research either pH level or RIN score could be

determined when brain tissue arrives in the laboratory, before protocol for purification of I/A protein fraction. This is particularly important since the homogenization and long purification processes could exacerbate protein degradation if the initial tissue quality is compromised. To check for protein degradation, samples could be stained for dihydropyrimidinase-related protein-2, a degradation-sensitive marker[513]. Franzen et al. showed a higher ratio of fragmented dihydropyrimidinase-related protein-2 to full-length version is connected to higher tissue degradation.

One of the main things shown in this thesis is the variability of protein aggregation among different individuals with CMIs and in controls. Identifying a subset of CMIs patients with protein aggregation as underlying mechanism based on biochemical approaches could improve diagnostic accuracy and pave the way for targeted treatments, rather than a one-size-fits-all approach. A possibility for future research could be creating a “selection process”. Individuals with CMIs should firstly be assessed for level of general protein insolubility, before checking proteins of interest. Ideally, the assessment would be done in multiple brain regions within the same individual, establishing a standardized threshold to classify individuals as "aggregation-positive" when their values exceed this limit. Future studies should prioritize the LOG, PiFC, and TC, due to their frequent and diagnosis-specific patterns of protein aggregation. The LOG stood out for its high aggregation signals of DISC1, CRMP1 Lv, and TRIOBP-1, especially in MDD and suicide victims, suggesting a role in emotional dysregulation and impulsivity. The PiFC showed elevated DISC1 and CRMP1 Sv aggregation, particularly in MDD, linking it to olfactory processing and mood-related circuitry. The TC consistently showed aggregation across proteins and diagnostic groups, making it a promising region for investigating common molecular pathways in CMIs. Additionally, the somatosensory cortex (BA 3, 1, 2) remains a valuable region for further exploration, particularly in suicide victims and SZ, due to high DISC1 and CRMP1 Sv aggregation, potentially reflecting altered sensory processing and tactile perception. Lastly, regions like the FC and BA4 (motor cortex) also warrant investigation, given their involvement in MDD and SZ and emerging evidence of DISC1 and TRIOBP-1 aggregation, respectively. These areas may help disentangle motor and executive dysfunctions associated with CMIs. Generally, if individuals with high overall protein insolubility show different

aggregating proteins compared to those with low insolubility—within the same diagnostic group—this method could provide a more straightforward way to identify subgroups where aggregation may have pathological significance. Ultimately, this analysis could highlight novel therapeutic targets or biomarkers. In literature, a suggested way to probe individuals with CMIs who could be affected by protein aggregation is based on the intensity of their symptoms or treatment resistance[453]. In the case of SZ, 70% of patients are responding to currently available treatment. The rest of the patients are resistant to conventional drugs such as haloperidol but still respond to clozapine. Those patients are diagnosed with TRS and they usually exhibit intense cognitive symptoms, which makes them a potential subset with protein aggregation pathology. Less than 10% of patients with treatment-resistant SZ are resistant to clozapine, making them non-responsive to any currently available treatment. They also exhibit the worst clinical picture and should be investigated for signs of protein aggregation. Isolating this subset of patients based on clinical features may be effective. Still, it requires a well-trained clinician(s) for accurate diagnosis and an extensive follow-up on treatment, which can be affected by multiple factors like a support system, socioeconomic status, genetic mutations that affect drug metabolism, and others. Hence, a biochemical approach to distinguish different variants of SZ and other CMIs is essential. So far, high levels of ubiquitination and insolubility have been correlated with patients with poor cognitive performance and high resistance to clozapine, one of the significant antipsychotics. So, in future "selection process", levels of ubiquitination can also be included, complementary to the general protein insolubility analysis. Nevertheless, these kind of analysis on human brain tissue are informative, but in long-term, analysis also need to be done on tissues more accessible than brain, such as cerebrospinal fluid, as those samples can be collected from living patients. If described phenomenon is detectable in peripheral tissues in the same manner as in brain tissue samples, it could move the whole research onto the peripheral tissues, and the CMIs could be tracked minimally invasively, during treatment, or even in clinical studies. An optimistic future end goal would be even to guide treatment strategies for CMIs.

Acknowledging that the proteins of interest were also detected in the I/A fraction of control individuals is essential. One potential explanation for this finding is that the experimental methodology

requires further optimization. Incomplete removal of the supernatant during the I/A protein purification process or inadequate pellet resuspension may have influenced the results. The protocol used for I/A protein purification was validated by previous research in brain tissue material from transgenic DISC1 rats[320,464]. Briefly, both high- and low-stringency protocols were tested in removing soluble proteins while retaining aggregated forms. Incomplete supernatant removal and inadequate pellet resuspension were observed to cause minor protein loss, but did not significantly impact the presence of accurate I/A aggregates. Moreover, to confirm that soluble proteins are not contaminating the purified I/A fraction, the I/A protein fraction can be stained for soluble housekeeping protein, like β-actin. However, it is essential to note that TRIOBP-1 binds β-actin in normal conditions, so it is possible TRIOBP-1 "pulls" β-actin in its aggregates, which could be seen as a low signal of β-actin in I/A protein fraction. So, other proteins like Glyceraldehyde-3-phosphate dehydrogenase could be used instead. Alternatively, this observation may indicate a baseline level of protein aggregation that is physiologically normal and efficiently managed by cellular clearance mechanisms. This interpretation is supported by demographic data, as controls, AD, and MDD patients were significantly older than suicide victims, suggesting that accumulated I/A proteins result from age-related declines in protein clearance. Notably, suicide victims, despite their younger age, exhibited similar signs of impaired clearance, highlighting the potential role of protein aggregation in cellular dysfunction and its broader impact on psychiatric pathology. Previously cited research [464] also showed that I/A TRIOBP-1 levels correlate with brain pH, suggesting that *post-mortem* changes affect aggregation, adding to how some aggregation is physiologically normal and influenced by cellular clearance. Finally, another suggestion to account for the presence of I/A proteins in control samples, would be to normalize the aggregation signal observed in patients with CMIs to the baseline levels of protein aggregation typically occurring in the brain.

For the individuals included in this project, no difference in PMI, age, sex, and social factors was connected to aggregating signals. However, future analyses should incorporate correlation methods like Pearson's to explore potential relationships. Moreover, additional data on substance or alcohol abuse, medication history, and other relevant health information would provide a clearer picture of their physiological

state before death. Samples collected for specific research can be at least analyzed for substances (alcohol, drugs, etc.) that were present in the individual at the time of death, so that can provide more information if medical history is not available. This would be especially significant for individuals used as a control since protein aggregation was observed in some control individuals, and it could be a consequence of other pathological mechanisms. Another essential aspect addressed by previous research[464] is the effect of ethnicity, which was impossible to include in this project since all analyzed individuals were Caucasians from Hungary. Briefly, previous research detected high levels of I/A TRIOBP-1 levels in patients with SZ and African American descent, compared to patients with SZ and Caucasian American descent. For MDD, the situation was reversed. This variation further supports the notion that protein aggregation is not purely pathological but involves genetic or environmental factors. Hence, in individuals with a genetic predisposition or chronic exposure to environmental stressors, the accumulation of protein aggregates could overwhelm the proteostasis network, disrupt neuronal cell function, and potentially lead to the development of CMIs.

When samples from IC of suicide victims, control individuals, and patients with either AD or MDD were analyzed for the first time, normalization between membranes was challenging. The starting material was the same for all samples (10% of tissue homogenized in a buffer), and the same amount of sample was loaded on all gels. In homogenates, the protein signal was normalized to the β-actin signal for each sample since the actin signal also varied for each individual. The signal after staining for β-actin was uneven and, in some cases, hard to detect. Hence, a part of the whole protein fraction (homogenate) should have been taken for standard protein quantification, with the buffer used for homogenization serving as a blank. A significant problem was normalization of ban intensity of I/A protein fractions across different membranes. The signal of I/A protein fraction from AD patients could have been normalized to phosphorylated tau, a known aggregating protein in the pathology of this disease. However, it also depends on the type of AD since phosphorylated tau is not involved in all cases. For CMIs, no equivalent reference protein has been identified, yet. However, in the follow up analysis with different brain regions, total protein content was determined, both in the homogenate (whole protein fraction) and the

aggregate (I/A protein fraction). This approach involves visualizing total proteins in gels using TCE, which binds to proteins and fluoresces under UV light. Compared to antibody-based immunodetection, total protein staining is less sensitive but also less prone to signal oversaturation. Additionally, because it relies on the entire protein load as a loading control, it is less influenced by variations in individual protein expression due to experimental conditions. In this project, applying this method showed no differences in total protein quantification in homogenates loaded on different gels. However, to ensure accuracy, this method should be validated with samples of known protein concentration. Additionally, total protein quantification in homogenates should be compared to β-actin signal quantification in the same samples. Protein quantification before transferring proteins onto the membrane can be useful, but only if the transfer is complete. In some cases, incomplete transfers can lead to inaccurate quantification. Ideally, proteins should be quantified after transfer using total protein stains like Ponceau or a stain-free approach, where the TCE signal is visualized under UV light. If total protein visualization on the membrane is not possible, the remaining protein signal on the gel after transfer should be subtracted from the pre-transfer signal to estimate the amount transferred. Another option is to quantify protein concentration using commercial kits. However, this would require using part of the already limited I/A material, reducing the number of specific proteins available for Western blot analysis. If a large number of proteins need to be analyzed, Western blot becomes a limiting method, and a more effective approach would be mass spectrometry analysis of proteins in the I/A material.

Finally, to determine if these proteins play a diagnostic or mechanistic role in CMIs, it would be interesting to analyze post-translational modifications. During purification of the I/A protein fraction, samples can be collected after resuspension in lysis and sarkosyl buffer from the supernatant after centrifugation. Mass spectrometry-based proteomics can identify novel post-translational modifications across patient-derived samples. In contrast, specific known post-translational modifications for each protein can be investigated with modification-specific antibodies in Western blot. If a particular post-translational modification site is identified as diagnosis-specific, including functional studies through CRISPR-mediated gene editing or site-directed mutagenesis would be interesting. A novel

method, single-cell proteomics, might provide more insights into cell-type-specific expression or modifications, which are often overlooked in tissue analyses. Another approach that should not be ignored is network-based analyses integrating transcriptomic and proteomic data, which could help identify functional pathways enriched in CMIs.

5.3 Aggregation of NPAS3, beyond the V304I mutation

NPAS3 is a transcription factor implicated in neurodevelopment and psychiatric disorders. Although the V304I mutation has been linked to SZ[453], its impact on protein aggregation is poorly understood. This section investigates whether NPAS3 aggregation occurs beyond this mutation and explores the factors influencing its dynamics.

Specifically, the localization, aggregation propensity, and critical regions of the transcription factor NPAS3 wt under normal and stress conditions were investigated. Both NPAS3 wt and V304I are primarily localized to the nucleus under normal conditions, consistent with their role as a transcription factor described in previous research. Interestingly, under oxidative stress induced by sodium arsenite, both protein variants exhibited a notable increase in a mixed phenotype (nuclear and cytoplasmic localization). The cytoplasmic localization was therefore interpreted as a possible early stage of aggregation, an approach previously described for other proteins such as TDP-43 and FUS.

The lack of significant differences between the wt and mutant variants in localization suggests that the V304I mutation does not drastically alter the protein's distribution in normal conditions. However, the increase in mixed localization under stress conditions highlights a potential vulnerability of NPAS3 to cellular stress, which may be relevant to the pathology of CMIs. Also, when the time factor was introduced, both NPAS3 wt and V304I exhibited an increase in insolubility. The V304I variant showed higher insolubility at 24 hrs; however, by 48 and 72 hrs, both variants demonstrated similar levels of insolubility, indicating that the mutation does not consistently affect NPAS3 aggregation under these experimental conditions. The transient increase in insolubility of V304I at 24 hours is interesting since it may indicate an early stage of aggregation, which disrupts NPAS3's interaction with other proteins and leads to CMIs pathology.

Analysis of NPAS3 fragments revealed that the PAS1 domain is critical for cytoplasmic localization, while the bHLH and C-terminal

regions predominantly localize to the nucleus. The introduction of the PAS1 domain increased cytoplasmic localization and, in some cases, led to aggregate formation, meaning PAS domains mediate both localization and aggregation. However, it is important to note that the perinuclear accumulation observed for the bHLH1-PAS1 region may not represent true protein aggregates. Such signals could instead reflect protein-filled vesicles or vacuoles, such as autophagosomes or lysosomes, accumulation of overexpressed protein in the endoplasmic reticulum or Golgi—both of which cluster near the nucleus—or even artifacts resulting from overexpression or fixation. Therefore, to draw more definitive conclusions, further validation is needed, such as testing the insolubility of the bHLH1-PAS1 region or performing co-localization studies with aggregate-associated markers like ubiquitin. The cytoplasmic localization observed for PAS1-containing fragments underlines its dual role in regulating protein interactions and cellular responses, which are influenced by stress and metabolic conditions. Despite the PAS1 domain's influence on cytoplasmic localization, co-expression experiments with full-length NPAS3 showed no disruption of nuclear localization. Hence, while individual regions may influence NPAS3 localization, the full-length protein retains a dominant nuclear localization pattern.

To conclude, the results of this thesis do not support the idea that mutation V304I can solely lead to NPAS3 aggregation. However, it may subtly alter NPAS3's interaction network or stability, for instance, by slightly altering binding affinities, folding kinetics, or subcellular localization, which could influence aggregation propensity under certain cellular conditions or in combination with other stressors. Given the strong association between NPAS3 mutations and CMIs such as SZ and BiPD, further studies are needed to determine whether this mutation affects transcriptional activity and targets expression. The observation that PAS1 domains influence aggregation propensity suggests that mutations or stress-induced modifications in these regions could predispose NPAS3 to aggregation, potentially disrupting its normal function in neurogenesis and metabolism.

Also, post-translational modification O-GlcNAc could affect the aggregation of NPAS3, so utilizing methods like Fluorescence Resonance Energy Transfer can provide more information about the effect of stress factors on O-GlcNAc dynamic while monitoring NPAS3 localization.

5.3.1 Limitations of cell-based assays with implications for future research

In this thesis, SH-SY5Y and HEK293 cell lines were used and there is a definitive need for replication results in other cell lines and more advanced cells cultures, like primary neuronal cultures, or induced pluripotent stem cell (iPSC)-derived neurons, which can better replicate complex environment of the brain, before moving on with other experiments.

Protein aggregation for this thesis involves punctate staining patterns examining overexpressed proteins in cells with immunofluorescence microscopy. However, it is unclear whether these structures are aggregates or represent an alternative localization, such as proteins sequestered within cellular vacuoles or organelles. To address this, the aggregation of proteins investigated in this thesis was additionally confirmed by a biochemical protocol, which purified I/A proteins and followed by Western blot in a similar manner as brain samples were analyzed.

Given the resolution limitations inherent in conventional fluorescent microscopy, there is also the possibility that punctate patterns arise from technical artifacts or the overlapping localization of proteins within the imaging plane. Several images shown here are overlapping, which should be avoided in future research. Future studies should also employ confocal microscopy, which offers higher resolution and can perform three-dimensional reconstruction of cellular structures. Confocal imaging would enable precise delineation of the spatial distribution and morphology of the puncta, thus enhancing the accuracy of aggregate identification. Additionally, on a confocal microscope, it is possible to perform a colocalization analysis using markers for other cellular compartments, such as lysosomes (e.g., LAMP1) or endoplasmic reticulum (e.g., calnexin), to investigate whether the puncta are associated with these organelles.

Another approach to distinguish between these possibilities is investigating aggresome formation, a cellular response to misfolded proteins. Aggresomes are dynamic structures characterized by the recruitment of aggregated proteins to a perinuclear region, encased by vimentin filaments, and often associated with markers such as vimentin, HDAC6, and γ-tubulin. The formation of aggresomes can be

further validated experimentally using the proteasome inhibitor MG-132, which enhances the accumulation of misfolded proteins and promotes aggresome assembly. This experimental setup can help confirm whether observed puncta align with the characteristics of aggresomes or represent other cellular phenomena.

To further elucidate the potential mechanisms underlying the formation of punctuated patterns, it will be essential to investigate whether the overexpression of these proteins influences key cellular pathways, including proteasomal degradation, autophagy, or apoptosis. These pathways represent the primary mechanisms for maintaining cellular homeostasis and responding to protein misfolding or aggregation. The ubiquitin-proteasome system is responsible for degrading the majority of short-lived, damaged, or misfolded proteins in eukaryotic cells. In contrast, autophagy primarily targets long-lived proteins, aggregated proteins, and even damaged organelles, particularly under cellular stress or nutrient deprivation conditions[307,308,328,329]. To discern the role of these pathways in our system, assays like proteasome activity assay and/or staining for autophagy markers and apoptosis indicators can be used. Specifically, proteasome activity assay involves using fluorescent substrates that report on proteasome function or monitoring the stabilization of proteasomal targets. MG-132 treatment can serve as a control to observe changes in proteasome inhibition. Co-staining proteins of interest and autophagy markers could provide more information about possible colocalize of our proteins with autophagic structures. Staining for apoptosis markers could show if overexpression of proteins of interest triggers apoptosis. Given that similar stimuli can trigger both autophagy and apoptosis, pharmacological tools that specifically modulate these pathways (e.g., autophagy or apoptosis inhibitors) could be used with imaging and biochemical assays to provide more information.

The system used for investigating protein co-aggregation in this thesis involved double transfection of plasmids containing human genes for CRMP1, DISC1, NPAS3, and TRIOBP-1, leading to their overexpression in cells. For future experiments employing this double transfection approach, evaluating the transfection rate for each plasmid individually and in combination will be essential. Additionally, testing multiple transfection reagents to determine which provides the

highest transfection efficiency for both plasmids would further optimize the system and improve the reliability of the results. Future experiments should also address endogenously expressed proteins. One approach could involve transfecting DISC1 or TRIOBP-1 into cells to induce aggregation through overexpression and then examine the interaction with endogenous CRMP1 using specific staining techniques. A more advanced strategy would be to utilize systems where the expression of DISC1 or TRIOBP-1 can be precisely regulated, such as Tet-On inducible systems. This would allow for controlled protein expression, enabling the study of CRMP1's role under more physiological conditions. Additionally, to confirm direct interactions between DISC1 and CRMP1 or other tested proteins, co-immunoprecipitation should be done. Meanwhile, technique such as Fluorescence Resonance Energy Transfer can show the dynamic of protein interactions. Moreover, the experiments were conducted under normal conditions. Future studies should explore the impact of stressors, such as oxidative stress, on co-aggregation dynamics, particularly for NPAS3. Also, it would be interesting to investigate the downstream effects of co-aggregation on cellular function, with assays like MTT for cell viability and apoptosis assays, live-cell imaging for cytoskeletal dynamics tracking, Seahorse XF Analyzer for mitochondrial function assays and RNA-Seq to detect transcriptional changes associated with cytoskeletal or mitochondrial stress.

5.4 Behavioral and molecular effects of *hflDISC1* expression in *Drosophila*

Studying the role of specific proteins implicated in CMIs often necessitates the development of animal models. These models serve as versatile tools for examining the impact of the human DISC1 protein on animal behavior within the intricate network of hormones and neurotransmitters that regulate brain function. This approach offers critical insights into mental illnesses' molecular mechanisms, bridging the gap between genetic abnormalities and observable behavioral phenotypes.

Thanks to their short lifespan and rapid reproduction, *Drosophila melanogaster* models address common challenges of traditional animal models, such as low statistical power, high costs, and lengthy breeding times[477–480]. Genetic flexibility and a well-mapped nervous system make *Drosophila* excellent tools for studying the molecular and cellular processes behind complex behaviors and diseases. While flies and

humans may seem vastly different initially, they share many fundamental evolutionary pathways and mechanisms. Their laboratory use is also unrestricted due to minimal ethical and safety concerns.

Moreover, *Drosophila* lacks an endogenous *DISC1* gene, making it an ideal model for studying the human DISC1 without the confounding effects of endogenous protein. In transgenic mouse and rat models, determining whether observed effects are primarily due to the introduced human *DISC1* or interactions with the endogenous *Disc1* is often challenging. In contrast, *Drosophila* eliminates this ambiguity while many interaction partner genes are conserved, allowing research of DISC1 aggregation mechanisms in a simplified yet biologically relevant system.

Furthermore, by using the GAL4-UAS system, which is a genetic tool widely used in *Drosophila* research, cell-specific expression of cloned genes[481,482], such as the *hflDISC1* can be achieved. Unlike mammalian models, the GAL4-UAS system in *Drosophila* enables the clean expression of human *DISC1* without interference. The GAL4 generally has minimal to no effects on the cells[482], however in this thesis it showed effect in some experiments (will be discussed in more details below).

For this thesis, transgenic *Drosophila* lines with inserted *hflDISC1* under the UAS promoter were created, with gene balanced on the 2nd (UAS-*hflDISC1*-2nd) or 3rd chromosome (UAS-*hflDISC1*-3rd). A cell-specific expression in neuronal cells driven by elav-GAL4 was used to study endophenotypes related to SZ. Both UAS-*hflDISC1* lines exhibited distinct behavioral and biochemical phenotypes, likely attributable to *DISC1* expression rather than insertion effects, as evidenced by consistent phenotypes and detectable DISC1 in both strains.

The expression of the *hflDISC1* was confirmed by Western blot with specific anti-DISC1 antibody in lysates collected from fly heads and bodies separately. *hflDISC1* expression was highest in elav-GAL4-UAS-*hflDISC1*-2nd for body samples and in UAS-*hflDISC1*-3rd line for head samples, surprisingly decreased in elav-GAL4 cross. The detected *hflDISC1* expression in UAS lines (UAS-*hflDISC1*-2nd and UAS-*hflDISC1*-3rd) is probably due to a typical „leaky gene" phenomenon, an unintended or basal expression of a gene under a UAS promoter, even in the absence of the GAL4 driver. This may induce phenotypes in UAS lines and/or create unintended effects that are difficult to explain about crosses.

The next set of analyses included measuring monoamine concentration in the heads, with and without activating localized expression induced by elav-GAL4 driver. Notably, dopamine and octopamine levels were highest in flies expressing *hflDISC1* on the 3rd chromosome (elav-GAL4-UAS-*hflDISC1*-3rd, purple bar with black crossing), suggesting that the chromosomal location of the gene can influence neurotransmitter synthesis regulation. This aligns with the known role of DISC1 as a scaffolding protein that integrates various cellular signaling pathways [373,374]. The elevated dopamine and octopamine levels may reflect disruptions in these pathways, potentially leading to altered neurotransmitter homeostasis. Interestingly, flies expressing *hflDISC1* on the 2nd chromosome (elav-GAL4-UAS-*hflDISC1*-2nd) also exhibited higher dopamine and octopamine levels than controls. However, the increase was less pronounced than in the 3rd chromosome model. This further emphasizes the influence of gene location and suggests potential variability in *DISC1*-mediated effects based on its integration site. Tyramine levels were elevated in all *DISC1*-expressing models (both 2nd and 3rd chromosomes), showing how DISC1 dysregulation can impact catecholaminergic pathways. The significant increase in tyramine in the elav-GAL4-UAS-*hflDISC1*-3rd model compared to controls may indicate a broader role for DISC1 in modulating biogenic amines beyond dopamine and octopamine. The results in this thesis show that glutamate levels were generally stable across groups but reduced in flies with UAS-hflDISC1 insertions (UAS-*hflDISC1*-2nd and UAS-*hflDISC1*-3rd) compared to CTRL. This suggests that gene insertion might suppress glutamatergic activity, though the mechanisms remain unclear. Acetylcholine levels showed slight variation but were lower in UAS-*hflDISC1*-3rd flies compared to CTRL and elav-GAL4-UAS-*hflDISC1*-2nd flies, pointing towards a subtle, gene location-dependent effect on cholinergic pathways, warranting additional investigation. While GABA levels did not differ significantly across groups, flies expressing DISC1 (elav-GAL4-UAS-*hflDISC1*-2nd and elav-GAL4-UAS-*hflDISC1*-3rd) tended to have higher GABA concentrations compared to UAS-only lines, aligning with the known complexity of DISC1's role in neuronal signaling[373,374] which suggests it may modulate inhibitory neurotransmission under certain conditions. Dopamine in *Drosophila* affects learning by modifying synapses between odor-responsive Kenyon cells and MBONs, reinforcing approach or avoidance behaviors. Specific dopaminergic neurons

encode positive or negative valence, targeting distinct mushroom body compartments. Beyond memory formation, dopamine also regulates memory expression based on factors like hunger or internal state, enabling the mushroom body to integrate sensory inputs with context for adaptive behavior. The DISC1 has also been implicated in modulating dopaminergic signaling[373,374], suggesting it may influence synaptic plasticity and behavior by regulating dopamine-dependent pathways. The observed changes in neurotransmitter levels and synaptic plasticity in *DISC1*-expressing flies suggest that similar dopamine and related pathway disruptions could underlie cognitive and behavioral deficits in SZ.

Both UAS-*hflDISC1*-2nd and UAS-*hflDISC1*-3rd lines exhibited consistent alterations in redox parameters: elevated H_2O_2 levels and reduced GSH concentrations, with no significant changes in GSSG compared to controls. These changes could imply that the overexpression of DISC1 impairs mitochondrial function, leading to increased oxidative stress as indicated by higher H_2O_2 levels and the oxidation of GSH to GSSG. Given the dual role of H_2O_2 in cellular signaling and as an indicator of oxidative stress, these disruptions may also impair redox-sensitive pathways, potentially influencing neurotransmitter systems involved in regulating behavior.

Social deficits are a core feature of SZ, profoundly impacting patients' quality of life and interpersonal relationships[55–57]. Given the involvement of *DISC1* in SZ, this study aimed to investigate its role in shaping social behaviors using *Drosophila* as a model. By applying SIN analysis, it is possible to examine the effect of *DISC1* expression on social organization and interaction dynamics, providing insights into the molecular basis of social impairments in mental illness. It is important to note GAL4 line showed different clustering coefficient than UAS or elav-UAS lines, hence it is possible driver elav-GAL4 can affect SIN and should be considered when discussing the results of lines with driver (elav-GAL4-UAS-*hflDISC1*-2nd or elav-GAL4-UAS-*hflDISC1*-3rd). The expression of *DISC1* did not significantly alter the global efficiency of the SIN, suggesting that the flies maintained tightly knit groups despite genetic modifications. This finding indicates that the locomotor phenotypes of the two transgenic lines were not severe enough to disrupt this parameter. Additionally, the experimental setup (12 flies and 25 minutes of recording) was adequate to ensure all flies had the

opportunity to interact. However, at the local level, UAS-*hflDISC1* lines exhibited a lower clustering coefficient than controls. This finding implies a disruption in the formation of tight social clusters, resulting in more diffuse or random interactions among individuals. The observed reduction in clustering may point to impairments in social organization, potentially linked to the underlying genetic modification. A lower closeness centrality in the UAS-*hflDISC1*-2nd line suggests reduced efficiency in accessing other individuals within the network, potentially reflecting delays in the flow of information or influence. Interestingly, the UAS-*hflDISC1*-3rd line did not exhibit changes in closeness centrality but showed increased betweenness centrality. This finding suggests that these flies facilitated more efficient communication between different parts of the network, possibly compensating for other deficits in social structure. The observed alterations in social network parameters, such as reduced clustering and changes in centrality measures, may reflect underlying disruptions in the neurotransmitter systems influenced by DISC1. Since in *Drosophila*, social interactions are predominantly mediated through olfactory communication[477,495], by influencing dopaminergic signaling, DISC1 may alter how sensory inputs, internal states, and memory processes are integrated. For example, reduced clustering could indicate that flies with altered *DISC1* expression struggle to maintain stable, cohesive interaction patterns. Such difficulties may arise if glutamatergic or cholinergic excitatory drive is diminished, making it harder for individuals to form tight-knit groups, or if GABAergic inhibition is imbalanced, leading to less predictable social engagement.

The results highlight the effect of *DISC1* expression on specific SIN parameters, emphasizing the importance of independently examining local and global measures. Applying SINs in *Drosophila* offers a novel and powerful approach to studying social behavior deficits, particularly in the context of SZ-related phenotypes. Traditional behavioral assays, while informative, often lack the resolution to capture the complexity and dynamics of social interactions in a networked context. SIN analysis, in contrast, provides quantitative insights into both global and local patterns of interaction, enabling the identification of specific disruptions in social organization and communication pathways. The findings from this study, such as the altered clustering coefficient and centrality measures in *DISC1*-expressing flies, underscore the relevance of SIN parameters in capturing subtle but critical aspects of social dysfunction. Nevertheless, SIN analysis has the potential to advance our understanding of social

deficits beyond what traditional assays can provide. For example, measures like clustering coefficient and centrality highlight group-level dynamics and offer insights into individual roles within the network, such as "hubs" that may mediate communication or "isolates" that reflect social withdrawal. These nuances mirror the heterogeneity of social impairments observed in SZ and can guide the development of more targeted therapeutic strategies.

In conclusion, no direct correlation was observed between DISC1 levels and the phenotypes' severity. As a complex scaffolding protein regulating various cellular pathways [374], disruptions in additional proteins likely contribute to the manifestation of these phenotypes.

5.4.1 Limitations of transgenic *DISC1 Drosophila* model with implications for future research

Creation of transgenic *DISC1* Drosophila model was done by Department of Genetics, University of Cambridge, however the gene insertion was never confirmed by sequencing of the UAS lines, to confirm the accuracy and integrity of the insertion. Moreover, the main issue described in this part of thesis is the "leaky gene" expression in the UAS-*hflDISC1* lines, where DISC1 was detected even without the GAL4 driver. Hence, it is difficult to distinguish the effects of targeted gene expression from background activity. In the future, lines should be analyzed with quantitative techniques like Real Time Quantitative PCR, or reporter assays to identify, and, if present, quantify leakage of the inserted gene. Future strategies to mitigate this effect would include using a stronger or more specific GAL4 driver or a Gal80, a GAL4 inhibitor, to suppress basal activity until explicitly activated.

Additionally, the chromosomal location of the *hflDISC1* insertion (2^{nd} vs. 3^{rd} chromosome) significantly affected dopamine, octopamine, and other neurotransmitter levels, adding an additional layer of variability. Since integration site effects were not systematically controlled, it remains unclear whether differences in neurotransmitter levels and behavioral phenotypes result from *DISC1* expression or from chromosomal positioning effects. Moreover, *hflDISC1* was expressed in all neuronal cells of Drosophila. Based on results of neurotransmitter analysis, future research should consider expressing *hflDISC1* in specific neurons, like mushroom body, to better understand the link between DISC1-mediated oxidative stress and behavioral phenotypes.

Another thing not included were stress conditions or account for endogenous protein levels, both of which could impact DISC1-related effects. Given that stress and internal states influence dopamine signaling and social behavior, the lack of these variables limits the generalizability of the findings.

Further, while social deficits were assessed, the specific mechanisms linking DISC1 expression to social network alterations were not fully explored. Since DISC1 aggregation has been identified in brain samples from patients with mental illness and in transgenic rat models, future research should focus on investigating DISC1 aggregation in these fly lines. Additionally, replicating these findings in rodent models will be essential to validate the results and enhance their translational relevance.

As for used methods, an example is the method for indirect measurement of H_2O_2 in *hflDISC1* models. Elevated H_2O_2 levels were particularly noted when fly lines containing the *hflDISC1* (UAS) were crossed with the elav driver line. This thesis employs DHE, which is not an ideal probe for directly detecting H_2O_2, as it primarily targets superoxide. To improve specificity, follow-up analyses with mass spectrometry, could help differentiate between superoxide-specific DHE oxidation and non-specific oxidation byproducts potentially influenced by H_2O_2.

5.5 Contribution to the field

This thesis made several critical advancements to the field of researching protein aggregation in CMIs.

The aggregation of NPAS3, DISC1, TRIOBP-1, and CRMP1 was shown in brains affected by CMIs and in control samples. However, the aggregation was not observed in all CMIs patients and it was observed in controls, suggesting that protein aggregation is a molecular subtype rather than a universal feature and potentially can be used as a biomarker for specific psychiatric subgroups.

Moreover, their aggregation patterns were region-specific, with DISC1 and CRMP1 accumulating in somatosensory areas (BA3,1,2) in SZ patients, linking them to sensory dysfunction, while TRIOBP-1 and CRMP1 aggregation in the LOG of suicide victims suggested a role in impulsivity and emotional regulation. Hence, it was shown that protein aggregation in CMIs probably follows defined pathways rather than occur randomly.

Additionally, protein co-aggregation, first hypotheses based on analysis of *post-mortem* brain samples, later investigated in more details in SH-SY5Y and HEK293 cells, was a key finding, particularly between DISC1 and CRMP1 Lv or DISC1 and TRIOBP-1, suggesting that protein-protein interactions can contribute to CMIs pathology. It was also strongly suggested that CRMP1 Sv may stabilize DISC1 aggregation, which in future could lead to development of potential therapeutic interventions aimed at modulating protein interactions rather than individual protein aggregation.

As for the influence of genetic mutations, NPAS3 V304I did not significantly alter aggregation under normal conditions, but under oxidative stress, both wild-type and V304I showed increased cytoplasmic localization. This finding reinforces the gene-environment interaction model of CMIs, where stress acts as a trigger for aggregation in genetically predisposed individuals.

Moreover, *Drosophila* was validated as a viable model for studying DISC1, with insights into neurotransmitter dysregulation and social deficits. As created *Drosophila* DISC1 model showed alterations in dopamine, octopamine, and social behaviors, it did indeed mimic key features of SZ. The chromosomal location of *hflDISC1* insertion had a strong effect on biochemical and behavioral phenotypes, which is an important experimental variable for transgenic *Drosophila* and other animal models in psychiatric research. However, studying DISC1 or other proteins implicated as aggregating in CMIs in flies might yield clues about the cellular dysfunctions contributing to SZ and other CMIs.

6 Conclusion

While protein aggregation is generally associated with NDs, it is also emerging as a potential mechanism in CMIs, as it can contribute to cellular dysfunction. In this thesis protein aggregation was explored by the combined analysis of *post-mortem* brain samples, cell models, and a transgenic *Drosophila* model. This approach offers a novel perspective for investigating the molecular mechanism of CMIs, paving the way for further studies into biomarkers and diagnostic tools and, hopefully, therapeutic target(s).

Key findings from this thesis include:

1. **Shared or overlapping pathological mechanisms in CMIs** as multiple proteins often aggregate within the same individuals. Moreover, it appears that protein aggregation in brains affected by CMIs is **region-specific**.
2. **Genetic predisposition alone is not necessarily to drive protein aggregation**. While the NPAS3 V304I mutation does not independently induce aggregation, environmental stressors such as oxidative stress can act as a trigger.
3. **Misfolded proteins may contribute to cellular stress and CMIs pathology**, as co-aggregation analysis indicates interactions between CRMP1 and either DISC1 or TRIOBP-1, forming a potential aggregation network.
4. **Disrupted DISC1 function affects neurotransmitter regulation and social behavior**, as demonstrated by altered biochemical and behavioral profiles in a transgenic *Drosophila* model.

These findings further support the investigation of protein aggregation as a mechanism for a subset of patients with CMIs diagnosis. Identifying proteins with the potential for aggregation and co-aggregation suggests a shared molecular mechanism, which could serve as novel diagnostic or therapeutic interventions.

Future research on protein aggregation in CMIs should build upon these findings by considering regional variability and the potential for parallel aggregation in patient tissues. Expanding analyses to a larger cohort and incorporating samples from living patients will be essential to capturing the full picture of aggregation. Additionally, the observed interactions between misfolded proteins suggest that future studies

should explore co-aggregation networks as potential drivers of cellular stress and pathology in psychiatric disorders. Developing transgenic *Drosophila* models for other aggregating proteins and assessing their effect could provide further mechanistic insights into how protein aggregation contributes to CMIs. These approaches will refine our understanding of proteinopathies in CMIs and pave the way for novel diagnostic and therapeutic strategies.

7 Appendix

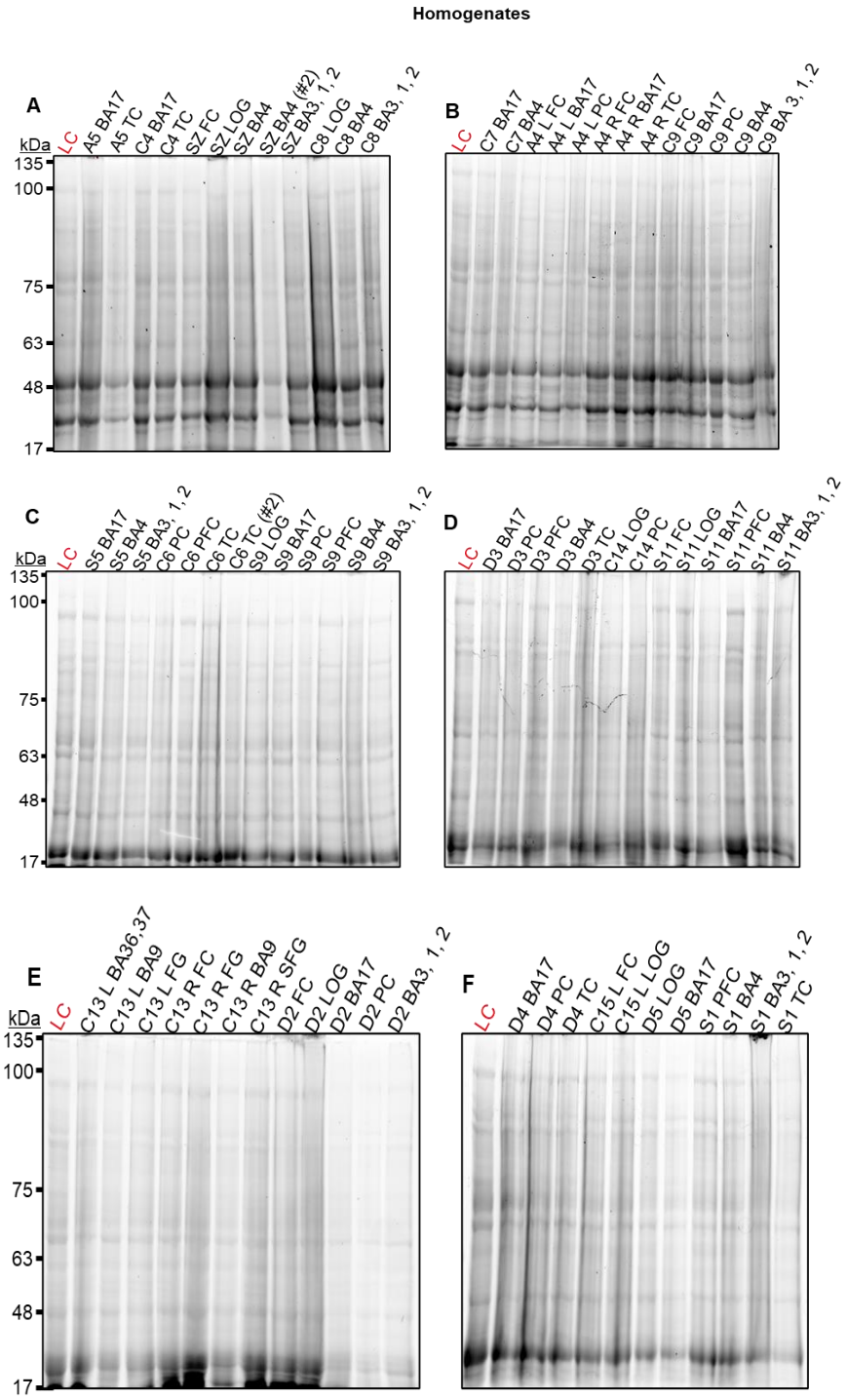

Figure 62: Comparable protein levels across all used samples. The samples were collected from suicide victims (S), control individuals (C), patients with either AD (A), SZ, or MDD (D) diagnosis. TCE was added to hand-casted acrylamide gels and proteins were visualized under UV light on ChemiDoc MP Imaging System, while the band signal intensity was quantified with Image Lab software (Bio-Rad). The gel was transferred on membrane later used to investigate proteins DISC1 and CRMP1.

Aggregates

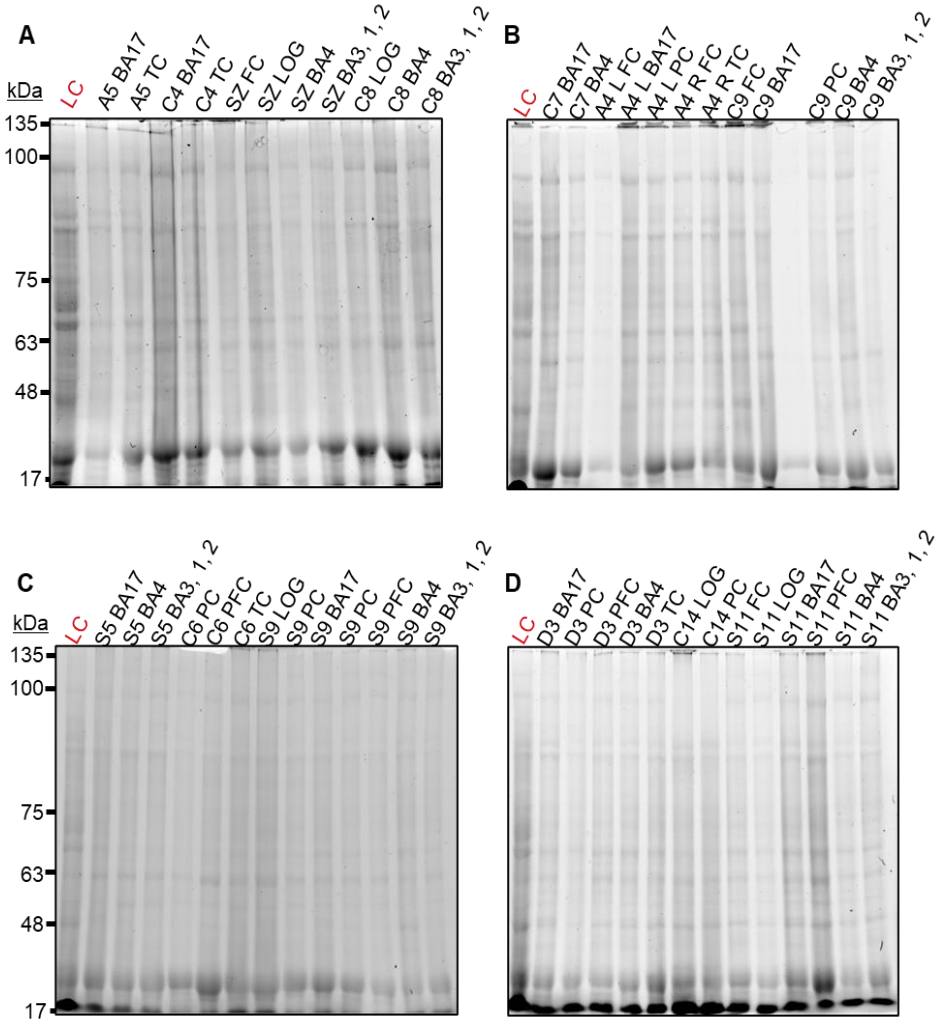
A
kDa
LC
A5 BA17
A5 TC
C4 BA17
C4 TC
SZ FC
SZ LOG
SZ BA4
SZ BA3, 1, 2
C8 LOG
C8 BA4
C8 BA3, 1, 2
135
100
75
63
48
17
B
LC
C7 BA17
C7 BA4
A4 L FC
A4 L BA17
A4 L PC
A4 R FC
A4 R TC
C9 FC
C9 BA17
C9 PC
C9 BA4
C9 BA3, 1, 2
C
kDa
LC
S5 BA17
S5 BA4
S5 BA3, 1, 2
C6 PC
C6 PFC
C6 TC
S9 LOG
S9 PC
S9 BA17
S9 PC
S9 PFC
S9 BA4
S9 BA3, 1, 2
135
100
75
63
48
17
D
LC
D3 BA17
D3 PC
D3 PFC
D3 BA4
D3 TC
C14 LOG
C14 PC
S11 FC
S11 LOG
S11 BA17
S11 PFC
S11 BA4
S11 BA3, 1, 2

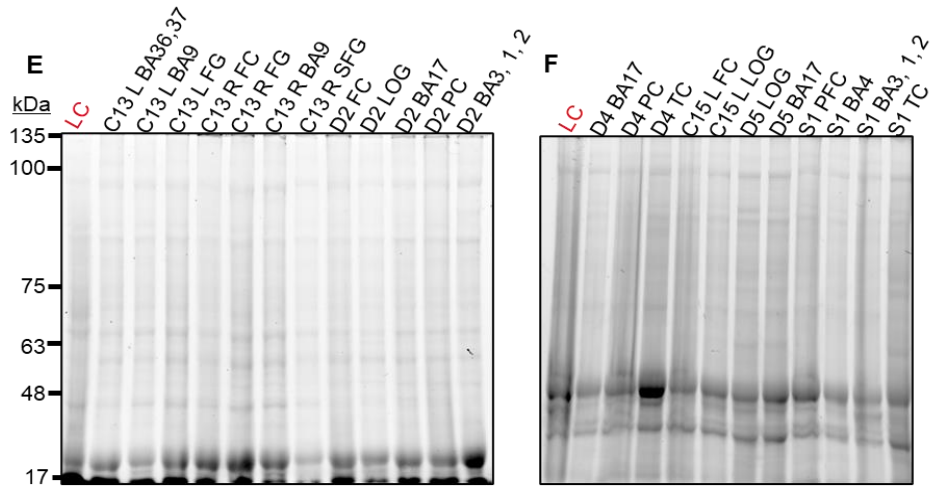

Figure 65: Total protein level does not vary across all aggregates. The samples were collected from suicide victims (S), control individuals (C), and patients with either AD (A), SZ, or MDD (D) diagnosis. TCE was added to hand-casted acrylamide gels and proteins were visualized under UV light on ChemiDoc MP Imaging System, while the band signal intensity was quantified with Image Lab software (Bio-Rad).

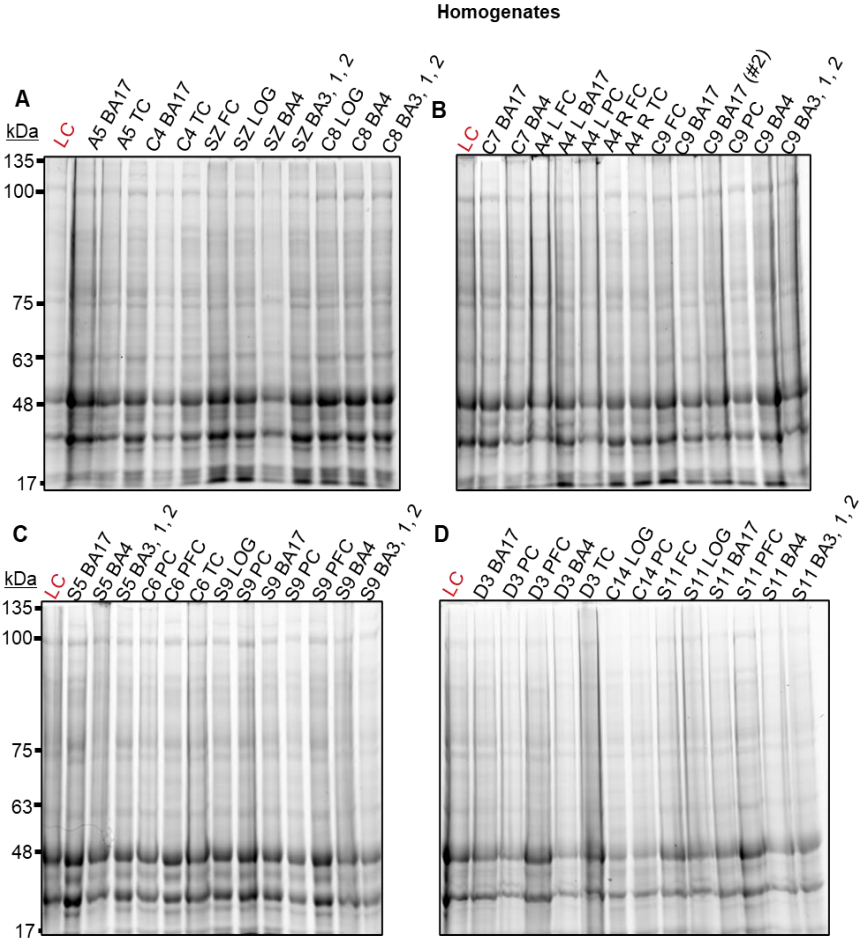

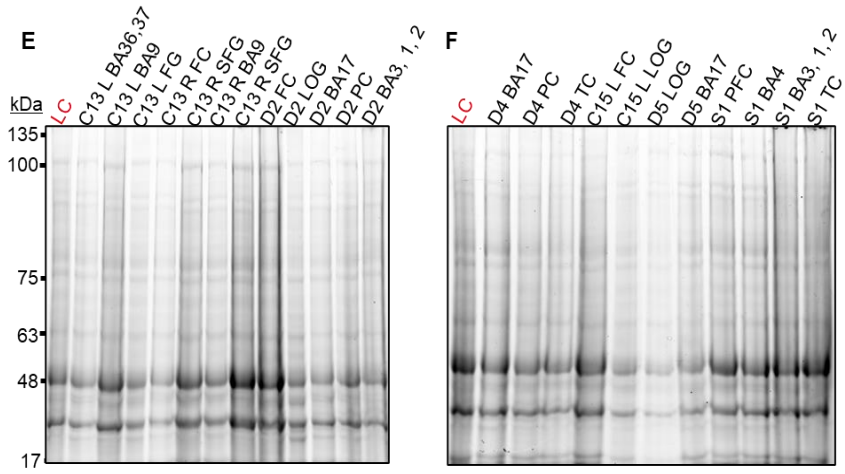

Figure 636: Comparable protein levels across all used samples. The samples were collected from suicide victims (S), control individuals (C), patients with either AD (A), SZ, or MDD (D) diagnosis. TCE was added to hand-casted acrylamide gels and proteins were visualized under UV light on ChemiDoc MP Imaging System, while the band signal intensity was quantified with Image Lab software (Bio-Rad).

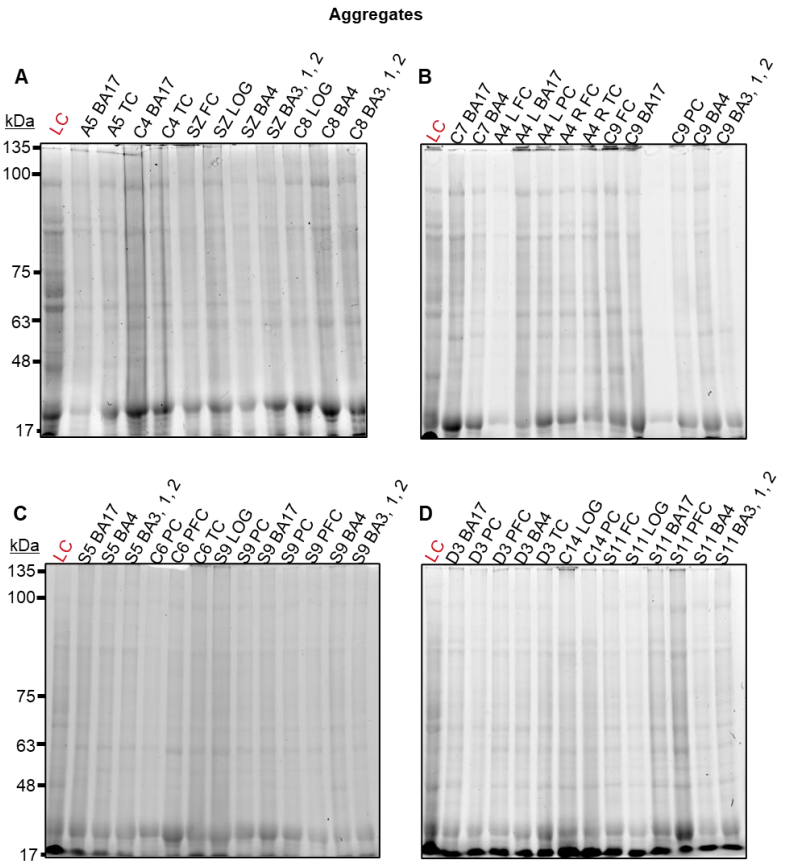

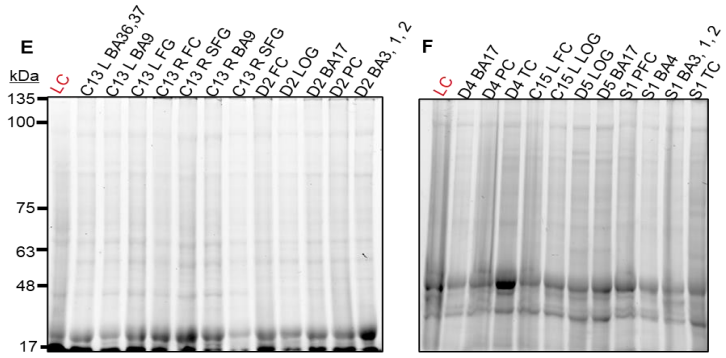

Figure 67: Comparable levels of total protein in I/A protein fraction, not correlating to diagnosis status. The samples were collected from suicide victims (S), control individuals (C), patients with either AD (A), SZ (SZ) or MDD (D) diagnosis. Analysis of samples included Western blot with anti-CRMP1 antibody, and appropriate secondary antibody for visualization. Samples were anonymized and randomly loaded on acrylamide gels. Visualization was performed with ECL kit and on a ChemiDoc MP Imaging System, while the band signal intensity was quantified with Image Lab software (Bio-Rad). Additionally, the samples were normalized to a loading control (LC) which contains pooled sample. Abbreviations: L: left hemisphere or R: right hemisphere, BAx: Brodmann area number x, FC: frontal cortex, LOG: lateral orbitofrontal gyrus, PC: parietal cortex, SFG: superior frontal gyrus, TC: temporal cortex, PiFC: piriform cortex.

8 Literature

1. *Diagnostic and Statistical Manual of Mental Disorders: DSM-5*. (American psychiatric association, Washington, 2013).
2. *International Classification of Diseases, Eleventh Revision (ICD-11)*. (World Health Organization (WHO), 2019).
3. GBD Results. *Institute for Health Metrics and Evaluation* https://vizhub.healthdata.org/gbd-results.
4. Kieling, C. *et al.* Worldwide Prevalence and Disability From Mental Disorders Across Childhood and Adolescence. *JAMA Psychiatry* **81**, 347–356 (2024).
5. Uher, R. Gene–Environment Interactions in Severe Mental Illness. *Front. Psychiatry* **5**, 48 (2014).
6. Gottesman, I. I., Laursen, T. M., Bertelsen, A. & Mortensen, P. B. Severe Mental Disorders in Offspring With 2 Psychiatrically Ill Parents. *Arch. Gen. Psychiatry* **67**, 252 (2010).
7. Shih, R. A., Belmonte, P. L. & Zandi, P. P. A review of the evidence from family, twin and adoption studies for a genetic contribution to adult psychiatric disorders. *Int. Rev. Psychiatry* **16**, 260–283 (2004).
8. Cardno, A. G. *et al.* Heritability Estimates for Psychotic Disorders: The Maudsley Twin Psychosis Series. *Arch. Gen. Psychiatry* **56**, 162–168 (1999).

9. McGuffin, P., Tandon, K. & Corsico, A. Linkage and association studies of schizophrenia. *Curr. Psychiatry Rep.* **5**, 121–127 (2003).
10. Lichtenstein, P. *et al.* Common genetic influences for schizophrenia and bipolar disorder: A population-based study of 2 million nuclear families. *Lancet* **373**, 10.1016/S0140-6736(09)60072–6 (2009).
11. Hilker, R. *et al.* Is an Early Age at Illness Onset in Schizophrenia Associated With Increased Genetic Susceptibility? Analysis of Data From the Nationwide Danish Twin Register. *EBioMedicine* **18**, 320–326 (2017).
12. Hilker, R. *et al.* Heritability of Schizophrenia and Schizophrenia Spectrum Based on the Nationwide Danish Twin Register. *Biol. Psychiatry* **83**, 492–498 (2018).
13. Song, J. *et al.* Polygenic Risk Scores and Twin Concordance for Schizophrenia and Bipolar Disorder. *JAMA Psychiatry* **81**, 1246–1252 (2024).
14. McGuffin, P., Katz, R., Watkins, S. & Rutherford, J. A Hospital-Based Twin Register of the Heritability of DSM-IV Unipolar Depression. *Arch. Gen. Psychiatry* **53**, 129–136 (1996).
15. Kendler, K. S., Gatz, M., Gardner, C. O. & Pedersen, N. L. A Swedish National Twin Study of Lifetime Major Depression. *Am. J. Psychiatry* **163**, 109–114 (2006).
16. Mather, L., Blom, V., Bergström, G. & Svedberg, P. An Underlying Common Factor, Influenced by Genetics and Unique Environment,

Explains the Covariation Between Major Depressive Disorder, Generalized Anxiety Disorder, and Burnout: A Swedish Twin Study. *Twin Res. Hum. Genet.* **19**, 619–627 (2016).

17. Sullivan, P. F., Neale, M. C. & Kendler, K. S. Genetic Epidemiology of Major Depression: Review and Meta-Analysis. *Am. J. Psychiatry* **157**, 1552–1562 (2000).
18. Polderman, T. J. C. *et al.* Meta-analysis of the heritability of human traits based on fifty years of twin studies. *Nat. Genet.* **47**, 702–709 (2015).
19. Green, E. K. *et al.* Genome-wide significant locus for Research Diagnostic Criteria Schizoaffective Disorder Bipolar type. *Am. J. Med. Genet. Part B Neuropsychiatr. Genet. Off. Publ. Int. Soc. Psychiatr. Genet.* **174**, 767–771 (2017).
20. Green, E. K. *et al.* The bipolar disorder risk allele at CACNA1C also confers risk of recurrent major depression and of schizophrenia. *Mol. Psychiatry* **15**, 1016–1022 (2010).
21. Schizophrenia Working Group of the Psychiatric Genomics Consortium. Biological insights from 108 schizophrenia-associated genetic loci. *Nature* **511**, 421–427 (2014).
22. Trubetskoy, V. *et al.* Mapping genomic loci implicates genes and synaptic biology in schizophrenia. *Nature* **604**, 502–508 (2022).

23. Palmer, D. S. *et al.* Exome sequencing in bipolar disorder identifies AKAP11 as a risk gene shared with schizophrenia. *Nat. Genet.* **54**, 541–547 (2022).
24. Dvir, Y., Denietolis, B. & Frazier, J. A. Childhood Trauma and Psychosis. *Child Adolesc. Psychiatr. Clin. N. Am.* **22**, 629–641 (2013).
25. Carbone, E. A. *et al.* Adverse childhood experiences and clinical severity in bipolar disorder and schizophrenia: A transdiagnostic two-step cluster analysis. *J. Affect. Disord.* **259**, 104–111 (2019).
26. Arango, C. *et al.* Risk and protective factors for mental disorders beyond genetics: an evidence-based atlas. *World Psychiatry* **20**, 417–436 (2021).
27. Solmi, M. *et al.* Incidence, prevalence, and global burden of schizophrenia - data, with critical appraisal, from the Global Burden of Disease (GBD) 2019. *Mol. Psychiatry* **28**, 5319–5327 (2023).
28. Arias, I. *et al.* Infectious agents associated with schizophrenia: A meta-analysis. *Schizophr. Res.* **136**, 128–136 (2012).
29. Khandaker, G. M., Zimbron, J., Dalman, C., Lewis, G. & Jones, P. B. Childhood infection and adult schizophrenia: A meta-analysis of population-based studies. *Schizophr. Res.* **139**, 161–168 (2012).
30. Khandaker, G. M., Zimbron, J., Lewis, G. & Jones, P. B. Prenatal maternal infection, neurodevelopment and adult schizophrenia: a

systematic review of population-based studies. *Psychol. Med.* **43**, 239–257 (2013).

31. Stilo, S. A. & Murray, R. M. Non-Genetic Factors in Schizophrenia. *Curr. Psychiatry Rep.* **21**, 100 (2019).
32. Ursini, G. *et al.* BDNF rs6265 methylation and genotype interact on risk for schizophrenia. *Epigenetics* **11**, 11–23 (2016).
33. Palacios-García, I. *et al.* Prenatal Stress Down-Regulates Reelin Expression by Methylation of Its Promoter and Induces Adult Behavioral Impairments in Rats. *PLoS ONE* **10**, e0117680 (2015).
34. Kundakovic, M. *et al.* DNA methylation of BDNF as a biomarker of early-life adversity. *Proc. Natl. Acad. Sci. U. S. A.* **112**, 6807–6813 (2015).
35. Smigielski, L., Jagannath, V., Rössler, W., Walitza, S. & Grünblatt, E. Epigenetic mechanisms in schizophrenia and other psychotic disorders: a systematic review of empirical human findings. *Mol. Psychiatry* **25**, 1718–1748 (2020).
36. Abate, B. B. *et al.* Adverse Childhood Experiences Are Associated with Mental Health Problems Later in Life: An Umbrella Review of Systematic Review and Meta-Analysis. *Neuropsychobiology* **84**, 48–64 (2025).
37. Malaspina, D. *et al.* Acute maternal stress in pregnancy and schizophrenia in offspring: A cohort prospective study. *BMC Psychiatry* **8**, 71 (2008).

38. Misiak, B. *et al.* Adverse childhood experiences and low socioeconomic status with respect to allostatic load in adulthood: A systematic review. *Psychoneuroendocrinology* **136**, 105602 (2022).
39. Patel, R. S. *et al.* Marijuana use and acute myocardial infarction: A systematic review of published cases in the literature. *Trends Cardiovasc. Med.* **30**, 298–307 (2020).
40. Hasan, A. *et al.* Cannabis use and psychosis: a review of reviews. *Eur. Arch. Psychiatry Clin. Neurosci.* **270**, 403–412 (2020).
41. van Os, J., Krabbendam, L., Myin-Germeys, I. & Delespaul, P. The schizophrenia envirome. *Curr. Opin. Psychiatry* **18**, 141–145 (2005).
42. Liechti, S., Capodilupo, G., Opler, D. J., Opler, M. & Yang, L. H. A Developmental History of the Positive and Negative Syndrome Scale (PANSS). *Innov. Clin. Neurosci.* **14**, 12–17 (2017).
43. Gronholm, P. C., Ali, S., Brohan, E. & Thornicroft, G. Discrimination reported by people with schizophrenia: cross-national variations in relation to the Human Development Index. *Epidemiol. Psychiatr. Sci.* **32**, e66 (2023).
44. Moran, E. K., Culbreth, A. J. & Barch, D. M. Anhedonia in Schizophrenia. *Curr. Top. Behav. Neurosci.* **58**, 129–145 (2022).

45. Temmingh, H. & Stein, D. J. Anxiety in Patients with Schizophrenia: Epidemiology and Management. *CNS Drugs* **29**, 819–832 (2015).
46. Ceskova, E. Pharmacological strategies for the management of comorbid depression and schizophrenia. *Expert Opin. Pharmacother.* **21**, 459–465 (2020).
47. Wang, Y. *et al.* Exploring the interplay between core and mood symptoms in schizophrenia: A network analysis. *Schizophr. Res.* **269**, 28–35 (2024).
48. Tao, Y., Zhao, R., Yang, B., Han, J. & Li, Y. Dissecting the shared genetic landscape of anxiety, depression, and schizophrenia. *J. Transl. Med.* **22**, 373 (2024).
49. Hany, M., Rehman, B., Rizvi, A. & Chapman, J. Schizophrenia. in *StatPearls* (StatPearls Publishing, Treasure Island (FL), 2025).
50. Moritz, S. *et al.* What Kurt Schneider Really Said and What the DSM Has Made of it in Its Different Editions: A Plea to Redefine Hallucinations in Schizophrenia. *Schizophr. Bull.* **50**, 22–31 (2024).
51. American Psychiatric Association & American Psychiatric Association. Task Force on DSM-IV. *Diagnostic and Statistical Manual of Mental Disorders : DSM-IV*. (Washington, DC : American Psychiatric Association, 1999).

52. Recio-Barbero, M., Losada-León, N., Mentxaka, O., Cabezas-Garduño, J. & Segarra, R. Neuropsychological and Functional Assessment of Cognitive Impairments in Schizophrenia. in *Schizophrenia: Methods and Protocols* (eds. Urigüen, L. & Díez-Alarcia, R.) 127–139 (Springer US, New York, NY, 2023). doi:10.1007/978-1-0716-3307-6_10.
53. Li, X. *et al.* The global burden of schizophrenia and the impact of urbanization during 1990–2019: An analysis of the global burden of disease study 2019. *Environ. Res.* **232**, 116305 (2023).
54. Carmona, V. R., Gómez-Benito, J. & Rojo-Rodes, J. E. Employment Support Needs of People with Schizophrenia: A Scoping Study. *J. Occup. Rehabil.* **29**, 1–10 (2019).
55. Eglit, G. M. L., Palmer, B. W., Martin, A. S., Tu, X. & Jeste, D. V. Loneliness in schizophrenia: Construct clarification, measurement, and clinical relevance. *PLOS ONE* **13**, e0194021 (2018).
56. Green, M. F. *et al.* Social Disconnection in Schizophrenia and the General Community. *Schizophr. Bull.* **44**, 242–249 (2018).
57. El-Monshed, A. & Amr, M. Association between perceived social support and recovery among patients with schizophrenia. *Int. J. Afr. Nurs. Sci.* **13**, 100236 (2020).
58. Widiyawati, W., Yusuf, A., Devy, S. R. & Widayanti, D. M. Family support and adaptation mechanisms of adults outpatients with schizophrenia. *J. Public Health Res.* **9**, 1848 (2020).

59. Du, H. M. *et al.* [Impact of social support for schizophrenia patients on their quality of life and family life satisfaction]. *Zhonghua Liu Xing Bing Xue Za Zhi Zhonghua Liuxingbingxue Zazhi* **44**, 786–790 (2023).
60. Isometsä, E. Suicidal Behaviour in Mood Disorders—Who, When, and Why? *Can. J. Psychiatry* **59**, 120–130 (2014).
61. Lee, H. *et al.* Comorbid health outcomes in patients with schizophrenia: an umbrella review of systematic reviews and meta-analyses. *Mol. Psychiatry* **30**, 1127–1137 (2025).
62. Lv, Y. *et al.* Schizophrenia in the genetic era: a review from development history, clinical features and genomic research approaches to insights of susceptibility genes. *Metab. Brain Dis.* **39**, 147–171 (2023).
63. Munafò, M. R., Attwood, A. S. & Flint, J. Neuregulin 1 genotype and schizophrenia. *Schizophr. Bull.* **34**, 9–12 (2008).
64. Bousman, C. A. *et al.* Neuregulin-1 (NRG1) polymorphisms linked with psychosis transition are associated with enlarged lateral ventricles and white matter disruption in schizophrenia. *Psychol. Med.* **48**, 801–809 (2018).
65. Yang, J. *et al.* Pharmacogenetic associations of NRG1 polymorphisms with neurocognitive performance and clinical symptom response to risperidone in the untreated schizophrenia. *Schizophr. Res.* **231**, 67–69 (2021).

66. Wang, X. *et al.* Neuregulin-1 immunoreactivity in peripheral plasma is associated with rs6982890 polymorphism-mediated psychotic symptoms in schizophrenia. *Brain Res. Bull.* **217**, 111075 (2024).
67. Ghashghaei, H. T. *et al.* The role of neuregulin-ErbB4 interactions on the proliferation and organization of cells in the subventricular zone. *Proc. Natl. Acad. Sci. U. S. A.* **103**, 1930–1935 (2006).
68. Nicodemus, K. K. *et al.* Biological validation of increased schizophrenia risk with NRG1, ERBB4, and AKT1 epistasis via functional neuroimaging in healthy controls. *Arch. Gen. Psychiatry* **67**, 991–1001 (2010).
69. Silberberg, G., Darvasi, A., Pinkas-Kramarski, R. & Navon, R. The involvement of ErbB4 with schizophrenia: association and expression studies. *Am. J. Med. Genet. Part B Neuropsychiatr. Genet. Off. Publ. Int. Soc. Psychiatr. Genet.* **141B**, 142–148 (2006).
70. Millar, J. K. *et al.* Disruption of two novel genes by a translocation co-segregating with schizophrenia. *Hum. Mol. Genet.* **9**, 1415–1423 (2000).
71. Blackwood, D. H. R. & Muir, W. J. Clinical phenotypes associated with DISC1, a candidate gene for schizophrenia. *Neurotox. Res.* **6**, 35–41 (2004).

72. Ma, J.-H. *et al.* Association on DISC1 SNPs with schizophrenia risk: A meta-analysis. *Psychiatry Res.* **270**, 306–309 (2018).
73. Wang, H.-Y. *et al.* Gene polymorphisms of DISC1 is associated with schizophrenia: Evidence from a meta-analysis. *Prog. Neuropsychopharmacol. Biol. Psychiatry* **81**, 64–73 (2018).
74. He, B.-S. *et al.* Association of the DISC1 and NRG1 genetic polymorphisms with schizophrenia in a Chinese population. *Gene* **590**, 293–297 (2016).
75. Millar, J. K. *et al.* Disrupted in schizophrenia 1 and phosphodiesterase 4B: towards an understanding of psychiatric illness. *J. Physiol.* **584**, 401–405 (2007).
76. Wang, H., Xu, J., Lazarovici, P. & Zheng, W. Dysbindin-1 Involvement in the Etiology of Schizophrenia. *Int. J. Mol. Sci.* **18**, 2044 (2017).
77. Howes, O. D., McCutcheon, R., Owen, M. J. & Murray, R. M. The Role of Genes, Stress, and Dopamine in the Development of Schizophrenia. *Biol. Psychiatry* **81**, 9–20 (2017).
78. Luykx, J. J., Broersen, J. L. & de Leeuw, M. The DRD2 rs1076560 polymorphism and schizophrenia-related intermediate phenotypes: A systematic review and meta-analysis. *Neurosci. Biobehav. Rev.* **74**, 214–224 (2017).
79. Taheri, N., Pirboveiri, R., Sayyah, M., Bijanzadeh, M. & Ghandil, P. Association of DRD2, DRD4 and COMT genes variants and their

gene-gene interactions with antipsychotic treatment response in patients with schizophrenia. *BMC Psychiatry* **23**, 781 (2023).

80. Kogure, M. *et al.* Interacting Roles of COMT and GAD1 Genes in Patients with Treatment-Resistant Schizophrenia: a Genetic Association Study of Schizophrenia Patients and Healthy Controls. *J. Mol. Neurosci.* **71**, 2575–2582 (2021).
81. Ma, J. *et al.* Association Between the COMT Val158Met Polymorphism and Antipsychotic Efficacy in Schizophrenia: An Updated Meta-Analysis. *Curr. Neuropharmacol.* **19**, 1780–1790 (2021).
82. Knable, M. B. *et al.* Molecular abnormalities of the hippocampus in severe psychiatric illness: postmortem findings from the Stanley Neuropathology Consortium. *Mol. Psychiatry* **9**, 609–620, 544 (2004).
83. Zhou, J. *et al.* Association between CpG island DNA methylation in the promoter region of RELN and positive and negative types of schizophrenia. *J. Int. Med. Res.* **50**, 3000605221100345 (2022).
84. Xu, H. *et al.* BDNF affects the mediating effect of negative symptoms on the relationship between age of onset and cognition in patients with chronic schizophrenia. *Psychoneuroendocrinology* **125**, 105121 (2021).
85. Schweiger, J. I. *et al.* Effects of BDNF Val66Met genotype and schizophrenia familial risk on a neural functional network for

cognitive control in humans. *Neuropsychopharmacol. Off. Publ. Am. Coll. Neuropsychopharmacol.* **44**, 590–597 (2019).

86. Bolat Kaya, Ö. *et al.* Association of BDNF Gene Val66Met Polymorphism with Suicide Attempts, Focused Attention and Response Inhibition in Patients with Schizophrenia. *Noro Psikiyatri Arsivi* **59**, 91–97 (2022).
87. Szeszko, P. R. *et al.* Brain-derived neurotrophic factor val66met polymorphism and volume of the hippocampal formation. *Mol. Psychiatry* **10**, 631–636 (2005).
88. Rodriguez, V. *et al.* Environmental Risk Factors in Bipolar Disorder and Psychotic Depression: A Systematic Review and Meta-Analysis of Prospective Studies. *Schizophr. Bull.* **47**, 959–974 (2021).
89. Krabbendam, L. Schizophrenia and Urbanicity: A Major Environmental Influence--Conditional on Genetic Risk. *Schizophr. Bull.* **31**, 795–799 (2005).
90. Mosolov, S. N. & Yaltonskaya, P. A. Primary and Secondary Negative Symptoms in Schizophrenia. *Front. Psychiatry* **12**, (2022).
91. Muñoz-Negro, J. E. *et al.* Negative symptoms across psychotic spectrum disorders. *Eur. J. Psychiatry* **31**, 37–41 (2017).
92. Meltzer, H. Y. & Sumiyoshi, T. Does stimulation of 5-HT(1A) receptors improve cognition in schizophrenia? *Behav. Brain Res.* **195**, 98–102 (2008).

93. Sa, K. 5-HT1A and 5-HT2A Signaling, Desensitization, and Downregulation: Serotonergic Dysfunction and Abnormal Receptor Density in Schizophrenia and the Prodrome. *Cureus* **13**, (2021).
94. Cheah, S.-Y., Lawford, B. R., Young, R. M., Morris, C. P. & Voisey, J. mRNA Expression and DNA Methylation Analysis of Serotonin Receptor 2A (HTR2A) in the Human Schizophrenic Brain. *Genes* **8**, 14 (2017).
95. Fomsgaard, L. *et al.* Differences in 5-HT2A and mGlu2 Receptor Expression Levels and Repressive Epigenetic Modifications at the 5-HT2A Promoter Region in the Roman Low- (RLA-I) and High- (RHA-I) Avoidance Rat Strains. *Mol. Neurobiol.* **55**, 1998–2012 (2018).
96. Hiser, J. & Koenigs, M. The Multifaceted Role of the Ventromedial Prefrontal Cortex in Emotion, Decision Making, Social Cognition, and Psychopathology. *Biol. Psychiatry* **83**, 638–647 (2018).
97. Ruzicka, W. B., Subburaju, S. & Benes, F. M. Circuit- and Diagnosis-Specific DNA Methylation Changes at γ-Aminobutyric Acid-Related Genes in Postmortem Human Hippocampus in Schizophrenia and Bipolar Disorder. *JAMA Psychiatry* **72**, 541–551 (2015).
98. Curley, A. A. *et al.* Role of glutamic acid decarboxylase 67 in regulating cortical parvalbumin and GABA membrane transporter

1 expression: implications for schizophrenia. *Neurobiol. Dis.* **50**, 179–186 (2013).

99. Gallinat, J., McMahon, K., Kühn, S., Schubert, F. & Schaefer, M. Cross-sectional Study of Glutamate in the Anterior Cingulate and Hippocampus in Schizophrenia. *Schizophr. Bull.* **42**, 425–433 (2016).

100. Orhan, F. *et al.* CSF GABA is reduced in first-episode psychosis and associates to symptom severity. *Mol. Psychiatry* **23**, 1244–1250 (2018).

101. Skilbeck, K. J., O'Reilly, J. N., Johnston, G. A. R. & Hinton, T. The effects of antipsychotic drugs on GABAA receptor binding depend on period of drug treatment and binding site examined. *Schizophr. Res.* **90**, 76–80 (2007).

102. Cassella, S. N. *et al.* Maternal immune activation alters glutamic acid decarboxylase-67 expression in the brains of adult rat offspring. *Schizophr. Res.* **171**, 195–199 (2016).

103. Egerton, A., Modinos, G., Ferrera, D. & McGuire, P. Neuroimaging studies of GABA in schizophrenia: a systematic review with meta-analysis. *Transl. Psychiatry* **7**, e1147 (2017).

104. Taylor, S. F. & Tso, I. F. GABA abnormalities in schizophrenia: a methodological review of in vivo studies. *Schizophr. Res.* **167**, 84–90 (2015).

105. O'Connor, W. T. & O'Shea, S. D. Clozapine and GABA transmission in schizophrenia disease models: establishing principles to guide treatments. *Pharmacol. Ther.* **150**, 47–80 (2015).

106. Singh, S. P. & Singh, V. Meta-analysis of the efficacy of adjunctive NMDA receptor modulators in chronic schizophrenia. *CNS Drugs* **25**, 859–885 (2011).

107. Plitman, E. *et al.* Glutamate-mediated excitotoxicity in schizophrenia: A review. *Eur. Neuropsychopharmacol. J. Eur. Coll. Neuropsychopharmacol.* **24**, 1591–1605 (2014).

108. Griffiths, K. *et al.* Treatment resistance NMDA receptor pathway polygenic score is associated with brain glutamate in schizophrenia. *Schizophr. Res.* **260**, 152–159 (2023).

109. Kruse, A. O. & Bustillo, J. R. Glutamatergic dysfunction in Schizophrenia. *Transl. Psychiatry* **12**, 1–13 (2022).

110. Yohn, S. E., Harvey, P. D., Brannan, S. K. & Horan, W. P. The potential of muscarinic M1 and M4 receptor activators for the treatment of cognitive impairment associated with schizophrenia. *Front. Psychiatry* **15**, 1421554 (2024).

111. Paul, S. M., Yohn, S. E., Brannan, S. K., Neugebauer, N. M. & Breier, A. Muscarinic Receptor Activators as Novel Treatments for Schizophrenia. *Biol. Psychiatry* **96**, 627–637 (2024).

112. Dietz, A. G., Goldman, S. A. & Nedergaard, M. Glial cells in schizophrenia: a unified hypothesis. *Lancet Psychiatry* **7**, 272–281 (2020).

113. Fillman, S. G. *et al.* Elevated peripheral cytokines characterize a subgroup of people with schizophrenia displaying poor verbal fluency and reduced Broca's area volume. *Mol. Psychiatry* **21**, 1090–1098 (2016).

114. Fond, G., Lançon, C., Korchia, T., Auquier, P. & Boyer, L. The Role of Inflammation in the Treatment of Schizophrenia. *Front. Psychiatry* **11**, (2020).

115. Murray, A. J., Rogers, J. C., Katshu, M. Z. U. H., Liddle, P. F. & Upthegrove, R. Oxidative Stress and the Pathophysiology and Symptom Profile of Schizophrenia Spectrum Disorders. *Front. Psychiatry* **12**, 703452 (2021).

116. Madireddy, S. & Madireddy, S. Regulation of Reactive Oxygen Species-Mediated Damage in the Pathogenesis of Schizophrenia. *Brain Sci.* **10**, 742 (2020).

117. Carletti, B., Banaj, N., Piras, F. & Bossù, P. Schizophrenia and Glutathione: A Challenging Story. *J. Pers. Med.* **13**, 1526 (2023).

118. Kumar, J. *et al.* Glutathione and glutamate in schizophrenia: a 7T MRS study. *Mol. Psychiatry* **25**, 873–882 (2020).

119. Oya, K., Kishi, T. & Iwata, N. Efficacy and tolerability of minocycline augmentation therapy in schizophrenia: a systematic

review and meta-analysis of randomized controlled trials. *Hum. Psychopharmacol.* **29**, 483–491 (2014).

120. Romanovsky, E., Choudhary, A., Peles, D., Abu-Akel, A. & Stern, S. Uncovering convergence and divergence between autism and schizophrenia using genomic tools and patients' neurons. *Mol. Psychiatry* **30**, 1019–1028 (2025).

121. Cross-Disorder Group of the Psychiatric Genomics Consortium *et al.* Genetic relationship between five psychiatric disorders estimated from genome-wide SNPs. *Nat. Genet.* **45**, 984–994 (2013).

122. Schmitt, A., Falkai, P. & Papiol, S. Neurodevelopmental disturbances in schizophrenia: evidence from genetic and environmental factors. *J. Neural Transm. Vienna Austria 1996* **130**, 195–205 (2023).

123. Paul, T. *et al.* Neurostructural changes in schizophrenia and treatment-resistance: a narrative review. *Psychoradiology* **4**, kkae015 (2024).

124. Winship, I. R. *et al.* An Overview of Animal Models Related to Schizophrenia. *Can. J. Psychiatry Rev. Can. Psychiatr.* **64**, 5–17 (2019).

125. Jones, C. A., Watson, D. J. G. & Fone, K. C. F. Animal models of schizophrenia. *Br. J. Pharmacol.* **164**, 1162–1194 (2011).

126. Białoń, M. & Wąsik, A. Advantages and Limitations of Animal Schizophrenia Models. *Int. J. Mol. Sci.* **23**, 5968 (2022).

127. Tseng, K. Y., Chambers, R. A. & Lipska, B. K. The neonatal ventral hippocampal lesion as a heuristic neurodevelopmental model of schizophrenia. *Behav. Brain Res.* **204**, 295–305 (2009).

128. Brady, A. M. The Neonatal Ventral Hippocampal Lesion (NVHL) Rodent Model of Schizophrenia. *Curr. Protoc. Neurosci.* **77**, 9.55.1-9.55.17 (2016).

129. Powell, S. B. & Swerdlow, N. R. The Relevance of Animal Models of Social Isolation and Social Motivation for Understanding Schizophrenia: Review and Future Directions. *Schizophr. Bull.* **49**, 1112–1126 (2023).

130. Moore, H., Jentsch, J. D., Ghajarnia, M., Geyer, M. A. & Grace, A. A. A neurobehavioral systems analysis of adult rats exposed to methylazoxymethanol acetate on E17: implications for the neuropathology of schizophrenia. *Biol. Psychiatry* **60**, 253–264 (2006).

131. Tendilla-Beltrán, H., Sanchez-Islas, N. D. C., Marina-Ramos, M., Leza, J. C. & Flores, G. The prefrontal cortex as a target for atypical antipsychotics in schizophrenia, lessons of neurodevelopmental animal models. *Prog. Neurobiol.* **199**, 101967 (2021).

132. Feigenson, K. A., Kusnecov, A. W. & Silverstein, S. M. Inflammation and the two-hit hypothesis of schizophrenia. *Neurosci. Biobehav. Rev.* **38**, 72–93 (2014).

133. Labouesse, M. A., Dong, E., Grayson, D. R., Guidotti, A. & Meyer, U. Maternal immune activation induces GAD1 and GAD2 promoter remodeling in the offspring prefrontal cortex. *Epigenetics* **10**, 1143–1155 (2015).

134. Ozawa, K. *et al.* Immune Activation During Pregnancy in Mice Leads to Dopaminergic Hyperfunction and Cognitive Impairment in the Offspring: A Neurodevelopmental Animal Model of Schizophrenia. *Biol. Psychiatry* **59**, 546–554 (2006).

135. Featherstone, R. E., Kapur, S. & Fletcher, P. J. The amphetamine-induced sensitized state as a model of schizophrenia. *Prog. Neuropsychopharmacol. Biol. Psychiatry* **31**, 1556–1571 (2007).

136. Kalinichev, M. *et al.* Comparison between intraperitoneal and subcutaneous phencyclidine administration in Sprague-Dawley rats: a locomotor activity and gene induction study. *Prog. Neuropsychopharmacol. Biol. Psychiatry* **32**, 414–422 (2008).

137. Li, D., Pan, Q., Xiao, Y. & Hu, K. Advances in the study of phencyclidine-induced schizophrenia-like animal models and the underlying neural mechanisms. *Schizophr. Heidelb. Ger.* **10**, 65 (2024).

138. Tse, M. T., Piantadosi, P. T. & Floresco, S. B. Prefrontal cortical gamma-aminobutyric acid transmission and cognitive function: drawing links to schizophrenia from preclinical research. *Biol. Psychiatry* **77**, 929–939 (2015).

139. Yamazaki, M., Honda, S., Tamaki, K., Irie, M. & Mihara, T. Effects of (+)-bicuculline, a GABAa receptor antagonist, on auditory steady state response in free-moving rats. *PloS One* **15**, e0236363 (2020).

140. Jaaro-Peled, H. Gene models of schizophrenia: DISC1 mouse models. *Prog. Brain Res.* **179**, 75–86 (2009).

141. Lipina, T. V. *et al.* Enhanced dopamine function in DISC1-L100P mutant mice: implications for schizophrenia. *Genes Brain Behav.* **9**, 777–789 (2010).

142. Lipina, T. V. & Roder, J. C. Disrupted-In-Schizophrenia-1 (DISC1) interactome and mental disorders: impact of mouse models. *Neurosci. Biobehav. Rev.* **45**, 271–294 (2014).

143. Schneider, S., Götz, K., Birchmeier, C., Schwegler, H. & Roskoden, T. Neuregulin-1 mutant mice indicate motor and sensory deficits, indeed few references for schizophrenia endophenotype model. *Behav. Brain Res.* **322**, 177–185 (2017).

144. Lossi, L., Castagna, C., Granato, A. & Merighi, A. The Reeler Mouse: A Translational Model of Human Neurological Conditions,

or Simply a Good Tool for Better Understanding Neurodevelopment? *J. Clin. Med.* **8**, 2088 (2019).

145. Hill, R. A. Sex differences in animal models of schizophrenia shed light on the underlying pathophysiology. *Neurosci. Biobehav. Rev.* **67**, 41–56 (2016).

146. Moslem, M., Olive, J. & Falk, A. Stem cell models of schizophrenia, what have we learned and what is the potential? *Schizophr. Res.* **210**, 3–12 (2019).

147. Nakazawa, T. Modeling schizophrenia with iPS cell technology and disease mouse models. *Neurosci. Res.* **175**, 46–52 (2022).

148. Santarriaga, S., Gerlovin, K., Layadi, Y. & Karmacharya, R. Human stem cell-based models to study synaptic dysfunction and cognition in schizophrenia: A narrative review. *Schizophr. Res.* **273**, 78–97 (2024).

149. Leucht, S., Priller, J. & Davis, J. M. Antipsychotic Drugs: A Concise Review of History, Classification, Indications, Mechanism, Efficacy, Side Effects, Dosing, and Clinical Application. *Am. J. Psychiatry* **181**, 865–878 (2024).

150. Peng, A. *et al.* New Therapeutic Targets and Drugs for Schizophrenia Beyond Dopamine D2 Receptor Antagonists. *Neuropsychiatr. Dis. Treat.* **20**, 607–620 (2024).

151. Howes, O. D. *et al.* Treatment-Resistant Schizophrenia: Treatment Response and Resistance in Psychosis (TRRIP) Working

Group Consensus Guidelines on Diagnosis and Terminology. *Am. J. Psychiatry* **174**, 216–229 (2017).

152. Correll, C. U. & Howes, O. D. Treatment-Resistant Schizophrenia: Definition, Predictors, and Therapy Options. *J. Clin. Psychiatry* **82**, MY20096AH1C (2021).

153. Nucifora, F. C., Woznica, E., Lee, B. J., Cascella, N. & Sawa, A. Treatment resistant schizophrenia: Clinical, biological, and therapeutic perspectives. *Neurobiol. Dis.* **131**, 104257 (2019).

154. Ying, J., Chew, Q. H., McIntyre, R. S. & Sim, K. Treatment-Resistant Schizophrenia, Clozapine Resistance, Genetic Associations, and Implications for Precision Psychiatry: A Scoping Review. *Genes* **14**, 689 (2023).

155. Nucifora, F. C., Mihaljevic, M., Lee, B. J. & Sawa, A. Clozapine as a Model for Antipsychotic Development. *Neurother. J. Am. Soc. Exp. Neurother.* **14**, 750–761 (2017).

156. Dell'Osso, L. *et al.* Rethinking Clozapine: Lights and Shadows of a Revolutionary Drug. *Brain Sci.* **14**, 103 (2024).

157. Lundberg, M. *et al.* Clozapine protects adult neural stem cells from ketamine-induced cell death in correlation with decreased apoptosis and autophagy. *Biosci. Rep.* **40**, BSR20193156 (2020).

158. Critchlow, H. M., Maycox, P. R., Skepper, J. N. & Krylova, O. Clozapine and haloperidol differentially regulate dendritic spine

formation and synaptogenesis in rat hippocampal neurons. *Mol. Cell. Neurosci.* **32**, 356–365 (2006).

159. Gurrera, R. J. *et al.* Recognition and management of clozapine adverse effects: A systematic review and qualitative synthesis. *Acta Psychiatr. Scand.* **145**, 423–441 (2022).

160. Mijovic, A. & MacCabe, J. H. Clozapine-induced agranulocytosis. *Ann. Hematol.* **99**, 2477–2482 (2020).

161. Nielsen, J. *et al.* Worldwide Differences in Regulations of Clozapine Use. *CNS Drugs* **30**, 149–161 (2016).

162. Wagner, E. *et al.* Efficacy and safety of clozapine in psychotic disorders-a systematic quantitative meta-review. *Transl. Psychiatry* **11**, 487 (2021).

163. Forte, A. *et al.* Effects on suicidal risk: Comparison of clozapine to other newer medicines indicated to treat schizophrenia or bipolar disorder. *J. Psychopharmacol. Oxf. Engl.* **35**, 1074–1080 (2021).

164. Delgado, A. *et al.* Clozapine in bipolar disorder: A systematic review and meta-analysis. *J. Psychiatr. Res.* **125**, 21–27 (2020).

165. Wang, D. *et al.* Long-Acting Injectable Second-Generation Antipsychotics vs Placebo and Their Oral Formulations in Acute Schizophrenia: A Systematic Review and Meta-Analysis of Randomized-Controlled-Trials. *Schizophr. Bull.* **50**, 132–144 (2024).

166. Hálfdánarson, Ó. *et al.* International trends in antipsychotic use: A study in 16 countries, 2005–2014. *Eur. Neuropsychopharmacol.* **27**, 1064–1076 (2017).

167. Most Common Prescribed Antipsychotic Medications. https://www.definitivehc.com/resources/healthcare-insights/top-antipsychotic-prescriptions.

168. Vukićević, T., Draganić, P., Škribulja, M., Puljak, L. & Došenović, S. Consumption of psychotropic drugs in Croatia before and during the COVID-19 pandemic: a 10-year longitudinal study (2012-2021). *Soc. Psychiatry Psychiatr. Epidemiol.* **59**, 799–811 (2024).

169. Szkultecka-Dębek, M. *et al.* Treatment patterns of schizophrenia based on the data from seven Central and Eastern European Countries. *Psychiatr. Danub.* **28**, 234–242 (2016).

170. Boyer, L. *et al.* Real-world effectiveness of long-acting injectable antipsychotic treatments in a nationwide cohort of 12,373 patients with schizophrenia-spectrum disorders. *Mol. Psychiatry* **28**, 3709–3716 (2023).

171. Bugarski-Kirola, D. *et al.* Efficacy and safety of adjunctive bitopertin versus placebo in patients with suboptimally controlled symptoms of schizophrenia treated with antipsychotics: results from three phase 3, randomised, double-blind, parallel-group, placebo-controlled, multicentre studies in the SearchLyte clinical trial programme. *Lancet Psychiatry* **3**, 1115–1128 (2016).

172. Weiden, P. J. *et al.* Antipsychotic Efficacy of KarXT (Xanomeline-Trospium): Post Hoc Analysis of Positive and Negative Syndrome Scale Categorical Response Rates, Time Course of Response, and Symptom Domains of Response in a Phase 2 Study. *J. Clin. Psychiatry* **83**, 21m14316 (2022).

173. Achtyes, E. D. *et al.* Ulotaront: review of preliminary evidence for the efficacy and safety of a TAAR1 agonist in schizophrenia. *Eur. Arch. Psychiatry Clin. Neurosci.* **273**, 1543–1556 (2023).

174. Correll, C. U. What Are We Looking for in New Antipsychotics? *J. Clin. Psychiatry* **72**, (2011).

175. Adam, O. *et al.* Efficacy of Transcranial Direct Current Stimulation to Improve Insight in Patients With Schizophrenia: A Systematic Review and Meta-analysis of Randomized Controlled Trials. *Schizophr. Bull.* **48**, 1284–1294 (2022).

176. Misiak, B. *et al.* Gut microbiota alterations in stable outpatients with schizophrenia: findings from a case-control study. *Acta Neuropsychiatr.* **35**, 147–155 (2023).

177. Scott, M. R. & McClung, C. A. Bipolar Disorder. *Curr. Opin. Neurobiol.* **83**, 102801 (2023).

178. Hara, T., Owada, Y. & Takata, A. Genetics of bipolar disorder: insights into its complex architecture and biology from common and rare variants. *J. Hum. Genet.* **68**, 183–191 (2023).

179. Mullins, N. *et al.* Genome-wide association study of more than 40,000 bipolar disorder cases provides new insights into the underlying biology. *Nat. Genet.* **53**, 817–829 (2021).

180. Palmer, D. S. *et al.* Exome sequencing in bipolar disorder identifies AKAP11 as a risk gene shared with schizophrenia. *Nat. Genet.* **54**, 541–547 (2022).

181. Ou, X. *et al.* CACNA1C rs1006737 genotype and bipolar disorder: Focus on intermediate phenotypes and cardiovascular comorbidity. *Neurosci. Biobehav. Rev.* **55**, 198–210 (2015).

182. Smedler, E., Abé, C., Pålsson, E., Ingvar, M. & Landén, M. CACNA1C polymorphism and brain cortical structure in bipolar disorder. *J. Psychiatry Neurosci. JPN* **45**, 182–187 (2019).

183. Yoldi-Negrete, M. *et al.* Looking for factors affecting functioning in euthymic patients with bipolar I disorder: the importance of cognitive complaints and BDNF's Val66Met polymorphism. *J. Affect. Disord.* **302**, 131–138 (2022).

184. Liberona, A. *et al.* Brain-Derived Neurotrophic Factor (BDNF) as a Predictor of Treatment Response in Schizophrenia and Bipolar Disorder: A Systematic Review. *Int. J. Mol. Sci.* **25**, 11204 (2024).

185. De Felice, G. *et al.* Can Brain-Derived Neurotrophic Factor Be Considered a Biomarker for Bipolar Disorder? An Analysis of the Current Evidence. *Brain Sci.* **13**, 1221 (2023).

186. Hammerschlag, A. R., de Leeuw, C. A., Middeldorp, C. M. & Polderman, T. J. C. Synaptic and brain-expressed gene sets relate to the shared genetic risk across five psychiatric disorders. *Psychol. Med.* **50**, 1695–1705 (2020).

187. Robinson, N. *et al.* Impact of Early-Life Factors on Risk for Schizophrenia and Bipolar Disorder. *Schizophr. Bull.* **49**, 768–777 (2023).

188. Chauhan, V. S. *et al.* Childhood trauma and bipolar affective disorder: Is there a linkage? *Ind. Psychiatry J.* **32**, S9–S14 (2023).

189. Rowland, T. A. & Marwaha, S. Epidemiology and risk factors for bipolar disorder. *Ther. Adv. Psychopharmacol.* **8**, 251–269 (2018).

190. Fond, G. *et al.* Association Between Mental Health Disorders and Mortality Among Patients With COVID-19 in 7 Countries: A Systematic Review and Meta-analysis. *JAMA Psychiatry* **78**, 1208–1217 (2021).

191. Jones, G. H., Vecera, C. M., Pinjari, O. F. & Machado-Vieira, R. Inflammatory signaling mechanisms in bipolar disorder. *J. Biomed. Sci.* **28**, 45 (2021).

192. Kathuria, A., Lopez-Lengowski, K., McPhie, D., Cohen, B. M. & Karmacharya, R. Disease-specific differences in gene expression, mitochondrial function and mitochondria-endoplasmic reticulum interactions in iPSC-derived cerebral organoids and cortical

neurons in schizophrenia and bipolar disorder. *Discov. Ment. Health* **3**, 8 (2023).

193. McCarthy, M. J. *et al.* Neurobiological and behavioral mechanisms of circadian rhythm disruption in bipolar disorder: A critical multi-disciplinary literature review and agenda for future research from the ISBD task force on chronobiology. *Bipolar Disord.* **24**, 232–263 (2022).

194. Scott, M. R. & McClung, C. A. Circadian Rhythms in Mood Disorders. *Adv. Exp. Med. Biol.* **1344**, 153–168 (2021).

195. Preuss, U. W., Schaefer, M., Born, C. & Grunze, H. Bipolar Disorder and Comorbid Use of Illicit Substances. *Med. Kaunas Lith.* **57**, 1256 (2021).

196. Schiweck, C. *et al.* Comorbidity of ADHD and adult bipolar disorder: A systematic review and meta-analysis. *Neurosci. Biobehav. Rev.* **124**, 100–123 (2021).

197. He, H. *et al.* Trends in the incidence and DALYs of bipolar disorder at global, regional, and national levels: Results from the global burden of Disease Study 2017. *J. Psychiatr. Res.* **125**, 96–105 (2020).

198. Bipolar disorder prevalence. *Our World in Data* https://ourworldindata.org/grapher/bipolar-disorder-prevalence.

199. Pini, S. *et al.* Prevalence and burden of bipolar disorders in European countries. *Eur. Neuropsychopharmacol. J. Eur. Coll. Neuropsychopharmacol.* **15**, 425–434 (2005).

200. Bipolar disorder prevalence. *Our World in Data* https://ourworldindata.org/grapher/bipolar-disorder-prevalence?time=latest.

201. Liang, L., Chen, J., Xiao, L., Wang, Q. & Wang, G. Mitochondrial modulators in the treatment of bipolar depression: a systematic review and meta-analysis. *Transl. Psychiatry* **12**, 4 (2022).

202. Tarzian, M., Ndrio, M., Kaja, S., Beason, E. & Fakoya, A. O. Cariprazine for Treating Schizophrenia, Mania, Bipolar Depression, and Unipolar Depression: A Review of Its Efficacy. *Cureus* **15**, e39309 (2023).

203. Elsayed, O. H., Ercis, M., Pahwa, M. & Singh, B. Treatment-Resistant Bipolar Depression: Therapeutic Trends, Challenges and Future Directions. *Neuropsychiatr. Dis. Treat.* **18**, 2927–2943 (2022).

204. Docherty, J. P. & Colbert, B. M. The evolution of psychotherapy: from Freud to prescription digital therapeutics. *Front. Psychiatry* **15**, 1477543 (2024).

205. Herzog, L. E. *et al.* Mouse mutants in schizophrenia risk genes GRIN2A and AKAP11 show EEG abnormalities in common with schizophrenia patients. *Transl. Psychiatry* **13**, 92 (2023).

206. Smedler, E. *et al.* Disrupted Cacna1c gene expression perturbs spontaneous Ca2+ activity causing abnormal brain development and increased anxiety. *Proc. Natl. Acad. Sci. U. S. A.* **119**, e2108768119 (2022).

207. Raju, S. *et al.* BDNF Val66Met genotype and adolescent glucocorticoid treatment induce sex-specific disruptions to fear extinction and amygdala GABAergic interneuron expression in mice. *Horm. Behav.* **144**, 105231 (2022).

208. Roybal, K. *et al.* Mania-like behavior induced by disruption of CLOCK. *Proc. Natl. Acad. Sci. U. S. A.* **104**, 6406–6411 (2007).

209. Schnell, A. *et al.* Mice lacking circadian clock components display different mood-related behaviors and do not respond uniformly to chronic lithium treatment. *Chronobiol. Int.* **32**, 1075–1089 (2015).

210. von Schantz, M., Leocadio-Miguel, M. A., McCarthy, M. J., Papiol, S. & Landgraf, D. Genomic perspectives on the circadian clock hypothesis of psychiatric disorders. *Adv. Genet.* **107**, 153–191 (2021).

211. Mishra, H. K. *et al.* Contributions of circadian clock genes to cell survival in fibroblast models of lithium-responsive bipolar disorder. *Eur. Neuropsychopharmacol. J. Eur. Coll. Neuropsychopharmacol.* **74**, 1–14 (2023).

212. Mishra, H. K. *et al.* Circadian rhythms in bipolar disorder patient-derived neurons predict lithium response: preliminary studies. *Mol. Psychiatry* **26**, 3383–3394 (2021).

213. Phalnikar, K. *et al.* Altered neuroepithelial morphogenesis and migration defects in iPSC-derived cerebral organoids and 2D neural stem cells in familial bipolar disorder. *Oxf. Open Neurosci.* **3**, kvae007 (2024).

214. Kim, Y. *et al.* Mitochondria, Metabolism, and Redox Mechanisms in Psychiatric Disorders. *Antioxid. Redox Signal.* **31**, 275–317 (2019).

215. Hewitt, T. *et al.* Bipolar disorder-iPSC derived neural progenitor cells exhibit dysregulation of store-operated Ca2+ entry and accelerated differentiation. *Mol. Psychiatry* **28**, 5237–5250 (2023).

216. Osete, J. R. *et al.* Lithium increases mitochondrial respiration in iPSC-derived neural precursor cells from lithium responders. *Mol. Psychiatry* **26**, 6789–6805 (2021).

217. Niemsiri, V. *et al.* Focal adhesion is associated with lithium response in bipolar disorder: evidence from a network-based multi-omics analysis. *Mol. Psychiatry* **29**, 6–19 (2024).

218. Osete, J. R. *et al.* Transcriptional and functional effects of lithium in bipolar disorder iPSC-derived cortical spheroids. *Mol. Psychiatry* **28**, 3033–3043 (2023).

219. Kathuria, A. *et al.* Transcriptomic Landscape and Functional Characterization of Induced Pluripotent Stem Cell-Derived Cerebral Organoids in Schizophrenia. *JAMA Psychiatry* **77**, 745–754 (2020).

220. Sawada, T. *et al.* Developmental excitation-inhibition imbalance underlying psychoses revealed by single-cell analyses of discordant twins-derived cerebral organoids. *Mol. Psychiatry* **25**, 2695–2711 (2020).

221. Seemüller, F. *et al.* A factor analytic comparison of three commonly used depression scales (HAMD, MADRS, BDI) in a large sample of depressed inpatients. *BMC Psychiatry* **23**, 548 (2023).

222. Cui, L. *et al.* Major depressive disorder: hypothesis, mechanism, prevention and treatment. *Signal Transduct. Target. Ther.* **9**, 30 (2024).

223. Bhatt, S., Devadoss, T., Manjula, S. N. & Rajangam, J. 5-HT3 Receptor Antagonism: A Potential Therapeutic Approach for the Treatment of Depression and other Disorders. *Curr. Neuropharmacol.* **19**, 1545–1559 (2021).

224. Bamalan, O. A., Moore, M. J. & Al Khalili, Y. Physiology, Serotonin. in *StatPearls* (StatPearls Publishing, Treasure Island (FL), 2025).

225. Bansal, Y., Codeluppi, S. A. & Banasr, M. Astroglial Dysfunctions in Mood Disorders and Rodent Stress Models: Consequences on

Behavior and Potential as Treatment Target. *Int. J. Mol. Sci.* **25**, 6357 (2024).

226. Lei, L., Wang, Y.-F., Chen, C.-Y., Wang, Y.-T. & Zhang, Y. Novel insight into astrocyte-mediated gliotransmission modulates the synaptic plasticity in major depressive disorder. *Life Sci.* **355**, 122988 (2024).

227. Arosio, B., Guerini, F. R., Voshaar, R. C. O. & Aprahamian, I. Blood Brain-Derived Neurotrophic Factor (BDNF) and Major Depression: Do We Have a Translational Perspective? *Front. Behav. Neurosci.* **15**, (2021).

228. Cavaleri, D. *et al.* The role of BDNF in major depressive disorder, related clinical features, and antidepressant treatment: Insight from meta-analyses. *Neurosci. Biobehav. Rev.* **149**, 105159 (2023).

229. Zhao, M. *et al.* BDNF Val66Met polymorphism, life stress and depression: A meta-analysis of gene-environment interaction. *J. Affect. Disord.* **227**, 226–235 (2018).

230. Kennis, M. *et al.* Prospective biomarkers of major depressive disorder: a systematic review and meta-analysis. *Mol. Psychiatry* **25**, 321–338 (2020).

231. Miola, A., Tondo, L., Pinna, M., Contu, M. & Baldessarini, R. J. Comparison of bipolar disorder type II and major depressive disorder. *J. Affect. Disord.* **323**, 204–212 (2023).

232. Arnaud, A. M. *et al.* Impact of Major Depressive Disorder on Comorbidities: A Systematic Literature Review. *J. Clin. Psychiatry* **83**, (2022).

233. Major depressive disorder - Level 4 cause | Institute for Health Metrics and Evaluation. https://www.healthdata.org/research-analysis/diseases-injuries-risks/factsheets/2021-major-depressive-disorder-level-4-disease.

234. The Prevalence and National Burden of Treatment-Resistant Depression and Major Depressive Disorder in the United States - PubMed. https://pubmed.ncbi.nlm.nih.gov/33989464/.

235. Fischer, F. *et al.* Prevalence estimates of major depressive disorder in 27 European countries from the European Health Interview Survey: accounting for imperfect diagnostic accuracy of the PHQ-8. *BMJ Ment. Health* **26**, e300675 (2023).

236. Arias-de la Torre, J. *et al.* Prevalence and variability of current depressive disorder in 27 European countries: a population-based study. *Lancet Public Health* **6**, e729–e738 (2021).

237. Medić, A. Epidemiology of depression in Croatia.

238. Depressive disorders prevalence. *Our World in Data* https://ourworldindata.org/grapher/depressive-disorders-prevalence-ihme.

239. Machado-Santos, A. R. *et al.* Beyond New Neurons in the Adult Hippocampus: Imipramine Acts as a Pro-Astrogliogenic Factor and

Rescues Cognitive Impairments Induced by Stress Exposure. *Cells* **11**, 390 (2022).

240. Van den Eynde, V. *et al.* The prescriber's guide to classic MAO inhibitors (phenelzine, tranylcypromine, isocarboxazid) for treatment-resistant depression. *CNS Spectr.* **28**, 427–440 (2023).

241. Dell'Osso, B., Palazzo, M. C., Oldani, L. & Altamura, A. C. The Noradrenergic Action in Antidepressant Treatments: Pharmacological and Clinical Aspects. *CNS Neurosci. Ther.* **17**, 723–732 (2010).

242. Terevnikov, V. & Joffe, G. Mirtazapine in schizophrenia - an undeservedly overlooked option? *Int. Clin. Psychopharmacol.* **37**, 131–142 (2022).

243. Krystal, J. H., Kavalali, E. T. & Monteggia, L. M. Ketamine and rapid antidepressant action: new treatments and novel synaptic signaling mechanisms. *Neuropsychopharmacol. Off. Publ. Am. Coll. Neuropsychopharmacol.* **49**, 41–50 (2024).

244. Daly, E. J. *et al.* Efficacy of Esketamine Nasal Spray Plus Oral Antidepressant Treatment for Relapse Prevention in Patients With Treatment-Resistant Depression: A Randomized Clinical Trial. *JAMA Psychiatry* **76**, 893–903 (2019).

245. Zanos, P. & Gould, T. D. Mechanisms of ketamine action as an antidepressant. *Mol. Psychiatry* **23**, 801–811 (2018).

246. Boldrini, M. *et al.* Hippocampal angiogenesis and progenitor cell proliferation are increased with antidepressant use in major depression. *Biol. Psychiatry* **72**, 562–571 (2012).

247. Boldrini, M. *et al.* Benzodiazepines and the potential trophic effect of antidepressants on dentate gyrus cells in mood disorders. *Int. J. Neuropsychopharmacol.* **17**, 1923–1933 (2014).

248. Shao, L.-X. *et al.* Psilocybin induces rapid and persistent growth of dendritic spines in frontal cortex in vivo. *Neuron* **109**, 2535-2544.e4 (2021).

249. Moliner, R. *et al.* Psychedelics promote plasticity by directly binding to BDNF receptor TrkB. *Nat. Neurosci.* **26**, 1032–1041 (2023).

250. Fava, M. *et al.* Esmethadone-HCl (REL-1017): a promising rapid antidepressant. *Eur. Arch. Psychiatry Clin. Neurosci.* **273**, 1463–1476 (2023).

251. Kato, T. & Duman, R. S. Rapastinel, a novel glutamatergic agent with ketamine-like antidepressant actions: Convergent mechanisms. *Pharmacol. Biochem. Behav.* **188**, 172827 (2020).

252. Nagele, P., Zorumski, C. F. & Conway, C. Exploring Nitrous Oxide as Treatment of Mood Disorders: Basic Concepts. *J. Clin. Psychopharmacol.* **38**, 144–148 (2018).

253. Reddy, D. S., Mbilinyi, R. H. & Estes, E. Preclinical and clinical pharmacology of brexanolone (allopregnanolone) for postpartum

depression: a landmark journey from concept to clinic in neurosteroid replacement therapy. *Psychopharmacology (Berl.)* **240**, 1841–1863 (2023).

254. Miller, A. H. *et al.* Advancing precision psychiatry and targeted treatments: Insights from immunopsychiatry. *Brain. Behav. Immun.* **125**, 319–329 (2025).

255. Hsieh, M. H. Electroconvulsive therapy for treatment-resistant depression. *Prog. Brain Res.* **281**, 69–90 (2023).

256. Song, J. & Kim, Y. Animal models for the study of depressive disorder. *CNS Neurosci. Ther.* **27**, 633–642 (2021).

257. Strekalova, T. *et al.* Resilience and Vulnerability to Stress-Induced Anhedonia: Unveiling Brain Gene Expression and Mitochondrial Dynamics in a Mouse Chronic Stress Depression Model. *Biomolecules* **13**, 1782 (2023).

258. Crawford, L. K., Rahman, S. F. & Beck, S. G. Social stress alters inhibitory synaptic input to distinct subpopulations of raphe serotonin neurons. *ACS Chem. Neurosci.* **4**, 200–209 (2013).

259. Anacker, C. *et al.* Neuroanatomic Differences Associated With Stress Susceptibility and Resilience. *Biol. Psychiatry* **79**, 840–849 (2016).

260. Vollmayr, B. & Gass, P. Learned helplessness: unique features and translational value of a cognitive depression model. *Cell Tissue Res.* **354**, 171–178 (2013).

261. Zhu, Z. & Reiser, G. The small heat shock proteins, especially HspB4 and HspB5 are promising protectants in neurodegenerative diseases. *Neurochem. Int.* **115**, 69–79 (2018).

262. Jaehne, E. J., Klarić, T. S., Koblar, S. A., Baune, B. T. & Lewis, M. D. Effects of Npas4 deficiency on anxiety, depression-like, cognition and sociability behaviour. *Behav. Brain Res.* **281**, 276–282 (2015).

263. Zeng, D. *et al.* Co-Expression Network Analysis Revealed That the ATP5G1 Gene Is Associated With Major Depressive Disorder. *Front. Genet.* **10**, 703 (2019).

264. Ludwig, B. & Dwivedi, Y. The concept of violent suicide, its underlying trait and neurobiology: A critical Perspective. *Eur. Neuropsychopharmacol. J. Eur. Coll. Neuropsychopharmacol.* **28**, 243–251 (2018).

265. Mergl, R. *et al.* What Are Reasons for the Large Gender Differences in the Lethality of Suicidal Acts? An Epidemiological Analysis in Four European Countries. *PloS One* **10**, e0129062 (2015).

266. Suicide rates. https://www.who.int/data/gho/data/themes/mental-health/suicide-rates.

267. Deaths by suicide down by almost 14% in a decade. https://ec.europa.eu/eurostat/web/products-eurostat-news/w/edn-20230908-3 (2023).

268. Favril, L., Yu, R., Uyar, A., Sharpe, M. & Fazel, S. Risk factors for suicide in adults: systematic review and meta-analysis of psychological autopsy studies. *Evid. Based Ment. Health* **25**, 148–155 (2022).

269. Hasin, D. S. *et al.* Epidemiology of Adult DSM-5 Major Depressive Disorder and Its Specifiers in the United States. *JAMA Psychiatry* **75**, 336–346 (2018).

270. Correll, C. U. *et al.* Mortality in people with schizophrenia: a systematic review and meta-analysis of relative risk and aggravating or attenuating factors. *World Psychiatry* **21**, 248–271 (2022).

271. De Sousa, A., Shah, B. & Shrivastava, A. Suicide and Schizophrenia: an Interplay of Factors. *Curr. Psychiatry Rep.* **22**, 65 (2020).

272. Plans, L. *et al.* Association between completed suicide and bipolar disorder: A systematic review of the literature. *J. Affect. Disord.* **242**, 111–122 (2019).

273. Dong, M. *et al.* Prevalence of suicide attempts in bipolar disorder: a systematic review and meta-analysis of observational studies. *Epidemiol. Psychiatr. Sci.* **29**, e63 (2019).

274. Na, P. J. *et al.* Social Determinants of Health and Suicide-Related Outcomes: A Review of Meta-Analyses. *JAMA Psychiatry* (2025) doi:10.1001/jamapsychiatry.2024.4241.

275. Hoertel, N. *et al.* Cerebrospinal fluid levels of monoamines among suicide attempters: A systematic review and random-effects meta-analysis. *J. Psychiatr. Res.* **136**, 224–235 (2021).

276. Hernández-Díaz, Y. *et al.* Association between the HTR1A rs6295 gene polymorphism and suicidal behavior: an updated meta-analysis. *Eur. Arch. Psychiatry Clin. Neurosci.* **273**, 5–14 (2023).

277. De Berardis, D. *et al.* Suicide and Genetic Biomarkers: Toward Personalized Tailored-treatment with Lithium and Clozapine. *Curr. Pharm. Des.* **27**, 3293–3304 (2021).

278. Serafini, G. *et al.* The Role of Inflammation in the Pathophysiology of Depression and Suicidal Behavior: Implications for Treatment. *Med. Clin. North Am.* **107**, 1–29 (2023).

279. O'Connor, D. B., Gartland, N. & O'Connor, R. C. Stress, cortisol and suicide risk. *Int. Rev. Neurobiol.* **152**, 101–130 (2020).

280. Sutar, R., Kumar, A. & Yadav, V. Suicide and prevalence of mental disorders: A systematic review and meta-analysis of world data on case-control psychological autopsy studies. *Psychiatry Res.* **329**, 115492 (2023).

281. Conner, K. R., Bridge, J. A., Davidson, D. J., Pilcher, C. & Brent, D. A. Metaanalysis of Mood and Substance Use Disorders in

Proximal Risk for Suicide Deaths. *Suicide Life. Threat. Behav.* **49**, 278–292 (2019).

282. Li, Q. S. *et al.* Genome-wide association study meta-analysis of suicide death and suicidal behavior. *Mol. Psychiatry* **28**, 891–900 (2023).

283. DiBlasi, E., Kang, J. & Docherty, A. R. Genetic contributions to suicidal thoughts and behaviors. *Psychol. Med.* **51**, 2148–2155 (2021).

284. Wilkerson, M. D. *et al.* Uncommon Protein-Coding Variants Associated With Suicide Attempt in a Diverse Sample of U.S. Army Soldiers. *Biol. Psychiatry* **96**, 15–25 (2024).

285. Zhang, J. *et al.* Predicting suicidal behavior in individuals with depression over 50 years of age: Evidence from the UK biobank. *Digit. Health* **10**, 20552076241287450 (2024).

286. Underwood, M. D. *et al.* A Stress Protein-Based Suicide Prediction Score and Relationship to Reported Early-Life Adversity and Recent Life Stress. *Int. J. Neuropsychopharmacol.* **26**, 501–512 (2023).

287. Zhao, H. *et al.* Identifying novel proteins for suicide attempt by integrating proteomes from brain and blood with genome-wide association data. *Neuropsychopharmacol. Off. Publ. Am. Coll. Neuropsychopharmacol.* **49**, 1255–1265 (2024).

288. Pandey, G. N., Sharma, A., Rizavi, H. S. & Ren, X. Dysregulation of Protein Kinase C in Adult Depression and Suicide: Evidence From

Postmortem Brain Studies. *Int. J. Neuropsychopharmacol.* **24**, 400–408 (2021).

289. Dean, B., Tsatsanis, A., Lam, L. Q., Scarr, E. & Duce, J. A. Changes in cortical protein markers of iron transport with gender, major depressive disorder and suicide. *World J. Biol. Psychiatry Off. J. World Fed. Soc. Biol. Psychiatry* **21**, 119–126 (2020).

290. Neupane, S. P. *et al.* Immune-related biomarkers and suicidal behaviors: A meta-analysis. *Eur. Neuropsychopharmacol. J. Eur. Coll. Neuropsychopharmacol.* **75**, 15–30 (2023).

291. Hess, E. M., Riggs, L. M., Michaelides, M. & Gould, T. D. Mechanisms of ketamine and its metabolites as antidepressants. *Biochem. Pharmacol.* **197**, 114892 (2022).

292. Song, J. *et al.* Suicidal Behavior During Lithium and Valproate Treatment: A Within-Individual 8-Year Prospective Study of 50,000 Patients With Bipolar Disorder. *Am. J. Psychiatry* **174**, 795–802 (2017).

293. Ramadan, A. M. & Mansour, I. A. Could ketamine be the answer to treating treatment-resistant major depressive disorder? *Gen. Psychiatry* **33**, (2020).

294. Mann, J. J., Michel, C. A. & Auerbach, R. P. Improving Suicide Prevention Through Evidence-Based Strategies: A Systematic Review. *Am. J. Psychiatry* **178**, 611–624 (2021).

295. Xiao, X. *et al.* Brain Functional Connectome Defines a Transdiagnostic Dimension Shared by Cognitive Function and Psychopathology in Preadolescents. *Biol. Psychiatry* **95**, 1081–1090 (2024).

296. de Menezes Galvão, A. C. *et al.* Pathophysiology of Major Depression by Clinical Stages. *Front. Psychol.* **12**, 641779 (2021).

297. Tomasik, J. *et al.* Metabolomic Biomarker Signatures for Bipolar and Unipolar Depression. *JAMA Psychiatry* **81**, 101–106 (2024).

298. Goud Alladi, C., Etain, B., Bellivier, F. & Marie-Claire, C. DNA Methylation as a Biomarker of Treatment Response Variability in Serious Mental Illnesses: A Systematic Review Focused on Bipolar Disorder, Schizophrenia, and Major Depressive Disorder. *Int. J. Mol. Sci.* **19**, 3026 (2018).

299. Howes, O. D., Thase, M. E. & Pillinger, T. Treatment resistance in psychiatry: state of the art and new directions. *Mol. Psychiatry* **27**, 58–72 (2022).

300. Bradshaw, N. J. & Korth, C. Protein misassembly and aggregation as potential convergence points for non-genetic causes of chronic mental illness. *Mol. Psychiatry* **24**, 936–951 (2019).

301. Balch, W. E., Morimoto, R. I., Dillin, A. & Kelly, J. W. Adapting proteostasis for disease intervention. *Science* **319**, 916–919 (2008).

302. Hipp, M. S., Kasturi, P. & Hartl, F. U. The proteostasis network and its decline in ageing. *Nat. Rev. Mol. Cell Biol.* **20**, 421–435 (2019).

303. Juković, M., Ratkaj, I., Kalafatovic, D. & Bradshaw, N. J. Amyloids, amorphous aggregates and assemblies of peptides - Assessing aggregation. *Biophys. Chem.* **308**, 107202 (2024).

304. Ochneva, A. *et al.* Protein Misfolding and Aggregation in the Brain: Common Pathogenetic Pathways in Neurodegenerative and Mental Disorders. *Int. J. Mol. Sci.* **23**, 14498 (2022).

305. Markossian, K. A. & Kurganov, B. I. Protein folding, misfolding, and aggregation. Formation of inclusion bodies and aggresomes. *Biochem. Biokhimiia* **69**, 971–984 (2004).

306. Fu, L. & Sztul, E. Characterization of intracellular aggresomes by fluorescent microscopy. *Methods Mol. Biol. Clifton NJ* **1258**, 307–317 (2015).

307. Zhao, Y., Lin, M., Zhai, F., Chen, J. & Jin, X. Exploring the Role of Ubiquitin-Proteasome System in the Pathogenesis of Parkinson's Disease. *Pharm. Basel Switz.* **17**, 782 (2024).

308. Pohl, C. & Dikic, I. Cellular quality control by the ubiquitin-proteasome system and autophagy. *Science* **366**, 818–822 (2019).

309. Korth, C. Aggregated proteins in schizophrenia and other chronic mental diseases: DISC1opathies. *Prion* **6**, 134–141 (2012).

310. Lashley, T., Rohrer, J. D., Mead, S. & Revesz, T. Review: an update on clinical, genetic and pathological aspects of frontotemporal lobar degenerations. *Neuropathol. Appl. Neurobiol.* **41**, 858–881 (2015).

311. Mehra, S., Sahay, S. & Maji, S. K. α-Synuclein misfolding and aggregation: Implications in Parkinson's disease pathogenesis. *Biochim. Biophys. Acta Proteins Proteomics* **1867**, 890–908 (2019).

312. Srinivasan, E., Ram, V. & Rajasekaran, R. A Review On Huntington Protein: Insight Into Protein Aggregation and Therapeutic Interventions. *Curr. Drug Metab.* **23**, 260–282 (2022).

313. Murakami, K. & Ono, K. Interactions of amyloid coaggregates with biomolecules and its relevance to neurodegeneration. *FASEB J.* **36**, e22493 (2022).

314. Xia, Z. *et al.* Co-aggregation with Apolipoprotein E modulates the function of Amyloid-β in Alzheimer's disease. *Nat. Commun.* **15**, 4695 (2024).

315. Jiang, L.-L., Zhang, X.-L. & Hu, H.-Y. Co-Aggregation of TDP-43 with Other Pathogenic Proteins and Their Co-Pathologies in Neurodegenerative Diseases. *Int. J. Mol. Sci.* **25**, 12380 (2024).

316. Goedert, M. & Spillantini, M. G. Ordered Assembly of Tau Protein and Neurodegeneration. *Adv. Exp. Med. Biol.* **1184**, 3–21 (2019).

317. Bourdenx, M. *et al.* Protein aggregation and neurodegeneration in prototypical neurodegenerative diseases: Examples of amyloidopathies, tauopathies and synucleinopathies. *Prog. Neurobiol.* **155**, 171–193 (2017).

318. Lee, S.-J., Lim, H.-S., Masliah, E. & Lee, H.-J. Protein aggregate spreading in neurodegenerative diseases: Problems and perspectives. *Neurosci. Res.* **70**, 339–348 (2011).

319. Levenson, R. W., Sturm, V. E. & Haase, C. M. Emotional and behavioral symptoms in neurodegenerative disease: A model for studying the neural bases of psychopathology. *Annu. Rev. Clin. Psychol.* **10**, 581–606 (2014).

320. Leliveld, S. R. *et al.* Insolubility of Disrupted-in-Schizophrenia 1 Disrupts Oligomer-Dependent Interactions with Nuclear Distribution Element 1 and Is Associated with Sporadic Mental Disease. *J. Neurosci.* **28**, 3839–3845 (2008).

321. Ottis, P. *et al.* Convergence of two independent mental disease genes on the protein level: recruitment of dysbindin to cell-invasive disrupted-in-schizophrenia 1 aggresomes. *Biol. Psychiatry* **70**, 604–610 (2011).

322. Bader, V. *et al.* Proteomic, genomic and translational approaches identify CRMP1 for a role in schizophrenia and its underlying traits. *Hum. Mol. Genet.* **21**, 4406–4418 (2012).

323. Bradshaw, N. J. *et al.* Aggregation of the protein TRIOBP-1 and its potential relevance to schizophrenia. *PloS One* **9**, e111196 (2014).

324. Nucifora, L. G. *et al.* Increased Protein Insolubility in Brains From a Subset of Patients With Schizophrenia. *Am. J. Psychiatry* **176**, 730–743 (2019).

325. Kim, C. S. & Johnston, D. A Possible Link Between HCN Channels and Depression. *Chronic Stress Thousand Oaks Calif* **2**, 2470547018787781 (2018).

326. Bengesser, S. A. *et al.* Endoplasmic reticulum stress in bipolar disorder? - BiP and CHOP gene expression- and XBP1 splicing analysis in peripheral blood. *Psychoneuroendocrinology* **95**, 113–119 (2018).

327. Barmaki, H., Nourazarian, A. & Khaki-Khatibi, F. Proteostasis and neurodegeneration: a closer look at autophagy in Alzheimer's disease. *Front. Aging Neurosci.* **15**, 1281338 (2023).

328. Cheon, S., Dean, M. & Chahrour, M. The ubiquitin proteasome pathway in neuropsychiatric disorders. *Neurobiol. Learn. Mem.* **165**, 106791 (2019).

329. Luza, S. *et al.* The ubiquitin proteasome system and schizophrenia. *Lancet Psychiatry* **7**, 528–537 (2020).

330. Yamashita, N. & Goshima, Y. Collapsin Response Mediator Proteins Regulate Neuronal Development and Plasticity by

Switching Their Phosphorylation Status. *Mol. Neurobiol.* **45**, 234–246 (2012).

331. Makihara, H. *et al.* CRMP1 and CRMP2 have synergistic but distinct roles in dendritic development. *Genes Cells Devoted Mol. Cell. Mech.* **21**, 994–1005 (2016).

332. Nakamura, F., Ohshima, T. & Goshima, Y. Collapsin Response Mediator Proteins: Their Biological Functions and Pathophysiology in Neuronal Development and Regeneration. *Front. Cell. Neurosci.* **14**, 188 (2020).

333. Charrier, E. *et al.* Collapsin response mediator proteins (CRMPs): involvement in nervous system development and adult neurodegenerative disorders. *Mol. Neurobiol.* **28**, 51–64 (2003).

334. Tang, Y. *et al.* Vertebrate paralogous CRMPs in nervous system: evolutionary, structural, and functional interplay. *J. Mol. Neurosci. MN* **55**, 324–334 (2015).

335. Leung, T. *et al.* p80 ROKalpha binding protein is a novel splice variant of CRMP-1 which associates with CRMP-2 and modulates RhoA-induced neuronal morphology. *FEBS Lett.* **532**, 445–449 (2002).

336. Gojkovic, Z. *et al.* Dihydropyrimidine amidohydrolases and dihydroorotases share the same origin and several enzymatic properties. *Nucleic Acids Res.* **31**, 1683–1692 (2003).

337. Brittain, J. M., Wang, Y., Eruvwetere, O. & Khanna, R. Cdk5-mediated phosphorylation of CRMP-2 enhances its interaction with CaV2.2. *FEBS Lett.* **586**, 3813–3818 (2012).

338. Muha, V. *et al.* Loss of CRMP2 O-GlcNAcylation leads to reduced novel object recognition performance in mice. *Open Biol.* **9**, 190192 (2019).

339. Princz, A. & Tavernarakis, N. SUMOylation in Neurodegenerative Diseases. *Gerontology* **66**, 122–130 (2020).

340. Taghian, K., Lee, J. Y. & Petratos, S. Phosphorylation and cleavage of the family of collapsin response mediator proteins may play a central role in neurodegeneration after CNS trauma. *J. Neurotrauma* **29**, 1728–1735 (2012).

341. Zhang, Z. *et al.* Calpain-mediated collapsin response mediator protein-1, -2, and -4 proteolysis after neurotoxic and traumatic brain injury. *J. Neurotrauma* **24**, 460–472 (2007).

342. Zhang, J.-N. *et al.* Calpain-mediated cleavage of collapsin response mediator protein-2 drives acute axonal degeneration. *Sci. Rep.* **6**, 37050 (2016).

343. Hou, S.-T. The regulatory and enzymatic functions of CRMPs in neuritogenesis, synaptic plasticity, and gene transcription. *Neurochem. Int.* **139**, 104795 (2020).

344. Deo, R. C. *et al.* Structural bases for CRMP function in plexin-dependent semaphorin3A signaling. *EMBO J.* **23**, 9–22 (2004).

345. Niwa, S. *et al.* Structural basis for CRMP2-induced axonal microtubule formation. *Sci. Rep.* **7**, 10681 (2017).

346. Buel, G. R., Rush, J. & Ballif, B. A. Fyn promotes phosphorylation of collapsin response mediator protein 1 at tyrosine 504, a novel, isoform-specific regulatory site. *J. Cell. Biochem.* **111**, 20–28 (2010).

347. Cole, A. R. *et al.* Collapsin response mediator protein-2 hyperphosphorylation is an early event in Alzheimer's disease progression. *J. Neurochem.* **103**, 1132–1144 (2007).

348. Yu-Kemp, H.-C., Kemp, J. P. & Brieher, W. M. CRMP-1 enhances EVL-mediated actin elongation to build lamellipodia and the actin cortex. *J. Cell Biol.* **216**, 2463–2479 (2017).

349. Yamane, M. *et al.* A functional coupling between CRMP1 and Nav1.7 for retrograde propagation of Semaphorin3A signaling. *J. Cell Sci.* **130**, 1393–1403 (2017).

350. Higurashi, M. *et al.* Localized role of CRMP1 and CRMP2 in neurite outgrowth and growth cone steering. *Dev. Neurobiol.* **72**, 1528–1540 (2012).

351. Yamashita, N. *et al.* Collapsin response mediator protein 1 mediates reelin signaling in cortical neuronal migration. *J. Neurosci. Off. J. Soc. Neurosci.* **26**, 13357–13362 (2006).

352. Su, K.-Y. *et al.* Mice Deficient in Collapsin Response Mediator Protein-1 Exhibit Impaired Long-Term Potentiation and Impaired Spatial Learning and Memory. *J. Neurosci.* **27**, 2513–2524 (2007).

353. Rogemond, V. *et al.* Processing and Nuclear Localization of CRMP2 during Brain Development Induce Neurite Outgrowth Inhibition. *J. Biol. Chem.* **283**, 14751–14761 (2008).

354. Johnston-Wilson, N. L. *et al.* Disease-specific alterations in frontal cortex brain proteins in schizophrenia, bipolar disorder, and major depressive disorder. The Stanley Neuropathology Consortium. *Mol. Psychiatry* **5**, 142–149 (2000).

355. Aylsworth, A., Jiang, S. X., Desbois, A. & Hou, S. T. Characterization of the role of full-length CRMP3 and its calpain-cleaved product in inhibiting microtubule polymerization and neurite outgrowth. *Exp. Cell Res.* **315**, 2856–2868 (2009).

356. Rosslenbroich, V. *et al.* Collapsin response mediator protein-4 regulates F-actin bundling. *Exp. Cell Res.* **310**, 434–444 (2005).

357. Blasco, H. *et al.* A rare motor neuron deleterious missense mutation in the DPYSL3 (CRMP4) gene is associated with ALS. *Hum. Mutat.* **34**, 953–960 (2013).

358. Jeanne, M. *et al.* Missense variants in DPYSL5 cause a neurodevelopmental disorder with corpus callosum agenesis and cerebellar abnormalities. *Am. J. Hum. Genet.* **108**, 951–961 (2021).

359. Desprez, F., Ung, D. C., Vourc'h, P., Jeanne, M. & Laumonnier, F. Contribution of the dihydropyrimidinase-like proteins family in synaptic physiology and in neurodevelopmental disorders. *Front. Neurosci.* **17**, 1154446 (2023).

360. Ohtani-Kaneko, R. Crmp4-KO Mice as an Animal Model for Investigating Certain Phenotypes of Autism Spectrum Disorders. *Int. J. Mol. Sci.* **20**, 2485 (2019).

361. Williamson, R. *et al.* CRMP2 hyperphosphorylation is characteristic of Alzheimer's disease and not a feature common to other neurodegenerative diseases. *J. Alzheimers Dis. JAD* **27**, 615–625 (2011).

362. Kanamori, T. *et al.* Suppressed phosphorylation of collapsin response mediator protein-2 in the hippocampus of HCNP precursor transgenic mice. *Brain Res.* **1355**, 180–188 (2010).

363. Watamura, N., Toba, J., Yoshii, A., Nikkuni, M. & Ohshima, T. Colocalization of phosphorylated forms of WAVE1, CRMP2, and tau in Alzheimer's disease model mice: Involvement of Cdk5 phosphorylation and the effect of ATRA treatment. *J. Neurosci. Res.* **94**, 15–26 (2016).

364. Noguchi, D. *et al.* Involvement of CRMP2 Phosphorylation in Amyloid Beta-induced Tau Phosphorylation of Hippocampal Neurons in Alzheimer's Disease Mouse Model. *Mol. Neurobiol.* (2025) doi:10.1007/s12035-025-04721-y.

365. Ravindran, E. *et al.* Monoallelic CRMP1 gene variants cause neurodevelopmental disorder. *eLife* **11**, e80793.

366. Wu, Z., Wang, G., Wei, Y., Xiao, L. & Wang, H. PI3K/AKT/GSK3β/CRMP-2-mediated neuroplasticity in depression induced by stress. *NeuroReport* **29**, 1256–1263 (2018).

367. Liu, Z. *et al.* The neuroprotective effect of lithium chloride on cognitive impairment through glycogen synthase kinase-3β inhibition in intracerebral hemorrhage rats. *Eur. J. Pharmacol.* **840**, 50–59 (2018).

368. Nakata, K. *et al.* The human dihydropyrimidinase-related protein 2 gene on chromosome 8p21 is associated with paranoid-type schizophrenia. *Biol. Psychiatry* **53**, 571–576 (2003).

369. Ujike, H. *et al.* Association study of the dihydropyrimidinase-related protein 2 gene and methamphetamine psychosis. *Ann. N. Y. Acad. Sci.* **1074**, 90–96 (2006).

370. Kedracka-Krok, S. *et al.* Clozapine influences cytoskeleton structure and calcium homeostasis in rat cerebral cortex and has a different proteomic profile than risperidone. *J. Neurochem.* **132**, 657–676 (2015).

371. Föcking, M. *et al.* Common proteomic changes in the hippocampus in schizophrenia and bipolar disorder and particular evidence for involvement of cornu ammonis regions 2 and 3. *Arch. Gen. Psychiatry* **68**, 477–488 (2011).

372. Stroedicke, M. *et al.* Systematic interaction network filtering identifies CRMP1 as a novel suppressor of huntingtin misfolding and neurotoxicity. *Genome Res.* **25**, 701–713 (2015).

373. Camargo, L. M. *et al.* Disrupted in Schizophrenia 1 Interactome: evidence for the close connectivity of risk genes and a potential synaptic basis for schizophrenia. *Mol. Psychiatry* **12**, 74–86 (2007).

374. Soares, D. C., Carlyle, B. C., Bradshaw, N. J. & Porteous, D. J. DISC1: Structure, Function, and Therapeutic Potential for Major Mental Illness. *ACS Chem. Neurosci.* **2**, 609–632 (2011).

375. Bradshaw, N. J. & Porteous, D. J. DISC1-binding proteins in neural development, signalling and schizophrenia. *Neuropharmacology* **62**, 1230–1241 (2012).

376. Yerabham, A. S. K. *et al.* A structural organization for the Disrupted in Schizophrenia 1 protein, identified by high-throughput screening, reveals distinctly folded regions, which are bisected by mental illness-related mutations. *J. Biol. Chem.* **292**, 6468–6477 (2017).

377. Brandon, N. J. *et al.* Understanding the role of DISC1 in psychiatric disease and during normal development. *J. Neurosci. Off. J. Soc. Neurosci.* **29**, 12768–12775 (2009).

378. Tropea, D., Hardingham, N., Millar, K. & Fox, K. Mechanisms underlying the role of DISC1 in synaptic plasticity. *J. Physiol.* **596**, 2747–2771 (2018).

379. Murphy, L. C. & Millar, J. K. Regulation of mitochondrial dynamics by DISC1, a putative risk factor for major mental illness. *Schizophr. Res.* **187**, 55–61 (2017).

380. Norkett, R. *et al.* DISC1-dependent Regulation of Mitochondrial Dynamics Controls the Morphogenesis of Complex Neuronal Dendrites. *J. Biol. Chem.* **291**, 613–629 (2016).

381. Bradshaw, N. J. *et al.* NDE1 and NDEL1: multimerisation, alternate splicing and DISC1 interaction. *Neurosci. Lett.* **449**, 228–233 (2009).

382. James, R. *et al.* Disrupted in Schizophrenia 1 (DISC1) is a multicompartmentalized protein that predominantly localizes to mitochondria. *Mol. Cell. Neurosci.* **26**, 112–122 (2004).

383. Atkin, T. A., MacAskill, A. F., Brandon, N. J. & Kittler, J. T. Disrupted in Schizophrenia-1 regulates intracellular trafficking of mitochondria in neurons. *Mol. Psychiatry* **16**, 122–124, 121 (2011).

384. Park, S. J. *et al.* DISC1 Modulates Neuronal Stress Responses by Gate-Keeping ER-Mitochondria Ca2+ Transfer through the MAM. *Cell Rep.* **21**, 2748–2759 (2017).

385. Kim, J. Y. *et al.* DISC1 regulates new neuron development in the adult brain via modulation of AKT-mTOR signaling through KIAA1212. *Neuron* **63**, 761–773 (2009).

386. Fuentes-Villalobos, F. *et al.* DISC1 promotes translation maintenance during sodium arsenite-induced oxidative stress. *Biochim. Biophys. Acta Gene Regul. Mech.* **1862**, 657–669 (2019).

387. Ogawa, F., Kasai, M. & Akiyama, T. A functional link between Disrupted-In-Schizophrenia 1 and the eukaryotic translation initiation factor 3. *Biochem. Biophys. Res. Commun.* **338**, 771–776 (2005).

388. Watanabe, M. *et al.* Evidence of DISC1 as an arsenic binding protein and implications regarding its role as a translational activator. *Front. Mol. Biosci.* **10**, 1308693 (2023).

389. Miyoshi, K. *et al.* Disrupted-In-Schizophrenia 1, a candidate gene for schizophrenia, participates in neurite outgrowth. *Mol. Psychiatry* **8**, 685–694 (2003).

390. Lipska, B. K. *et al.* Functional genomics in postmortem human brain: abnormalities in a DISC1 molecular pathway in schizophrenia. *Dialogues Clin. Neurosci.* **8**, 353–357 (2006).

391. Blackwood, D. H. *et al.* Schizophrenia and affective disorders--cosegregation with a translocation at chromosome 1q42 that directly disrupts brain-expressed genes: clinical and P300 findings in a family. *Am. J. Hum. Genet.* **69**, 428–433 (2001).

392. Szeszko, P. R. *et al.* DISC1 is associated with prefrontal cortical gray matter and positive symptoms in schizophrenia. *Biol. Psychol.* **79**, 103–110 (2008).

393. Callicott, J. H. *et al.* Variation in DISC1 affects hippocampal structure and function and increases risk for schizophrenia. *Proc. Natl. Acad. Sci. U. S. A.* **102**, 8627–8632 (2005).

394. Singh, K. K. *et al.* Common DISC1 polymorphisms disrupt Wnt/GSK3β signaling and brain development. *Neuron* **72**, 545–558 (2011).

395. Raznahan, A. *et al.* Common functional polymorphisms of DISC1 and cortical maturation in typically developing children and adolescents. *Mol. Psychiatry* **16**, 917–926 (2011).

396. Atkin, T. A., Brandon, N. J. & Kittler, J. T. Disrupted in Schizophrenia 1 forms pathological aggresomes that disrupt its function in intracellular transport. *Hum. Mol. Genet.* **21**, 2017–2028 (2012).

397. Pils, M. *et al.* Disrupted-in-schizophrenia 1 protein aggregates in cerebrospinal fluid are elevated in patients with first-episode psychosis. *Psychiatry Clin. Neurosci.* **77**, 665–671 (2023).

398. Kaefer, K. *et al.* Disrupted-in-schizophrenia 1 overexpression disrupts hippocampal coding and oscillatory synchronization. *Hippocampus* **29**, 802–816 (2019).

399. Tanaka, M. *et al.* Aggregation of scaffolding protein DISC1 dysregulates phosphodiesterase 4 in Huntington's disease. *J. Clin. Invest.* **127**, 1438–1450.

400. Endo, R. *et al.* TDP-43 and DISC1 Co-Aggregation Disrupts Dendritic Local Translation and Mental Function in FTLD. *Biol. Psychiatry* **84**, 509–521 (2018).

401. Trossbach, S. V. *et al.* Misassembly of full-length Disrupted-in-Schizophrenia 1 protein is linked to altered dopamine homeostasis and behavioral deficits. *Mol. Psychiatry* **21**, 1561–1572 (2016).

402. Seidisarouei, M. *et al.* Social anhedonia as a Disrupted-in-Schizophrenia 1-dependent phenotype. *Sci. Rep.* **12**, 10182 (2022).

403. Wang, A.-L. *et al.* Disrupted-in-schizophrenia 1 Protein Misassembly Impairs Cognitive Flexibility and Social Behaviors in a Transgenic Rat Model. *Neuroscience* **493**, 41–51 (2022).

404. Hamburg, H. *et al.* Simultaneous effects on parvalbumin-positive interneuron and dopaminergic system development in a transgenic rat model for sporadic schizophrenia. *Sci. Rep.* **6**, 34946 (2016).

405. Ma, T. M. *et al.* Pathogenic disruption of DISC1-serine racemase binding elicits schizophrenia-like behavior via D-serine depletion. *Mol. Psychiatry* **18**, 557–567 (2013).

406. Jacobi, A. A., Halawani, S., Lynch, D. R. & Lin, H. Neuronal serine racemase associates with Disrupted-In-Schizophrenia-1 and

DISC1 agglomerates: Implications for schizophrenia. *Neurosci. Lett.* **692**, 107–114 (2019).

407. Pickard, B. S., Pieper, A. A., Porteous, D. J., Blackwood, D. H. & Muir, W. J. The NPAS3 gene--emerging evidence for a role in psychiatric illness. *Ann. Med.* **38**, 439–448 (2006).

408. OpenLibrary.org. McGill Lodish 5E Package - Molecular Cell Biology & McGill Activation Code by Harvey Lodish. *Open Library* https://openlibrary.org/books/OL10525774M/McGill_Lodish_5E_Package_-_Molecular_Cell_Biology_McGill_Activation_Code.

409. Trejo-Solís, C. *et al.* Metabolic Roles of HIF1, c-Myc, and p53 in Glioma Cells. *Metabolites* **14**, 249 (2024).

410. Henry, J. T. & Crosson, S. Ligand-binding PAS domains in a genomic, cellular, and structural context. *Annu. Rev. Microbiol.* **65**, 261–286 (2011).

411. Teh, C. H. L. *et al.* Neuronal PAS domain protein 1 is a transcriptional repressor and requires arylhydrocarbon nuclear translocator for its nuclear localization. *J. Biol. Chem.* **281**, 34617–34629 (2006).

412. Stanco, A. *et al.* NPAS1 represses the generation of specific subtypes of cortical interneurons. *Neuron* **84**, 940–953 (2014).

413. Troppoli, T. A. *et al.* Neuronal PAS domain 1 identifies a major subpopulation of wakefulness-promoting GABAergic neurons in the

basal forebrain. *Proc. Natl. Acad. Sci. U. S. A.* **121**, e2321410121 (2024).

414. Rutter, J., Reick, M., Wu, L. C. & McKnight, S. L. Regulation of Clock and NPAS2 DNA Binding by the Redox State of NAD Cofactors. *Science* **293**, 510–514 (2001).

415. Uchida, T. *et al.* CO-dependent Activity-controlling Mechanism of Heme-containing CO-sensor Protein, Neuronal PAS Domain Protein 2. *J. Biol. Chem.* **280**, 21358–21368 (2005).

416. Reick, M., Garcia, J. A., Dudley, C. & McKnight, S. L. NPAS2: An Analog of Clock Operative in the Mammalian Forebrain. *Science* **293**, 506–509 (2001).

417. Dudley, C. A. *et al.* Altered patterns of sleep and behavioral adaptability in NPAS2-deficient mice. *Science* **301**, 379–383 (2003).

418. Franken, P. *et al.* NPAS2 as a transcriptional regulator of non-rapid eye movement sleep: genotype and sex interactions. *Proc. Natl. Acad. Sci. U. S. A.* **103**, 7118–7123 (2006).

419. Garcia, J. A. *et al.* Impaired Cued and Contextual Memory in NPAS2-Deficient Mice. *Science* **288**, 2226–2230 (2000).

420. Sun, X. & Lin, Y. Npas4: Linking Neuronal Activity to Memory. *Trends Neurosci.* **39**, 264–275 (2016).

421. Spiegel, I. *et al.* Npas4 regulates excitatory-inhibitory balance within neural circuits through cell type-specific gene programs. *Cell* **157**, 1216–1229 (2014).

422. Yoshihara, S.-I. *et al.* Npas4 regulates Mdm2 and thus Dcx in experience-dependent dendritic spine development of newborn olfactory bulb interneurons. *Cell Rep.* **8**, 843–857 (2014).

423. Luoma, L. M. & Berry, F. B. Molecular analysis of NPAS3 functional domains and variants. *BMC Mol. Biol.* **19**, 14 (2018).

424. Wu, D., Su, X., Potluri, N., Kim, Y. & Rastinejad, F. NPAS1-ARNT and NPAS3-ARNT crystal structures implicate the bHLH-PAS family as multi-ligand binding transcription factors. *eLife* **5**, e18790 (2016).

425. Kamnasaran, D., Muir, W., Ferguson-Smith, M. & Cox, D. Disruption of the neuronal PAS3 gene in a family affected with schizophrenia. *J. Med. Genet.* **40**, 325–332 (2003).

426. Pickard, B. S., Malloy, M. P., Porteous, D. J., Blackwood, D. H. R. & Muir, W. J. Disruption of a brain transcription factor, NPAS3, is associated with schizophrenia and learning disability. *Am. J. Med. Genet. B Neuropsychiatr. Genet.* **136B**, 26–32 (2005).

427. Macintyre, G. *et al.* Association of NPAS3 exonic variation with schizophrenia. *Schizophr. Res.* **120**, 143–149 (2010).

428. Whalen, S. & Pollard, K. S. Enhancer Function and Evolutionary Roles of Human Accelerated Regions. *Annu. Rev. Genet.* **56**, 423–439 (2022).

429. Caporale, A. L., Cinalli, A. R., Rubinstein, M. & Franchini, L. F. The Human Accelerated Region HAR202 Controls NPAS3 Expression in the Developing Forebrain Displaying Differential Enhancer Activity Between Modern and Archaic Human Sequences. *Mol. Biol. Evol.* **41**, msae186 (2024).

430. Lee, B. E., Suh, P.-G. & Kim, J.-I. O-GlcNAcylation in health and neurodegenerative diseases. *Exp. Mol. Med.* **53**, 1674–1682 (2021).

431. Marotta, N. P. *et al.* O-GlcNAc modification blocks the aggregation and toxicity of the protein α-synuclein associated with Parkinson's disease. *Nat. Chem.* **7**, 913–920 (2015).

432. Bilbrough, T., Piemontese, E. & Seitz, O. Dissecting the role of protein phosphorylation: a chemical biology toolbox. *Chem. Soc. Rev.* **51**, 5691–5730 (2022).

433. Hart, G. W. & Ball, L. E. Post-translational modifications: a major focus for the future of proteomics. *Mol. Cell. Proteomics MCP* **12**, 3443 (2013).

434. van der Laarse, S. A. M., Leney, A. C. & Heck, A. J. R. Crosstalk between phosphorylation and O-GlcNAcylation: friend or foe. *FEBS J.* **285**, 3152–3167 (2018).

435. Wang, X. *et al.* MK-8719, a Novel and Selective O-GlcNAcase Inhibitor That Reduces the Formation of Pathological Tau and Ameliorates Neurodegeneration in a Mouse Model of Tauopathy. *J. Pharmacol. Exp. Ther.* **374**, 252–263 (2020).

436. Sha, L. *et al.* Transcriptional regulation of neurodevelopmental and metabolic pathways by NPAS3. *Mol. Psychiatry* **17**, 267–279 (2012).

437. Yang, D. *et al.* NPAS3 Regulates Transcription and Expression of VGF: Implications for Neurogenesis and Psychiatric Disorders. *Front. Mol. Neurosci.* **9**, 109 (2016).

438. Wong, J. *et al.* Expression of NPAS3 in the Human Cortex and Evidence of Its Posttranscriptional Regulation by miR-17 During Development, With Implications for Schizophrenia. *Schizophr. Bull.* **39**, 396–406 (2013).

439. Tissue expression of NPAS3 - Summary - The Human Protein Atlas. https://www.proteinatlas.org/ENSG00000151322-NPAS3/tissue.

440. Mandl, M. & Depping, R. Hypoxia-inducible aryl hydrocarbon receptor nuclear translocator (ARNT) (HIF-1β): is it a rare exception? *Mol. Med. Camb. Mass* **20**, 215–220 (2014).

441. Sun, X. *et al.* Structures of NPAS4-ARNT and NPAS4-ARNT2 heterodimers reveal new dimerization modalities in the bHLH-PAS

transcription factor family. *Proc. Natl. Acad. Sci. U. S. A.* **119**, e2208804119 (2022).

442. Sharma, N. *et al.* ARNT2 Tunes Activity-Dependent Gene Expression through NCoR2-Mediated Repression and NPAS4-Mediated Activation. *Neuron* **102**, 390-406.e9 (2019).

443. Tapescu, I. & Cherry, S. DDX RNA helicases: key players in cellular homeostasis and innate antiviral immunity. *J. Virol.* **98**, e0004024 (2024).

444. Wolfrum, P., Fietz, A., Schnichels, S. & Hurst, J. The function of p53 and its role in Alzheimer's and Parkinson's disease compared to age-related macular degeneration. *Front. Neurosci.* **16**, 1029473 (2022).

445. Edwards, M., Hall, J., Gong, G. & O'Bryant, S. E. Arsenic exposure, AS3MT polymorphism, and neuropsychological functioning among rural dwelling adults and elders: a cross-sectional study. *Environ. Health Glob. Access Sci. Source* **13**, 15 (2014).

446. Erbel-Sieler, C. *et al.* Behavioral and regulatory abnormalities in mice deficient in the NPAS1 and NPAS3 transcription factors. *Proc. Natl. Acad. Sci. U. S. A.* **101**, 13648–13653 (2004).

447. Pieper, A. A. *et al.* The neuronal PAS domain protein 3 transcription factor controls FGF-mediated adult hippocampal

neurogenesis in mice. *Proc. Natl. Acad. Sci. U. S. A.* **102**, 14052–14057 (2005).

448. Pieper, A. A. *et al.* Discovery of a proneurogenic, neuroprotective chemical. *Cell* **142**, 39–51 (2010).

449. Liu, J.-W., Li, H. & Zhang, Y. Npas3 regulates stemness maintenance of radial glial cells and neuronal migration in the developing mouse cerebral cortex. *Front. Cell. Neurosci.* **16**, 865681 (2022).

450. Ilievski, B., Rodzevski, K., Gibbon, M. & Dwork, A. J. Fahr's disease and schizophrenia in a patient with secondary hypoparathyroidism. *J. Neuropsychiatry Clin. Neurosci.* **14**, 357–358 (2002).

451. Segurado, R. *et al.* Genome scan meta-analysis of schizophrenia and bipolar disorder, part III: Bipolar disorder. *Am. J. Hum. Genet.* **73**, 49–62 (2003).

452. Schlade-Bartusiak, K., Ardinger, H. & Cox, D. W. A child with terminal 14q deletion syndrome: consideration of genotype-phenotype correlations. *Am. J. Med. Genet. A.* **149A**, 1012–1018 (2009).

453. Nucifora, L. G. *et al.* A Mutation in NPAS3 That Segregates with Schizophrenia in a Small Family Leads to Protein Aggregation. *Mol. Neuropsychiatry* **2**, 133–144 (2016).

454. Wong, J. *et al.* Expression of NPAS3 in the Human Cortex and Evidence of Its Posttranscriptional Regulation by miR-17 During Development, With Implications for Schizophrenia. *Schizophr. Bull.* **39**, 396–406 (2013).

455. Pickard, B. S. *et al.* Interacting haplotypes at the NPAS3 locus alter risk of schizophrenia and bipolar disorder. *Mol. Psychiatry* **14**, 874–884 (2009).

456. Lavedan, C. *et al.* Association of the NPAS3 gene and five other loci with response to the antipsychotic iloperidone identified in a whole genome association study. *Mol. Psychiatry* **14**, 804–819 (2009).

457. Govindarajalu, G., Selvam, M., Palchamy, E. & Baluchamy, S. N-terminal truncations of human bHLH transcription factor Twist1 leads to the formation of aggresomes. *Mol. Cell. Biochem.* **439**, 75–85 (2018).

458. Sepp, M., Pruunsild, P. & Timmusk, T. Pitt-Hopkins syndrome-associated mutations in TCF4 lead to variable impairment of the transcription factor function ranging from hypomorphic to dominant-negative effects. *Hum. Mol. Genet.* **21**, 2873–2888 (2012).

459. Zaharija, B., Samardžija, B. & Bradshaw, N. J. The TRIOBP Isoforms and Their Distinct Roles in Actin Stabilization, Deafness, Mental Illness, and Cancer. *Molecules* **25**, 4967 (2020).

460. Yu, J. *et al.* The E3 ubiquitin ligase HECTD3 regulates ubiquitination and degradation of Tara. *Biochem. Biophys. Res. Commun.* **367**, 805–812 (2008).

461. Maycox, P. R. *et al.* Analysis of gene expression in two large schizophrenia cohorts identifies multiple changes associated with nerve terminal function. *Mol. Psychiatry* **14**, 1083–1094 (2009).

462. Bradshaw, N. J. *et al.* The NDE1 genomic locus can affect treatment of psychiatric illness through gene expression changes related to microRNA-484. *Open Biol.* **7**, 170153 (2017).

463. Knight, H. M. *et al.* Homozygosity mapping in a family presenting with schizophrenia, epilepsy and hearing impairment. *Eur. J. Hum. Genet. EJHG* **16**, 750–758 (2008).

464. Zaharija, B. *et al.* TRIOBP-1 Protein Aggregation Exists in Both Major Depressive Disorder and Schizophrenia, and Can Occur through Two Distinct Regions of the Protein. *Int. J. Mol. Sci.* **23**, 11048 (2022).

465. Katsuno, T. *et al.* TRIOBP-5 sculpts stereocilia rootlets and stiffens supporting cells enabling hearing. *JCI Insight* **4**, e128561, 128561 (2019).

466. Javed, K., Reddy, V. & Lui, F. Neuroanatomy, Cerebral Cortex. in *StatPearls* (StatPearls Publishing, Treasure Island (FL), 2025).

467. Nolte, J. *The Human Brain: An Introduction to Its Functional Anatomy*. (Mosby, 1981).

468. Ochoa-Lantigua, P., Moreira-Mendoza, J., García Ríos, C. A., Rodas, J. A. & Leon-Rojas, J. E. The Little-Known Ribbon-Shaped Piriform Cortex: A Key Node in Temporal Lobe Epilepsy—Anatomical Insights and Its Potential for Surgical Treatment. *Diagnostics* **14**, 2838 (2024).

469. Goldberg, I. I., Harel, M. & Malach, R. When the brain loses its self: prefrontal inactivation during sensorimotor processing. *Neuron* **50**, 329–339 (2006).

470. Rolls, E. T., Cheng, W. & Feng, J. The orbitofrontal cortex: reward, emotion and depression. *Brain Commun.* **2**, fcaa196 (2020).

471. Wray, N. R. *et al.* Genome-wide association analyses identify 44 risk variants and refine the genetic architecture of major depression. *Nat. Genet.* **50**, 668–681 (2018).

472. Gray, J. P., Müller, V. I., Eickhoff, S. B. & Fox, P. T. Multimodal Abnormalities of Brain Structure and Function in Major Depressive Disorder: A Meta-Analysis of Neuroimaging Studies. *Am. J. Psychiatry* **177**, 422–434 (2020).

473. Boldrini, M. *et al.* Resilience Is Associated With Larger Dentate Gyrus, While Suicide Decedents With Major Depressive Disorder Have Fewer Granule Neurons. *Biol. Psychiatry* **85**, 850–862 (2019).

474. Van Hooijdonk, C. F. M. *et al.* The substantia nigra in the pathology of schizophrenia: A review on post-mortem and molecular imaging findings. *Eur. Neuropsychopharmacol.* **68**, 57–77 (2023).

475. Sonne, J., Reddy, V. & Beato, M. R. Neuroanatomy, Substantia Nigra. in *StatPearls* (StatPearls Publishing, Treasure Island (FL), 2025).

476. McCutcheon, R. A., Keefe, R. S. E. & McGuire, P. K. Cognitive impairment in schizophrenia: aetiology, pathophysiology, and treatment. *Mol. Psychiatry* **28**, 1902–1918 (2023).

477. Androschuk, A., Al-Jabri, B. & Bolduc, F. V. From Learning to Memory: What Flies Can Tell Us about Intellectual Disability Treatment. *Front. Psychiatry* **6**, 85 (2015).

478. van der Voet, M., Nijhof, B., Oortveld, M. A. W. & Schenck, A. Drosophila models of early onset cognitive disorders and their clinical applications. *Neurosci. Biobehav. Rev.* **46 Pt 2**, 326–342 (2014).

479. van Alphen, B. & van Swinderen, B. Drosophila strategies to study psychiatric disorders. *Brain Res. Bull.* **92**, 1–11 (2013).

480. Furukubo-Tokunaga, K. Modeling schizophrenia in flies. *Prog. Brain Res.* **179**, 107–115 (2009).

481. Her, Y., Pascual, D. M., Goldstone-Joubert, Z. & Marcogliese, P. C. Variant functional assessment in Drosophila by overexpression: what can we learn? *Genome* **67**, 158–167 (2024).

482. Velentzas, A. D. *et al.* Proteomic mapping of Drosophila transgenic elav.L-GAL4/+ brain as a tool to illuminate neuropathology mechanisms. *Sci. Rep.* **10**, 5430 (2020).

483. Berger, C., Renner, S., Lüer, K. & Technau, G. M. The commonly used marker ELAV is transiently expressed in neuroblasts and glial cells in the Drosophila embryonic CNS. *Dev. Dyn. Off. Publ. Am. Assoc. Anat.* **236**, 3562–3568 (2007).

484. Honjo, K. & Furukubo-Tokunaga, K. Distinctive neuronal networks and biochemical pathways for appetitive and aversive memory in Drosophila larvae. *J. Neurosci. Off. J. Soc. Neurosci.* **29**, 852–862 (2009).

485. Barnstedt, O. *et al.* Memory-Relevant Mushroom Body Output Synapses Are Cholinergic. *Neuron* **89**, 1237–1247 (2016).

486. Ganguly, I., Heckman, E. L., Litwin-Kumar, A., Clowney, E. J. & Behnia, R. Diversity of visual inputs to Kenyon cells of the Drosophila mushroom body. *Nat. Commun.* **15**, 5698 (2024).

487. Furukubo-Tokunaga, K. *et al.* DISC1 Causes Associative Memory and Neurodevelopmental Defects in Fruit Flies. *Mol. Psychiatry* **21**, 1232–1243 (2016).

488. Sawamura, N. *et al.* Nuclear DISC1 regulates CRE-mediated gene transcription and sleep homeostasis in the fruit fly. *Mol. Psychiatry* **13**, 1138–1148, 1069 (2008).

489. Andretic, R. & Shaw, P. J. Essentials of sleep recordings in Drosophila: moving beyond sleep time. *Methods Enzymol.* **393**, 759–772 (2005).

490. Furukubo-Tokunaga, K. *et al.* DISC1 causes associative memory and neurodevelopmental defects in fruit flies. *Mol. Psychiatry* **21**, 1232–1243 (2016).

491. Millar, J. K., James, R., Christie, S. & Porteous, D. J. Disrupted in schizophrenia 1 (DISC1): subcellular targeting and induction of ring mitochondria. *Mol. Cell. Neurosci.* **30**, 477–484 (2005).

492. Shao, L. *et al.* Disrupted-in-Schizophrenia-1 (DISC1) protein disturbs neural function in multiple disease-risk pathways. *Hum. Mol. Genet.* **26**, 2634–2648 (2017).

493. Pandey, H. *et al.* Genetic interaction of DISC1 and Neurexin in the development of fruit fly glutamatergic synapses. *NPJ Schizophr.* **3**, 39 (2017).

494. Petrović, M., Meštrović, A., Andretić Waldowski, R. & Filošević Vujnović, A. A network-based analysis detects cocaine-induced changes in social interactions in Drosophila melanogaster. *PloS One* **18**, e0275795 (2023).

495. Schneider, J., Dickinson, M. H. & Levine, J. D. Social structures depend on innate determinants and chemosensory processing in Drosophila. *Proc. Natl. Acad. Sci. U. S. A.* **109 Suppl 2**, 17174–17179 (2012).

496. Liu, G. *et al.* A simple computer vision pipeline reveals the effects of isolation on social interaction dynamics in Drosophila. *PLoS Comput. Biol.* **14**, e1006410 (2018).

497. Schneider, J. & Levine, J. D. Automated identification of social interaction criteria in Drosophila melanogaster. *Biol. Lett.* **10**, 20140749 (2014).

498. Palkovits, M. Isolated removal of hypothalamic or other brain nuclei of the rat. *Brain Res.* **59**, 449–450 (1973).

499. Palkovits, M. Microdissection of Individual Brain Nuclei and Areas. in *General Neurochemical Techniques* vol. 1 1–18 (Humana Press, New Jersey, 1986).

500. Samardžija, B. *et al.* Protein Aggregation of NPAS3, Implicated in Mental Illness, Is Not Limited to the V304I Mutation. *J. Pers. Med.* **11**, 1070 (2021).

501. Samardžija, B. *et al.* Co-Aggregation and Parallel Aggregation of Specific Proteins in Major Mental Illness. *Cells* **12**, 1848 (2023).

502. Zaharija, B. & Bradshaw, N. J. Aggregation of Disrupted in Schizophrenia 1 arises from a central region of the protein. *Prog. Neuropsychopharmacol. Biol. Psychiatry* **130**, 110923 (2024).

503. Agrotis, A., Pengo, N., Burden, J. J. & Ketteler, R. Redundancy of human ATG4 protease isoforms in autophagy and LC3/GABARAP processing revealed in cells. *Autophagy* **15**, 976–997 (2019).

504. Filošević Vujnović, A., Saftić Martinović, L., Medija, M. & Andretić Waldowski, R. Distinct and Dynamic Changes in the Temporal Profiles of Neurotransmitters in Drosophila melanogaster Brain following Volatilized Cocaine or Methamphetamine Administrations. *Pharmaceuticals* **16**, 1489 (2023).

505. Filošević Vujnović, A., Rubinić, M., Starčević, I. & Andretić Waldowski, R. Influence of Redox and Dopamine Regulation in Cocaine-Induced Phenotypes Using Drosophila. *Antioxidants* **12**, 933 (2023).

506. Fernandes, D. C., Gonçalves, R. C. & Laurindo, F. R. M. Measurement of Superoxide Production and NADPH Oxidase Activity by HPLC Analysis of Dihydroethidium Oxidation. *Methods Mol. Biol. Clifton NJ* **1527**, 233–249 (2017).

507. Alisik, M., Neselioglu, S. & Erel, O. A colorimetric method to measure oxidized, reduced and total glutathione levels in erythrocytes. *J. Lab. Med.* **43**, 269–277 (2019).

508. GitHub - kristinbranson/FlyTracker. https://github.com/kristinbranson/FlyTracker.

509. Wice, E. W. & Saltz, J. B. Selection on heritable social network positions is context-dependent in Drosophila melanogaster. *Nat. Commun.* **12**, 3357 (2021).

510. milanXpetrovic/drosophila-social-network-analysis: v1.0.0 Initial Release. https://zenodo.org/records/10355543.

511. Kearney, B. E. & Lanius, R. A. The brain-body disconnect: A somatic sensory basis for trauma-related disorders. *Front. Neurosci.* **16**, 1015749 (2022).

512. Tian, J. *et al.* An analysis of RNA quality metrics in human brain tissue. *J. Neuropathol. Exp. Neurol.* **84**, 236–243 (2025).

513. Franzén, B. *et al.* Dihydropyrimidinase related protein-2 as a biomarker for temperature and time dependent ***post mortem*** changes in the mouse brain proteome. *PROTEOMICS* **3**, 1920–1929 (2003).

9 List of figures

Appendix

10 List of tables

Bobana Samardžija

Nationality: Serbian **Date of birth:** 25/01/1996 **Gender:** Female

Phone number: (+385) 921502617

Email address: bobana.samardzija@uniri.hr

Home: Javornik 21, 44440 Dvor (Croatia)

WORK EXPERIENCE

Early-stage researcher [2016 – Current]

City: Rijeka | **Country:** Croatia

- Awarded FENS scholarship to attend course "Current approaches in neurological disorder research: from animal models to human brain on the chip", Warsaw 2023
- Awarded Early Career Award by Schizophrenia International Research Society, Florence 2022
- Member of national organizations: Hrvatsko društvo za neuroznanost and Hrvatsko društvo za biokemiju imolekularnu biologiju
- Member of international organisations: FENS: Federation of European Neuroscience Societies and Society forNeuroscience
- Member of scientific committee for Student congress of neuroscience NeuRi since 2020

Quality Assurance Student Expert [2022 – Current]

City: Rijeka | **Country:** Croatia

- member of Quality Assurance Pool in European Student Union since 2022

EDUCATION AND TRAINING

PhD in Medicinal Chemistry

University of Rijeka [15/10/2020 – 13/06/2025]

- Co-ordinator of the activities at the Department of biotechnology for the Science Festival 2022.
- Active member of organisation of the Night of the Researchers activities 2020 – now

Erasmus+ ***John Hopkins University, School of Medicine*** [01/10/2024 – 25/12/2024]

City: Baltimore | **Country:** United States

- Precision Medicine Center of Excellence for Schizoaffective Disorder

Master's degree in Drug research and development (mag. pharm. inv.)

University of Rijeka [2017 – 2020]

- Active member of the Office for science of the University of Rijeka Students' Council
- Leader of a project:"Summer school for first-year students" at the Department of Biotechnology University of Rijeka
- Active member of organisation of the Night of the Researchers activities 2019 – 2020

Erasmus+ ***Forschungszentrum Jülich GmbH*** [01/03/2020 – 30/06/2020]

City: Jülich | **Country:** Germany

- Institute of Biological Information processing - Structural biochemistry (IBI-7)

Bachelor's degree in Biotechnology and drug research (univ. bacc. biotechn. et pharm. inv.)

University of Rijeka [2014 – 2017]

- Active member of the Office for science of the University of Rijeka Students' Council and the Student organisation at the Department of Biotechnology

LANGUAGE SKILLS

Mother tongue(s): Croatian

Other language(s):

English	**LISTENING** C2	**READING** C2
	WRITING C2	
	SPOKEN PRODUCTION C2	**SPOKEN INTERACTION** C2

Levels: A1 and A2: Basic user; B1 and B2: Independent user; C1 and C2: Proficient user

List of publications:

Research articles

1. **Samardžija, B**.; Petrović, M.; Zaharija, B.; Medija, M.; Meštrović, A.; Bradshaw, NJ.; Filošević Vujnović, A.; Andretić Waldowski, R.; Transgenic Drosophila melanogaster Carrying a Human Full-Length DISC1 Construct (UAS-hflDISC1) Showing Effects on Social Interaction Networks, Current Issues in Molecular Biology 2024, 46, 8, 8526, doi: 10.3390/cimb46080502
2. Batel, A.; Polović, M.; Glumac, M.; Šuman, O.; Jadrijević, S.; Lozić, B.; Petrović, M.; **Samardžija, B**.; Bradshaw, NJ.; Skube, K.; Palada, V.; Acman, M.; Marinović Terzić, I.: SPRTN is involved in hepatocellular carcinoma development through the ER stress response, Cancer gene therapy 2024, 1, 3, 376-386, doi: 10.1038/s41417-023-00708-w
3. **Samardžija, B**.; Juković, M.; Zaharija, B.; Renner, É.; Palkovits, M.; Bradshaw, N.J. Co-Aggregation and Parallel Aggregation of Specific Proteins in Major Mental Illness. Cells 2023, 12, 1848. doi:10.3390/cells12141848
4. Zaharija B.; Odorčić M.; Hart A.; **Samardžija B.**; Marreiros R.; Prikulis I.; Juković M.; Hyde T.M.; Kleinman J.E.; Korth C.; Bradshaw N.J.: TRIOBP-1 Protein Aggregation Exists in Both Major Depressive Disorder and Schizophrenia, and Can Occur through Two Distinct Regions of the Protein. International journal of molecular sciences, 2022, 18; 11048, 19 doi:10.3390/ijms231911048
5. **Samardžija, B.**; Pavešić Radonja, A.; Zaharija, B.; Bergman, M.; Renner, É.; Palkovits, M.; Rubeša, G.;Bradshaw, N.J. Protein Aggregation of NPAS3, Implicated in Mental Illness, Is Not Limited to the V304I Mutation. J. Pers. Med. 2021, 11, 1070. doi:10.3390/jpm11111070
6. Zaharija B.; **Samardžija B.**; Bradshaw NJ. The TRIOBP Isoforms and Their Distinct Roles in Actin Stabilization, Deafness, Mental Illness, and Cancer. Molecules. 2020 25(21):4967. doi: 10.3390/molecules25214967
7. Giacometti, J.; Milin, Č.; Ćuk, M.; **Samardžija, B.**; Radosević-Stašić, B.: Partial Hepatectomy and Diets Enriched with Olive and Corn Oil Altered the Phospholipid Fatty Acid Profile in the Spleen.

Journal of Nutrition and Food, Science Forecast, 2018, 1005, 9, urn:nbn:hr:184:004903

Conference abstracts:

1. Samardžija, B.; Juković, M.; Zaharija, B.; Renner, E.; Palkovits, M.; Bradshaw NJ.: AGGREGATION OF DISC1 AND RELATED PROTEINS IN MENTAL ILLNESS OCCURS ACROSS THE BRAIN, BUT IS NOT HOMOGENOUS (poster) *19th International Conference on Alzheimer's and Parkinson's Diseases: Mechanisms, Clinical Strategies and promising Treatments of Neurodegenerative Diseases Vienna, Austria 1. - 5.4.2025.*
2. Samardžija, B.; Juković, M.; Zaharija, B.; Renner, E.; Palkovits, M.; Bradshaw NJ.: Protein aggregation of DISC1, as assayed by insolubility, varies across the brain of an individual with schizophrenia and Alzheimer's disease (poster) *Neuroscience 2024, Chicago USA 5.-9.10.2024*
3. Samardžija, B.: Sampled Smirks: Unraveling Protein Aggregation in Mental Health, Budapest Style (invited plenary lecture) *13th Student Congress of Neuroscience NeuRi 2024, Rijeka and Rab Croatia 19. - 21.4.2024.*
4. Samardžija, B.; Juković, M.; Zaharija, B.; Renner, E.; Palkovits, M.; Bradshaw NJ.: Unveiling the molecular tango: Specific pairs of protein co-aggregate in the brains of individuals with mental illness (poster) *Second Congress of Molecular Biologist of Serbia, Beograd Serbia 6. - 8.10.2023.*
5. Samardžija, B.: UNVEILING THE MOLECULAR TANGO IN MENTAL ILLNESS: what connects human brain samples, cell models and Drosophila? (oral presentation) *Dani doktoranada, Rijeka, Croatia 15.09.2023.*
6. Samardžija, B.: Multiverzum agregacije (oral presentation) *PhD Science café, Rijeka Croatia 21.03.2023.*
7. Samardžija, B.; Juković, M.; Zaharija, B.; Renner, E.; Palkovits, M.; Bradshaw NJ.: Aggregation and co-aggregation of specific proteins in *post-mortem* brain samples (poster) *2022 Congress of the Schizophrenia International Research Society, Florence Italy 6.04.2022. - 10.04.2022.*
8. Samardžija, B.; Bradshaw NJ.: NPAS3 aggregation, implicated in schizophrenia, is common in post mortem brain samples and can be induced by oxidative stress in neuroblastoma cells (poster) *FENS Regional Meeting 2021, virtual 25.08.2021. - 27.08.2021.*

9. Samardžija, B.; Pavešić Radonja, A.; Bradshaw NJ.: NPAS3 aggregation, seen in schizophrenia, is not dependent on a previously reported familial mutation (poster) *MIND & BRAIN - 60th International Neuropsychiatric Congress Pula, virtual 27.5.2021. - 30.5.2021.*